

AD-A070 537

NAVAL UNDERSEA CENTER SAN DIEGO CA  
ACRYLIC PLASTIC VIEWPORTS FOR OCEAN ENGINEERING APPLICATIONS. A--ETC(U)  
FEB 77 J D STACHW  
NUC-TP-562-APP

F/G 11/9

UNCLASSIFIED

1 OF 2  
AD  
A070537

NL



⑨ Research rept.,

NUC TP 562  
APPENDICES



LEVEL III

ADA 070537

⑥ ACRYLIC PLASTIC VIEWPORTS  
FOR OCEAN ENGINEERING  
APPLICATIONS. Appendices.

by

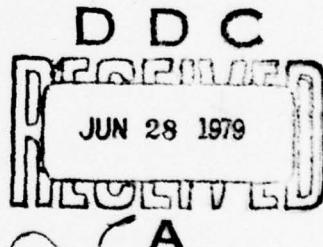
⑩ J.D. Stachiw

Ocean Technology Department

⑪ February 1977

⑭ NUC-TP-562-APP

⑫ 189 p.



ORIGINAL CONTAINS COLOR PLATES: ADD DDC  
REPRODUCTIONS WILL BE IN BLACK AND WHITE

Approved for public release; distribution unlimited.

DDC FILE COPY

390 458

79 06 28 003



NAVAL UNDERSEA CENTER, SAN DIEGO, CA. 92132

---

A N A C T I V I T Y O F T H E N A V A L M A T E R I A L C O M M A N D

**R. B. GILCHRIST, CAPT, USN**

Commander

**HOWARD L. BLOOD, PhD**

Technical Director

#### ADMINISTRATIVE INFORMATION

This design handbook summarizes research on viewports with acrylic plastic windows. Its preparation was supported by the Naval Facilities Engineering Command and the Director of Navy Laboratories.

Accession For	
NTIS GRA&I	<input checked="" type="checkbox"/>
DDC TAB	<input type="checkbox"/>
Unannounced	<input type="checkbox"/>
Justification	<input type="checkbox"/>
By _____	
Distribution/	
Availability Codes	
Dist	Available and/or special

Released by

H. R. Talkington, Head  
Ocean Technology Department

#### ACKNOWLEDGEMENTS

This handbook represents not only the efforts of the author but also those of researchers without whose data the formulation of the design guidelines would not have been feasible. Section 1 was authored by J. L. Atkerson of the New York Historical Society; section 2 by H. Mukamal, N. G. Nixon, and W. Yamaguchi of Swedlow, Inc.; section 5 by J. L. Stachiw of San Diego City Schools; section 14 by J. J. Lones of Adroit Engineering; and section 15 by the Committee on Viewports, Ocean Engineering Division, American Society of Mechanical Engineers. All other sections and appendices are the work of J. D. Stachiw of the Ocean Technology Department.

1  
2  
3  
4  
5  
6  
7  
8  
9  
0  
D  
A  
B  
C  
E  
F  
G  
H  
I  
J  
K  
L  
M  
N  
O  
P  
Q  
R  
S  
T  
U  
V  
W  
X  
Y  
Z  
a  
b  
c  
d  
e  
f  
g  
h  
i  
j  
k  
l  
m  
n  
o  
p  
q  
r  
s  
t  
u  
v  
w  
x  
y  
z

79 06 28 003

APPENDIX A. CONSTRUCTION OF ACRYLIC SPHERES . . . A-1

A.1 CONSTRUCTION BY BONDING THERMOFORMED  
SPHERICAL PENTAGONS . . . A-1

- A.1.1 Fabrication . . . A-1
- A.1.2 Construction . . . A-2
- A.1.3 Quality Control . . . A-3
- A.1.4 Conclusion . . . A-5
- A.1.5 Bibliography . . . A-5

A.2 CONSTRUCTION BY BONDING OF CAST HEMISPHERES . . . A-19

- A.2.1 Tooling . . . A-19
- A.2.2 Casting Process . . . A-20
- A.2.3 Inspection of Castings . . . A-21
- A.2.4 Fabrication of Spherical Hull . . . A-22
- A.2.5 Inspection of Assembled Sphere . . . A-23
- A.2.6 Findings . . . A-24
- A.2.7 Conclusion . . . A-24
- A.2.8 Bibliography . . . A-24

## APPENDIX A. CONSTRUCTION OF ACRYLIC SPHERES

### A.1 CONSTRUCTION BY BONDING THERMOFORMED SPHERICAL PENTAGONS\*

The procedure of producing an acrylic sphere by this process is graphically shown in figures A.1 through A.26.

#### A.1.1 Fabrication

The first step was to thermoform a flat blank of acrylic, 2.5 inches (6.4 centimeters) thick and 46 inches (117 centimeters) in diameter, into a spherical shell sector with a 33-inch (84 centimeters) radius in a concave spherical mold. The blank was cut from a 4- by 5-foot (1.2 by 1.5 meters) commercial sheet of 2.5-inch-thick (6.4 centimeters) acrylic. The thermoforming mold was a custom-built aluminum dish with a surface texture of 32 microinches (0.0008 millimeter). Four 3/32-inch-diameter (0.2 centimeter) vacuum holes were drilled at the bottom of the mold. Before thermoforming, the cylindrical surface of the acrylic blank was machined to a 200-microinch (0.005 millimeter) surface texture to promote a good vacuum seal between the heated blank and the mold. Four 1/8-inch-diameter (0.3 centimeter) by 2-inch-deep (5 centimeters) holes were drilled into the outside edge of the circular blank perpendicular to the cylindrical surface and parallel to the flat surface of the blank for installation of iron-constantan thermocouples. These thermocouples were spaced 90 degrees (1.57 radians) to each other.

After positioning the acrylic blank in the mold, both were placed in an oven and gradually heated to 300°F (149°C) over a period of 24 hours. The sequence of thermoforming events was as follows:

- a. 1545 hours: parts placed in oven with temperature at 165°F (74°C) and allowed to remain overnight; fan on.
- b. 0745 hours: oven temperature raised to 300°F (149°C); fan on.
- c. 1030 hours: acrylic blank sagged a constant amount with temperature at  
254°F (123°C) at 0.25 inch (0.6 centimeter) from air-exposed surface  
275°F (135°C) at both midpoints of blank thickness  
297°F (147°C) at 0.25 inch (0.6 centimeter) from mold surface  
299°F (148°C) at the mold surface
- d. 1530 hours: oven temperature raised to 310°F (154°C); fan on.
- e. 1545 hours: all temperatures became  $300^{\circ}\text{F} \pm 1^{\circ}$  (149°C); vacuum of 25-inch (64 centimeters) mercury applied to mold; blank immediately sagged and held completely to mold contour; fan on.
- f. 1600 hours: oven and fan turned off; oven door remained closed; vacuum left on all night.

---

\*This process was developed by the U.S. Navy at the Naval Missile Center, Point Mugu, California, and at the Naval Civil Engineering Laboratory, Port Hueneme, California, in 1966. The description of the process for a 2.5-inch-thick (6.4 centimeters) sphere with a 33-inch (84 centimeters) radius is applicable to spheres of any thickness and radius.

g. 0800 hours: vacuum turned off; oven temperature at 110°F (43°C); oven door opened and oven allowed to cool to room temperature; thermoformed acrylic shell removed.

Each thermoformed shell sector was stored in a contoured box with soft lining to prevent damage to the acrylic surface. A vacuum-operated chuck was built to hold, rotate, and position the acrylic shell sector for cutting and machining into a pentagonal shape. The chuck utilized vacuum to hold the shell sectors in the fixture, and air pressure to rotate and index the shell sector for the five straight cuts to form a pentagon. The acrylic shell sectors were first rough cut on a band saw into pentagon-shaped segments. Final machining was performed on a numerically controlled automatic milling machine. The milling cutter was a 2-inch-diameter (5 centimeters), helical type that rotated at 3800 rpm and fed at 10 inches per minute (25 centimeters per minute). A coolant of detergent-based water was used during the milling operation. The resulting surface texture at the pentagon edge was 63 micro-inches (0.0016 millimeter), which was satisfactory for cementing purposes. Two of the spherical acrylic pentagons were conically bored for their metal end plate insert. These holes were conical with their projected apex at the center of curvature of the spherical pentagon surface. After the machining operations, each spherical pentagon was annealed at 160°F (71°C) for 24 hours to reduce residual internal stresses and crazing potential in the acrylic plastic. Annealing was performed while the spherical pentagon rested in its contoured box.

#### A.1.2 Construction

Assembly of the 5.5-foot-diameter (1.7 meters) acrylic hull was accomplished by a two-phase bonding technique in which two quasihemispheres composed of six bonded spherical pentagons were bonded together into a sphere. To prepare the pentagon for bonding, the cemented surfaces were sanded with 240- and 400-grit sandpapers to develop adequate joint strength. A bonding procedure, suggested by the maker of the PS-30 polymerizing cement, was to use a butt joining gap of 1/8 inch (0.3 centimeter) between the adjacent 2.5-inch-thick (6.4 centimeters) acrylic pentagons. One polar pentagon with its conical hole and five regular pentagons were hemispherically positioned in an assembly fixture. The assembly fixture was preadjusted by means of an accurately dimensioned, dummy, glass-reinforced plastic sphere to produce the 66-inch-diameter (168 centimeters) NEMO sphere. The pentagons were spaced 0.125 inch (0.3 centimeter) apart with 0.25-inch-diameter (0.6 centimeter) acrylic spacers. Two spacers were placed on each 24-inch-long (61 centimeters) side of the pentagon at 2 inches (5 centimeters) from the corners. The joints were matched on the outside surface (convex) to form a continuous smooth contour between adjacent pentagons. Because of the variation in the thickness of the pentagons, the inside surface at the joints was not expected to be even. The joints were masked with cellophane fiber tape and a preformed aluminum foil to create a protruding bead of cement at the joint to account for any shrinkage of the bonded joint. The excess beads were polished away to ensure a bonded joint flush with the surface.

PS-30, the polymerizing acrylic cement, consisted of two components: component A (base resin) and component B (catalyst). The catalyst, 50 milliliters of component B, was dissolved in 950 milliliters of the resin at 60°F (16°C) by stirring the mix slowly beneath the surface to avoid entrapment of air bubbles in the cement. The cement mixture was then placed under vacuum and degassed for 10 minutes to remove all air bubbles before pouring

into the prepared joints. The pot life of this mixture was 30 minutes which was adequate for degassing and pouring purposes.

The cement was poured simultaneously into two vertical masked joints at opposite sides of the hemisphere by means of funnels and polyethylene squeeze bottles. The cavity in the joint area was filled by gravity, while each funnel or bottle attached to the cavity was kept full to prevent air bubbles from entering. New batches of adhesive were continuously prepared as the pouring proceeded to maintain constant head in the funnel. This process continued until the adhesive filled all the joints in the hemisphere, including the other three vertical joints. If air was trapped in some of the horizontal joints between advancing columns of adhesive, a hole was punched in the tape at that location with a needle. After all the trapped air escaped and the adhesive began to ooze out, the hole was sealed with a tape patch prepared for this purpose. Utilizing this technique, a continuous joint was prepared in the hemisphere with only a minimum of entrapped air. The few resulting bubbles were less than 0.25 inch (0.6 centimeter) in diameter, and in most cases they were located at the edges of the joint where they could be easily refilled with adhesive after the tape was removed from the joints.

The final assembly into a sphere was performed by matching and bonding the two previously constructed hemispheres of six bonded pentagons each. The cement was allowed to cure at room temperature for 48 hours before the protruding bead at the joint was ground and polished. The whole hull was then polished to minimize surface blemishes. The completed hull was annealed in the oven at 160°F (71°C) for 24 hours and allowed to cool at a rate of approximately 7°F (-14°C) per hour until room temperature was reached.

#### A.1.3 Quality Control

The first measurement was the thickness of each flat sheet of acrylic used as the thermoforming blank. The thickness of the acrylic sheet was within the MIL-P-21105C specifications for type G acrylic of 2.5 inches (6.4 centimeters) thickness, which was +0.079 inch (0.2 centimeter) and -0.181 inch (0.5 centimeter)

The second measurement was of the acrylic thickness after thermoforming. In general, the acrylic blank increased in thickness around its periphery and decreased in thickness at the center after the thermoforming operation in the female mold. The increase at the periphery was approximately 0.080 to 0.110 inch (0.2 to 0.3 centimeter). At the center of the thermoformed blank the thickness decreased approximately 0.020 inch (0.05 centimeter).

A third measurement was the acrylic thickness after annealing of a machined pentagon; no net change in thickness was found between the thermoformed and the annealed pentagon.

The curvature of an acrylic blank was compared with the curvature of the forming mold. The concave surfaces of the mold and the blank were measured by swinging an arc with a dial indicator about the center of the spherical surface.

The acrylic blank generally appeared to flatten near the apex and acquire increased curvature in its skirt region. The largest deviation in radius was less than 0.1 percent of the spherical radius of the thermoformed blank. It should be noted that the mold was made with a shorter radius at the skirt region to compensate for an expected incomplete contact between the thermoformed acrylic blank and the corresponding mold surfaces. As expected, the acrylic blank acquired less curvature than the mold in the skirt region, but still short of the specified 33.000 outside radius.

The convex surface of the thermoformed acrylic blank showed some mark-off where the acrylic was in contact with the mold which had a surface texture of 32 microinches (0.0008 millimeter). These marks were less than 0.003 inch (0.008 centimeter) in height and disappeared when in contact with water because of the small dissimilarity in index of refraction between acrylic (1.49) and water (1.33). Since nothing contacted the concave surface of the acrylic blank during thermoforming, the acrylic remained unmarred on this side. When viewed through polarized plates, the skirt region of the acrylic blank showed more stress pattern than the apex region.

The radial mismatch between adjacent pentagons was less than 0.032 inch (0.08 centimeter) on the outside surface; however, the inside-surface mismatch at the joint was dependent on the difference in pentagon thicknesses. Typical mismatches were less than 3/16 inch (0.5 centimeter) on the inside surface. The mismatch on the outside surface was reduced by producing a faired contour when the hull was polished.

Uniaxial tensile loads were applied to acrylic specimens with PS-30 bonded joints within 1 month of bonding. The test specimens were machined from acrylic samples made by duplicating the bonding procedure used to assemble the 5.5-foot-diameter (1.7 meters) hull. In three tests, the breaking stresses were 8779, 8893, and 6573 pounds per square inch (60.5, 61.3, and 45.3 megapascals). In compression, the samples could not be fractured at stresses as high as 16,000 pounds per square inch (110.3 megapascals), although the PS-30 joint took a permanent distortion of about 5 percent.

To insure proper fit into a sphere, dimensions for each pentagon were verified during manufacture. The assembled hull was measured for diameter with an improvised micrometer and for curvature with a template and feeler gages. A total of 30 diameter measurements was taken in a controlled atmosphere room, and time, temperature, and humidity for each measurement were recorded. To summarize these measurements, the mean diameter of the hull across centers of the pentagons was 66.126 inches (167.96 centimeters); across the corners, which are adjacent to the polar pentagons, it was 66.049 inches (167.76 centimeters); and across the corners in the equatorial zone, it was 65.982 inches (167.59 centimeters). These measurements indicated that the NEMO serial number 0 hull was probably slightly prolate with slight bulges centered on the pentagons. The mean diameter was 66.030 inches (167.72 centimeters) with the maximum diameter at 66.158 inches (168.04 centimeters) and the minimum at 65.920 inches (167.44 centimeters). The maximum deviation on radius of curvature of the hull surface was within 0.5 percent of the design radius of the hull.

The 5.5-foot-diameter (1.7 meters) capsule assembly, including acrylic hull, stainless-steel bottom plate, and mating ring with the hatch at the top, weighed 1526 pounds (692 kilograms). No optical distortion other than spherical aberration was noticeable, and the transmissivity was not affected by minor surface flaws at the water-to-acrylic interface.

Although the quality of the assembled capsule was structurally satisfactory and constructed according to plans in terms of thermoforming and machining operations, the hull assembly procedure and the bonding operations with polymerizing acrylic cement invited improvements in terms of cement curing and elimination of undesirable voids in the joints. The joints also showed minor amounts of residual stress when viewed through polarized plates.

#### A.1.4 Conclusion

Fabrication and construction procedures for a 5.5-foot-diameter (1.7 meters), 2.5-inch-thick (6.3 centimeters), acrylic hull in the form of a spherical dodecahedron were successfully developed using commercial acrylic sheet stock. Similar fabrication procedures have also successfully produced 5.5-foot-diameter (1.7 meters), 4.0-inch-thick (10 centimeters) hulls meeting ANSI/ASME PVHO-1 and U.S. Navy specifications for pressure vessels for human occupancy.

#### A.1.5 Bibliography

1. Tsuji, K., and Sheldon R., "Fabrication of NEMO-Type Spherical Acrylic Capsules for Underwater Vehicles," ASME Paper No. 70-WA/UnT-4.
2. Stachiw, J. D., "Acrylic Pressure Hull for Submersible NEMO," ASME Paper No. 71-UnT-2.
3. Maison, J. R., and Stachiw, J. D., "Acrylic Pressure Hull for Johnson Sea-Link Submersible," ASME Paper No. 71-WA/UnT-6.

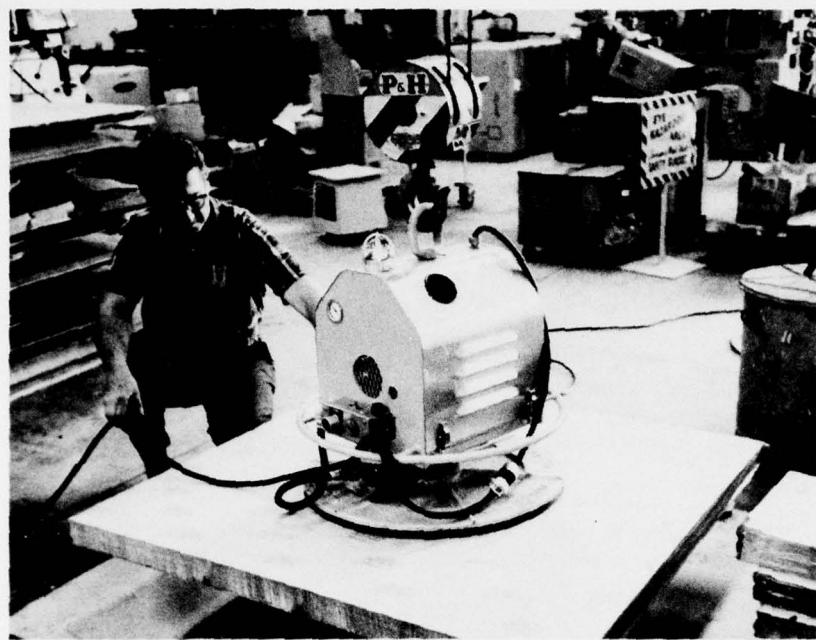


Figure A.1. Lifting a sheet of acrylic plastic with a vacuum chuck from the pallet.

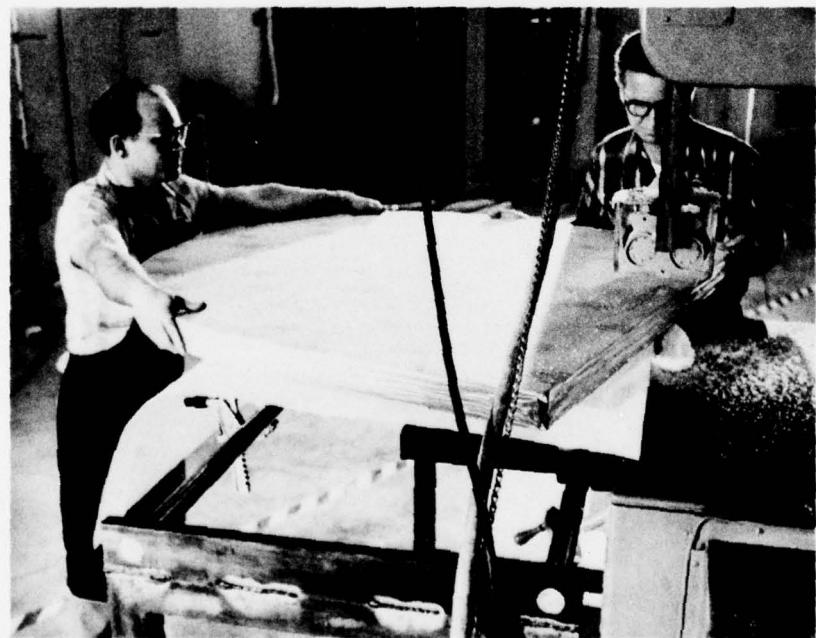


Figure A.2. Cutting a disc from the acrylic sheet with a band saw.

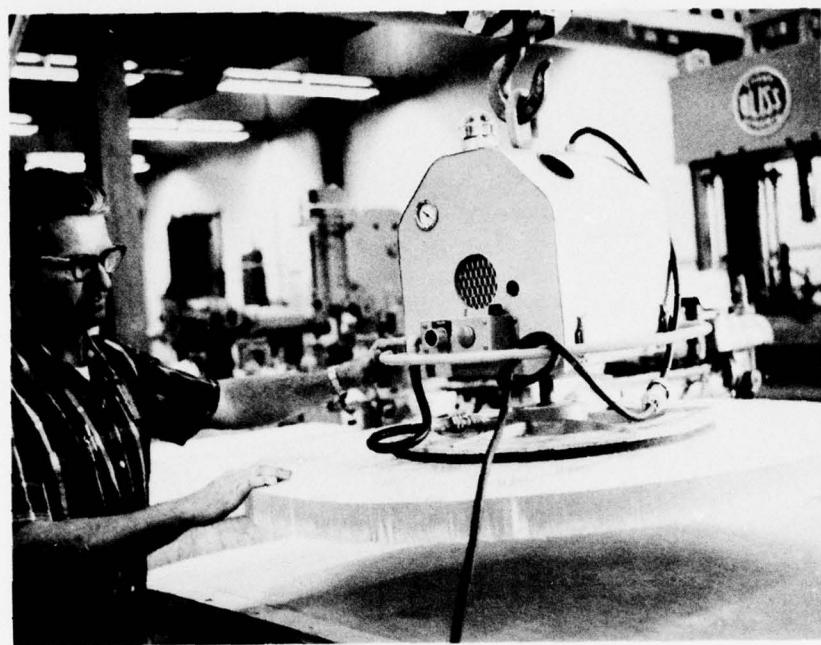


Figure A.3. Transporting the disc from the band saw to a milling machine where the edge of the disc will be milled smooth.

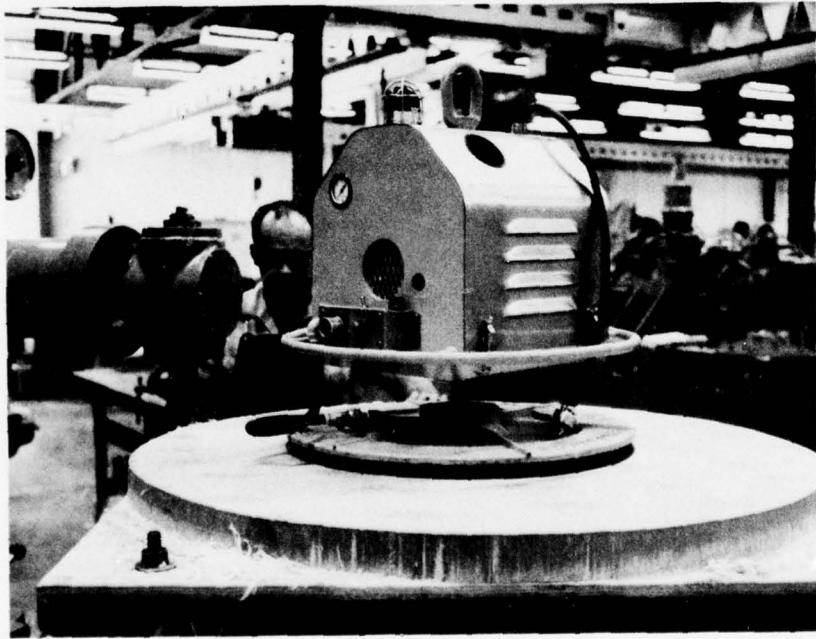


Figure A.4. Milling the edge of the disc smooth so that an airtight seal with the concave surface of the mold can be achieved.

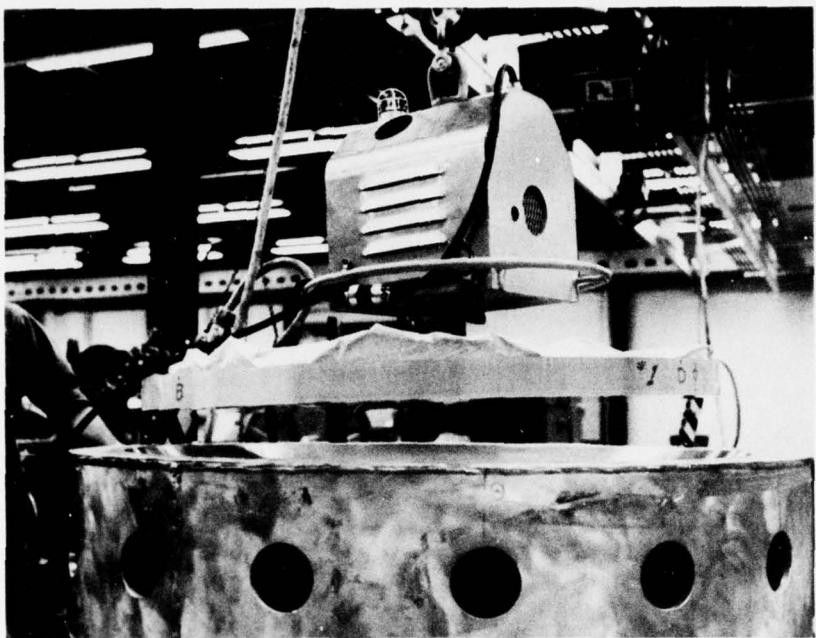


Figure A.5. Placing the disc into a vacuum mold after the protective paper has been stripped from the bottom surface.

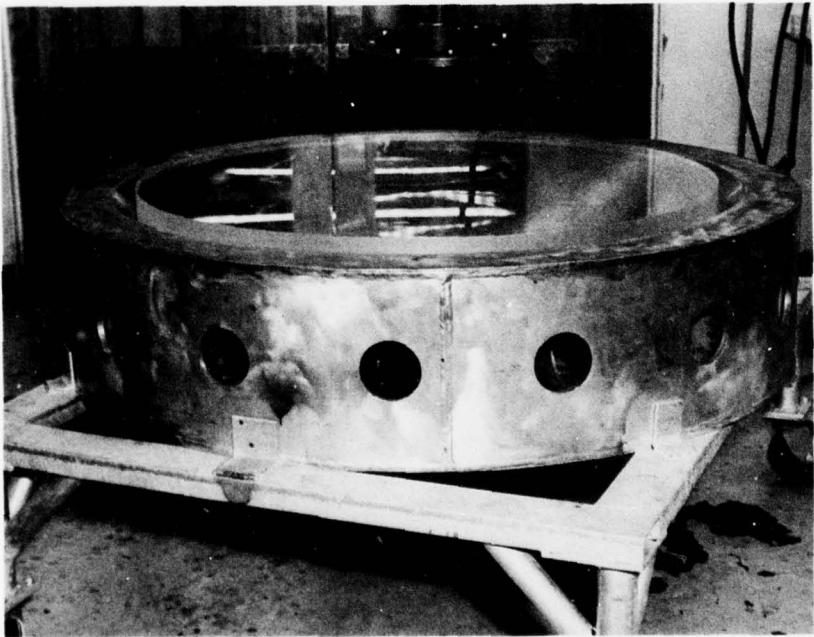


Figure A.6. Disc after the protective paper has also been stripped from the top surface.

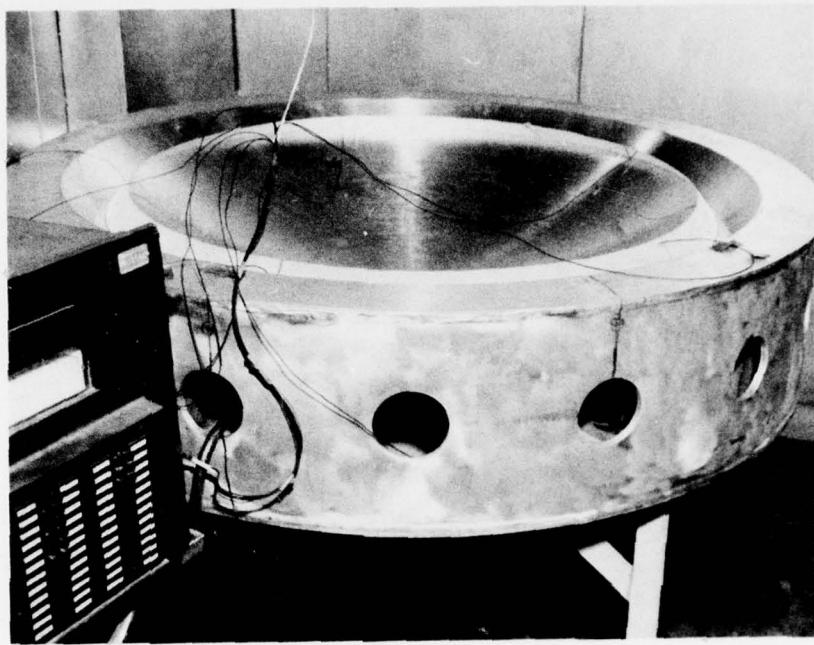


Figure A.7. Disc after thermoforming in a hot air oven. Note the thermocouples used for measurement of temperature in the acrylic.

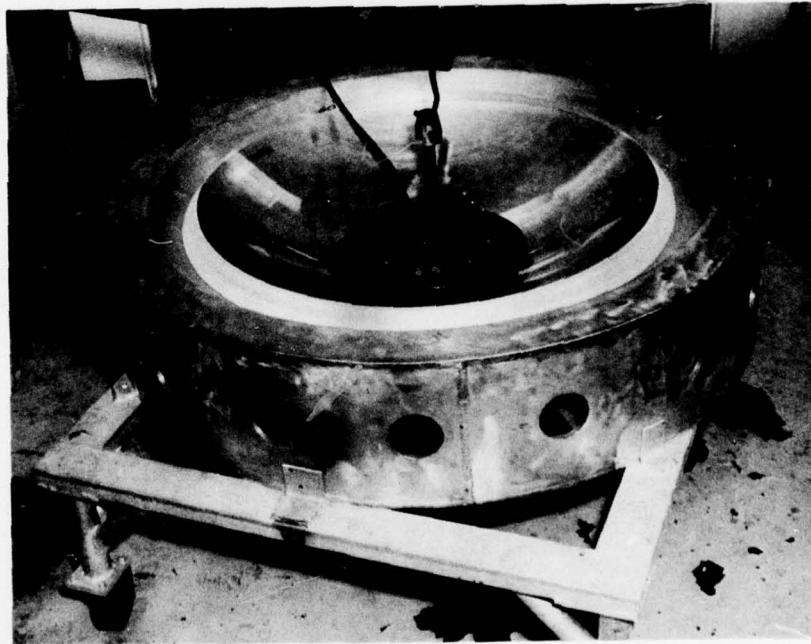


Figure A.8. Removing the thermoformed sector from the mold with a vacuum chuck.

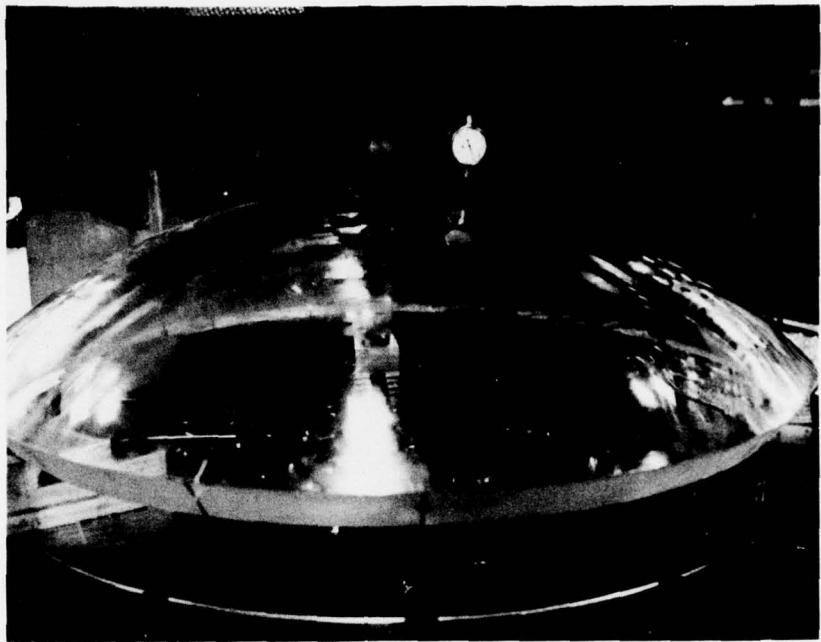


Figure A.9. Checking the sphericity of the spherical sector.

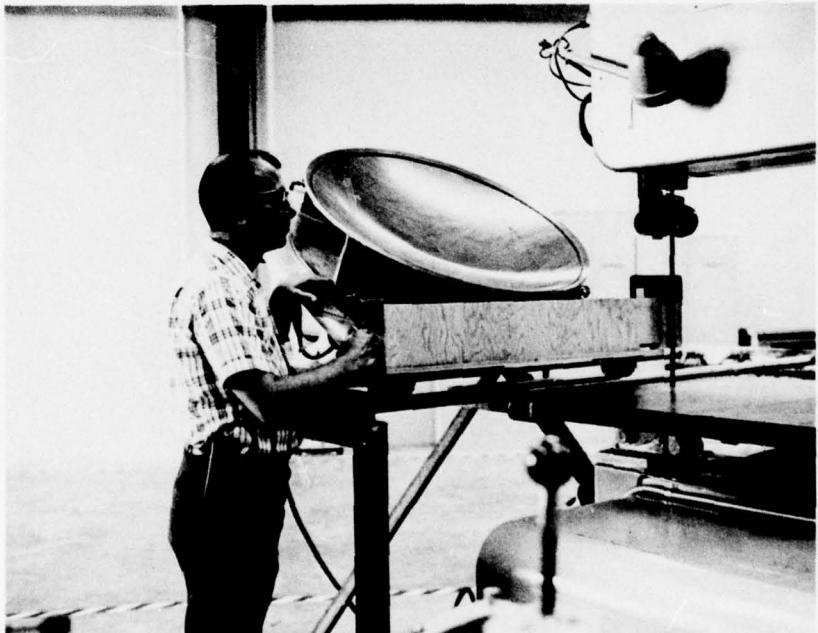


Figure A.10. Vacuum chuck that can be sequentially indexed to five positions and held there firmly during cutting and milling of the acrylic sector.

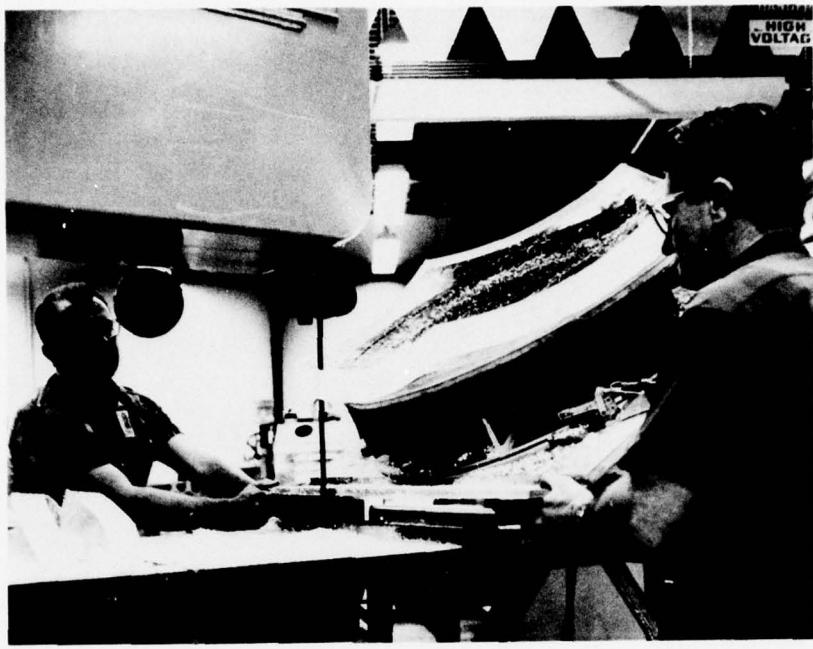


Figure A.11. Band sawing the sector into pentagonal shape.



Figure A.12. Milling the sawed edges with a numerically controlled vertical mill.

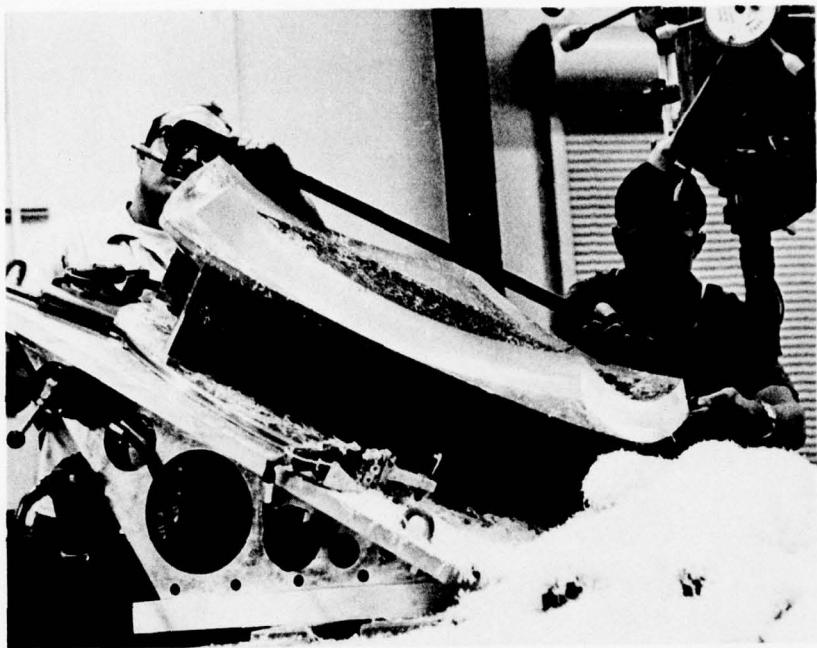


Figure A.13. Checking the dimensions of the pentagon.

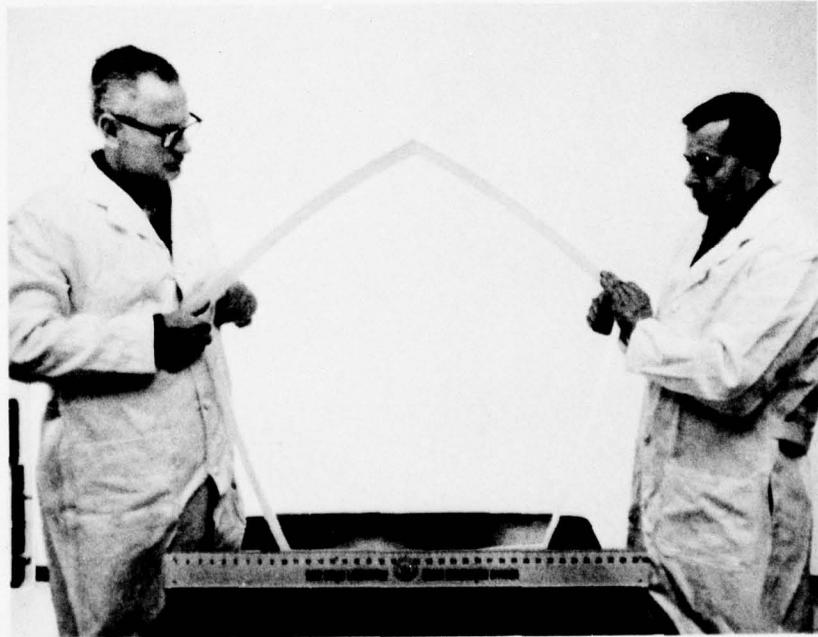


Figure A.14. Visual inspection of milled edges on the finished spherical pentagon.

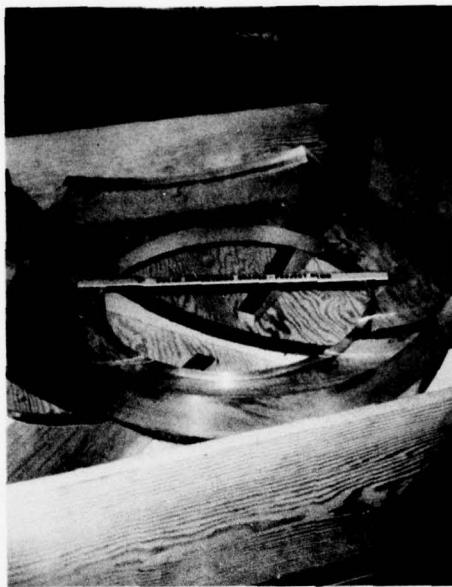


Figure A.15. Storage of finished pentagons in individual padded boxes prior to their assembly into hemispheres. At this time two of the pentagons have conical openings machined in them to fit metallic closures.

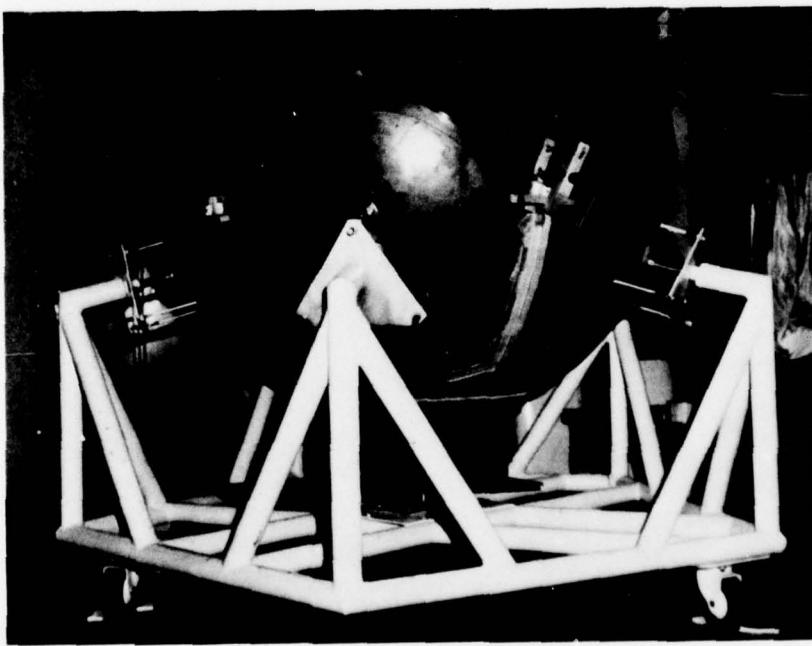


Figure A.16. Aligning spherical pentagons in the assembly jig prior to bonding.



Figure A.17. Bonded hemisphere after removal from the assembly jig.

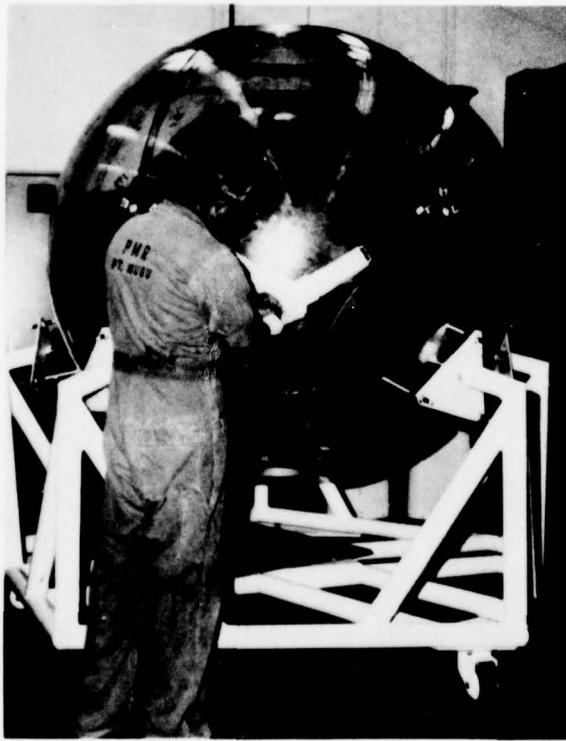


Figure A.18. Aligning two hemispheres prior to bonding of the equatorial joint.

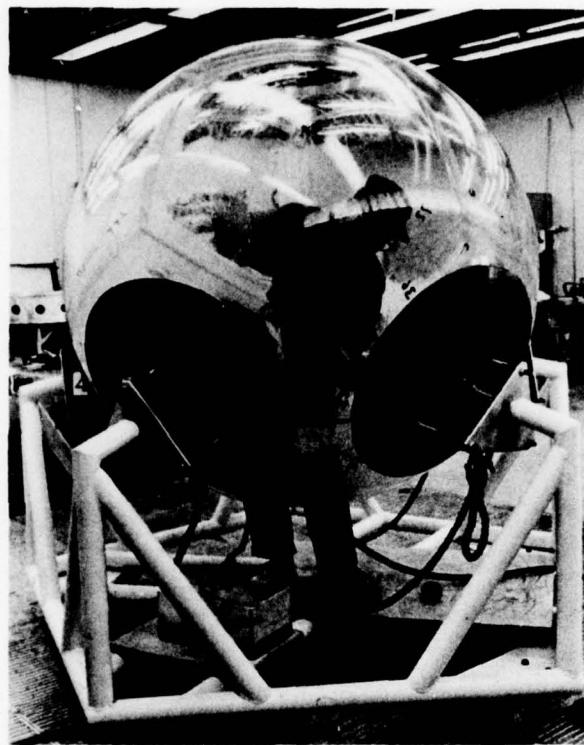


Figure A.19. Sanding and polishing bonded joints on the sphere.

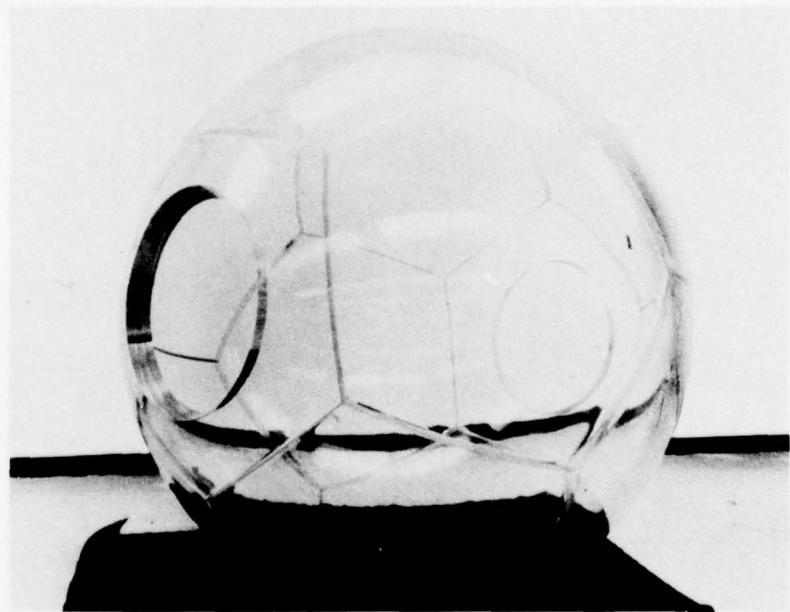


Figure A.20. Completed sphere after annealing in a heated air oven.

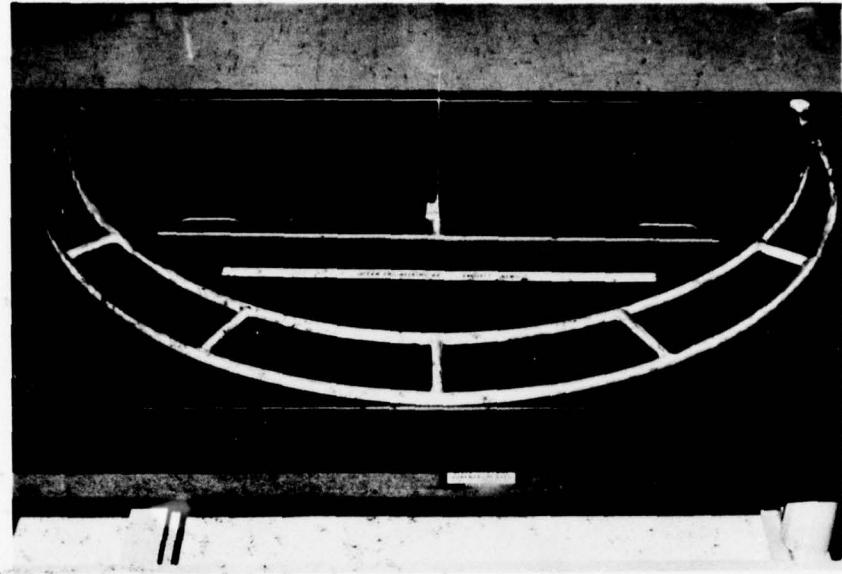


Figure A.21. Instruments used in quality control.



Figure A.22. Measuring the sphericity with a template and feeler gages.

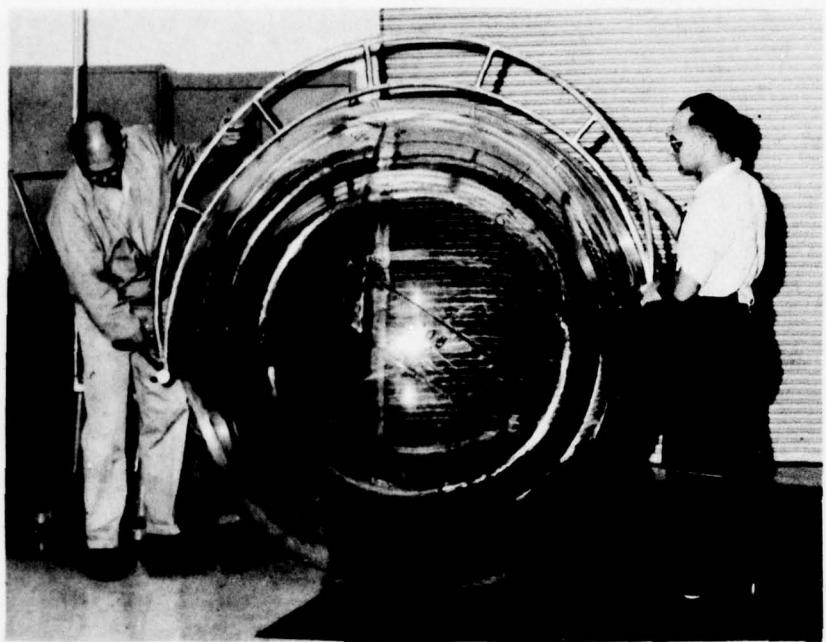


Figure A.23. Measuring the external diameter at selected locations.



Figure A.24. Visual inspection of bonded joints for presence of inclusions.

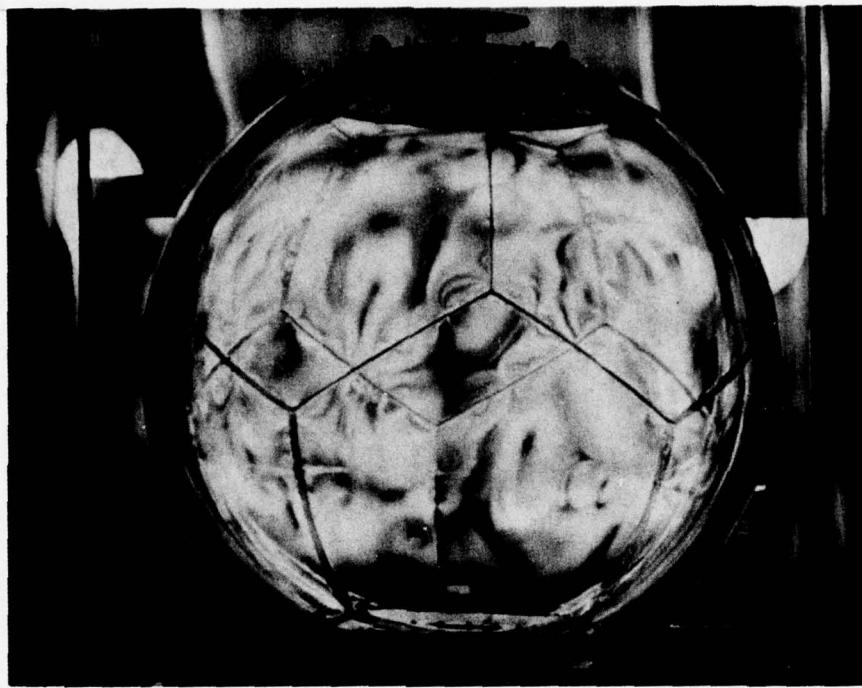


Figure A.25. Inspecting the sphere for residual strains with the aid of polarized light.



Figure A.26. Inspecting the operation of the hatch.

## A.2 CONSTRUCTION BY BONDING OF CAST HEMISPHERES\*

The procedure of producing an acrylic sphere by this process is graphically shown in figures A.27 through A.52.

### A.2.1 Tooling

Tooling for precision casting of acrylic plastic hemispheres consisted of a mold assembly, autoclave cart, and strongback.

The mold assembly was a matched set of male and female molds. Considerable care went into its design. It was to serve as the form for gelling and polymerizing the acrylic plastic and also as a power-assisted jig for separating the polymerized casting from the mold assembly. In addition, the mold assembly had to fit the autoclave where polymerization occurred under elevated temperature and pressure.

The major components of the assembly were a female mold (serving as foundation for four flanged wheels), a male mold (serving as foundation for six hydraulic lifting jacks and six elevation adjusting screws), and a manually operated hydraulic pump (for pressurization of hydraulic jacks). The entire assembly was fabricated from welded low-carbon steel.

The hydraulic jacks mounted on the extensions of the male mold served to separate the male mold from the polymerized casting that gripped the mold. Since the shrinkage of the casting was known to be in the 5 to 10 percent range, a substantial shrinkage grip was exerted on the male mold by the cured casting. To overcome the friction between the mold and the casting, each jack was designed to exert up to 10 tons of thrust against the equatorial surface of the casting. A manually operated hydraulic pump provided pressurized oil through flexible hoses to the hydraulic jacks.

The thrust of the hydraulic jacks was augmented by air pressure applied through a fitting in the bottom of the male mold to the interface between the mold and the casting. The provision for applying air pressure to this interface was found during subsequent casting operations to be very helpful, as the hydraulic jacks alone could not always insure separation between the male mold and the casting.

The separation between the female mold and the casting was accomplished by pressurized water that was pumped into the annular space between them through a fitting located at the bottom of the mold. After they were further separated, an influx of water made the casting float up in the mold until a lifting jig could be attached to it.

The elevation-adjusting screws, located on the extensions of the male mold, were used to adjust the clearance between the bottom of the male mold and the female mold. They also helped to locate the center of the male mold in the center of the female mold. With the help of these screws it was possible to center the male mold within 0.030 inch (0.08 centimeter) of the desired location.

\*The casting process was developed jointly by the Naval Undersea Center, Harbor Branch Foundation, and Polymer Products in 1975. The description of the process is for a 4.250-inch-thick (10.7 centimeters) sphere with a 33.25 inch (84.5 centimeters) outside radius; it also applies as to spheres of other thicknesses and radii.

Flanged wheels, attached to the lower external circumferential stiffener on the female mold, were designed for moving the mold assembly on rails in and out of the autoclave located at Polymer Products. In this manner, the mold assembly could be easily filled with casting mix outside the autoclave and then without disturbing the gelling mixture moved inside the autoclave.

The strongback consisted of a circular frame with a lifting sling. The diameter of the circular frame was smaller than the outer diameter of the acrylic hemisphere to permit lifting of the hemisphere from the female mold after the hemisphere was partially raised in the mold by forcing water between the casting and the mold. The strongback was attached to the casting by disassembling it into two halves, placing them around the casting, and clamping them together with bolts.

#### A.2.2 Casting Process

The casting process developed for this purpose by Polymer Products of Oakland, California, consisted of five distinct steps: (1) mixing of resin with additives; (2) pouring the resin mix into the mold assembly; (3) gellation of the resin mix in the mold at atmospheric pressure and temperature; (4) polymerization of the gelled resin mix inside the autoclave under elevated temperature and pressure; and (5) removal of the polymerized casting from the mold.

Mixing the acrylic and the required additive was done under atmospheric pressure and temperature. The basic casting mix was 1000 milliliters of Du Pont methyl methacrylate monomer, 1500 grams of Du Pont polymer 4FNC99 passing number 77 sieve, 2 grams of Du Pont catalyst Vazo 52, and 10 milliliters of Sartomer Resins Company methylene glycol methacrylate for cross-linking. The materials were mixed together with an electric rotary mixer and placed under 80 millimeters of vacuum. After several minutes, the vacuum was released, and the mix was stirred until it thickened to a thick creamy consistency. At that time, the mix was poured into the mold assembly previously cleaned with methyl or ethyl alcohol. The mixing of batches was repeated many times until the annular space between the male and female molds was completely filled.

Gellation of the casting inside the mold assembly occurred under atmospheric pressure and temperature. Although the length of time varied with atmospheric temperature, several hours were usually sufficient.

Polymerization of the gelled resin mixture took place inside a horizontal autoclave. The resin-filled mold assembly was rolled into the autoclave on tracks, extending from the general assembly area into the interior of the autoclave, and the door was locked in place. The door was then closed and pressurization with compressed air initiated. After approximately 6 hours, the internal pressure reached 150 pounds per square inch (1.03 megapascals). This served as a signal for initiation of the thermal cycle, which consisted of raising the temperature of the pressurized autoclave from 80 to 180°F (27 to 82°C) in 3 hours and 30 minutes. This temperature was maintained for 18 hours.

The cooling down of the pressurized autoclave to 120°F (49°C) took 24 hours. At 120°F (49°C), the autoclave was depressurized, the door opened, the male mold separated

from the casting, and the unpressurized autoclave was allowed to cool down to 80°F (27°C).

The crucial step in the polymerization process was the separation of the male mold from the already polymerized, but still hot, casting. The separation between the tightly wedged male mold and the hemispherical casting was achieved by simultaneously applying air pressure to the fitting in the bottom of the male mold and hydraulic pressure to the six hydraulic jacks spaced around the circumference of the mold. While the hydraulic jacks attached to the rim of the male mold pushed against the rim of the casting, compressed air applied through an opening in the base of the male mold to the interface between the male mold and the casting eliminated the vacuum generated by upward movement of the male mold. After raising the male mold about 2 inches (5 centimeters), it was placed on wedges resting on the rim of the female mold. Upon completion of this step the door to the autoclave was closed again and the gradual lowering of ambient temperature initiated.

The lifting of the male mold generated a small clearance between the male mold and the interior surface of the casting. Because of this clearance, the casting could be cooled without generating tensile hoop stresses in the rim of the hemispherical casting. If the casting was cooled to ambient atmospheric temperature without prior release of the male mold, tensile cracks appeared in the casting. Opening the autoclave door and rolling out the mold assembly completed the polymerization process.

The casting was removed from the mold assembly in the general work area outside the autoclave. The male mold was completely removed from the interior of the casting with a forklift; the casting was partially raised inside the female mold by injecting tap water through the bottom of the mold into the interface between the female mold and the exterior of the casting; and, the split strongback frame was clamped around the casting protruding from the mold and lifted with the forklift from the mold.

#### A.2.3 Inspection of Castings

After removal from the mold, the casting was subjected to inspection, whose objectives were to determine the quality of the product. The inspection took place in several steps: (1) visual observation, (2) dimensional measurement, and (3) testing of material specimens for determination of physical properties.

Visual observation was conducted by utilizing transmitted sunlight as a source of illumination. The observation focused on smoothness of casting surface, clarity of casting, and size and number of inclusions in the casting. The concave and convex surfaces possessed the same surface roughness as did the metallic molds, and no further finishing was required, except for fine sanding and polishing. The equatorial edge was in the form of a meniscus with a 2 inch (5 centimeters) depth caused by shrinking of the resin mix during the polymerization process. This was as expected and allowed for in the design of the mold assembly. The clarity of casting was equivalent to Plexiglas G of a similar thickness. After fine sanding and polishing of both the convex and concave surfaces, the casting was found to satisfy the

ANSI/ASME-PVHO-1 requirement for clarity\* in acrylic plastic viewports. The amount of inclusions varied from one casting to another. Some of the castings were completely free of inclusions, while others contained some.

Dimensional measurements were to determine the actual wall thickness at all locations. There was little need to check the sphericity, as the sphericity of a casting always closely conforms to the sphericity of the mold. Since the mold surfaces were machined within  $\pm 0.060$  inch (0.15 centimeter) of the specified radius, the sphericity of resulting castings was more than adequate to meet ANSI/ASME PVHO-1 specifications\*\* for man-rated spherical pressure hulls of acrylic plastic ( $\pm 0.5$  percent of external radius).

The wall thickness of the casting was checked, since during assembly of the molds the male mold might not have been properly aligned with respect to the female mold. If the alignment between the molds was not correct, the wall thickness varied from point to point on the hemisphere although the sphericity of the surfaces was within specification.

The wall thickness of the hemispheres varied from one location to another, the largest deviation in thickness being found at the pole. Since the variation in the thickness was less than the specified 5 percent, it was considered to be within the range of existing tolerances imposed by machining tolerances of the mold and thus acceptable.

Physical properties of the castings were determined by testing material specimens cut from the poles of hemispheres, the future location of metallic hatches. Two specimens were used per test for each hemisphere. The results of the tests were satisfactory, as the physical properties of the material in all cases met or surpassed the ANSI/ASME PVHO-1 specifications for acrylic plastic in man-rated, pressure-resistance structures.

#### A.2.4 Fabrication of Spherical Hull

Fabrication of the spherical submersible hull consisted of machining and bonding hemispherical castings, followed by polishing and inspecting the completed sphere. At the conclusion of these operations, the finished hull was mated with aluminum inserts that served as hatches and penetration plates.

Machining the hemispheres was preceded by rough grinding of the equatorial surface with a rotary file. After the equatorial surface was ground down to within 1 inch (2.5 centimeters) of the final dimensions, the hemisphere was mounted in a vertical mill and the polar penetration machined to its final dimension. After the polar opening was completed, the hemisphere was turned over in the mill and the equatorial surface was machined to its final dimension. Machining the equatorial surface to its final dimension completed the machining operations of the hemispheres.

---

\*Clear print of size 7 inches per column inch and 16 letters to the linear inch will be clearly visible when viewed from a distance of 20 inches (51 centimeters) through the thickness of the casting with opposite faces polished.

\*\*For 66-inch-OD (168 centimeters) spherical hulls the maximum permitted deviation in sphericity is  $+0.165$  inch (0.419 centimeter).

Bonding the hemispheres into a single structural entity was achieved by placing one hemisphere on top of the other. The width of the joint was controlled by placing small acrylic plastic spacers of 0.25 inch (0.6 centimeter) thickness between the equatorial surfaces of the hemispheres. The joint space between carefully aligned hemispheres was subsequently taped over with adhesive-backed aluminum foil tape. To facilitate pouring the adhesive into the joint cavity, three pouring spouts were plumbed to openings in the tape covering provided for this purpose.

The adhesive was prepared by mixing the same ingredients that made up the basic casting mix. The mix was poured concurrently into the three pouring spouts around the circumference of the sphere. At the same time, the mix was also poured in the test block joint. This block later served as a source of test specimens for determination of joint strength. As soon as the mix gelled in the joints, the sphere assembly with the associated test blocks was placed into the autoclave, where it was subjected to temperature and pressure until polymerization of the mix serving as adhesive was completed.

Polishing of the completed sphere consisted of rough sanding the edges of the joint followed by fine sanding and polishing of both the internal and external surfaces of the assembled sphere.

#### A.2.5 Inspection of Assembled Sphere

Inspection of the finished sphere consisted of detailed visual observation, dimensional measurements, and testing of bond samples. The objective of the visual observation was to ascertain the effects of the joint and repaired voids in the castings on the optical properties of the hull. The dimensional measurements were performed to determine conformance of the as-built sphere dimensions to the specified dimensional tolerances. The testing of bond samples served as quality control for the bonding technique used for joining the hemispheres.

The visual inspection showed that the optical properties of the sphere are usually more than adequate for underwater search, salvage, or work missions where panoramic visibility is of paramount importance. The only area on the sphere that showed optical distortion was the equatorial joint. The distortion was not severe enough to lower significantly the value of the acrylic sphere as a panoramic observation capsule. It was, however, sufficiently severe to preclude the use of cameras at the equator for photographing objects outside the acrylic capsule.

Dimensional measurements of the capsule showed that the diameter and angle of the top and bottom polar openings, as well as the outside diameter of the capsule, were within specified dimensional tolerances.

Installation of polar inserts consisted of placing the top hatch and bottom penetration plate and associated polycarbonate gaskets into the respective polar penetrations and locking them in place by bolting the split retaining rings.

#### **A.2.6 Findings**

1. It is technically feasible to fabricate spherical pressure hulls of any size by bonding together acrylic plastic hemispheres that are precision cast in metallic mold assemblies composed of male and female molds.
2. Precision-cast hemispheres do not require subsequent machining on spherical surfaces to satisfy ASME specified tolerances for sphericity and thickness.
3. The physical properties of the massive acrylic plastic castings produced by Polymer Products satisfy ANSI/ASME PVHO-1 specifications for acrylic plastic used in man-rated, external- or internal-pressure vessels.
4. Bonding joints with the same resin mix used to cast the hemispheres produces joints with tensile strength in excess of 9000 pounds per square inch (62 megapascals).
5. Large hollow inclusions in massive acrylic plastic hemispheres can be successfully recast by filling them with standard casting resin mix and subjecting the whole hemisphere for a second time to the polymerization process.
6. The repaired hemisphere is structurally as strong under external hydrostatic loading as is a hemisphere without recast hollow inclusions.
7. The repaired hollow inclusions are optically objectionable if located in the crew's main field-of-vision.

#### **A.2.7 Conclusion**

The NEMO Mod 2000 B assembly fabricated by bonding two precision-cast acrylic hemispheres met all the certification criteria for manned service. The maximum safe operational depth of 2500 feet (762 meters) is based on ANSI/ASME PVHO-1 Safety Standard For Pressure Vessels For Human Occupancy and the requirements of American Bureau of Shipping and of Det Norske Veritas.

#### **A.2.8 Bibliography**

1. Stachiw, J.D., and Lones, J.J., "Development of Economical Casting Process for NEMO-Type Acrylic Submersible Hulls," ASME Paper No. 76-WA/OcE-7, 1976.

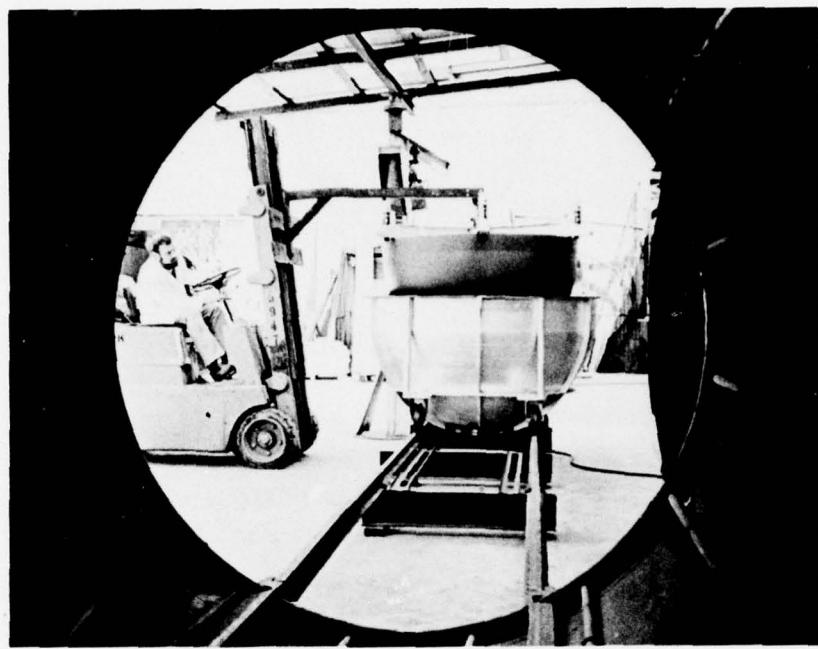


Figure A.27. Male and female molds for casting hemispheres. Note the tracks for moving the mold assembly into the autoclave without disturbing the casting slurry in the mold assembly.

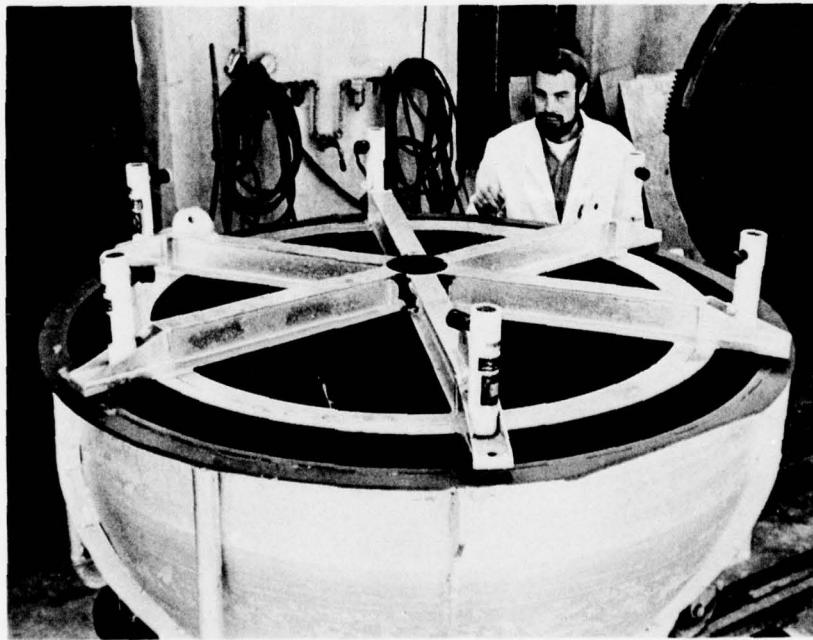
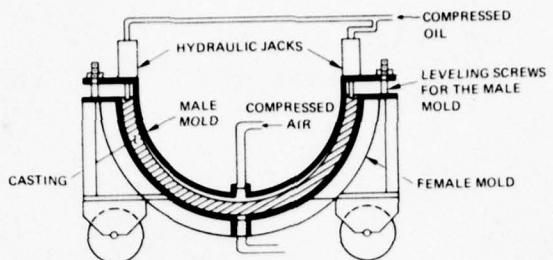
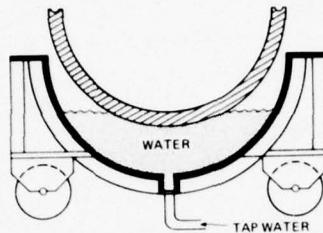


Figure A.28. Mold assembly. Note hydraulic jacks for lifting the male mold out of the casting.



STEP A. REMOVING THE MALE MOLD FROM INSIDE THE CASTING  
WITH THE AID OF (1) HYDRAULIC JACKS PRESSING AGAINST  
THE EDGE OF CASTING AND (2) COMPRESSED AIR LIFTING  
THE MOLD FROM BELOW



STEP B. REMOVING THE CASTING FROM INSIDE THE FEMALE  
MOLD BY INJECTING WATER INTO THE ANNULAR SPACE  
BETWEEN THE CASTING AND THE MOLD

Figure A.29. Procedures for removing the male mold  
and then casting from the female mold.

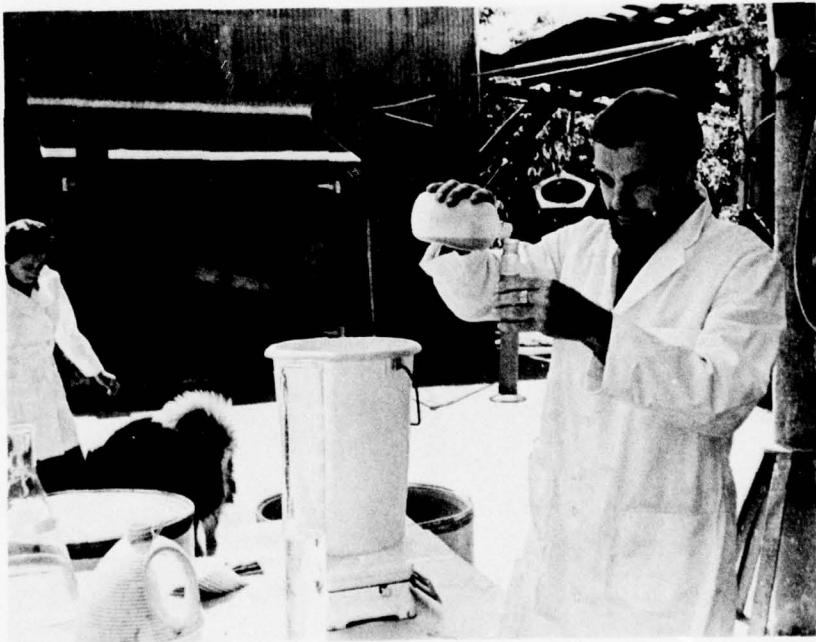


Figure A.30. Mixing ingredients for the casting slurry.



Figure A.31. Degassing a batch of casting slurry under vacuum prior to pouring it into the mold.



Figure A.32. Pouring degassed casting slurry into the annular space between the male and female molds.

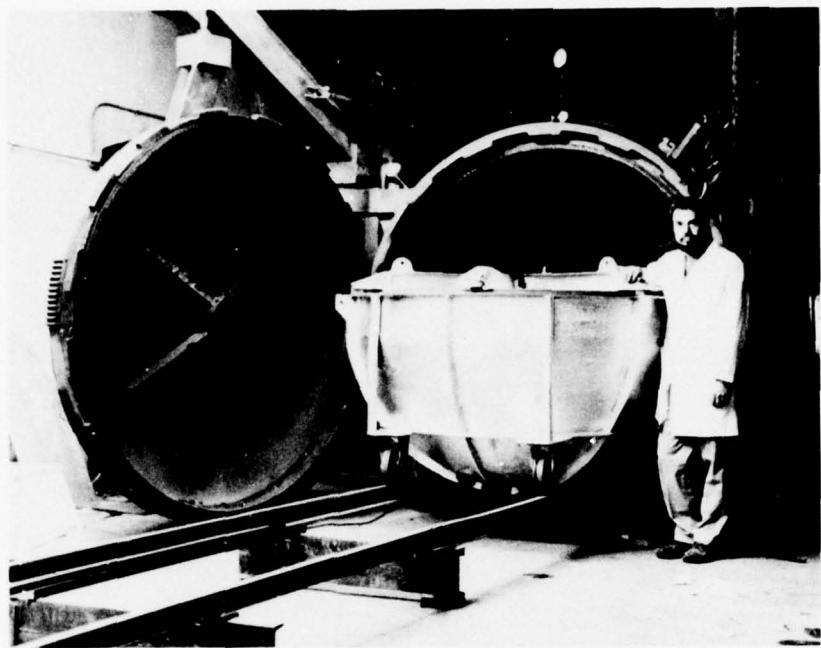


Figure A.33. Placing the slurry-filled mold assembly into an autoclave where the acrylic slurry will be subjected to heat and pressure.

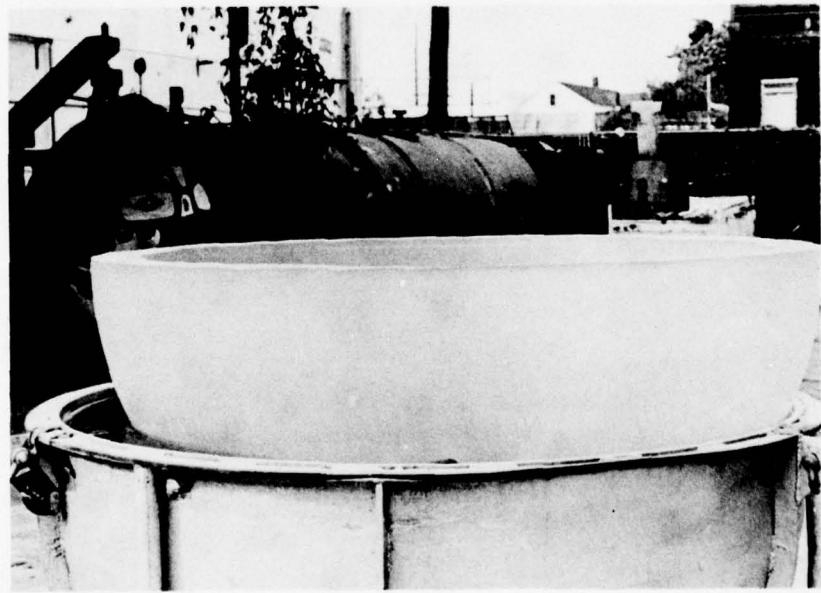


Figure A.34. Mold assembly after the male mold has been removed and the casting has floated up with water.

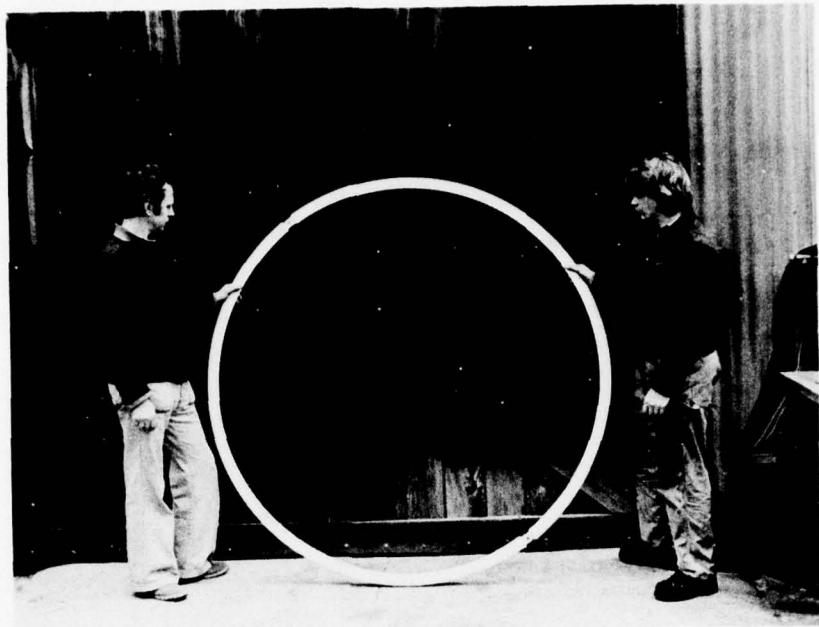


Figure A.35. Lifting ring for the casting.

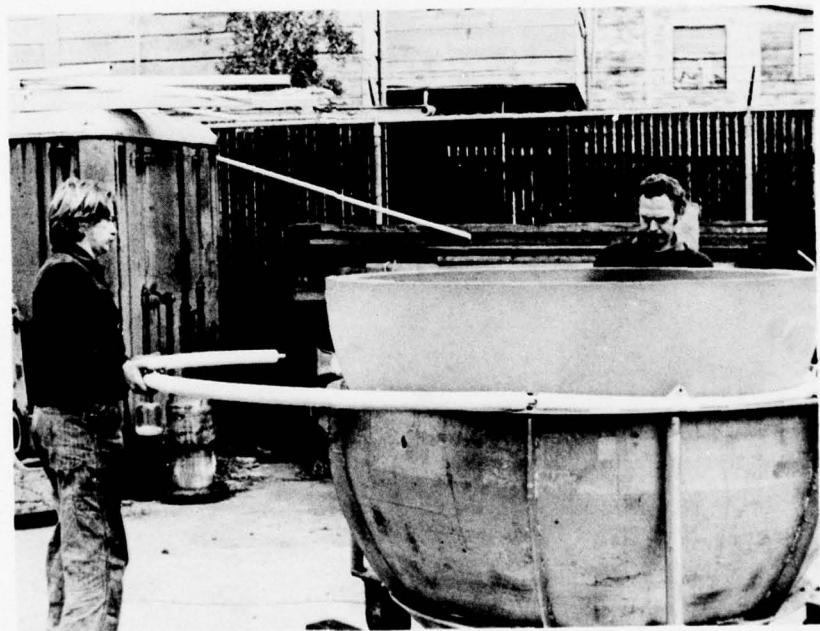


Figure A.36. Placing the locking ring around the casting.

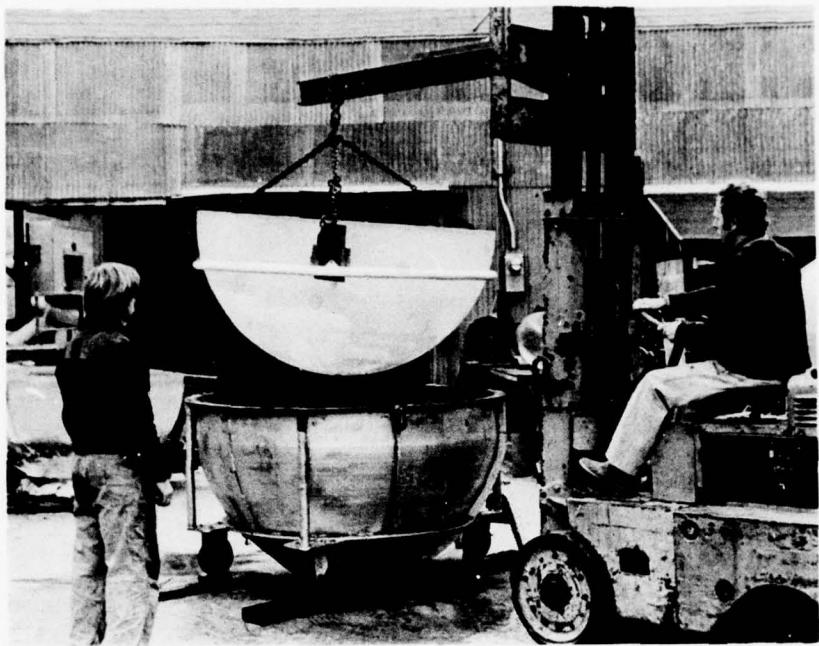


Figure A.37. Lifting the casting out of the female mold.

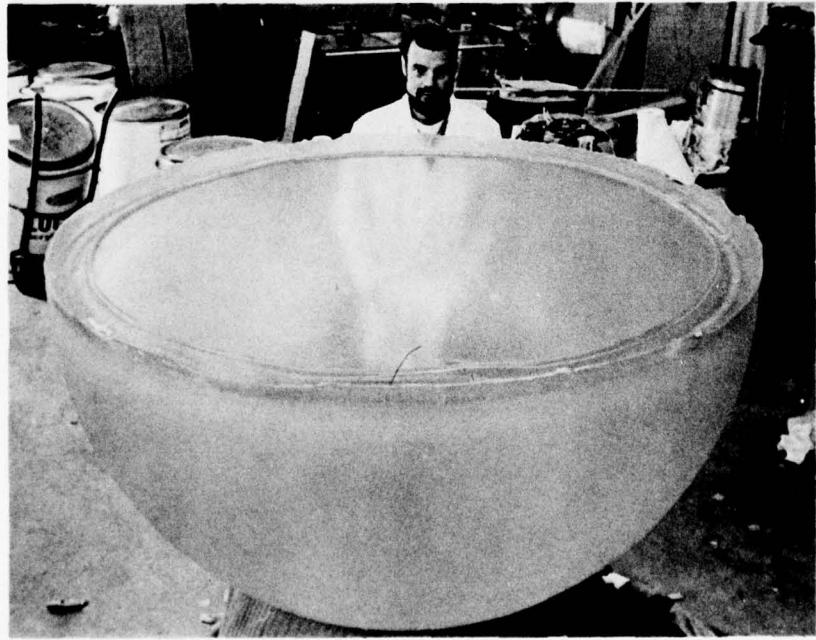


Figure A.38. Casting after removal from the mold.

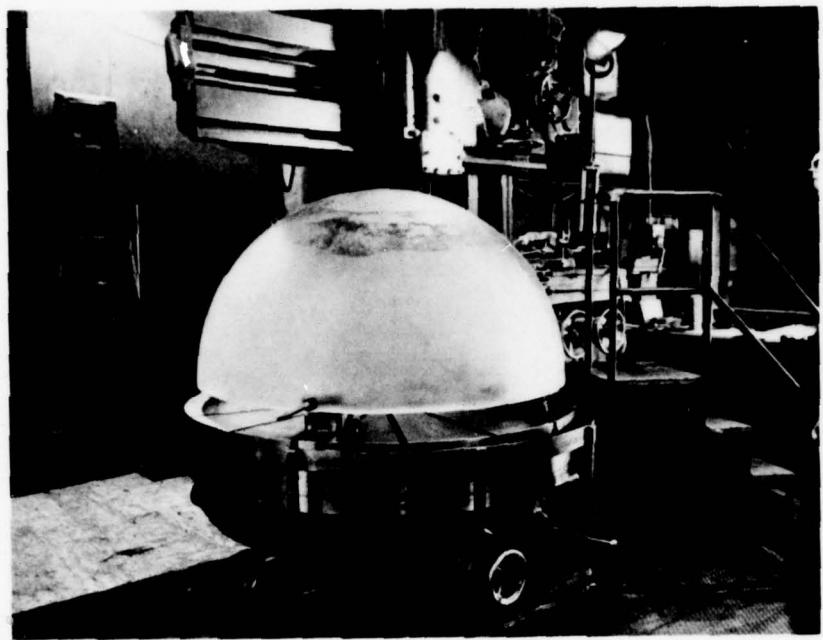


Figure A.39. Vertical mill used in machining the equatorial joint surface and polar penetration.

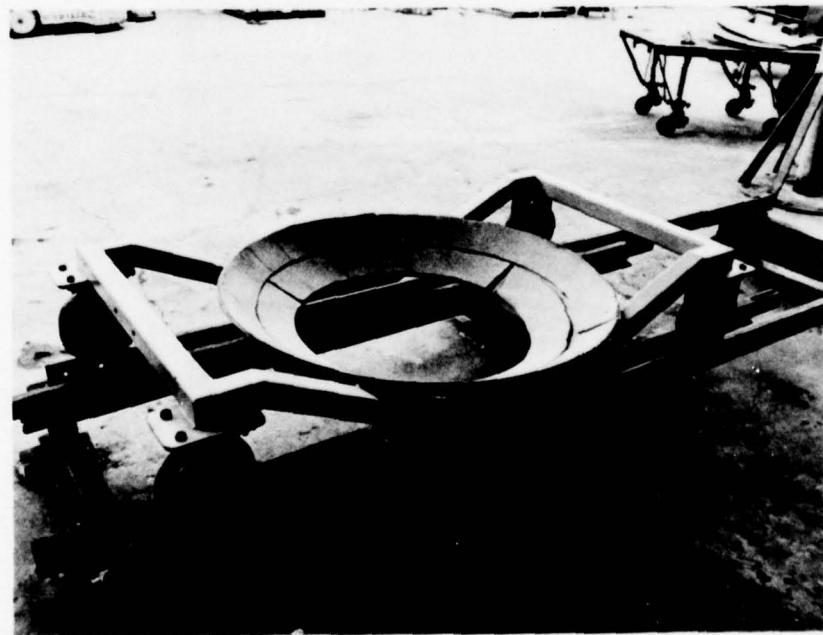


Figure A.40. Padded cart for transportation of acrylic hemispheres and spheres into the interior of the autoclave.

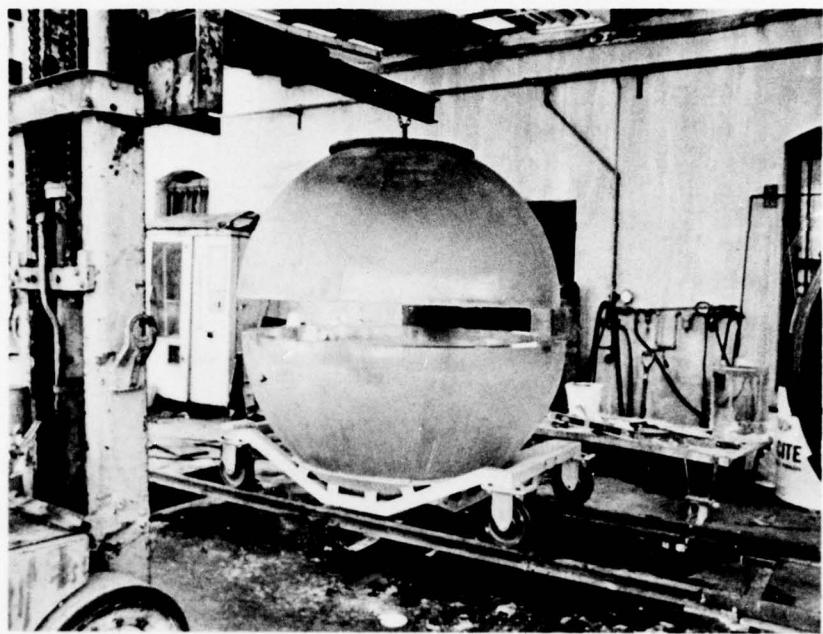


Figure A.41. Assembling the sphere from two hemispheres with machined openings and equatorial joint surfaces. Acrylic spacers are used to maintain a 0.25-inch (0.6 centimeter) clearance between hemispheres.

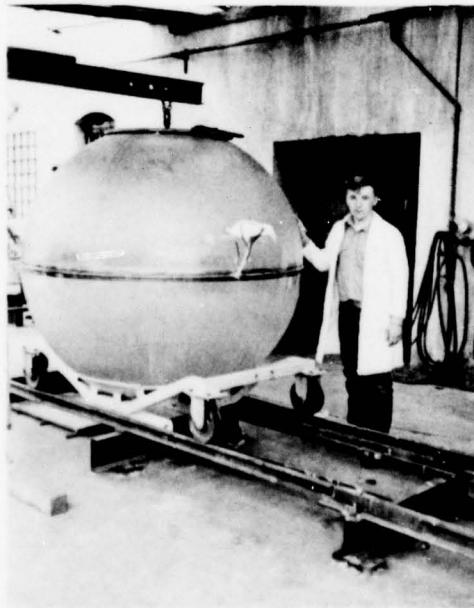


Figure A.42. Adhesive-coated aluminum tape used to seal the joint prior to filling it with a casting slurry through two funnels located at opposite sides of the sphere.



Figure A.43. The joint in a bond test specimen is filled with the same casting slurry as the equatorial joint in the sphere.

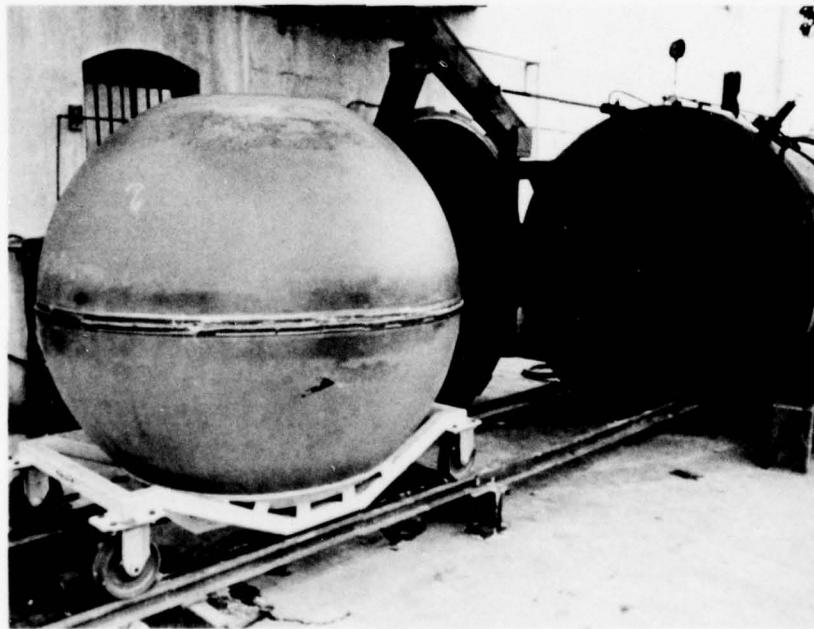


Figure A.44. Test specimen is placed together with the sphere into the autoclave and subjected to the same temperature and pressure that was previously used for polymerization of the hemispheres.

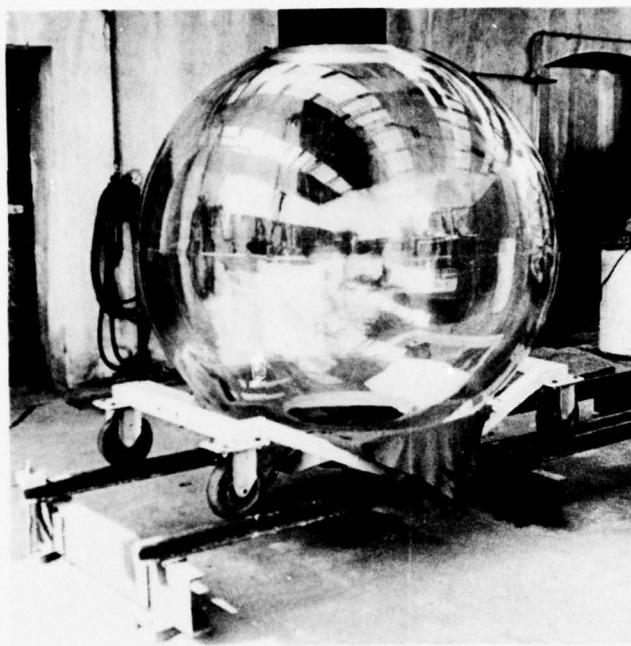


Figure A.45. Bonded sphere after sanding, polishing, and annealing.



Figure A.46. Measuring the thickness of the casting at the penetration.

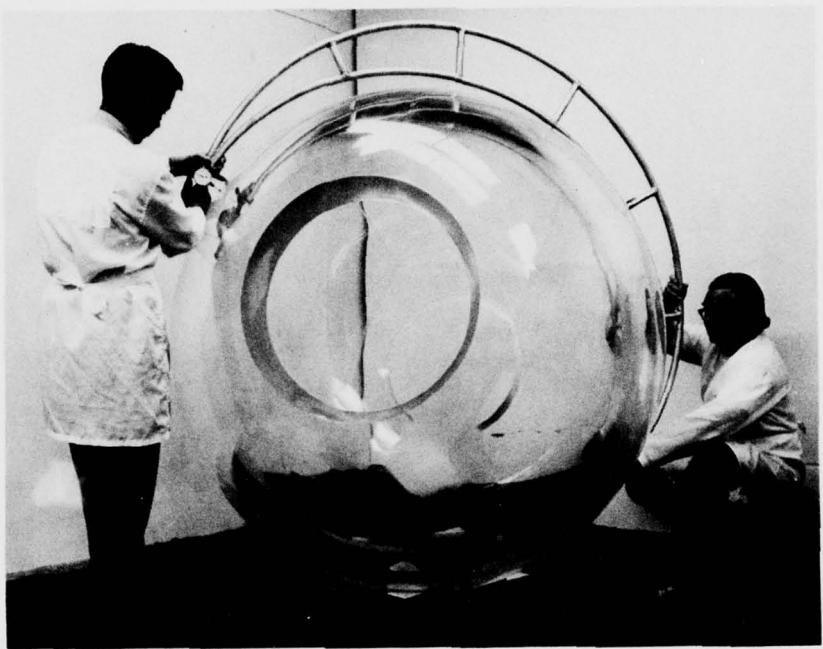


Figure A.47. Measuring the external diameter of the sphere.



Figure A.48. Completed sphere prior to installation of penetration closures.  
Note that the equatorial joint is almost invisible.



Figure A.49. Aluminum penetration closure serving as a bulkhead for feedthroughs.



Figure A.50. Polycarbonate gasket for metallic penetration closures.

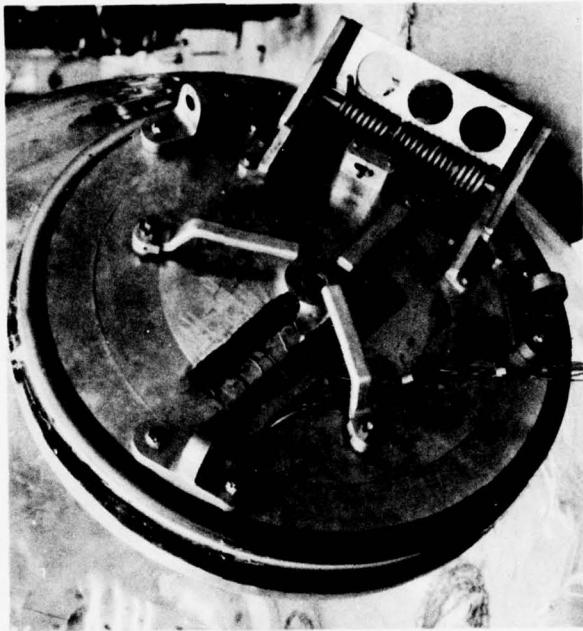


Figure A.51. Aluminum penetration closure, serving as personnel hatch, after installation.

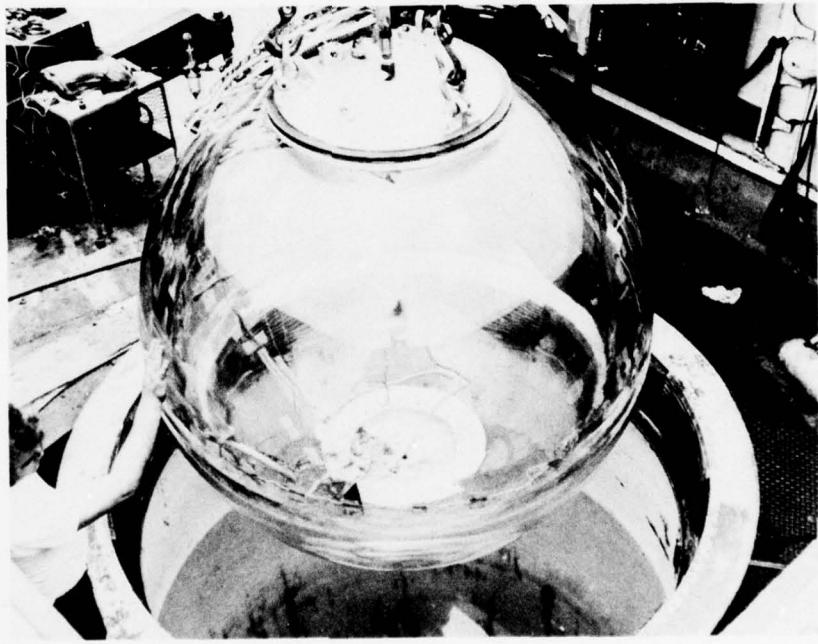


Figure A.52. Instrumented sphere with 33.4 inch (85 centimeters) outside radius and 4.35 inch (11 centimeters) thickness being placed in a deep ocean pressure simulator for hydrostatic testing to 1.33 X design depth, i.e.,  $1.33 \times 3000$  feet (914 meters) = 4000 feet (1218 meters).



APPENDIX B. CRITICAL PRESSURES AND DISPLACEMENTS OF  
CONICAL FRUSTUMS . . . B-1

B.1 SHORT-TERM PRESSURE LOADING . . . B-1

- B.1.1 Critical Pressures (Varying Included Angle) . . . B-3
- B.1.2 Axial Displacements (Varying Included Angle) . . . B-11
- B.1.3 Critical Pressures (Varying Temperatures) . . . B-19
- B.1.4 Axial Displacements (Varying Temperatures) . . . B-30

B.2 LONG-TERM PRESSURE LOADING . . . B-52

- B.2.1 Axial Displacements (5000 Pounds Per Square Inch) . . . B-54
- B.2.2 Axial Displacements (10,000 Pounds Per Square Inch) . . . B-63
- B.2.3 Axial Displacements (20,000 Pounds Per Square Inch) . . . B-73
- B.2.4 Permanent Deformations . . . B-91

## APPENDIX B. CRITICAL PRESSURES AND DISPLACEMENTS OF CONICAL FRUSTUMS

### B.1 SHORT-TERM PRESSURE LOADING

Short-term pressure loading consisted of pressurizing the viewport assembly at a rate of 650 pounds per square inch (4.48 megapascals) per minute until catastrophic failure of the window occurred. During the pressurization, axial displacement was measured at the center of the window's low-pressure face. This axial displacement represents the sum of the window's deflection and sliding inside the conical mounting.

Data generated by windows under short-term loading operationally represent the behavior of windows during a dive by a submersible or during the pressurization process of a hyperbaric chamber. As soon as the submersible ceases to sink or the hyperbaric chamber ceases to be pressurized by its operator, the behavior of the window starts to deviate from short-term data. Its axial displacement increases even though the pressure loading remains constant and the potential critical pressure value decreases, both as functions of time and magnitude of sustained pressure loading.

As a result of their operational limitations, short-term data should be utilized only with a complete understanding of their limitations. For this reason, short-term data are generally used only for four purposes:

- a. Evaluation of new window materials, mounting designs, mounting seat finishes, and other design and material variables.
- b. Evaluation of damage to a window in the form of crazing, scratches, cracks, weathering, nuclear radiation, etc.
- c. Determination of the displacements of windows during temporary overpressurization.
- d. Determination of the critical pressures of windows under temporary overpressurization.

The data generated by windows tested in mountings with  $D_i/D_f = 1.0$  (sections B.1.1 and B.1.2) are from the operational viewpoint conservative, since usually in operational viewports  $D_i/D_f > 1.0$  which is known to increase the short-term critical pressure and to decrease the short-term displacement of any window. For 90-degree (1.57 radians) conical frustums, the beneficial effects of an increased  $D_i/D_f$  ratio on the critical pressure and axial displacement under short-term loading have been experimentally established (sections B.1.3 and B.1.4).

Data generated by windows at ambient room temperature are directly applicable only to operational conditions at room temperature (65 to 75°F) (18 to 24°C). For operational temperatures below room temperature the room-temperature data become conservative; while for temperatures above room temperature, they are unacceptable unless properly discounted. The amounts that the critical pressures must be decreased and the axial displacements increased can be estimated from tests performed at 32, 50, 70, and 90°F (0, 10, 21, and 32°C) ambient temperature on conical frustums with a 90-degree (1.57 radians) included angle (sections B.1.3 and B.1.4) in mountings with  $D_i/D_f = 1.0$  and  $D_i/D_f = 1.5$ .

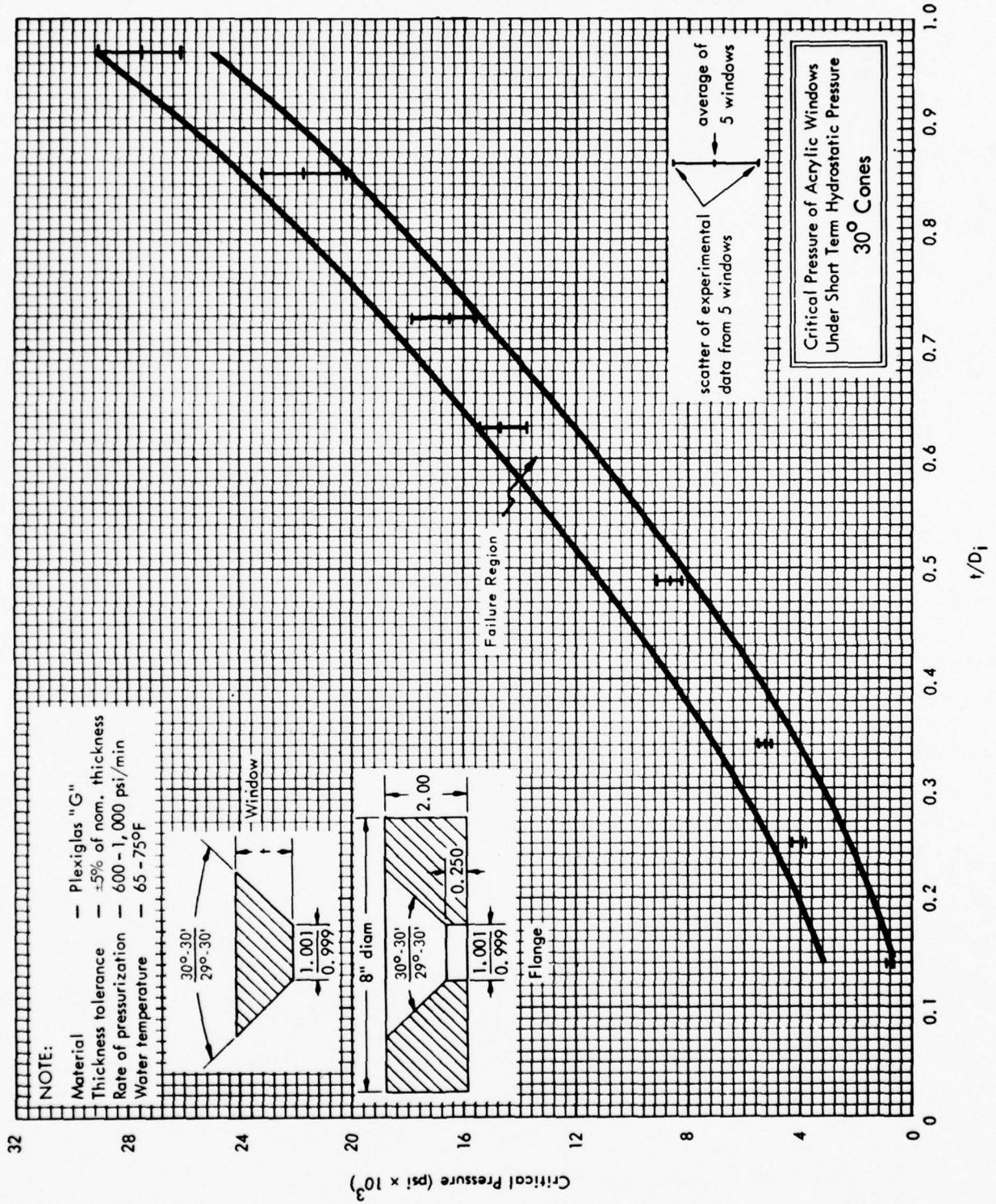
Most data have been generated with model-scale windows for reasons of economy. Since it has been proven, however, that there is no size effect for acrylic plastic (while it is known to exist for concrete, glass, and other brittle materials), data from model-scale windows can be used with confidence for predicting the performance of full-scale, acrylic plastic, conical frustums. The critical pressures can be directly used, as the critical pressure for model- and full-scale windows is the same, if both have the same included angle and  $t/D_i$  ratio and are tested in mountings with the same  $D_i/D_f$  ratio at identical ambient temperatures. Axial displacements of full-scale windows can be extrapolated from displacements of model-scale windows, if the displacements of the model-scale windows are multiplied by a ratio of full-scale to model-scale window diameters.

### B.1.1 Critical Pressures (Varying Included Angle)

The data in this section are concerned with the critical pressures of conical frustums with included angles of 30, 60, 90, 120, and 150 degrees (0.5, 1.04, 1.57, 2.09, and 2.6 radians) under short-term pressure loading at ambient room temperature in mountings with  $D_i/D_f = 1.0^*$ .

---

\*On many figures in this appendix  $D_i$  is noted either as D or d, thus  $t/D_i = t/D = t/d$ .



32

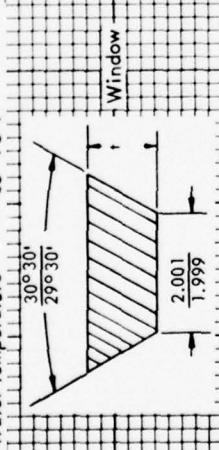
## NOTE:

Material      = Plexiglas "G"

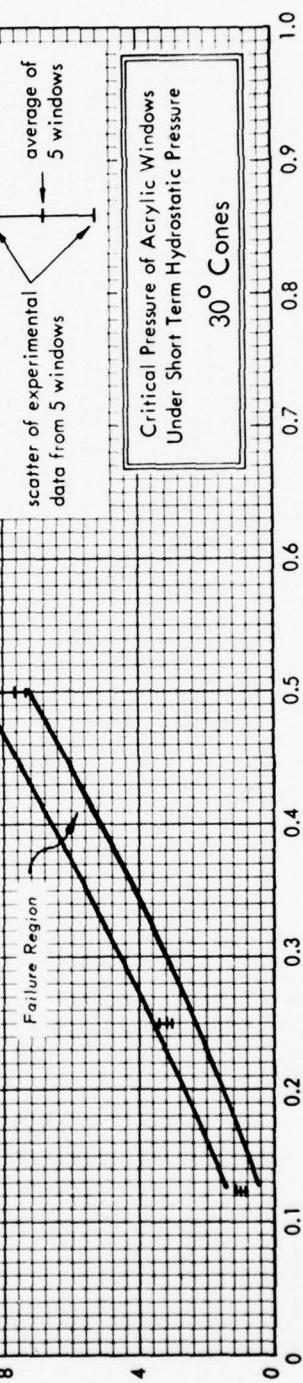
Thickness tolerance      =  $\pm 5\%$  nom. thickness

Rate of pressurization      = 500 - 1,000 psi/min

Water temperature      = 65 - 75°F

Critical Pressure (psi  $\times 10^3$ )28  
24  
20  
16  
12  
8  
4  
0

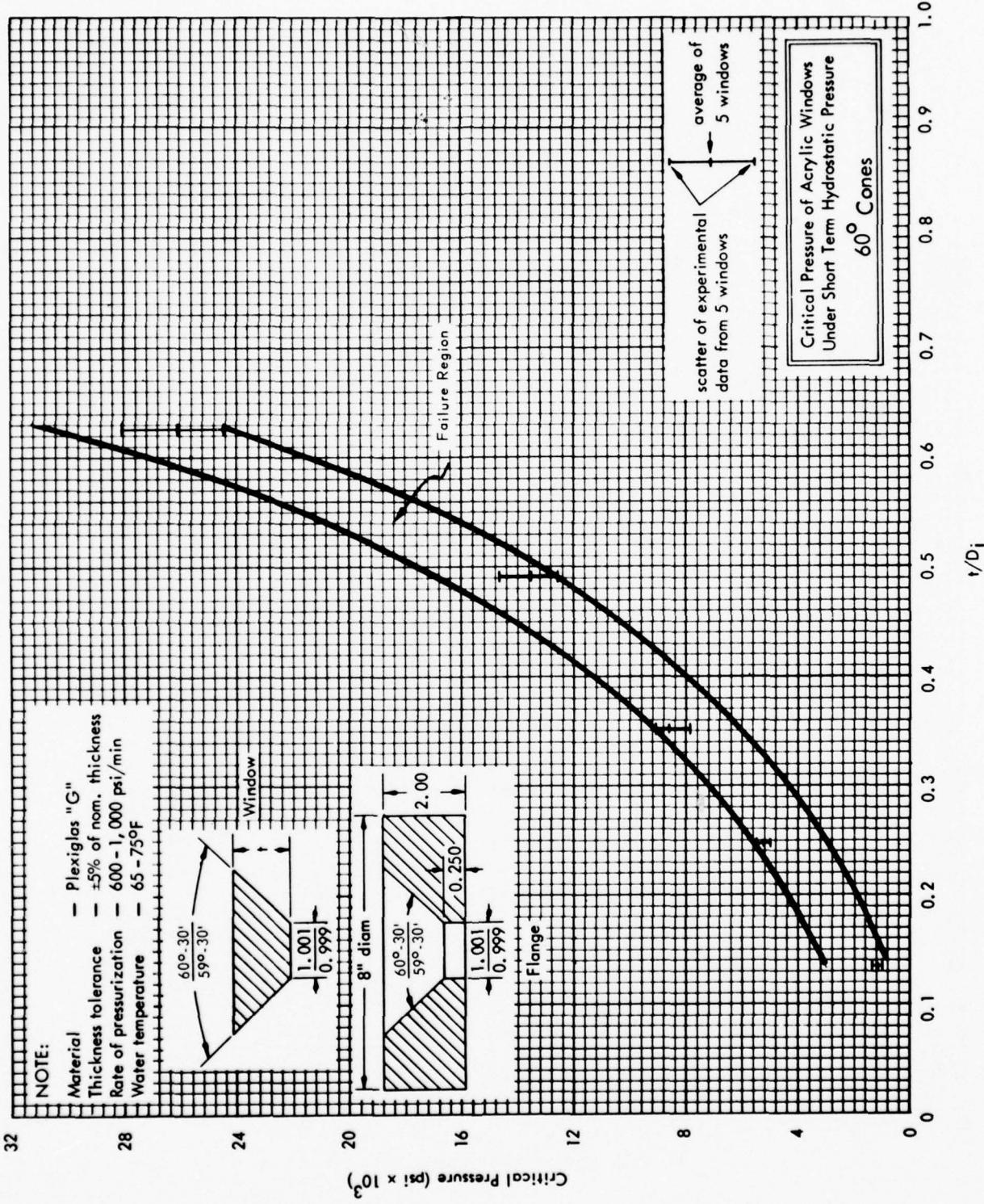
B-5

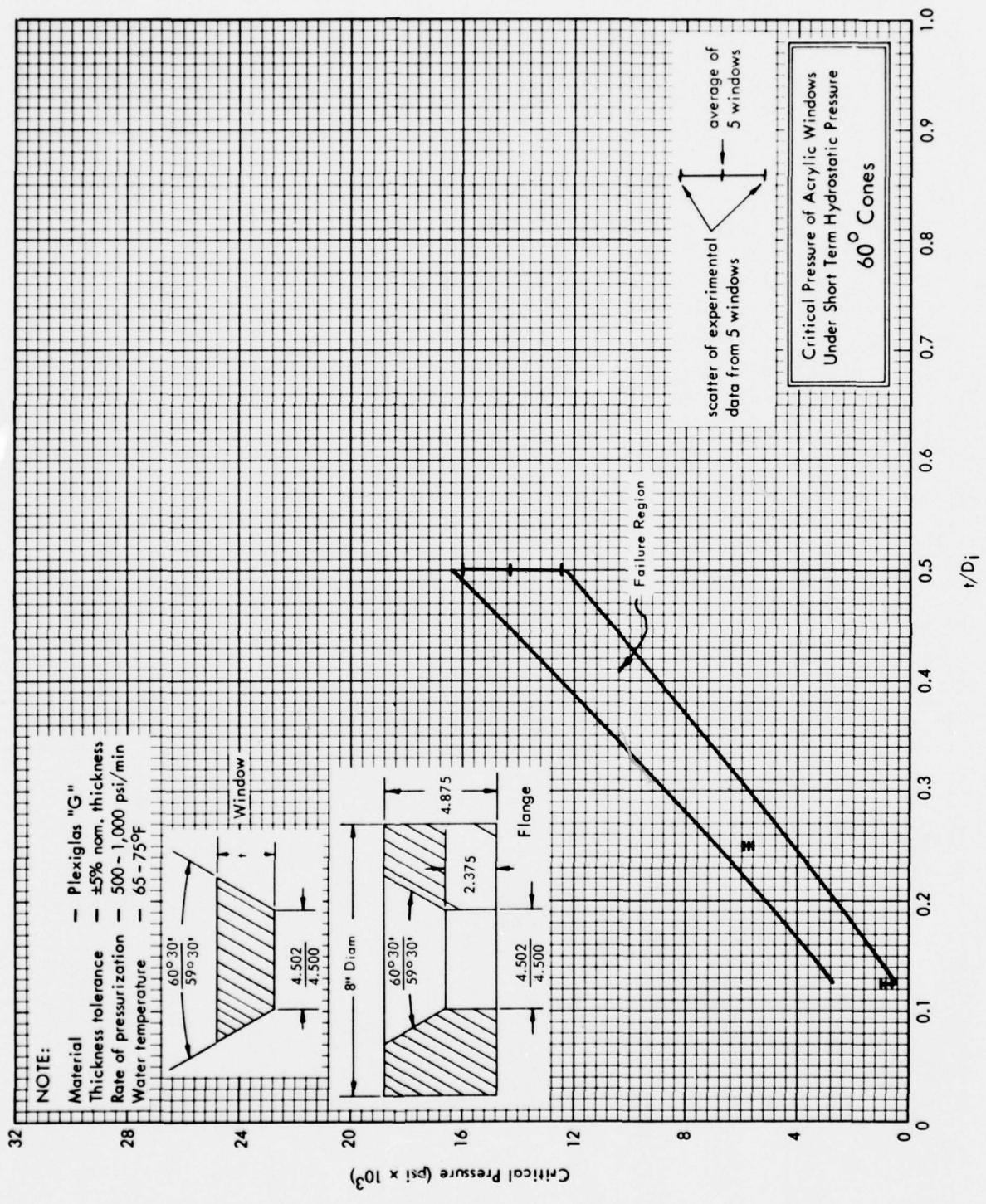


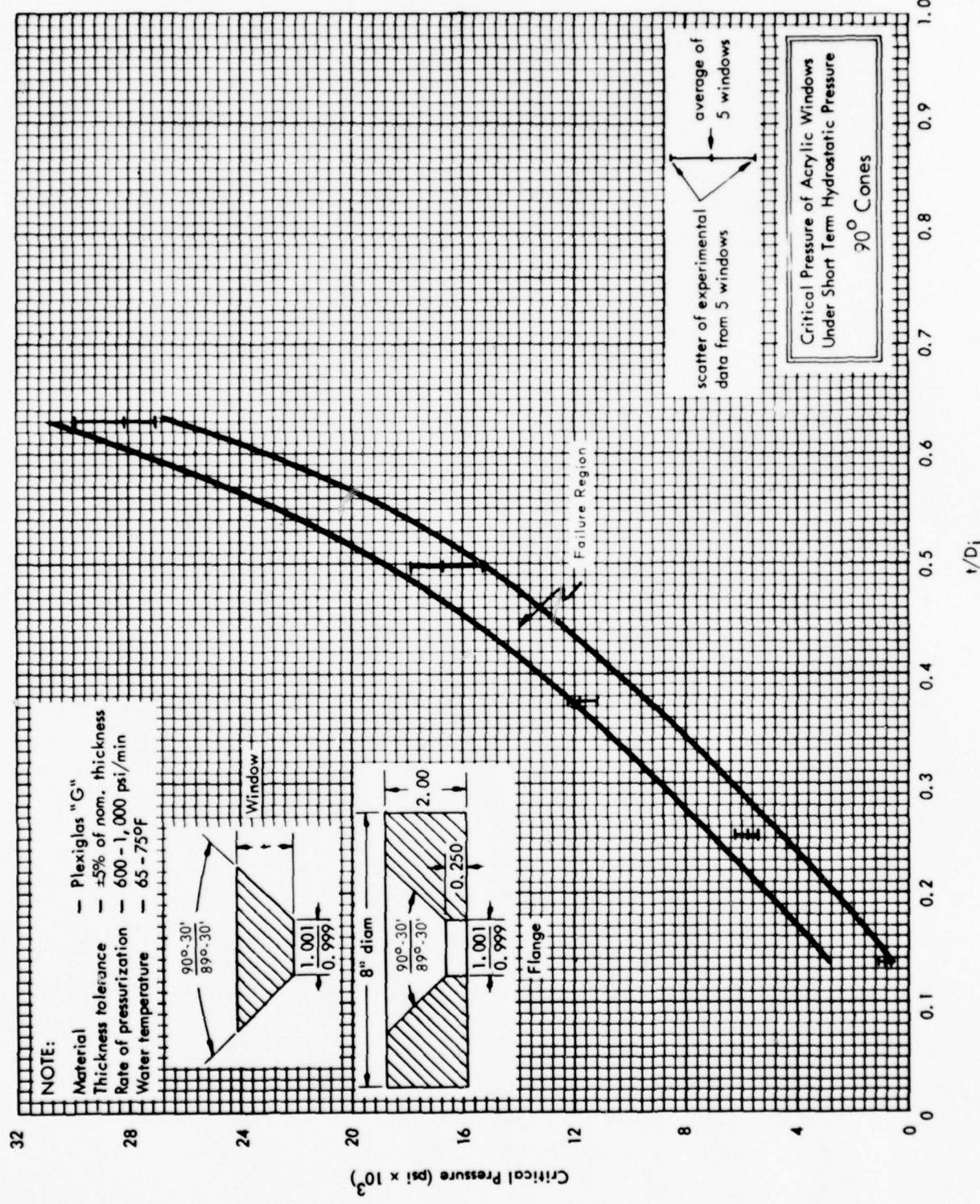
Critical Pressure of Acrylic Windows  
Under Short Term Hydrostatic Pressure  
30° Cones

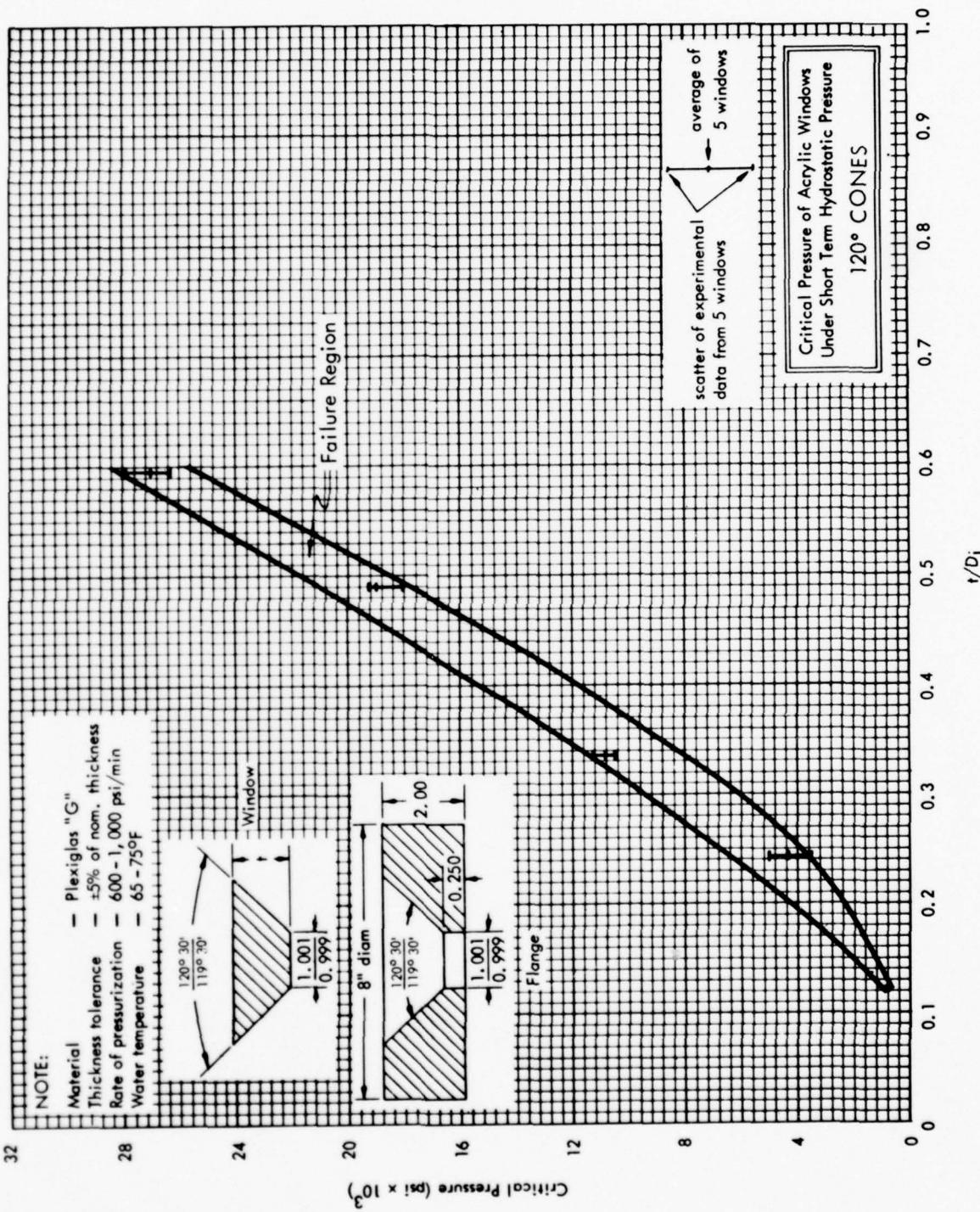
average of  
5 windows

scatter of experimental  
data from 5 windows



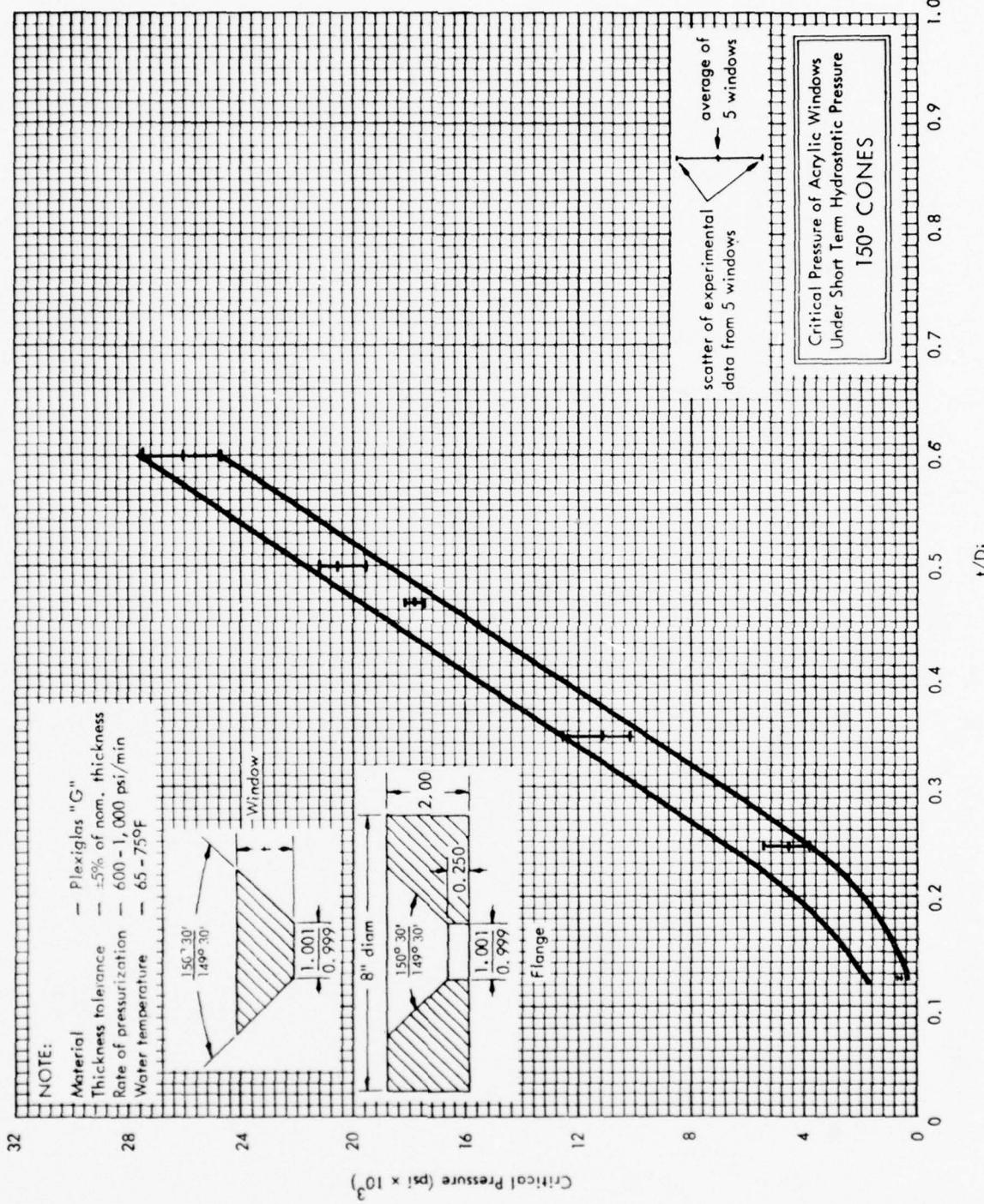






NOTE

Material	Plexiglas "G"
Thickness tolerance	±5% of nom. thickness
Rate of pressurization	600-1,000 psi/min
Water temperature	65-75°F



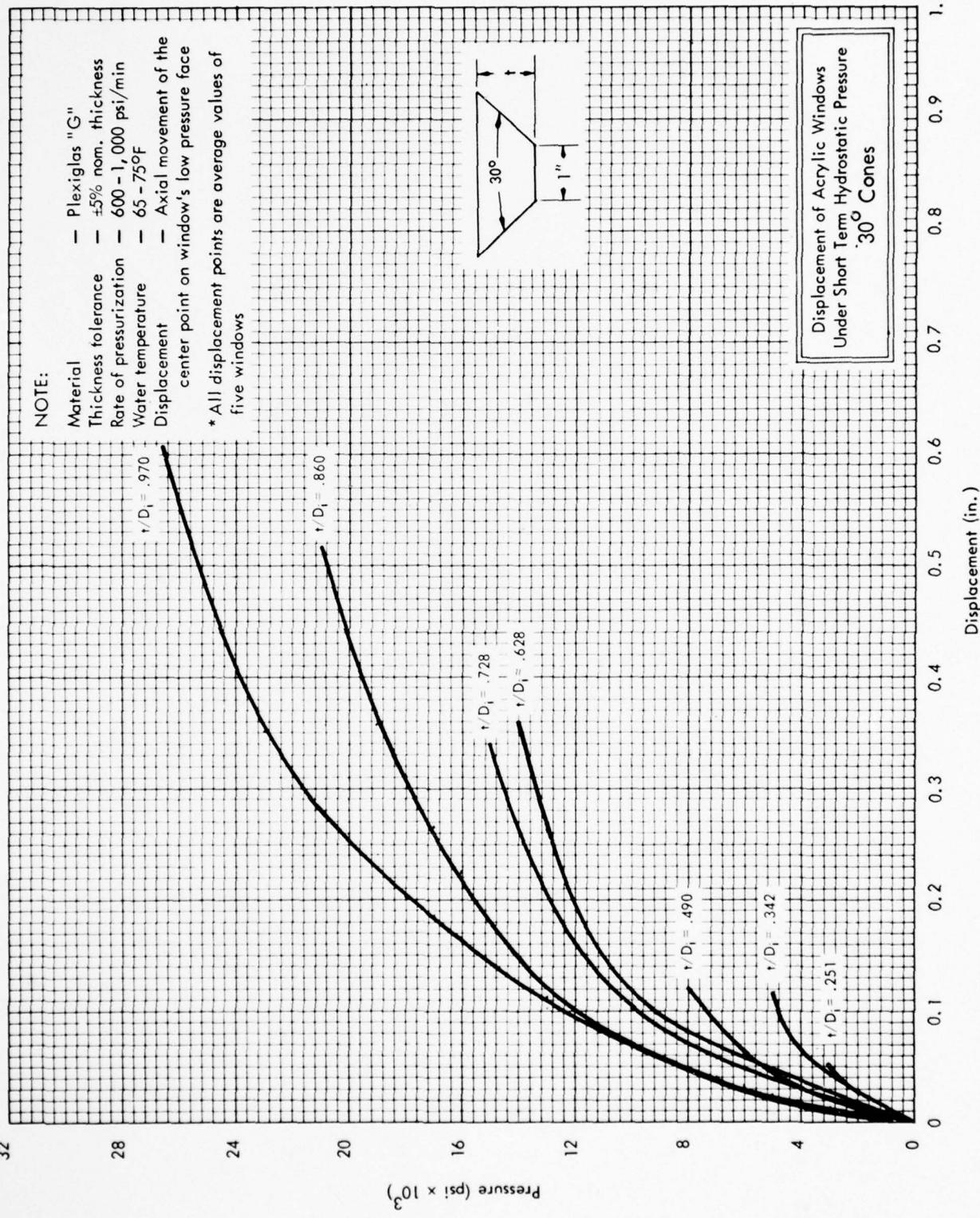
### B.1.2 Axial Displacements (Varying Included Angle)

The data in this section are concerned with the axial displacements of conical frustums with included angles of 30, 60, 90, 120, and 150 degrees (0.5, 1.04, 1.57, 2.09, and 2.6 radians) under short-term loading at ambient room temperature in mountings with  $D_i/D_f = 1.0$ .

## NOTE:

Material — Plexiglas "G"  
 Thickness tolerance —  $\pm 5\%$  nom. thickness  
 Rate of pressurization — 600 - 1,000 psi/min  
 Water temperature — 65 - 75°F  
 Displacement — Axial movement of the  
 center point on window's low pressure face

\* All displacement points are average values of five windows

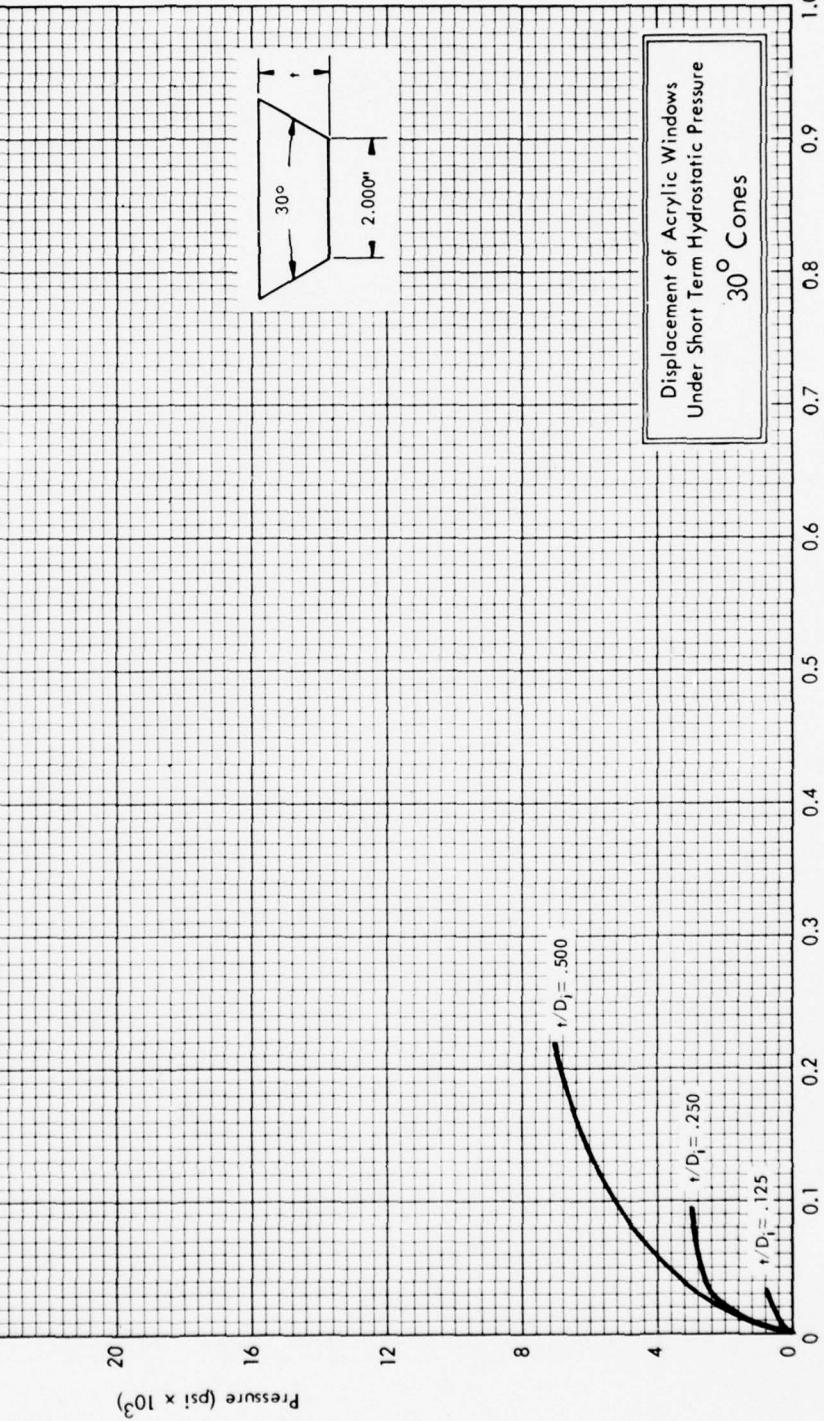


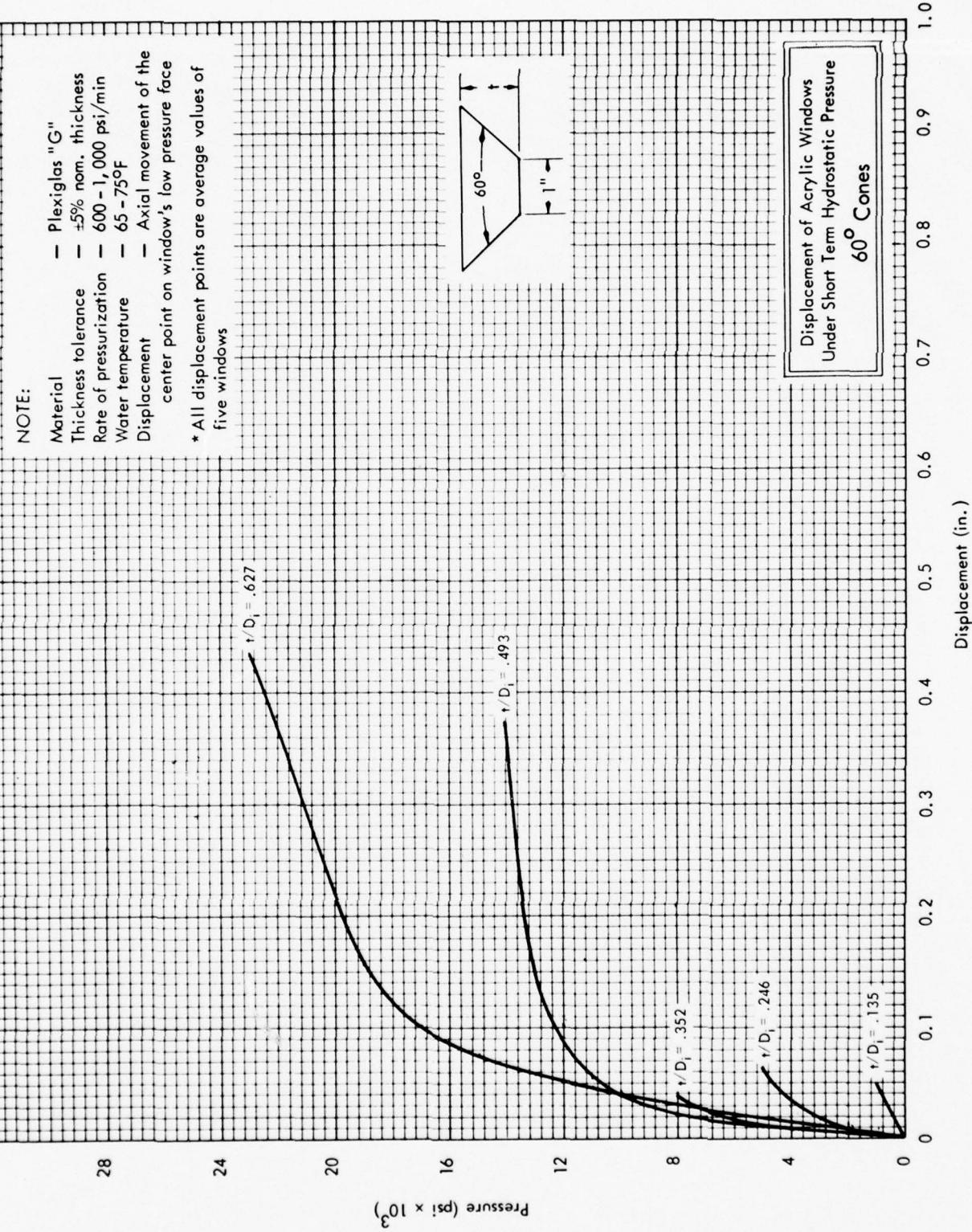
Pressure ( $\text{psi} \times 10^3$ )

## NOTE:

Material	Plexiglas "G"
Thickness tolerance	$\pm 5\%$ nom. thickness
Rate of pressurization	500 - 1,000 psi/min
Water temperature	65 - 75°F
Displacement	Axial movement of the center point on window's low pressure face

\*All displacement points are average values of five windows



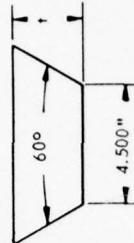


Pressure ( $\text{psi} \times 10^3$ )

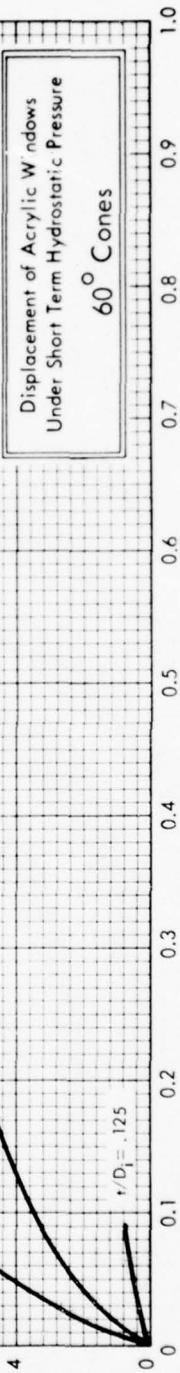
## NOTE:

Material	Plexiglas "G"
Thickness tolerance	$\pm 5\%$ nom. thickness
Rate of pressurization	500 - 1,000 psi/min
Water temperature	65 - 75°F
Displacement	Axial movement of the center point on window's low pressure face

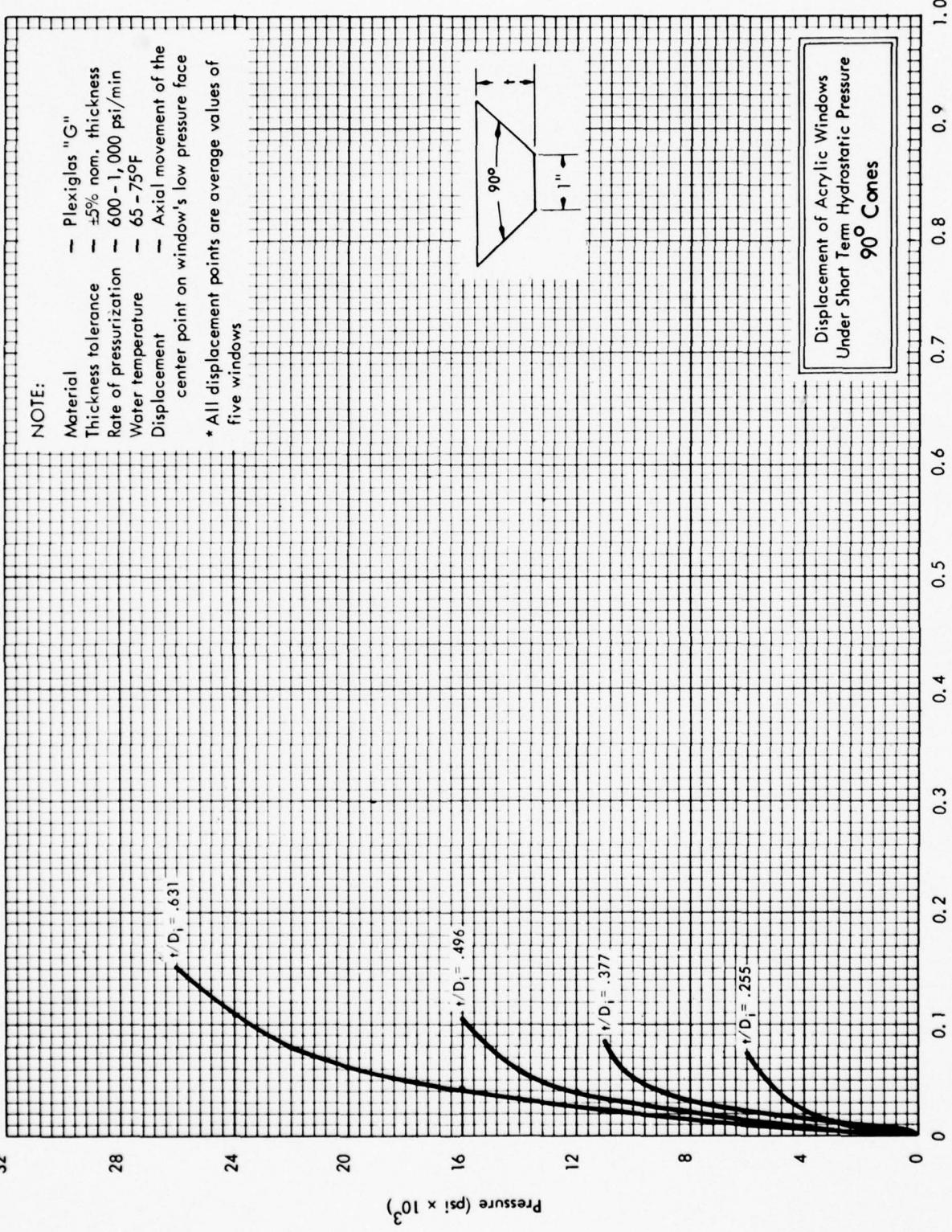
\*All displacement points are average values of five windows

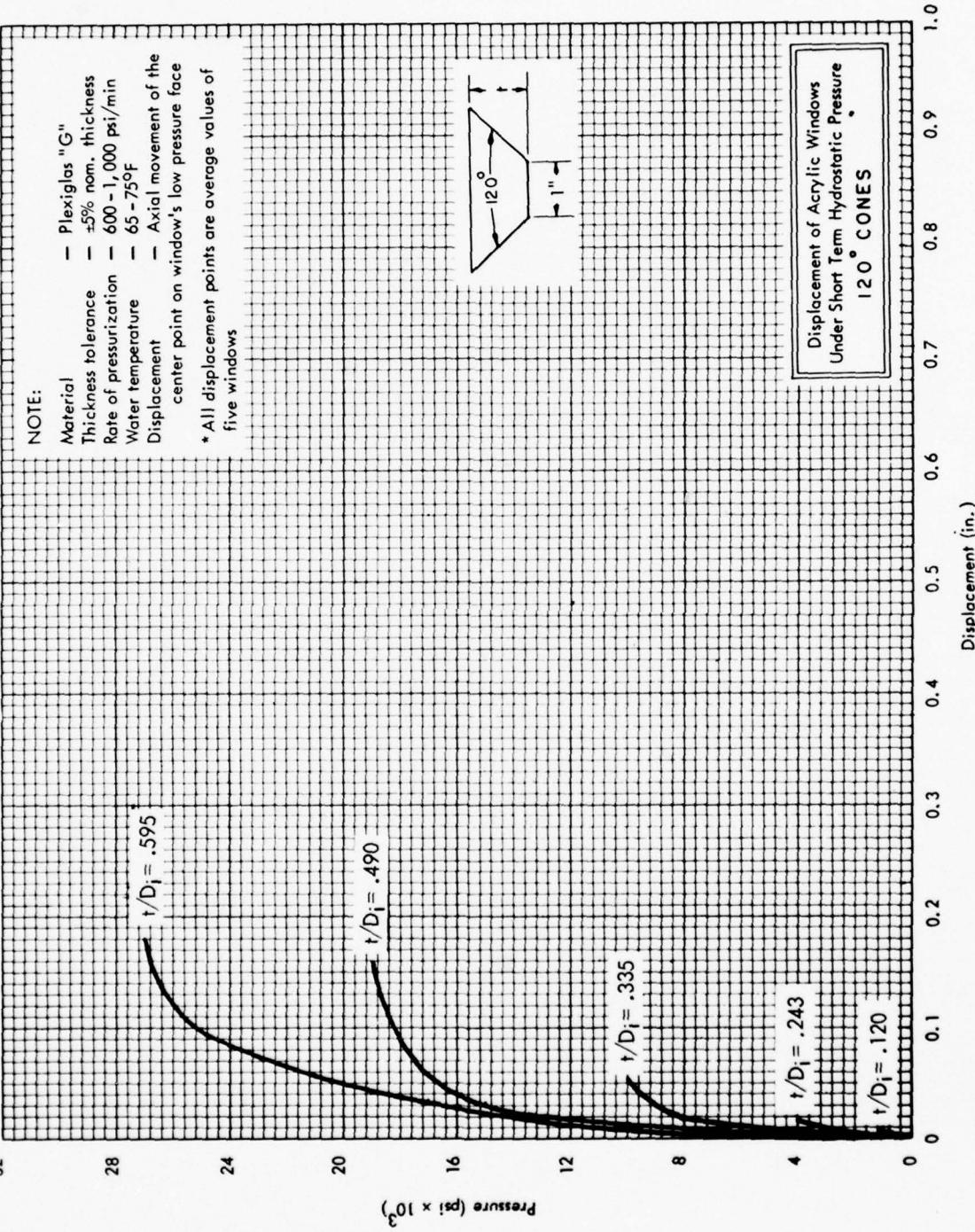
 $r/D_i = .500$ 

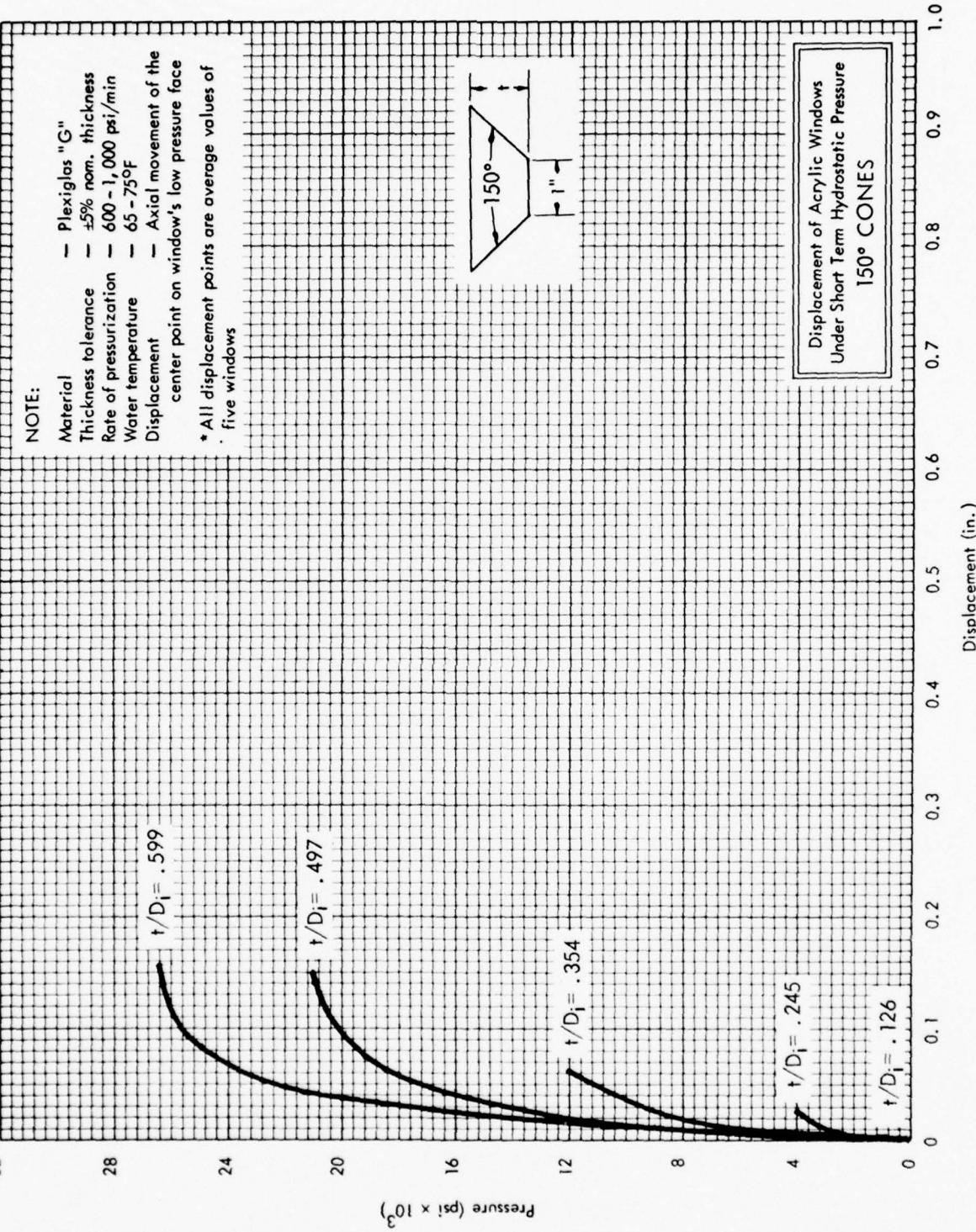
B-15



Displacement (in.)





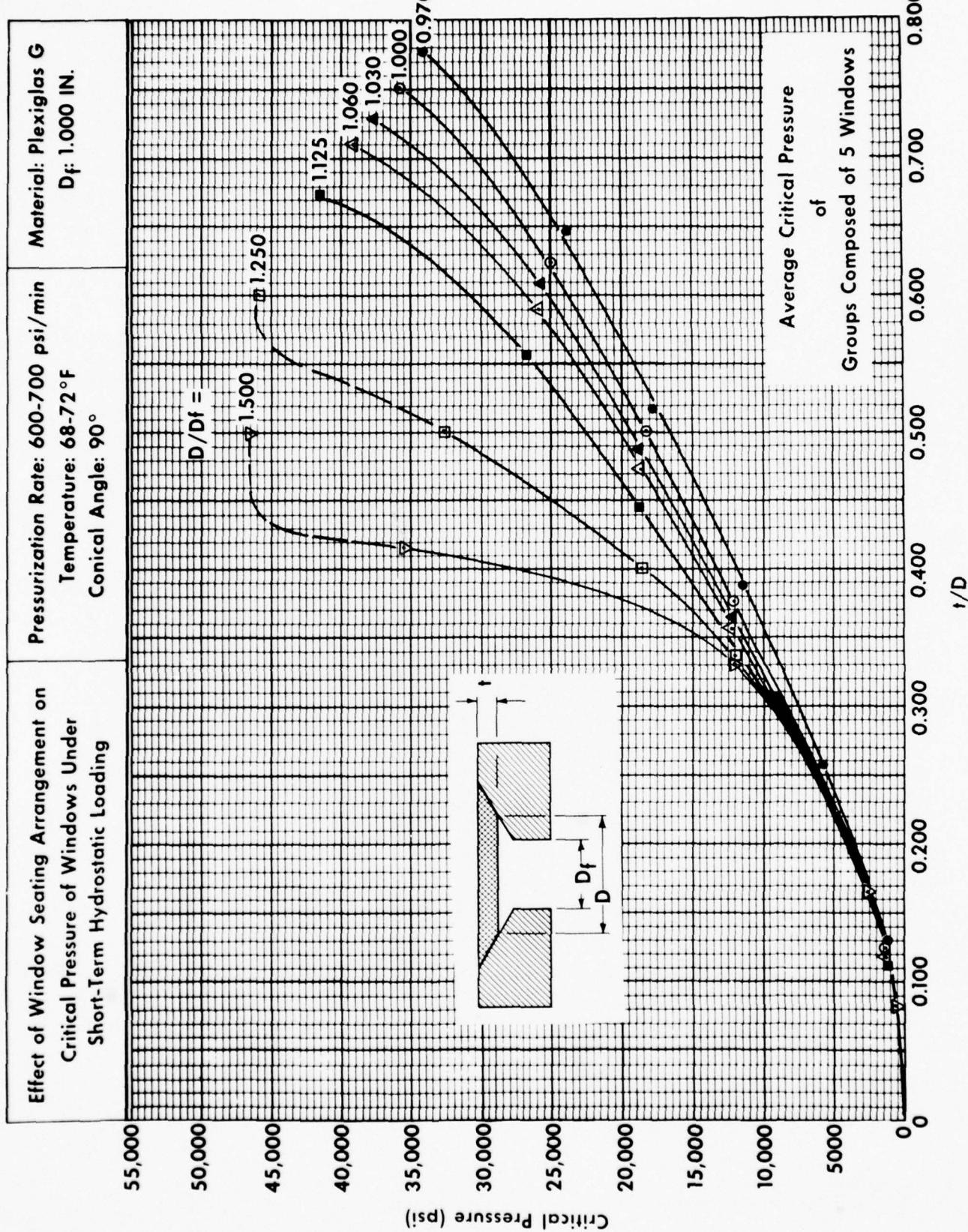


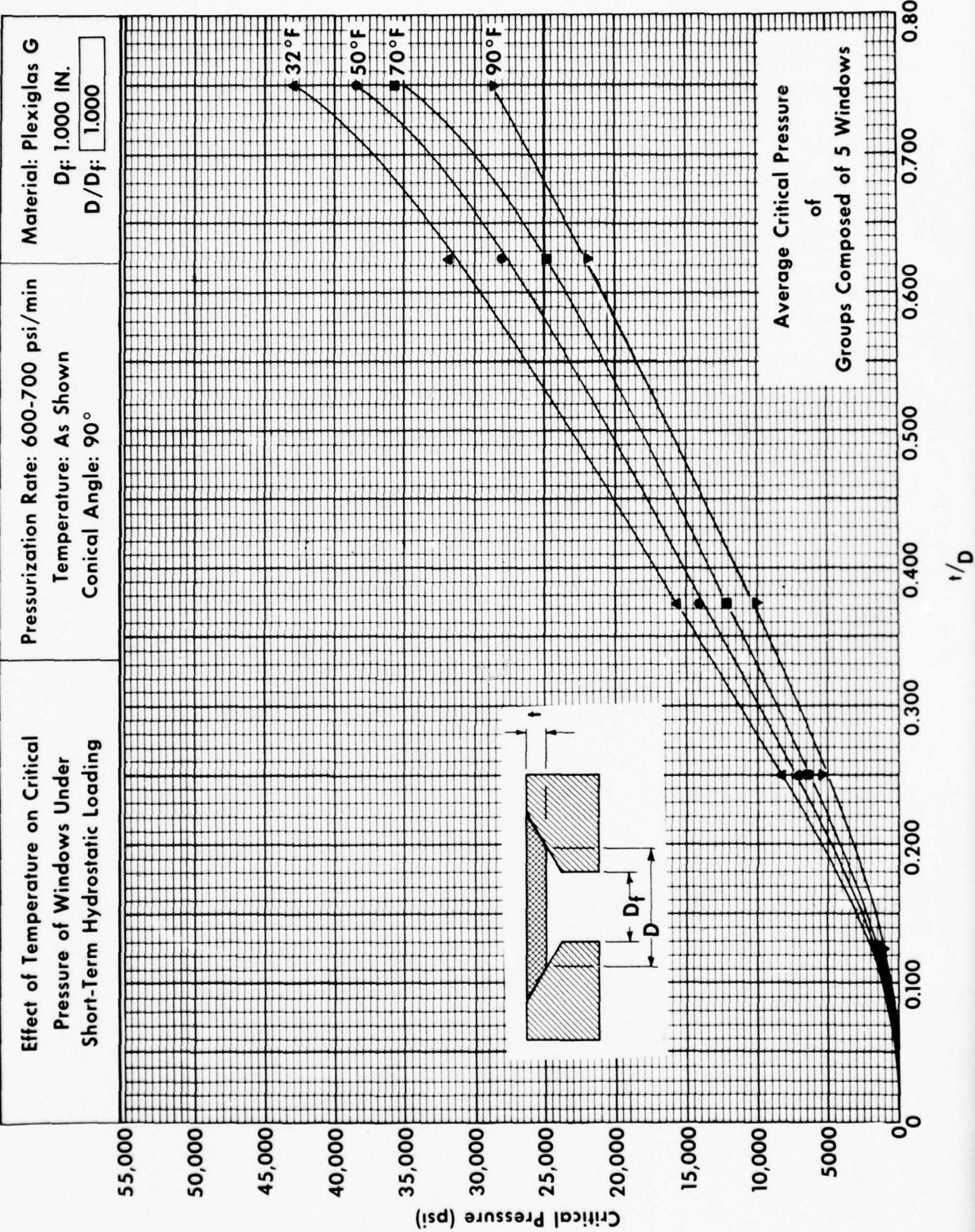
### B.1.3 Critical Pressures (Varying Temperatures)

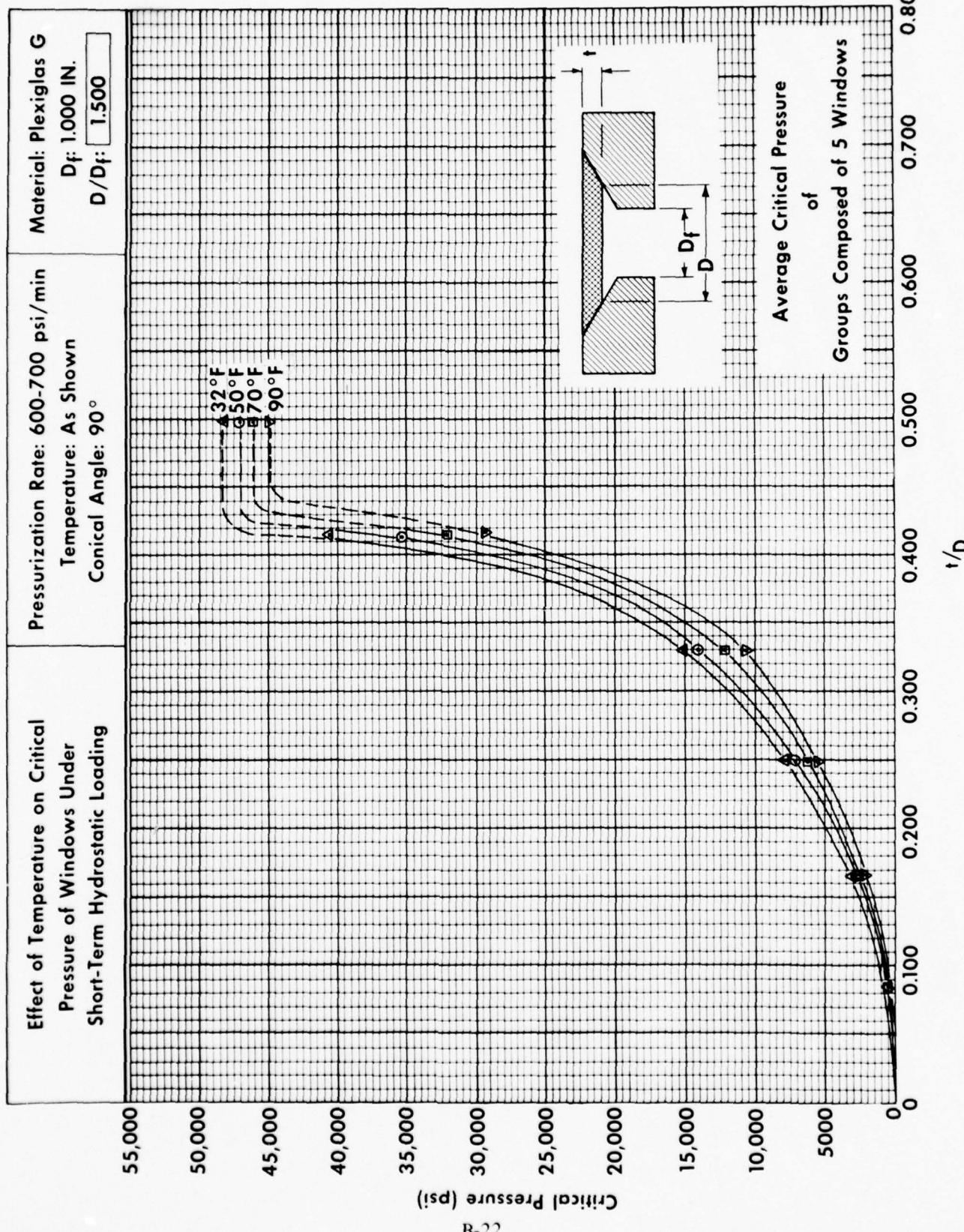
The data in this section are concerned with the critical pressures of conical frustums with 90-degree (1.57 radians) included angles under short-term pressure loading at 32, 50, 70, and 90°F (0, 10, 21, and 32°C) ambient temperatures in mountings with  $0.970 \leq D_i/D_f \leq 1.500$ .\*

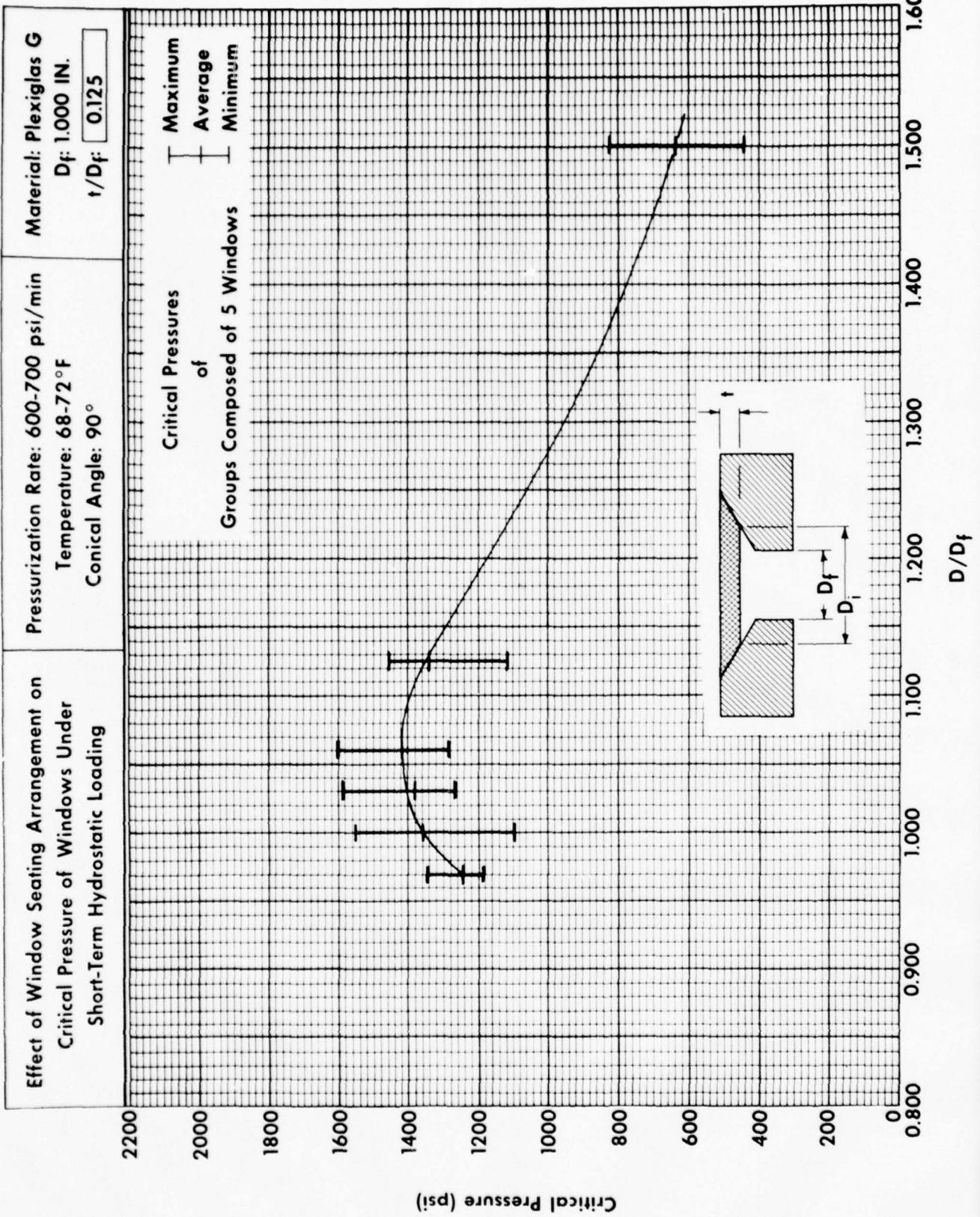
---

\*On many figures in this appendix  $D_i$  is noted as either  $D$  or  $d$ , thus  $t/D_i = t/D = t/d$ .





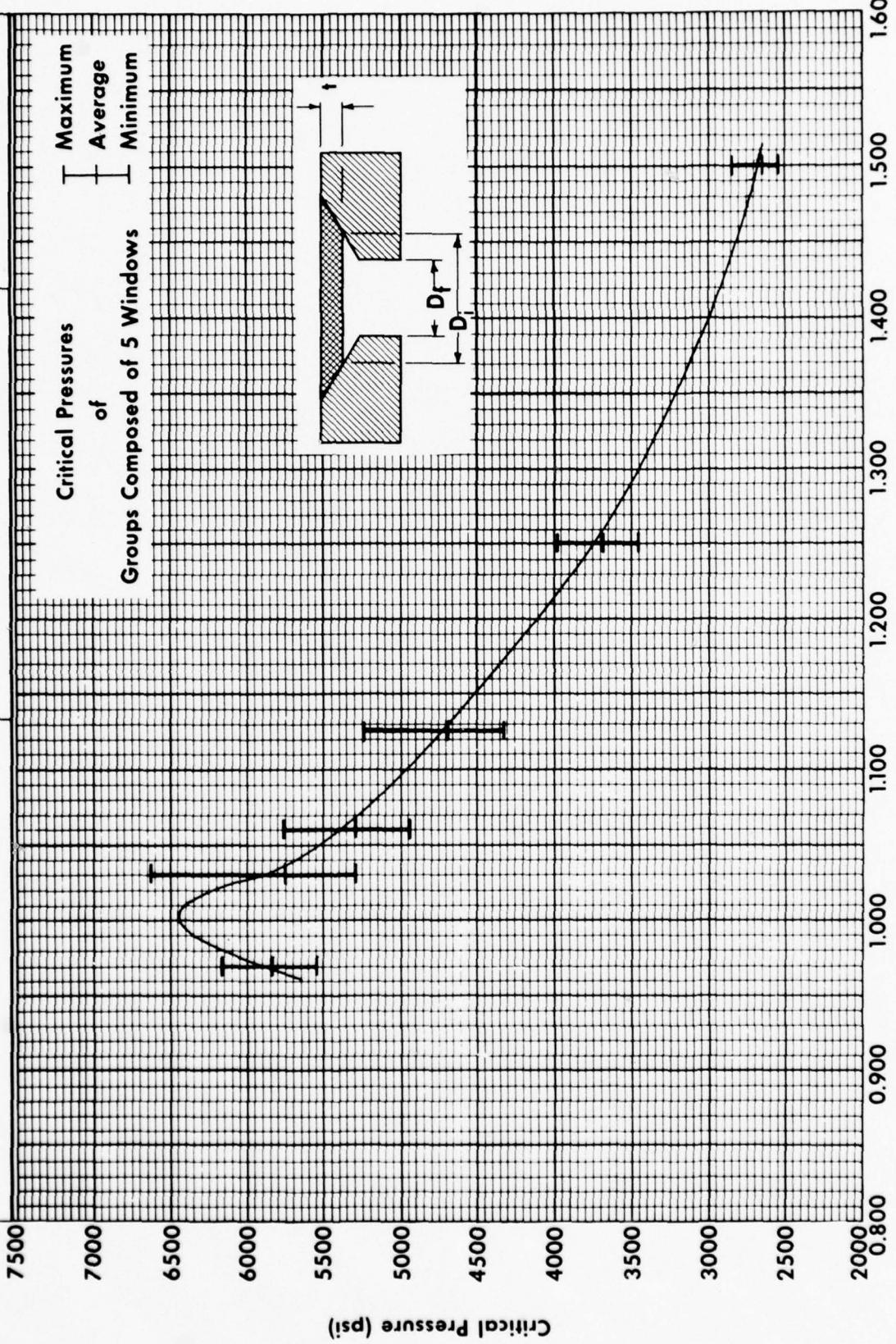




**Effect of Window Seating Arrangement on  
Critical Pressure of Windows Under  
Short-Term Hydrostatic Loading**

Pressurization Rate: 600-700 psi/min  
Temperature: 68-72°F  
Conical Angle: 90°

Material: Plexiglas G  
 $D_f$ : 1.000 IN.  
 $t/D_f$ : 0.250



**Effect of Window Seating Arrangement on Critical Pressure of Windows Under Short-Term Hydrostatic Loading**

Pressurization Rate: 600-700 psi/min  
Temperature: 68-72 °F  
Conical Angle: 90°

Material: Plexiglas G  
 $D_f$ : 1.000 IN.  
 $t/D_f$ : 0.375

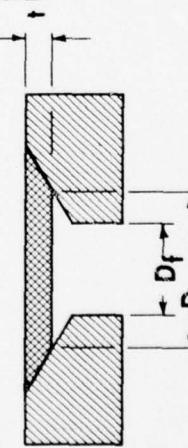
Critical Pressures

of Groups Composed of 5 Windows

Maximum  
Average  
Minimum

Critical Pressure (psi)

B-25



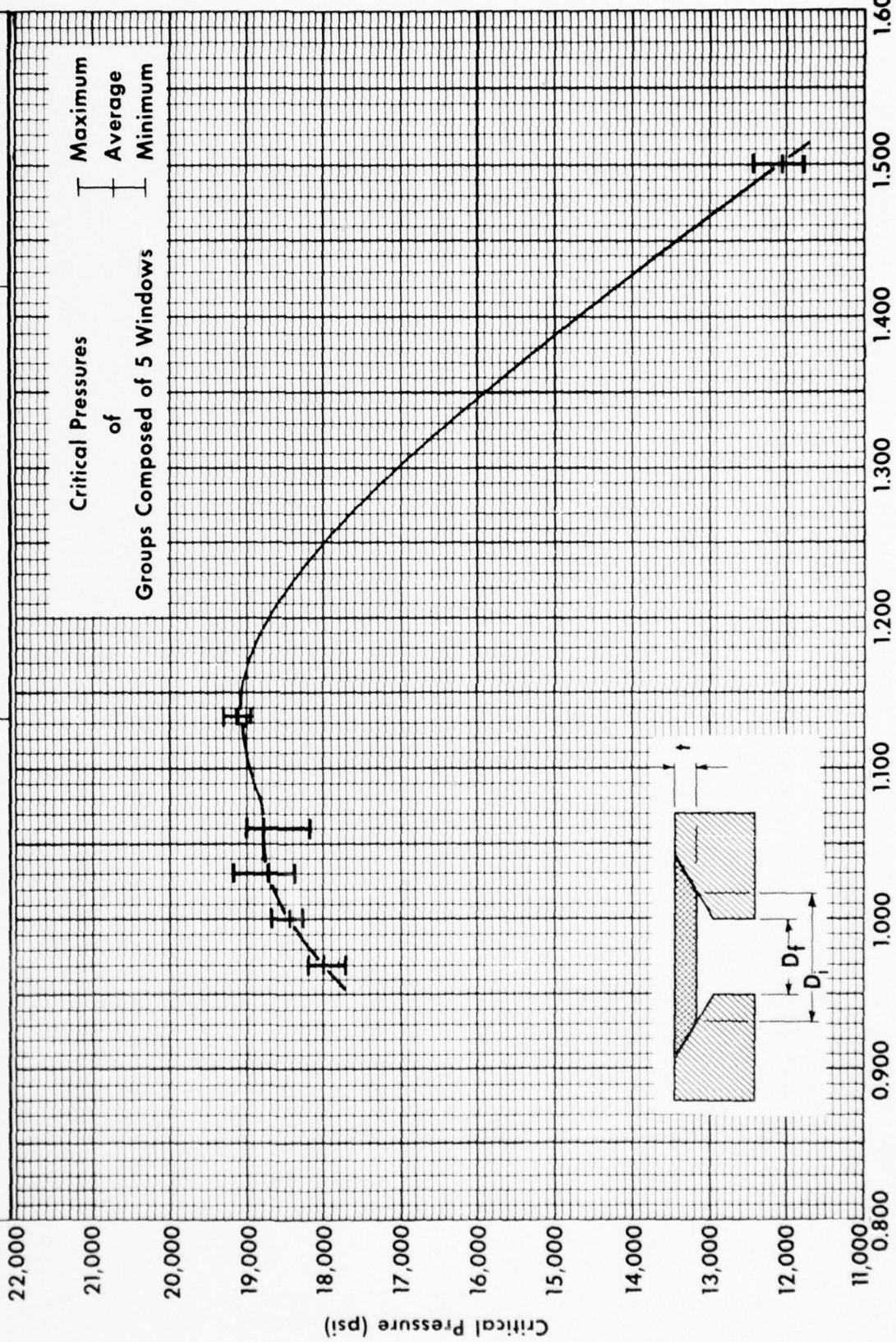
$D/D_f$

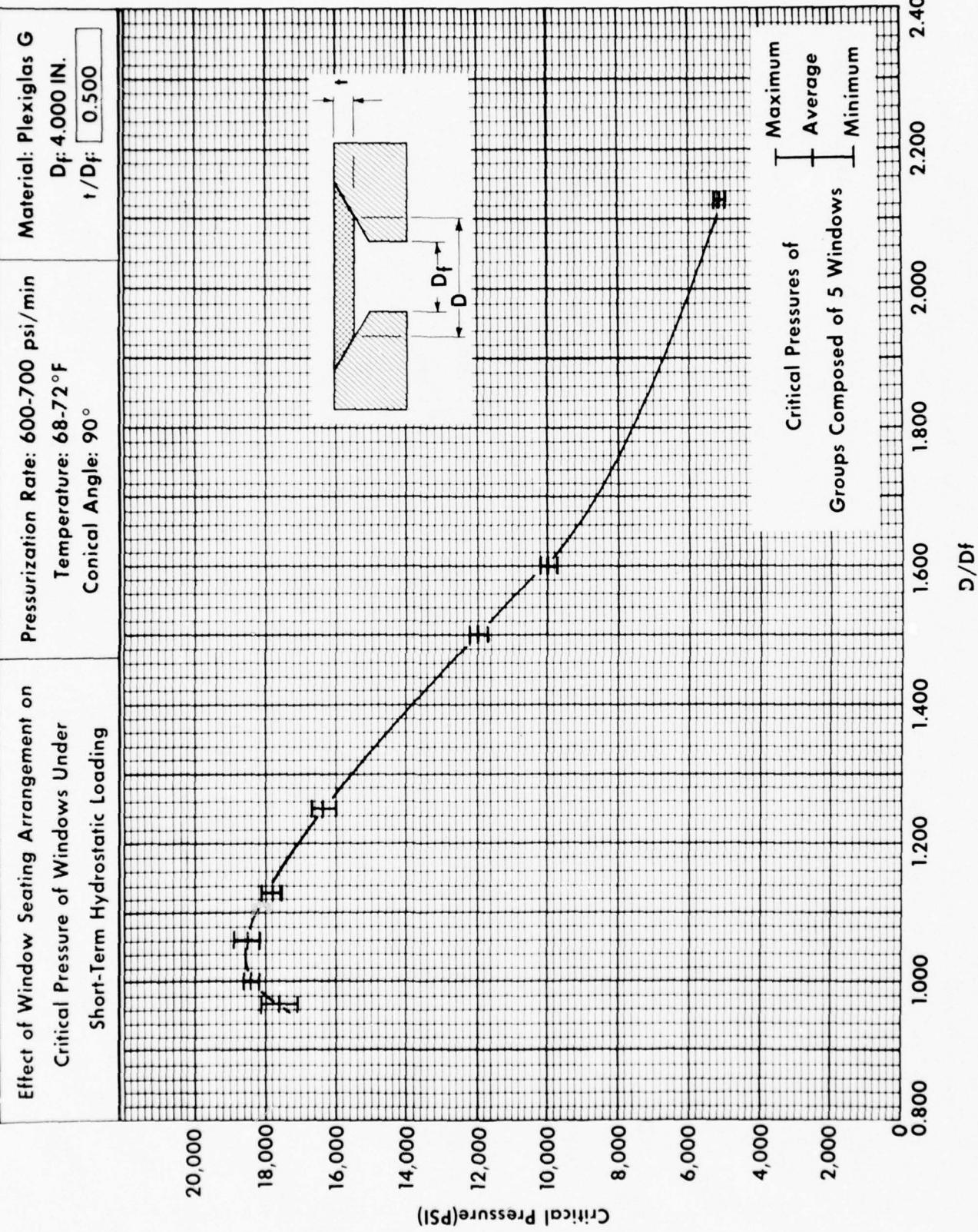
1.600  
1.500  
1.400  
1.300  
1.200  
1.100  
1.000  
0.900  
0.800

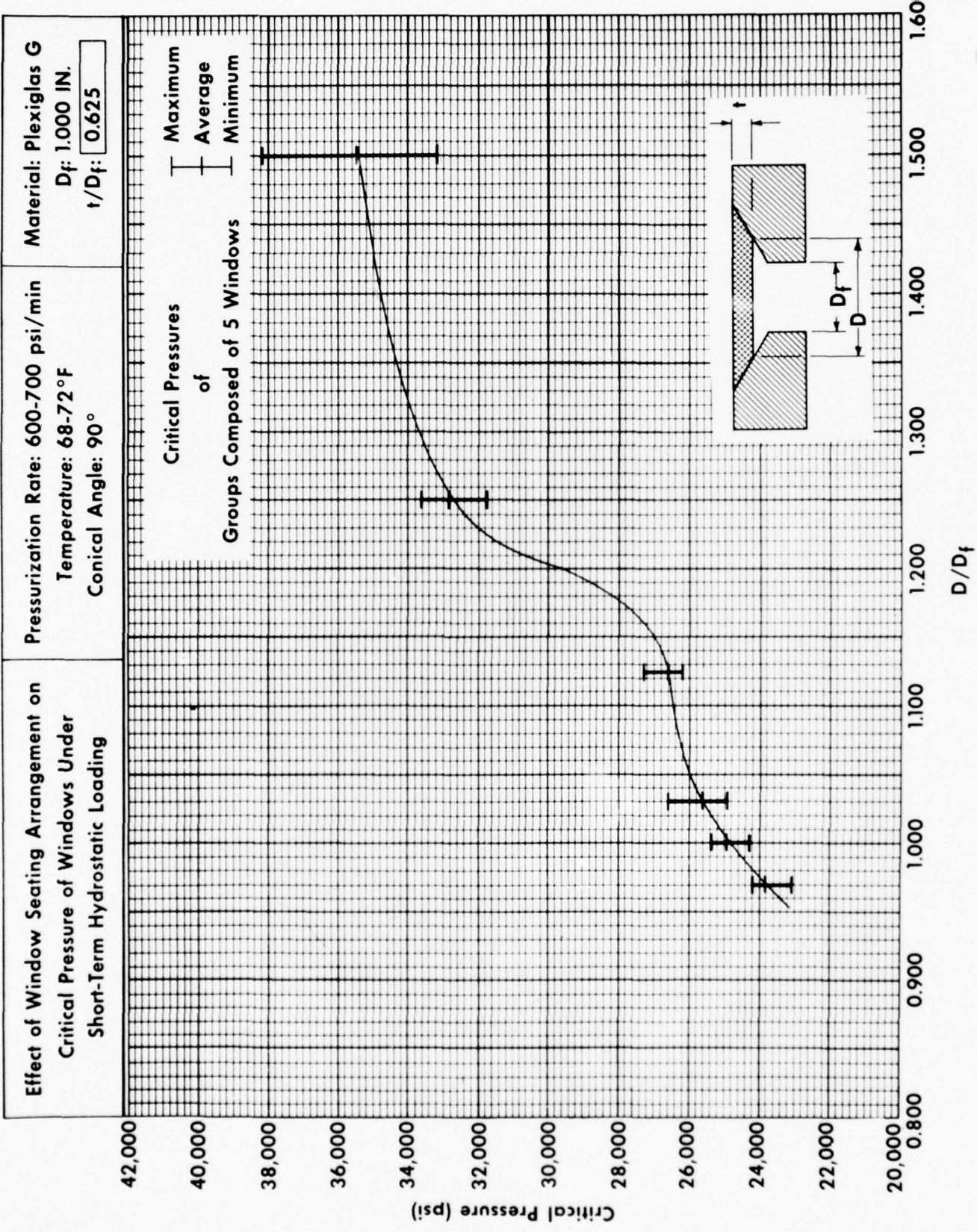
**Effect of Window Sealing Arrangement on Critical Pressure of Windows Under Short-Term Hydrostatic Loading**

Pressurization Rate: 600-700 psi/min  
Temperature: 68-72°F  
Conical Angle: 90°

Material: Plexiglas G  
 $D_f$ : 1.000 IN.  
 $t/D_f$ : 0.500



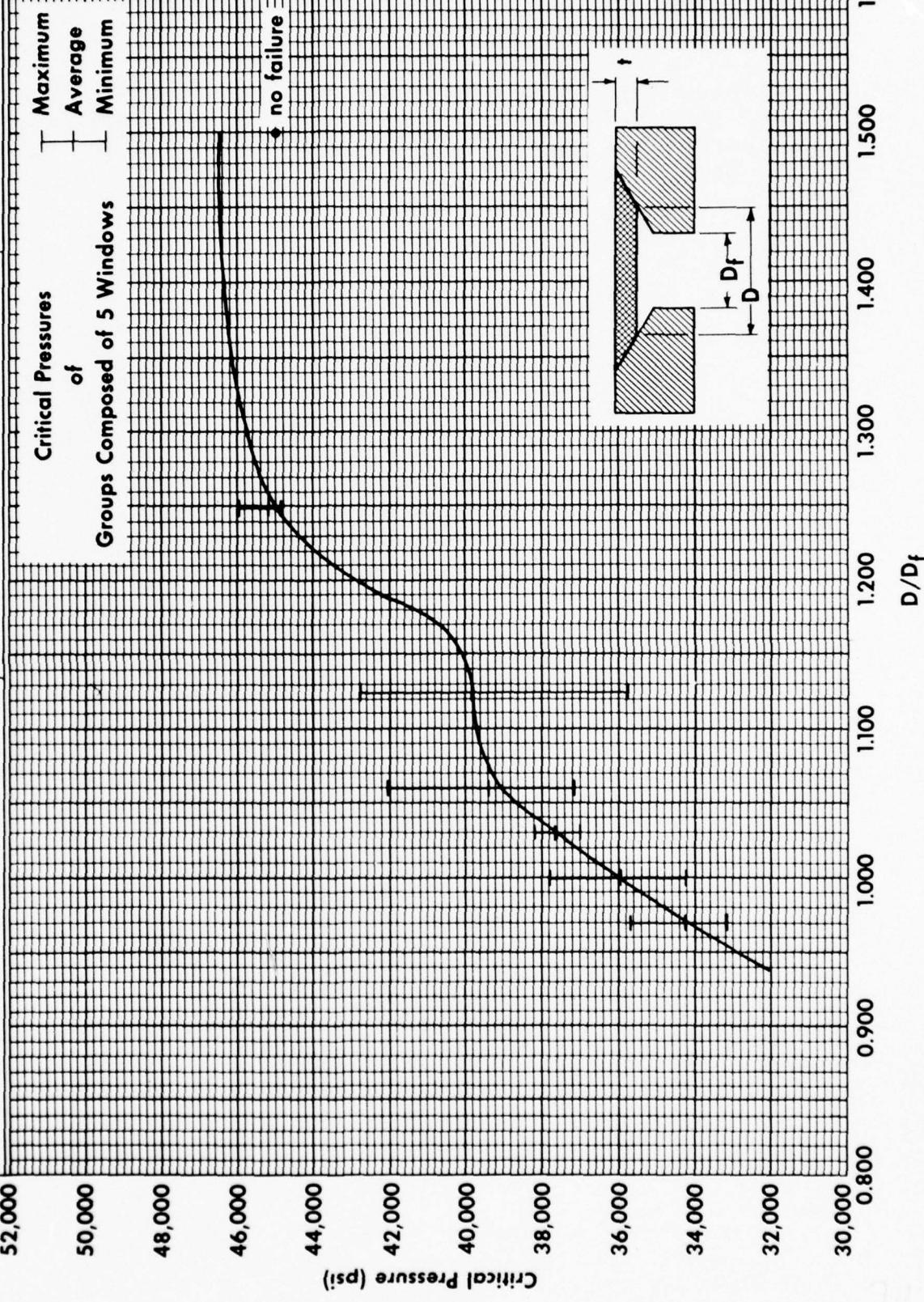




**Effect of Window Seating Arrangement on Critical Pressure of Windows Under Short-Term Hydrostatic Loading**

Pressurization Rate: 600-700 psi/min  
Temperature: 68-72°F  
Conical Angle: 90°

Material: Plexiglas G  
 $D_f$ : 1.000 IN.  
 $t/D_f$ : 0.75

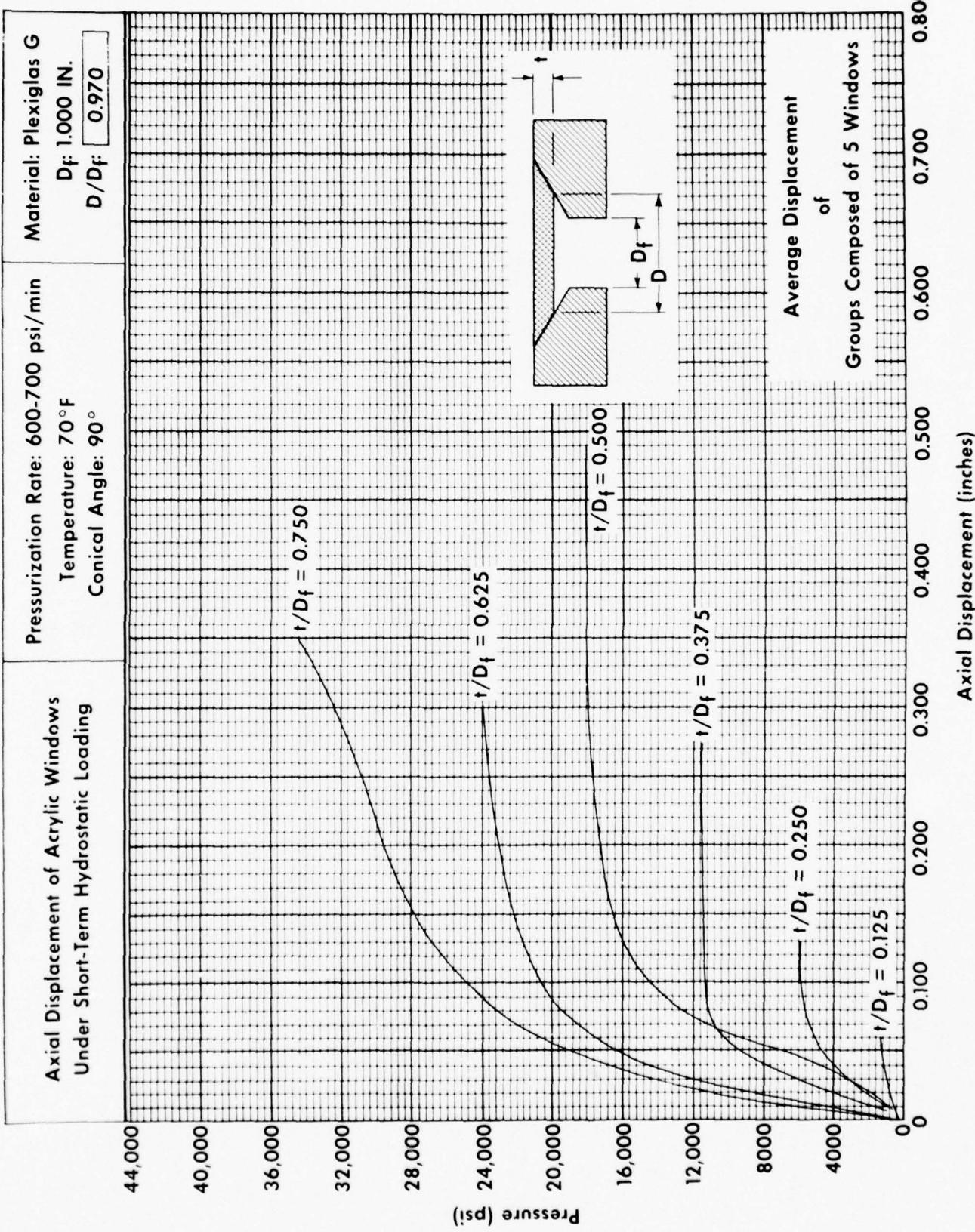


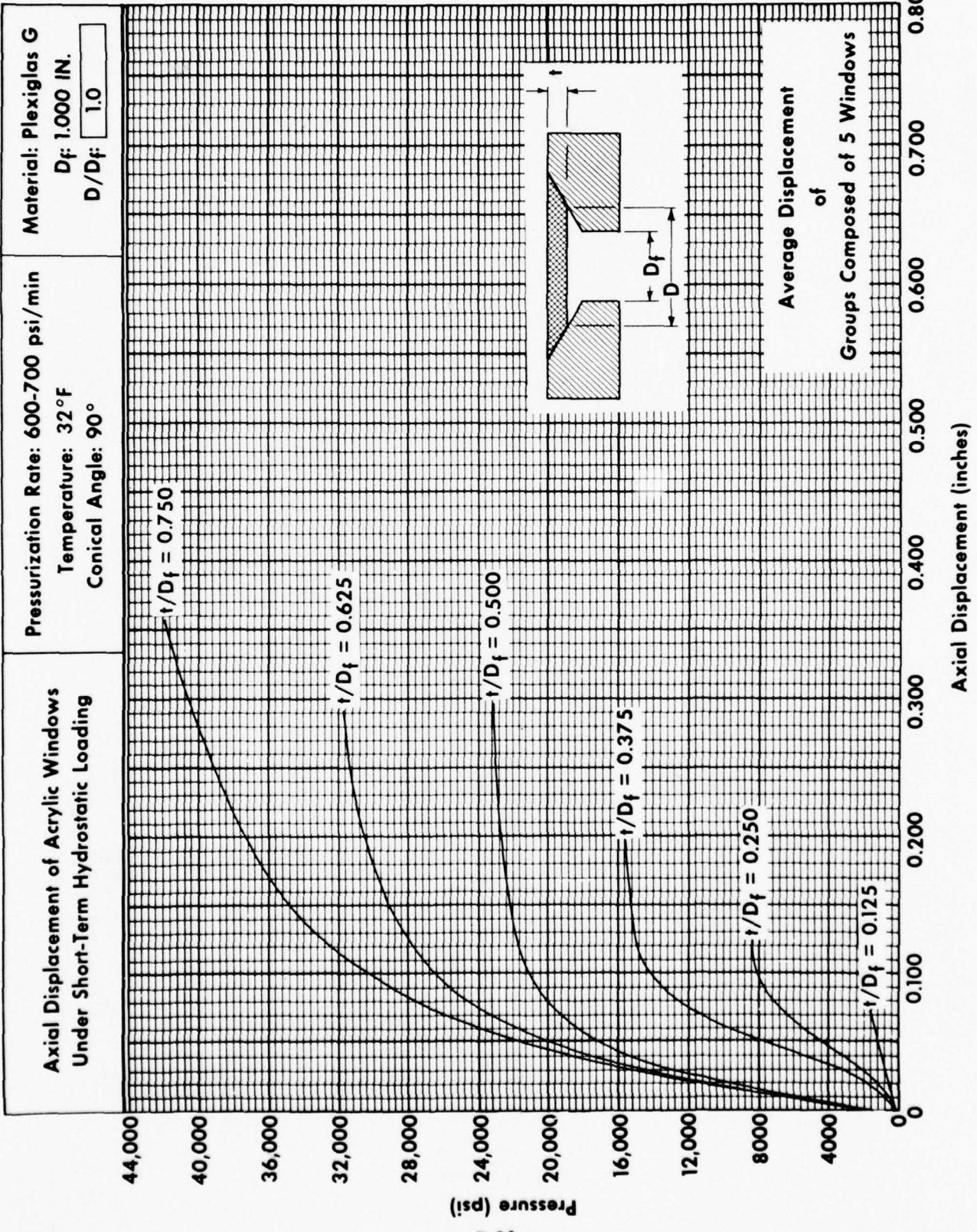
#### B.1.4 Axial Displacements (Varying Temperatures)

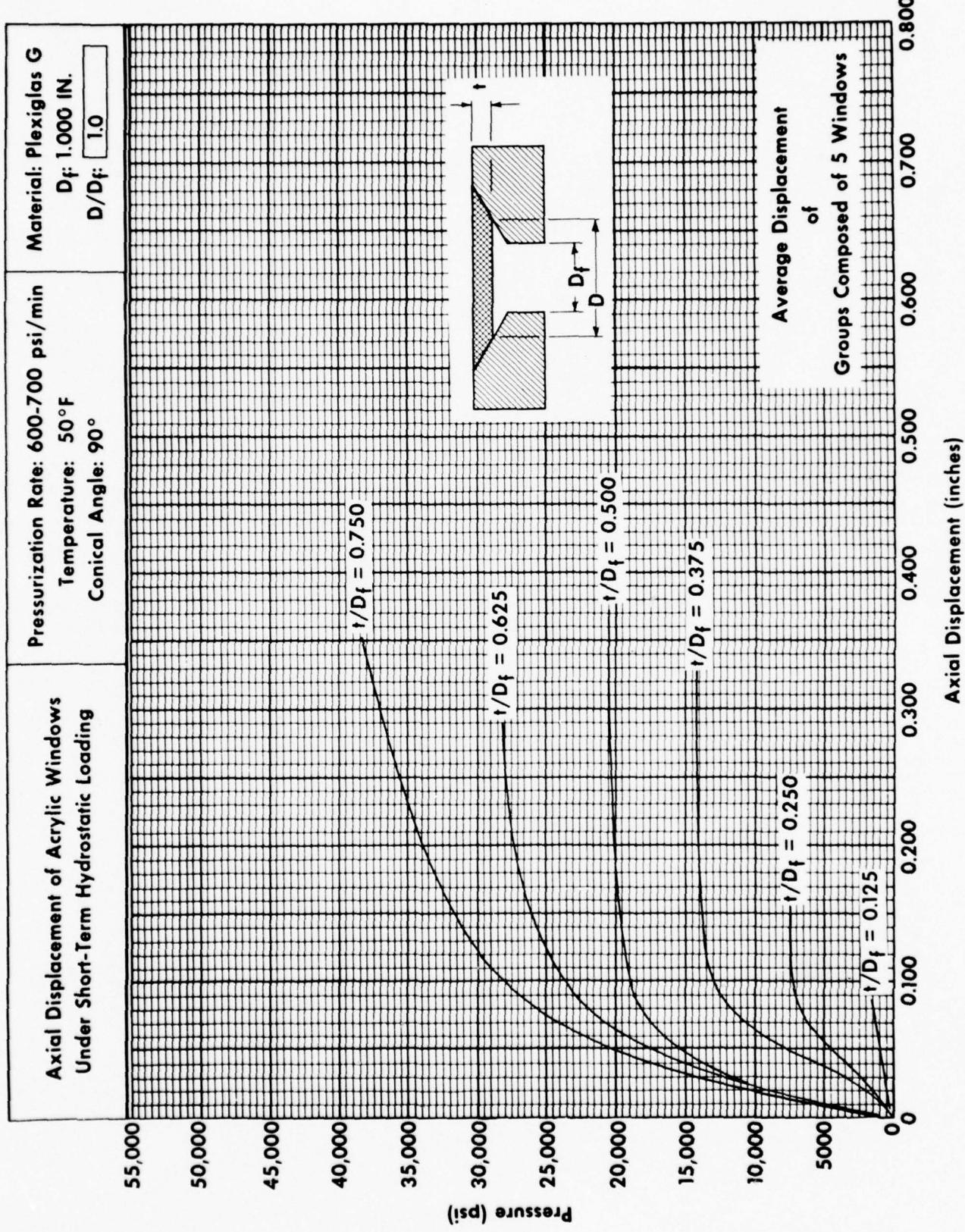
The data in this section are concerned with the axial displacements of conical frustums with 90-degree (1.57 radians) included angles under short-term pressure loading at 32, 50, 70, and 90°F (0, 10, 21, and 32°C) ambient temperatures in mountings with  $0.970 \leq D_i/D_f \leq 1.500$ .\*

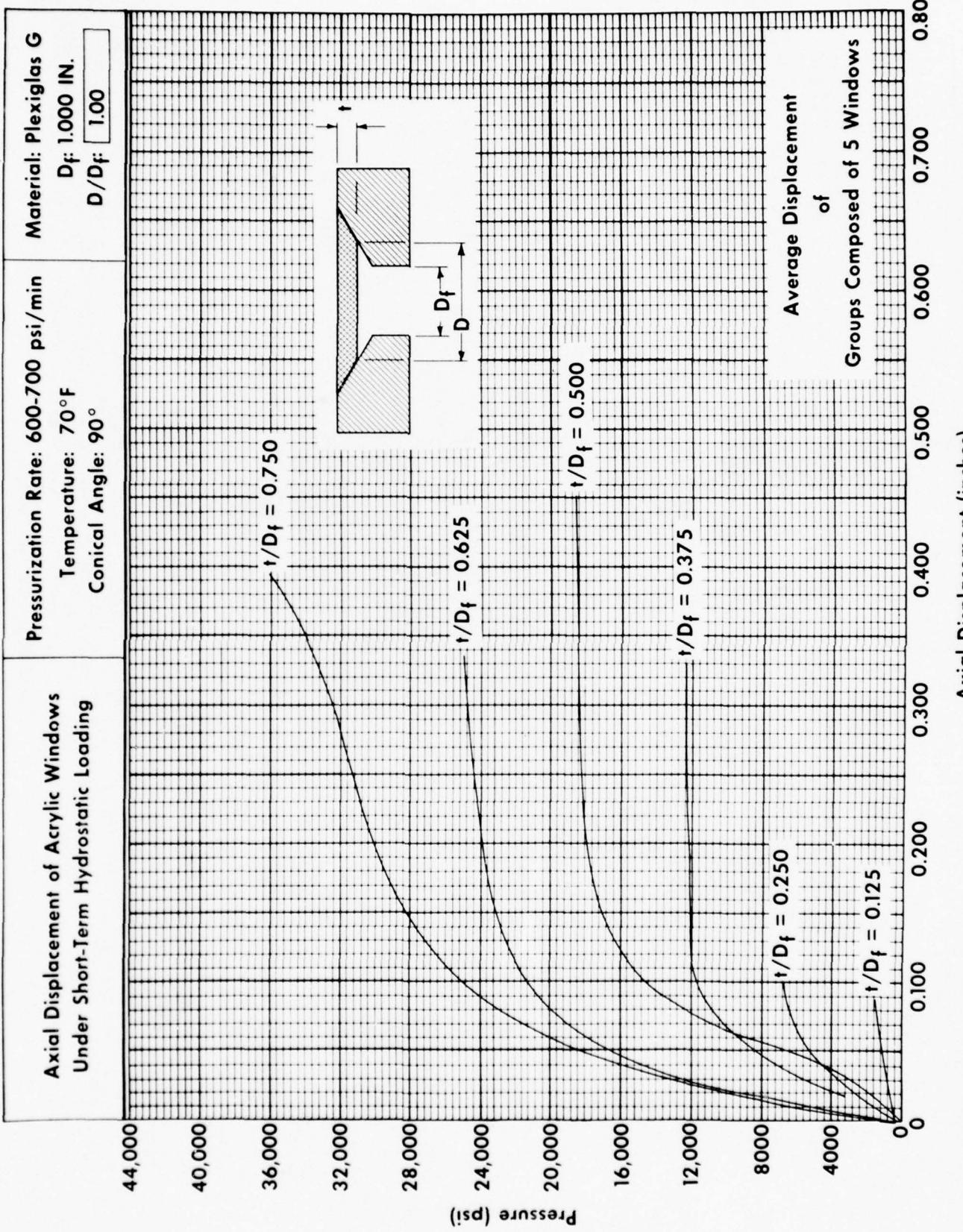
---

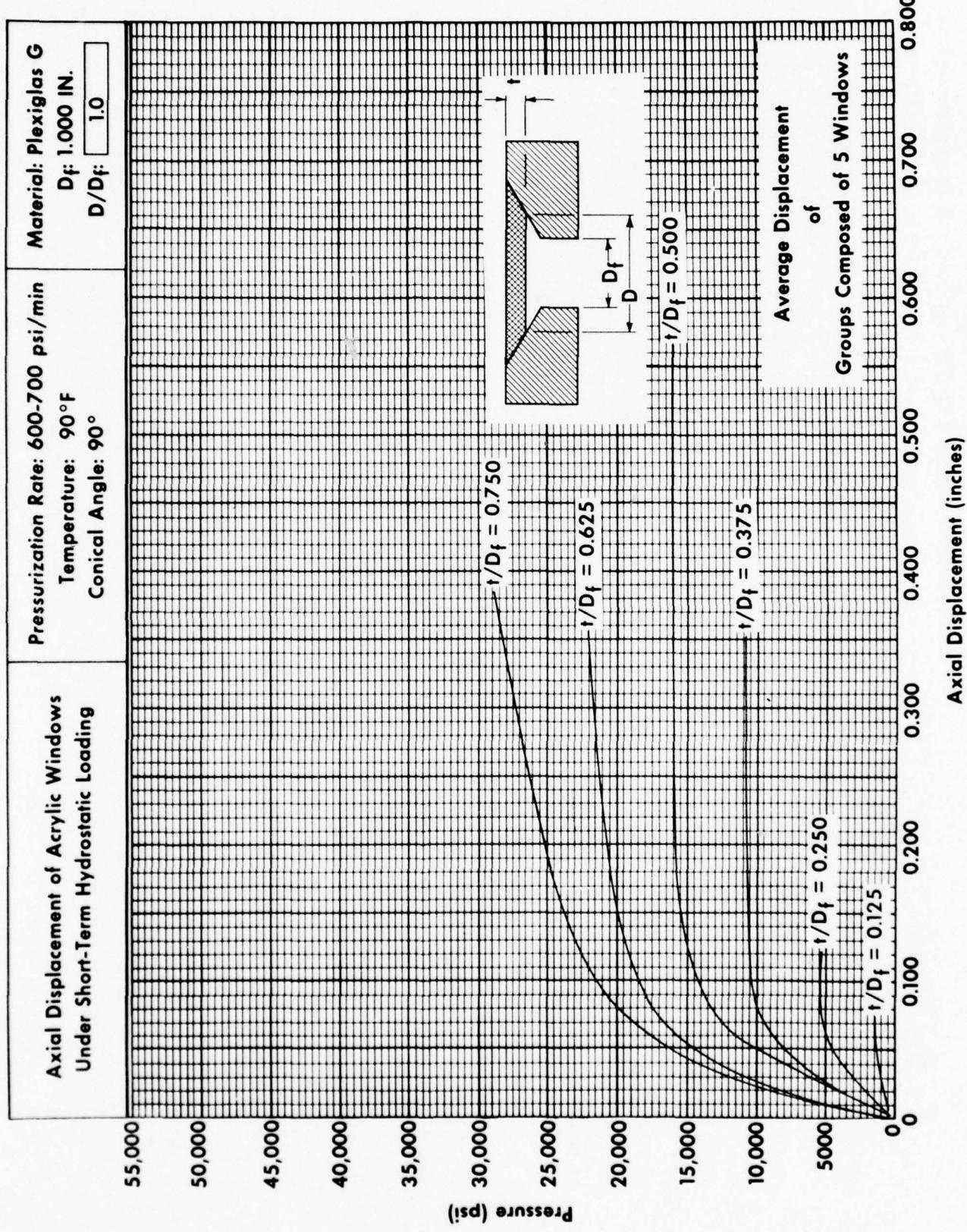
\*On many figures in this appendix  $D_i$  is noted either as  $D$  or  $d$ , thus  $D_i = D = d$ .

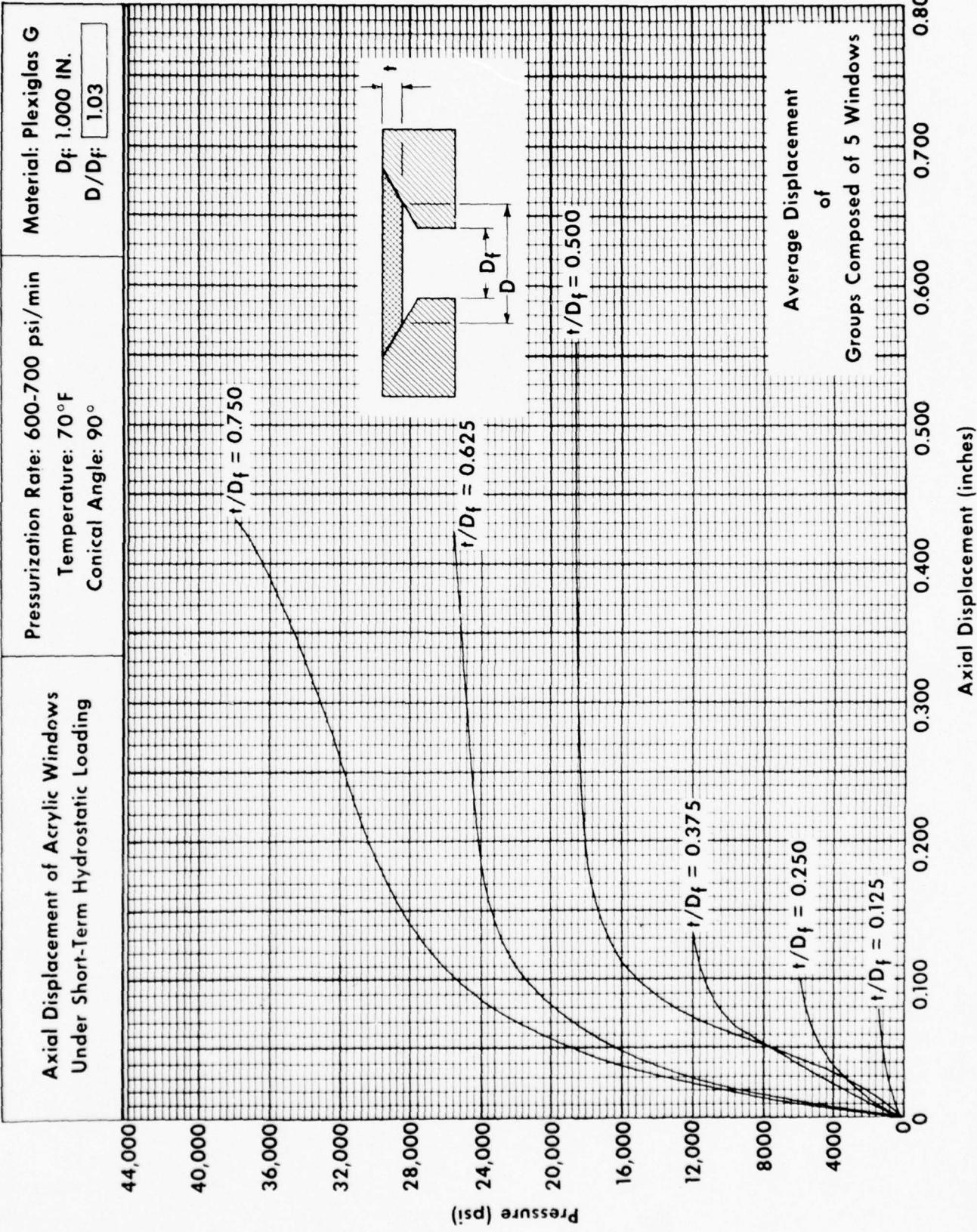


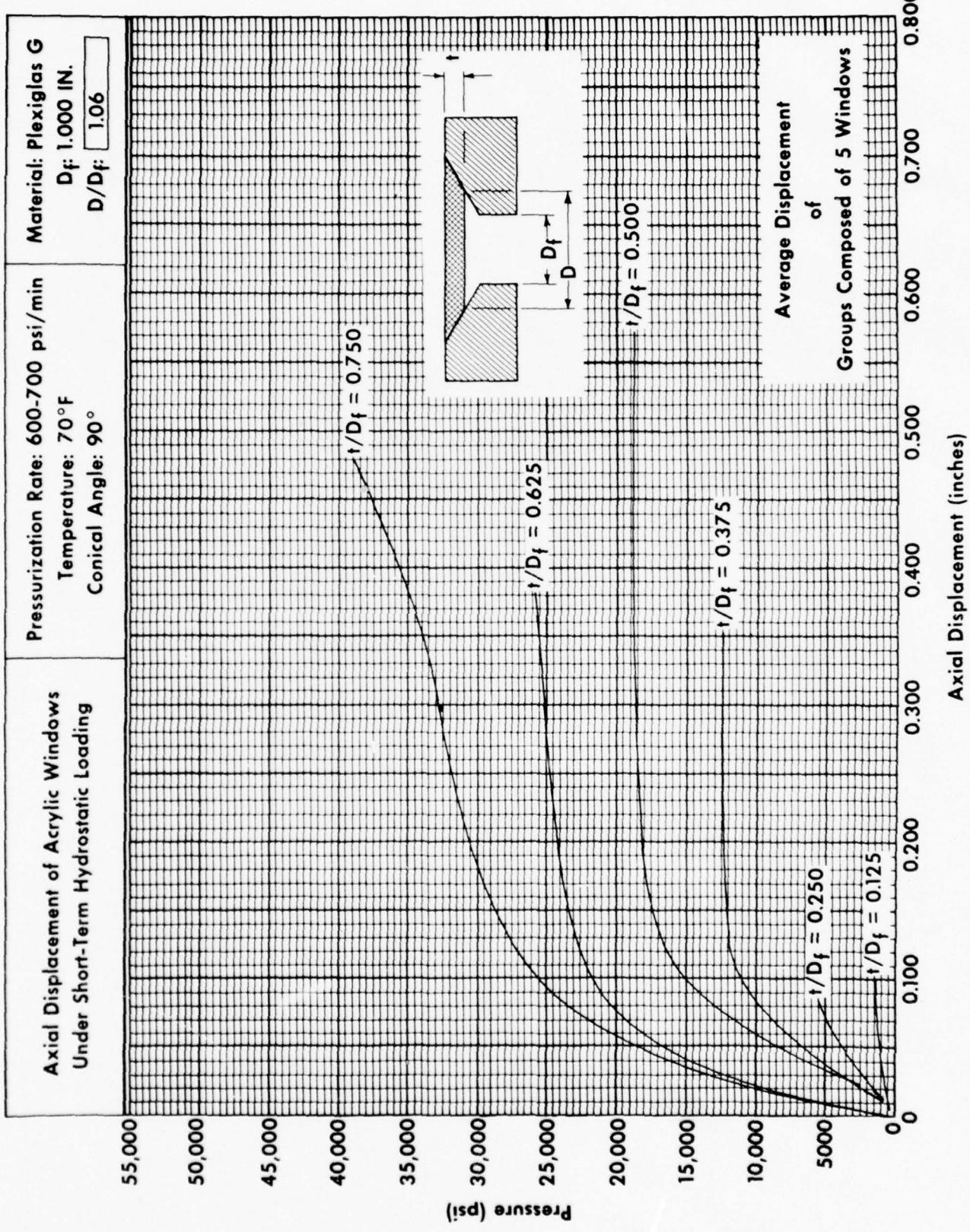


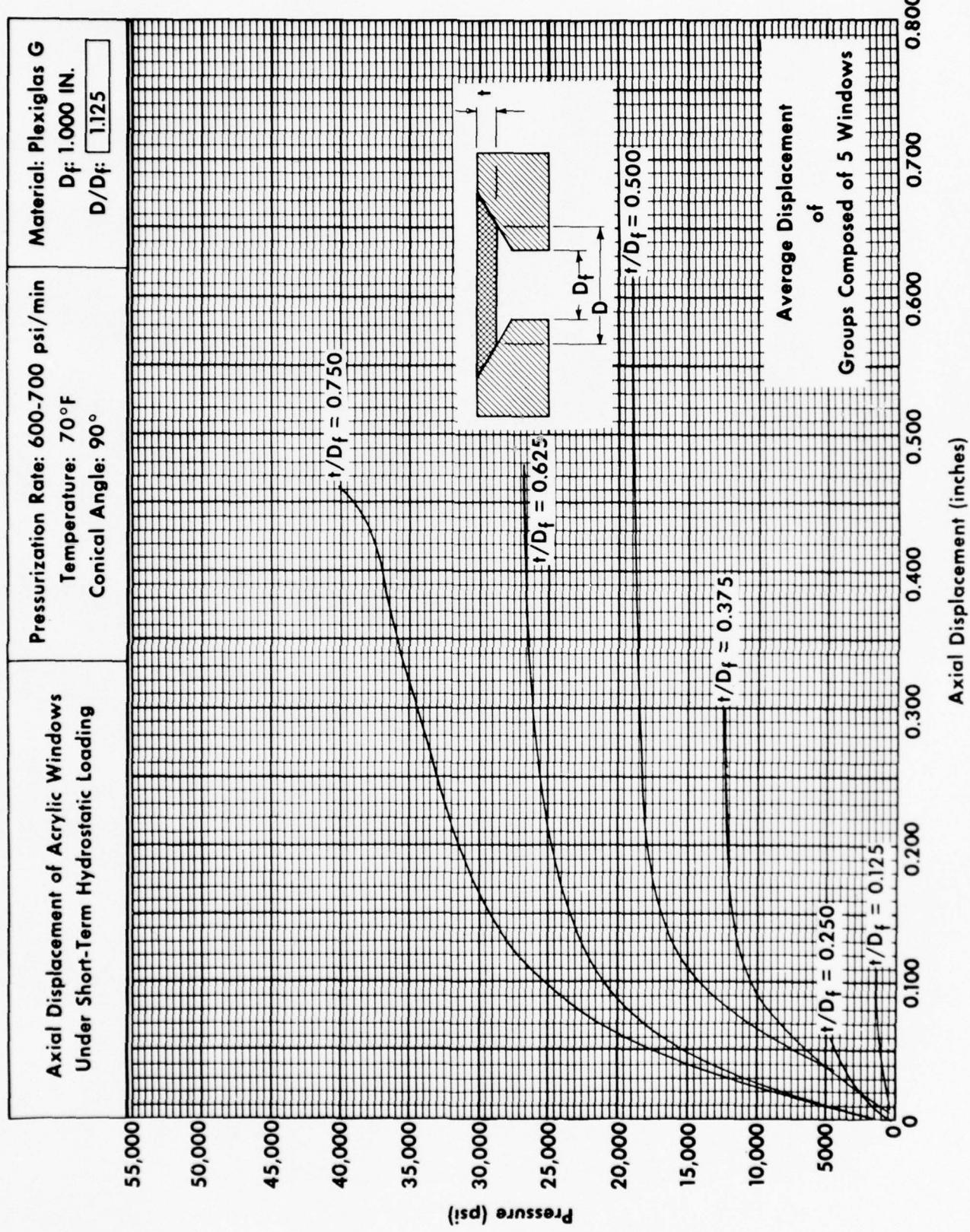


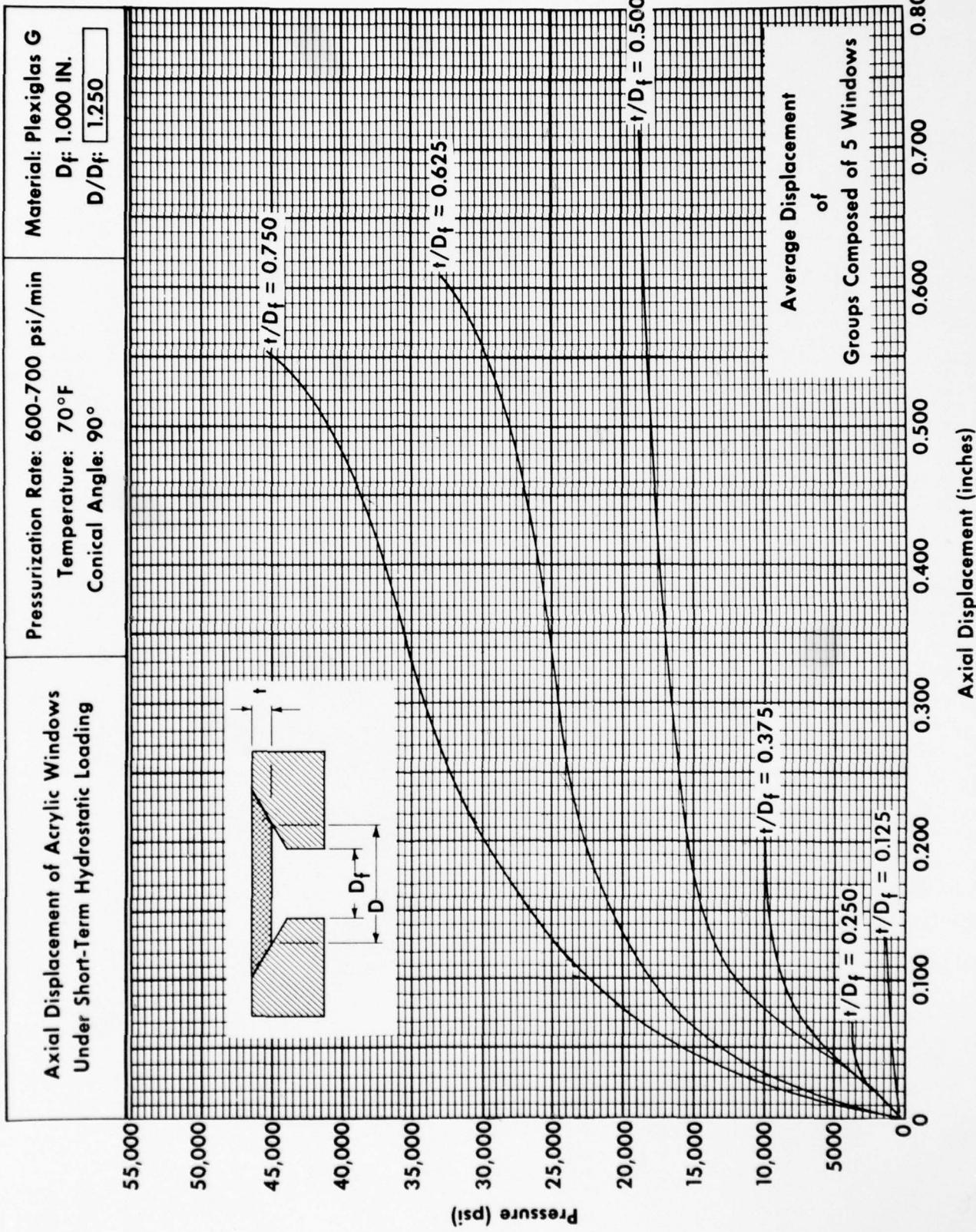


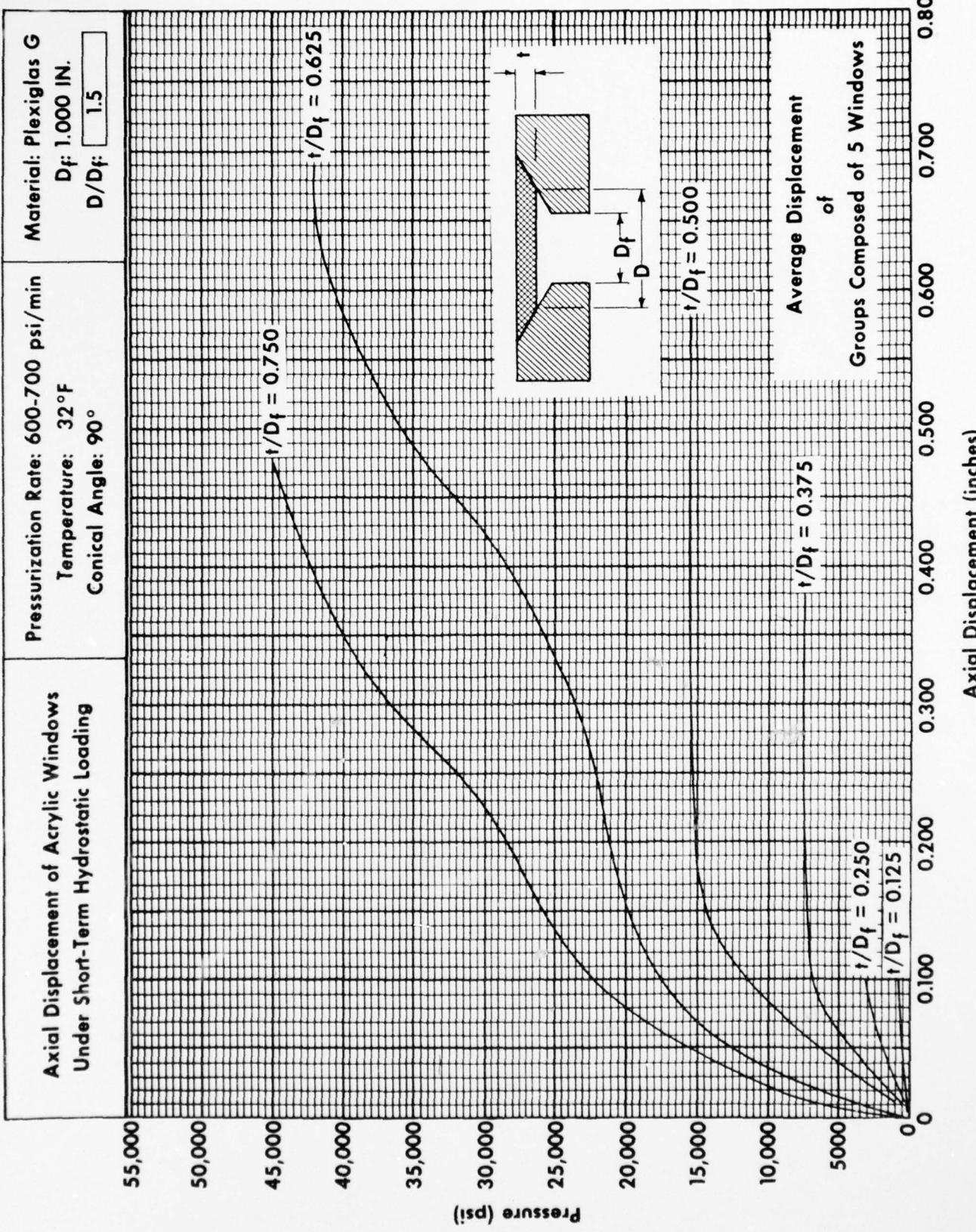


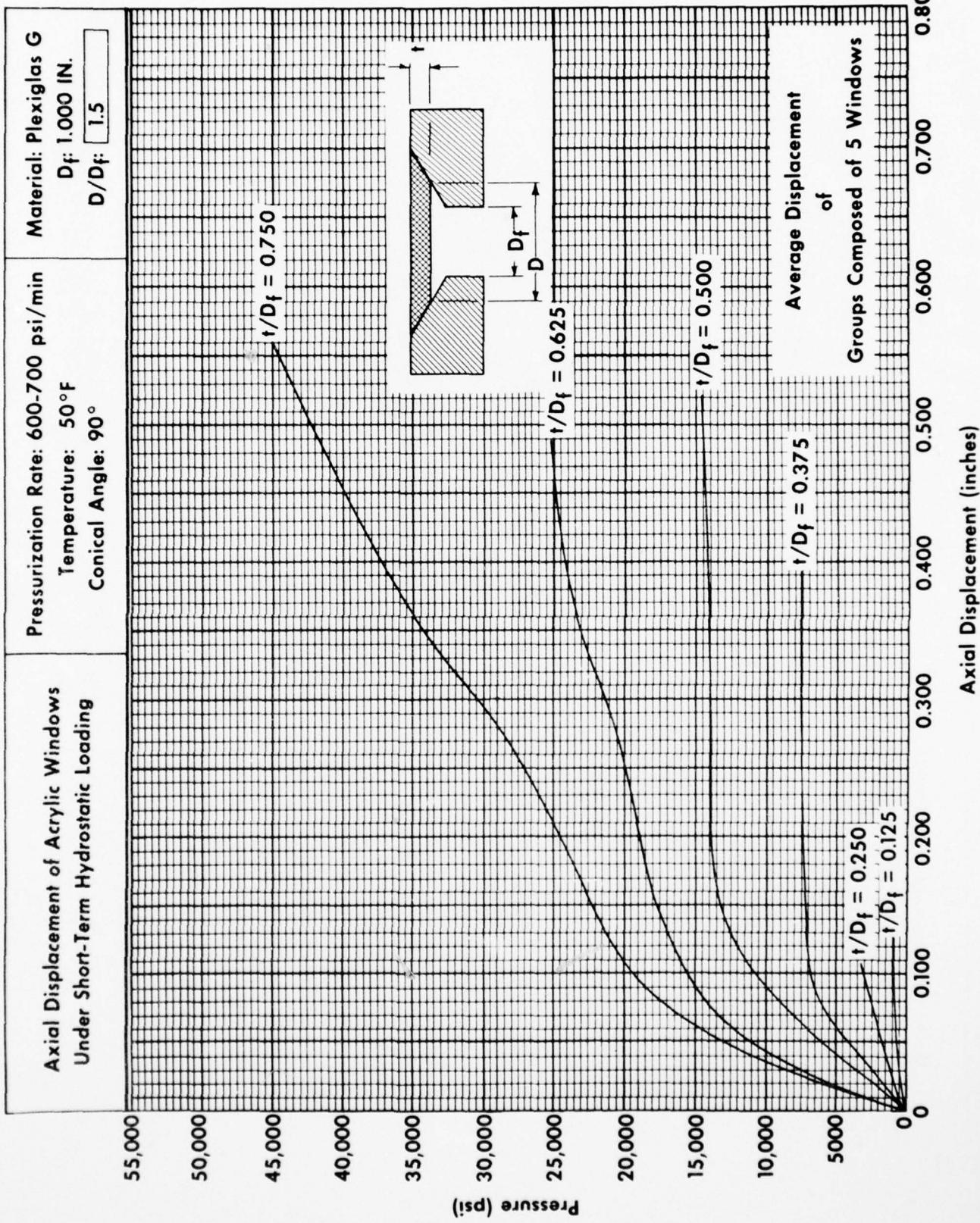


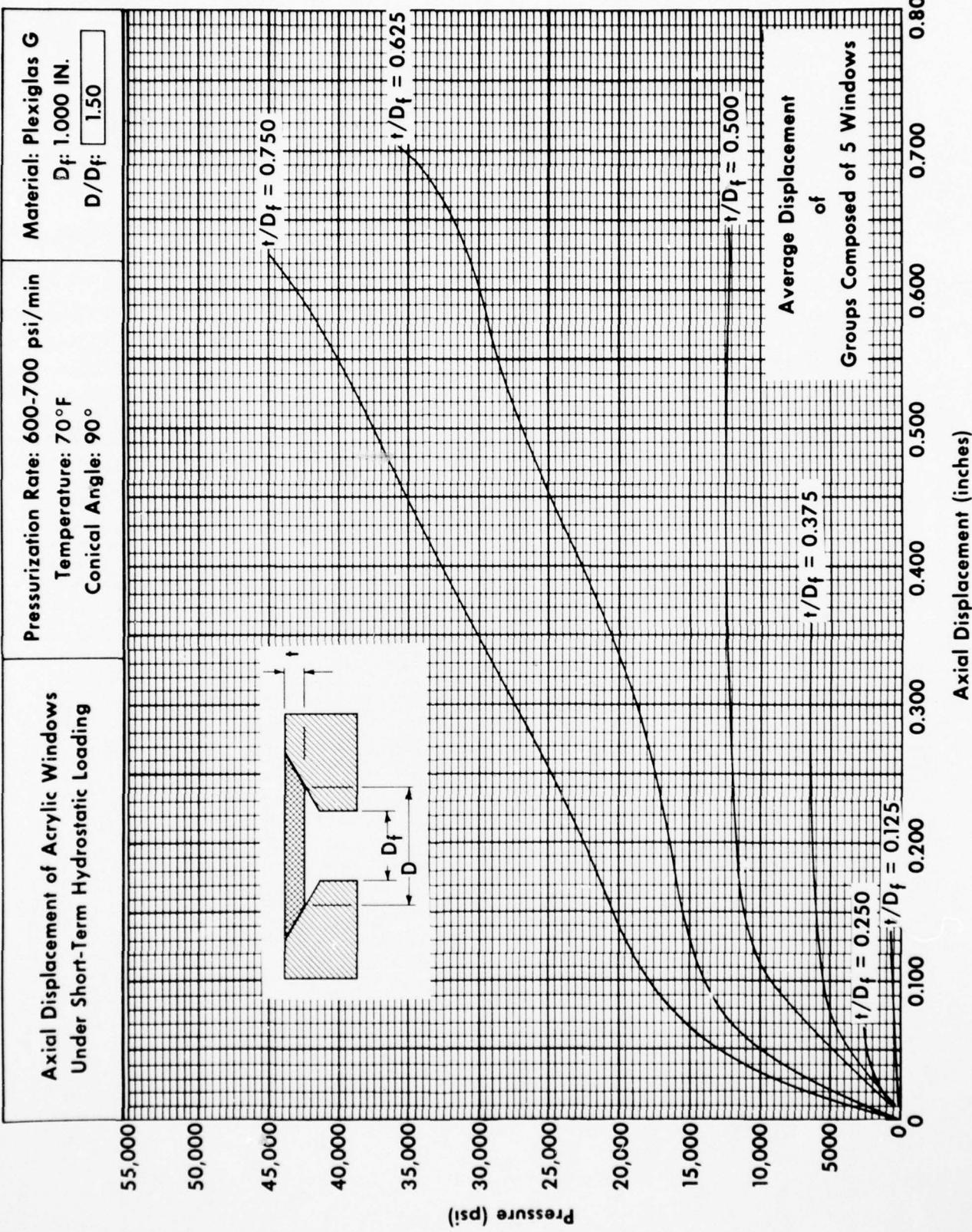


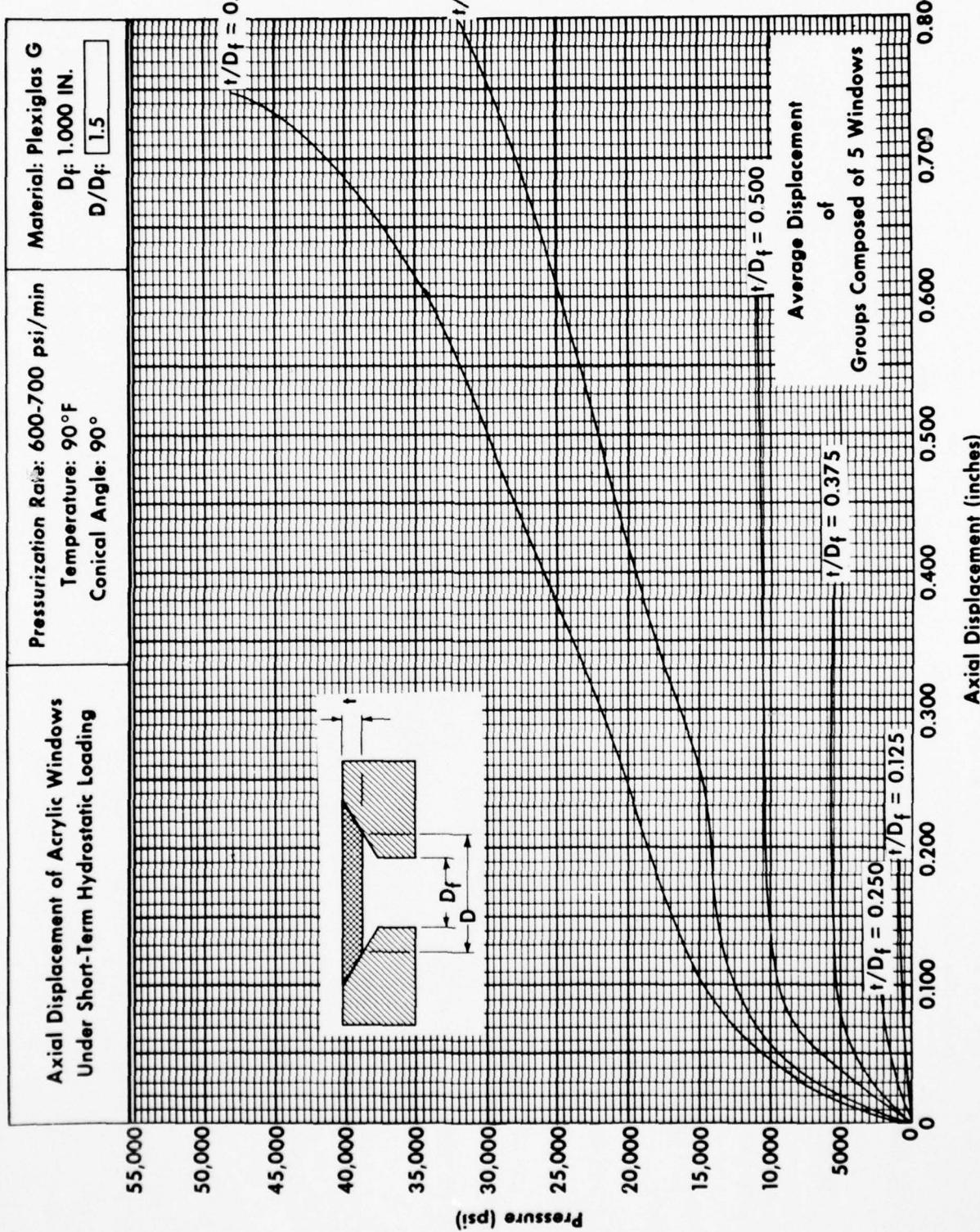


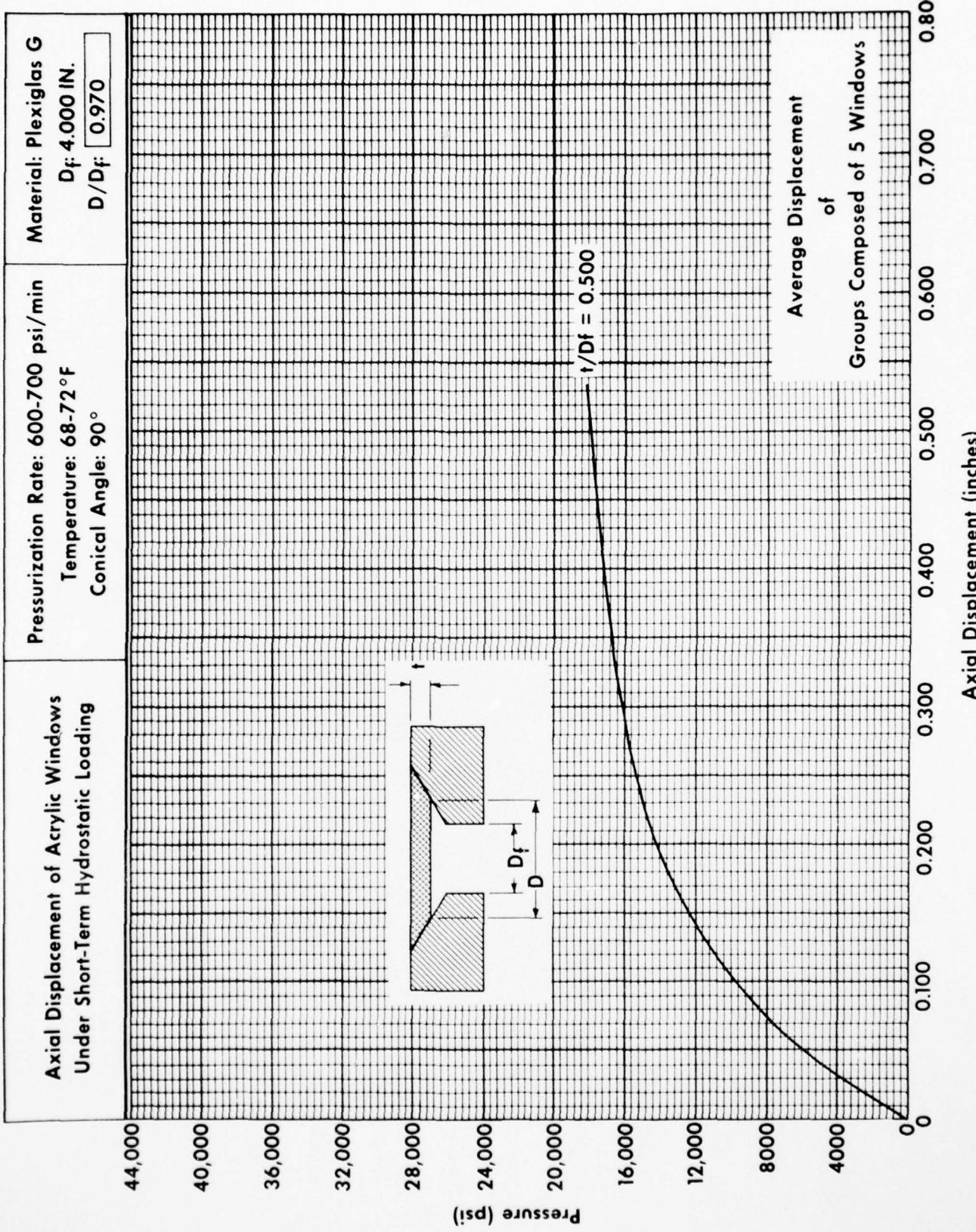


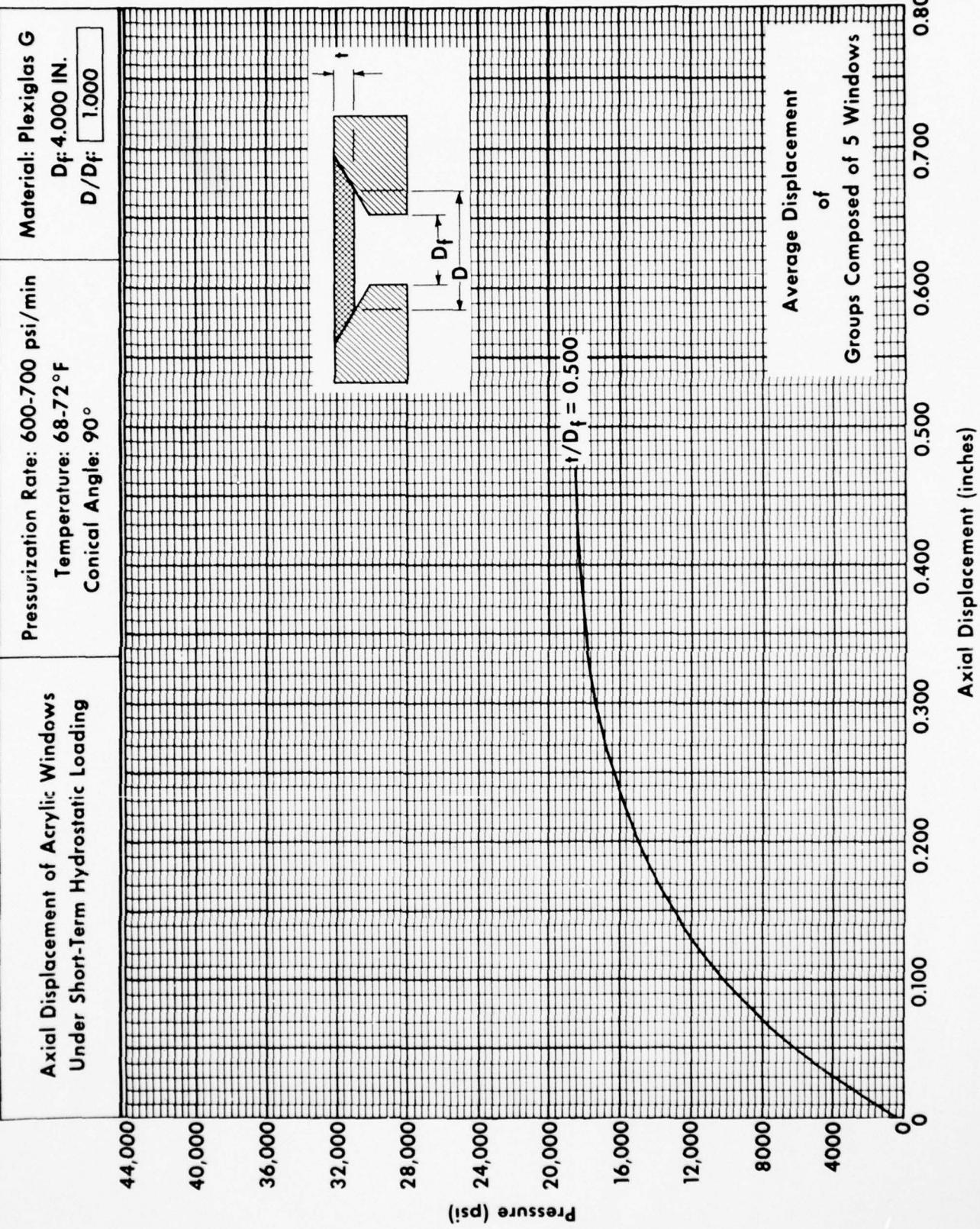


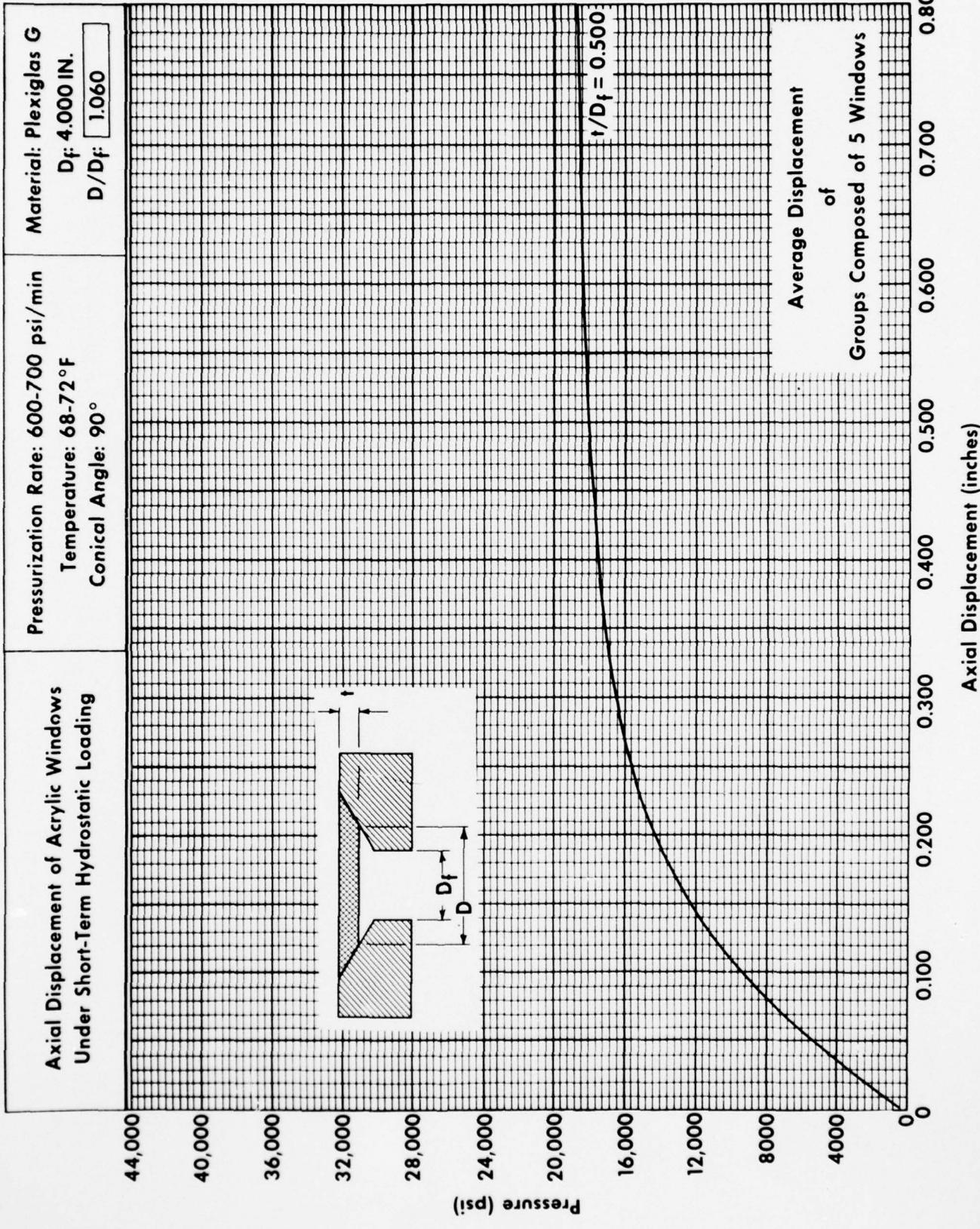


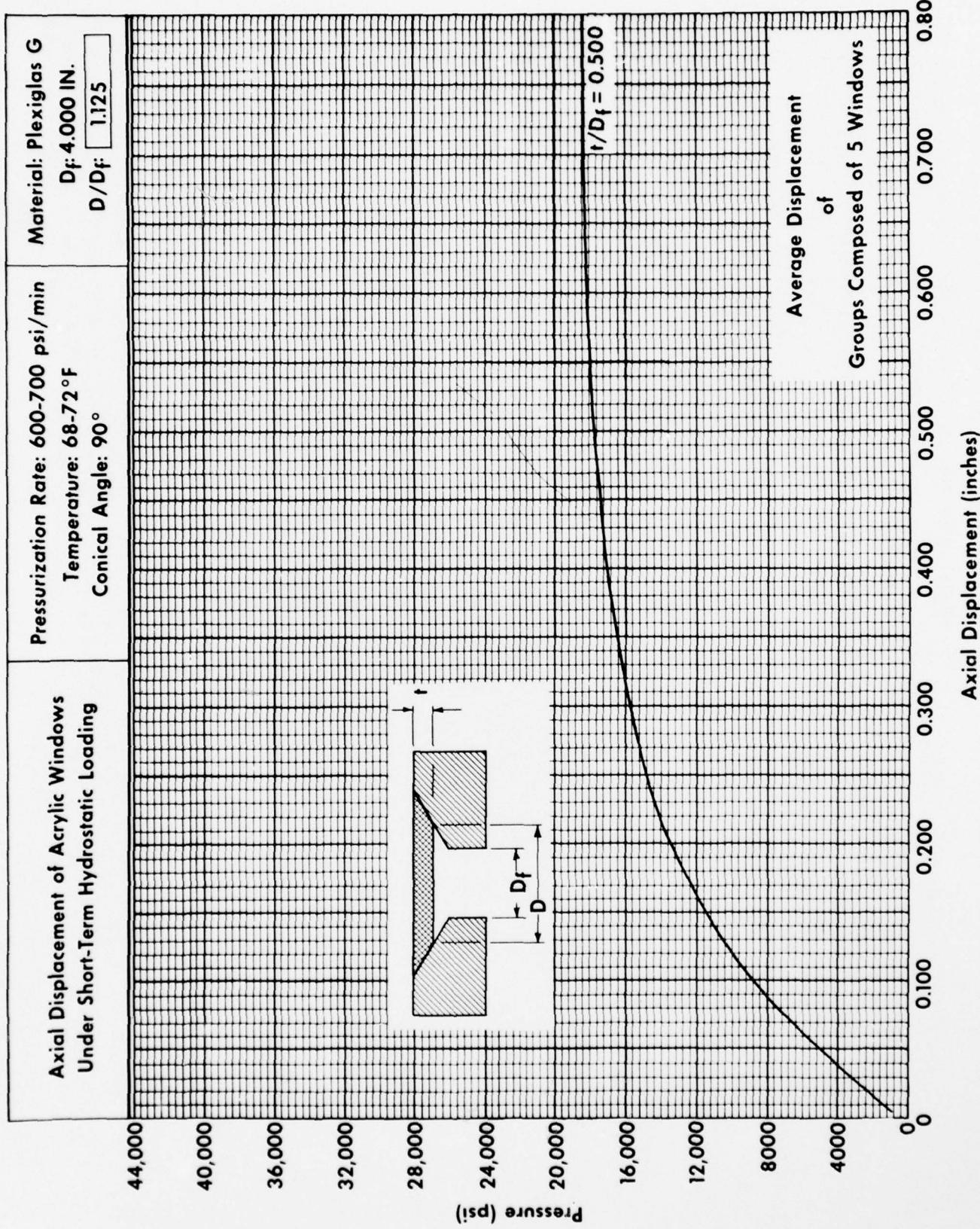


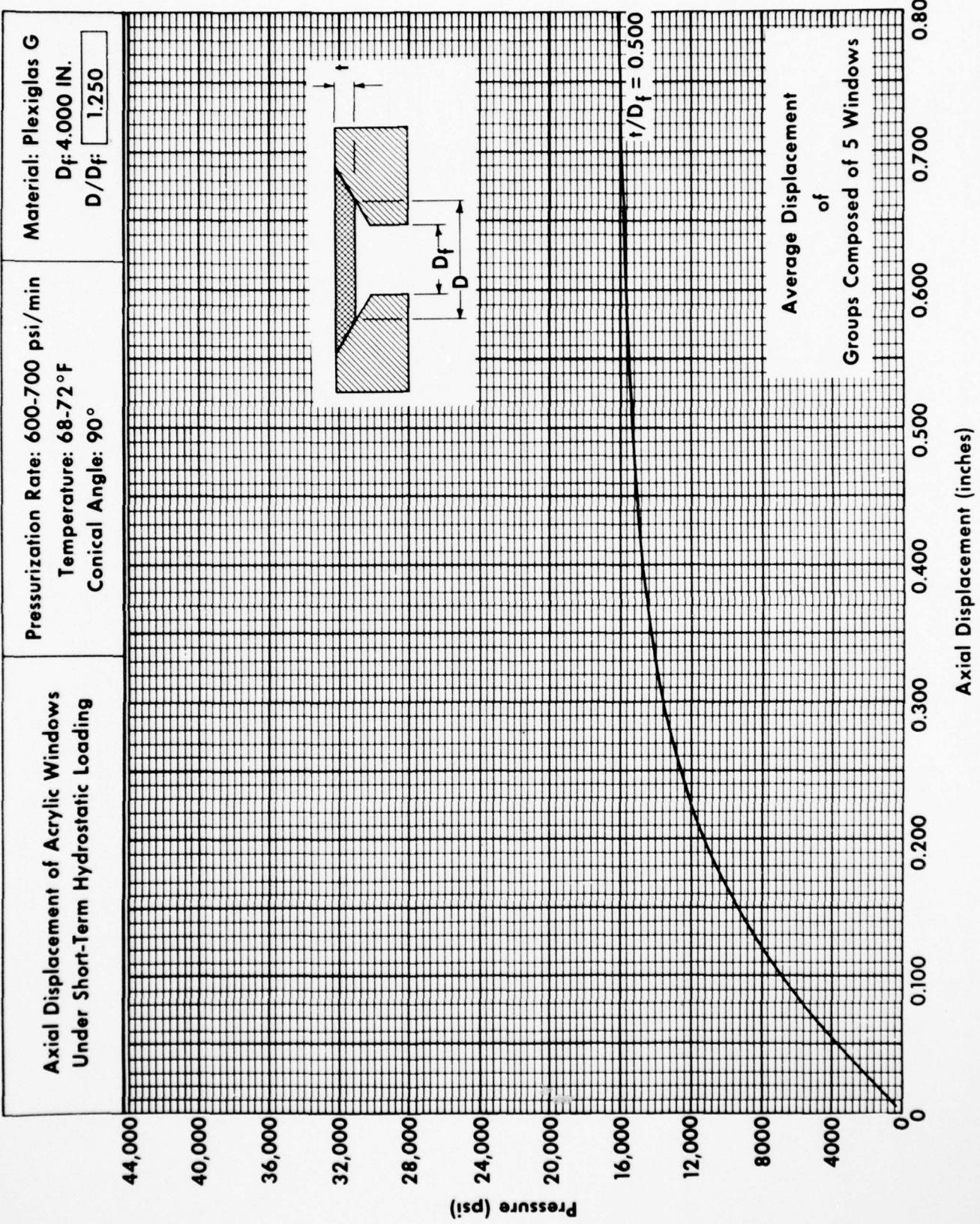


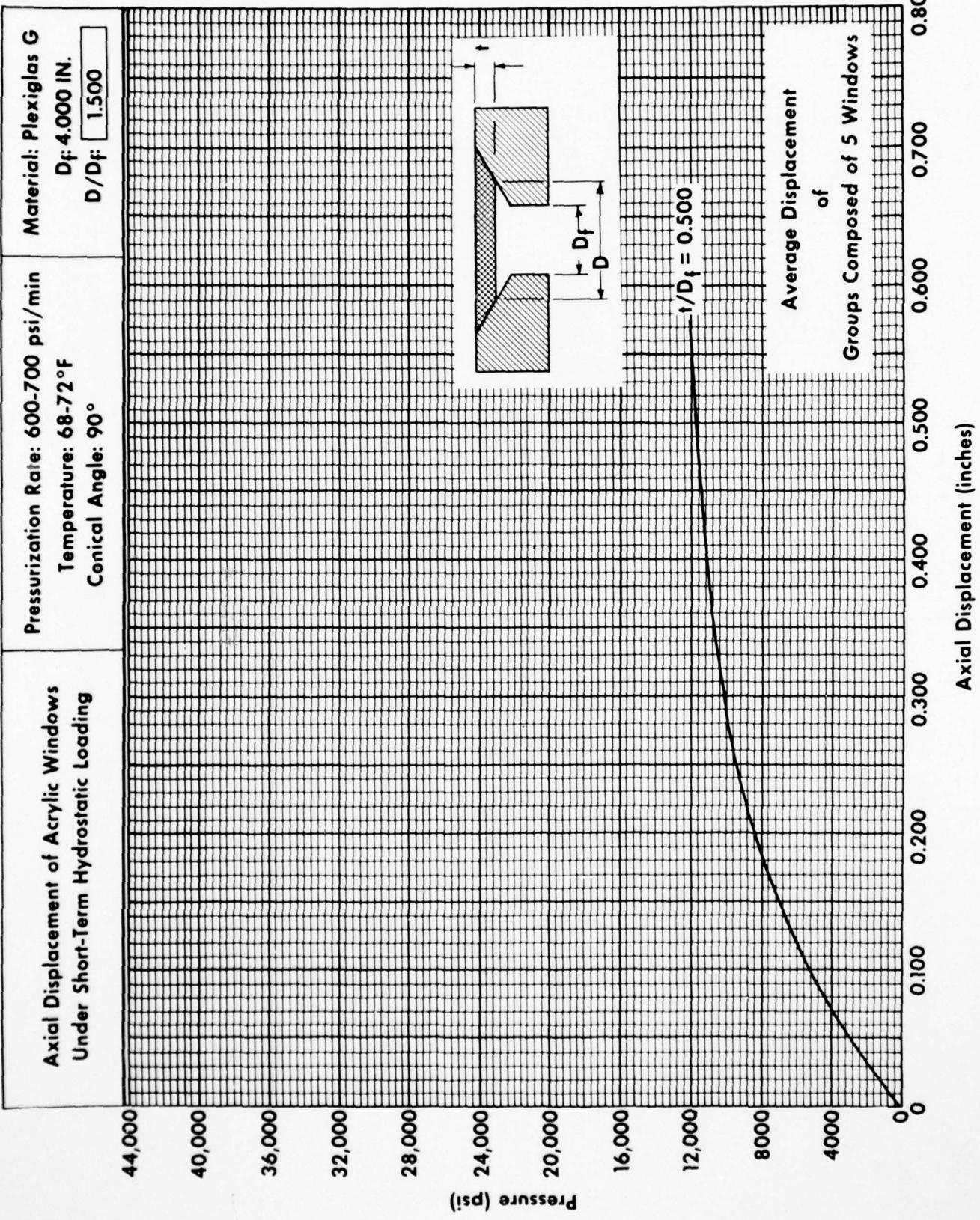


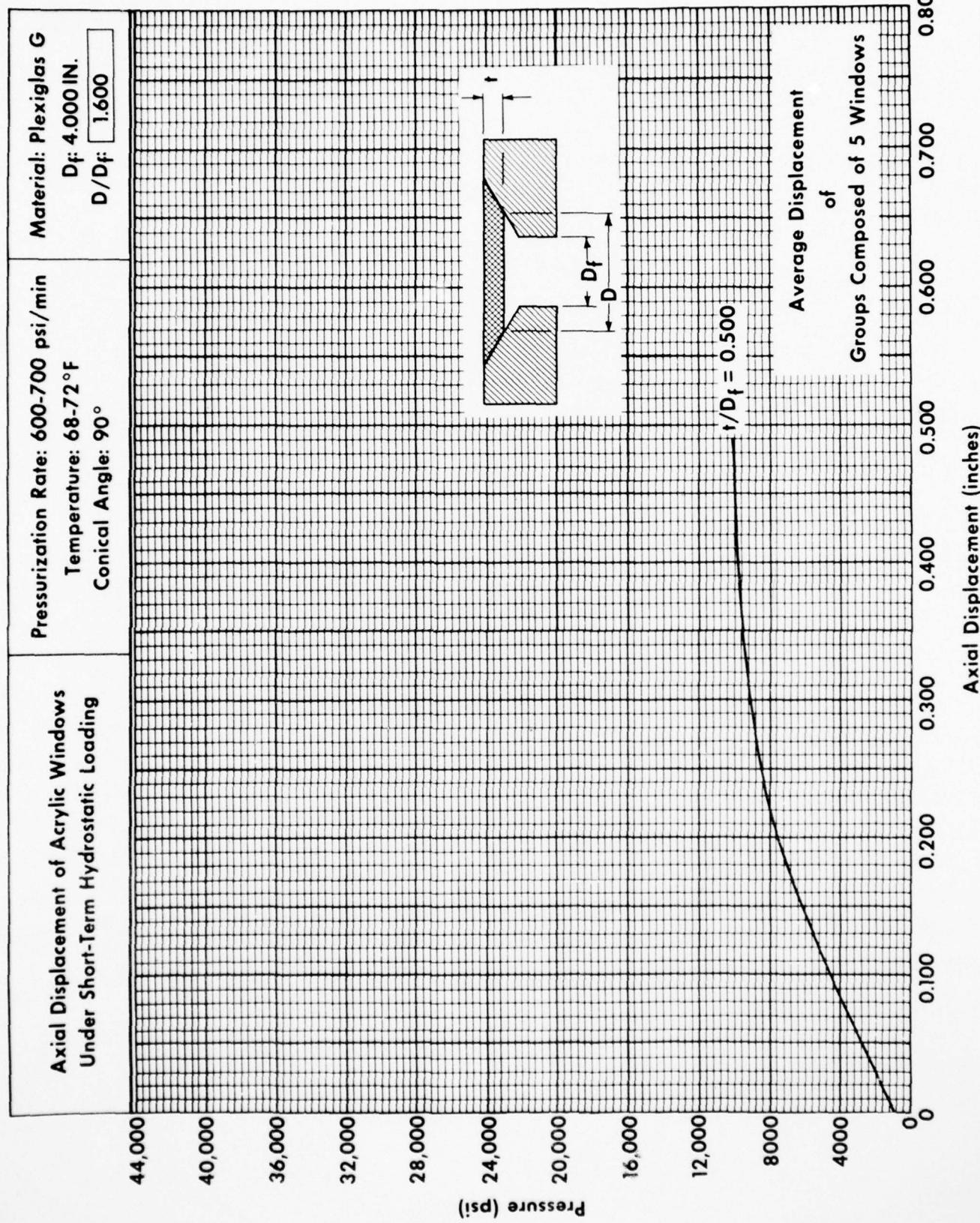


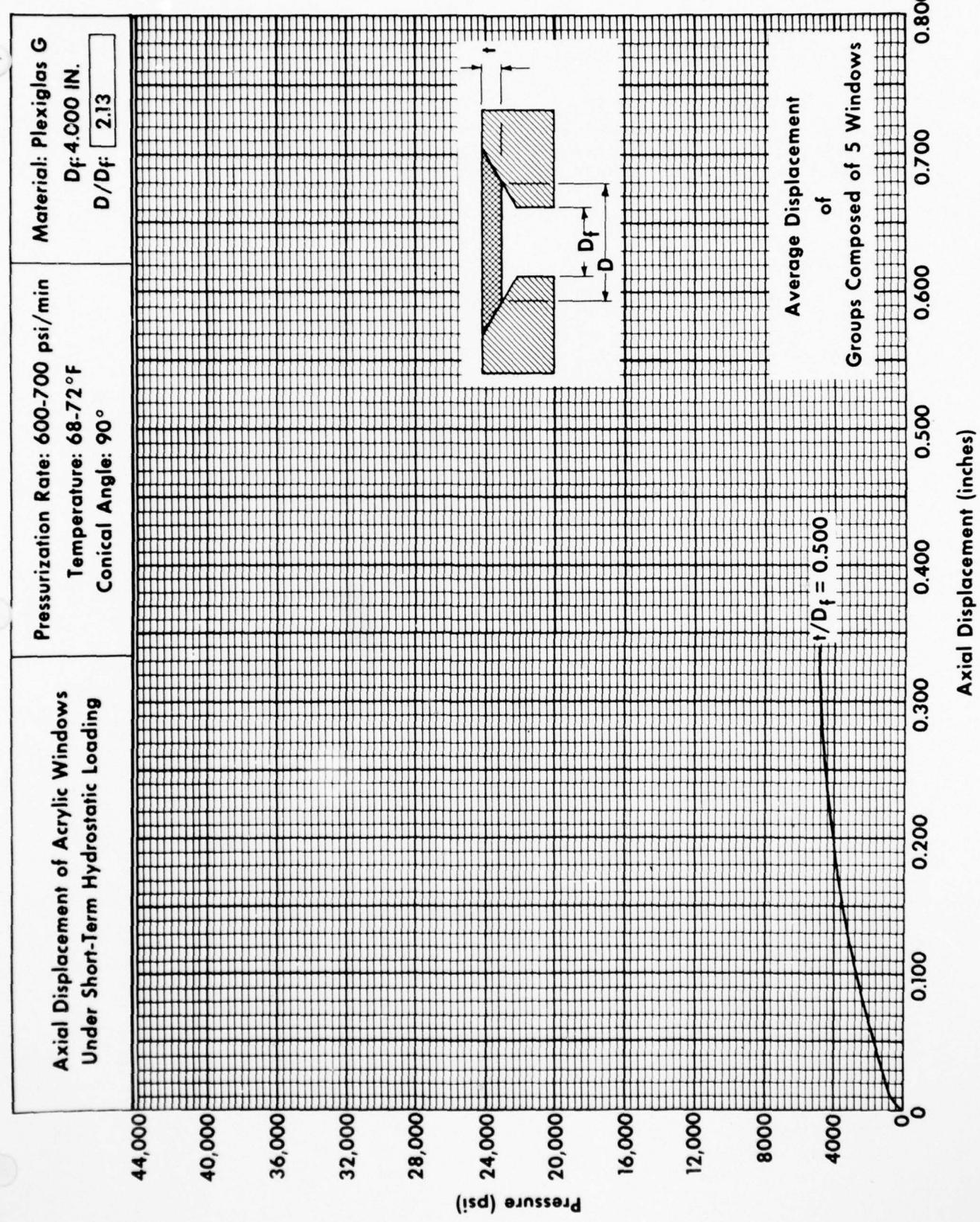












## B.2 LONG-TERM PRESSURE LOADING

Long-term pressure loading consisted of pressurizing the viewport assembly at a rate of 650 pounds per square inch (4.48 megapascals) per minute to the desired pressure, holding it for 1000 hours, and then depressurizing to 0 pound per square inch (0 megapascals). The windows were subsequently inspected for cracks, measured for permanent deformation, and photographed. Most tests were performed with model-scale windows at room temperature in mountings with  $D_i/D_f = 1.0$ .

The axial displacements of model-scale windows can be used to predict the displacement of full-scale windows, if the displacements of the model-scale windows are multiplied by a ratio of the full-scale to model-scale window diameters. Because the test data were generated at room temperature, they are directly applicable only to operational conditions at room temperature. For operational temperatures below room temperature, the displacement data for a given long-term pressure loading become very conservative, as there is a significant decrease in displacement and permanent deformation at lower temperatures. For temperatures above room temperature, the displacement data cannot be safely used. However, for temperatures up to 120°F (49°C), it is feasible to use existing room-temperature data for estimating displacements, if the operational pressures for which the displacements are sought are multiplied by a factor of 1.5. Thus, for example, to estimate the displacements of conical frustums at 120°F (49°C) under 3333-, 6666-, and 13,333-pound-per-square-inch (22.9, 45.9, and 91.9 megapascals) long-term pressure loading, the experimental displacements at room temperature under 5000-, 10,000-, and 20,000-pound-per-square-inch (34.4, 68.9, and 137.9 megapascals) long-term pressure loading are used.

Because all long-term displacement data have been generated in mountings with  $D_i/D_f = 1.0$ , they are directly applicable only to operational viewports with  $D_i/D_f = 1.0$ . Since operational viewports have mountings with  $D_i/D_f > 1.0$ , the data are conservative in operational applications, as window displacements in operational viewports are somewhat less than those shown in this appendix for conical frustums.

The primary operational application for long-term displacement data is to serve as the basis for the selection of  $D_i/D_f$  ratios in the design of mountings for conical frustums to be used as windows in pressure-resistant viewports. The magnitude of the  $D_i/D_f$  ratio is generally established by following this procedure:

a. Determine from the operational scenario, the maximum operational pressure and the predicted duration of its application. Multiply the predicted value of maximum operational pressure by at least a factor of 2, and use it to find the maximum axial displacement.

b. Select the window's  $t/D_i$  on the basis of maximum operational pressure, maximum operational temperature, maximum duration of operational pressure, and desirable cyclic fatigue life. If the maximum operational pressure  $\leq 20,000$  pounds per square inch (137.9 megapascals), maximum operational temperature  $\leq 151^\circ\text{F}$  (66°C), the cyclic fatigue life at maximum pressure  $\leq 10,000$  cycles, the design criteria in section 15 should be used to determine a safe  $t/D_i$  ratio. If any of the operational parameters exceed these limits, the designer must select the  $t/D_i$  ratio on the basis of a thorough study of all structural and operational variables affecting the life of the acrylic plastic window.

c. Find the maximum axial displacement from experimental data generated at 5000-, 10,000-, and 20,000-pound-per-square-inch (34.4, 68.9, and 137.9 megapascals) long-term pressure loadings. If the maximum operational pressure differs from any pressures used to generate the experimental data in appendix B, interpolation must be used to find the maximum predicted axial displacement under long-term loading.

d. Select the minimum value of the  $D_i/D_f$  ratio on the basis of providing the conical frustum with radial support when it is at its maximum calculated axial displacement during the maximum duration of the long-term loading. The relationship between the maximum predicted axial displacement of the window and the  $D_f$  in the ratio is expressed as:

$$D_f = D_i - 2L \tan \frac{\alpha}{2} , \quad (B1)$$

where

$D_i$  = nominal minor diameter of conical frustum

$D_f$  = nominal minor diameter of the conical seat in the window mounting

$L$  = maximum predicted axial displacement

$\alpha$  = included angle of the conical frustum.

If the calculated value of  $D_i/D_f$  is smaller than the value shown in section 15, the larger value must be used in the design of the window mounting seat.

e. If the  $D_i/D_f$  ratio chosen for the window mounting is too small, during operation of the pressure vessel at maximum pressure and duration of loading the minor diameter of the window will extend beyond the minor diameter of the seat in the mounting. This is not a cause for immediate alarm as catastrophic failure will not occur unless the length of unsupported extrusion is very great, as a rule in excess of at least 50 percent of the nominal window thickness. Still, even if the window is not in imminent danger of catastrophic failure, the situation should be remedied by redesign. If not redesigned, the portion of the window extending past the minor diameter of the flange seat will exhibit crazing, minor cracking, and a cylindrical deformation that will significantly decrease the cyclic fatigue life of the window.

AD-A070 537

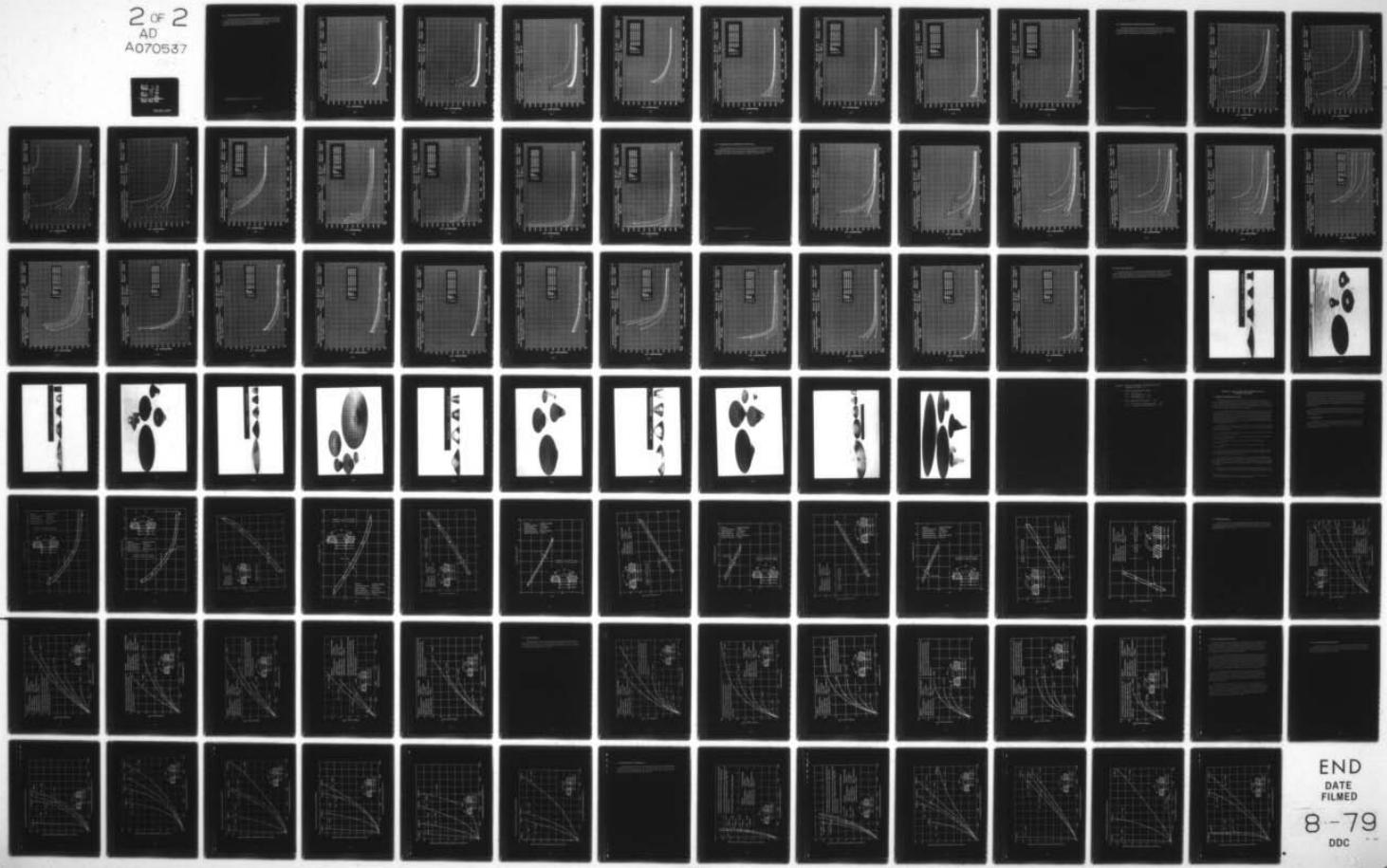
NAVAL UNDERSEA CENTER SAN DIEGO CA  
ACRYLIC PLASTIC VIEWPORTS FOR OCEAN ENGINEERING APPLICATIONS. A--ETC(U)  
FEB 77 J D STACHW  
NUC-TP-562-APP

F/G 11/9

UNCLASSIFIED

NL

2 OF 2  
AD  
A070537



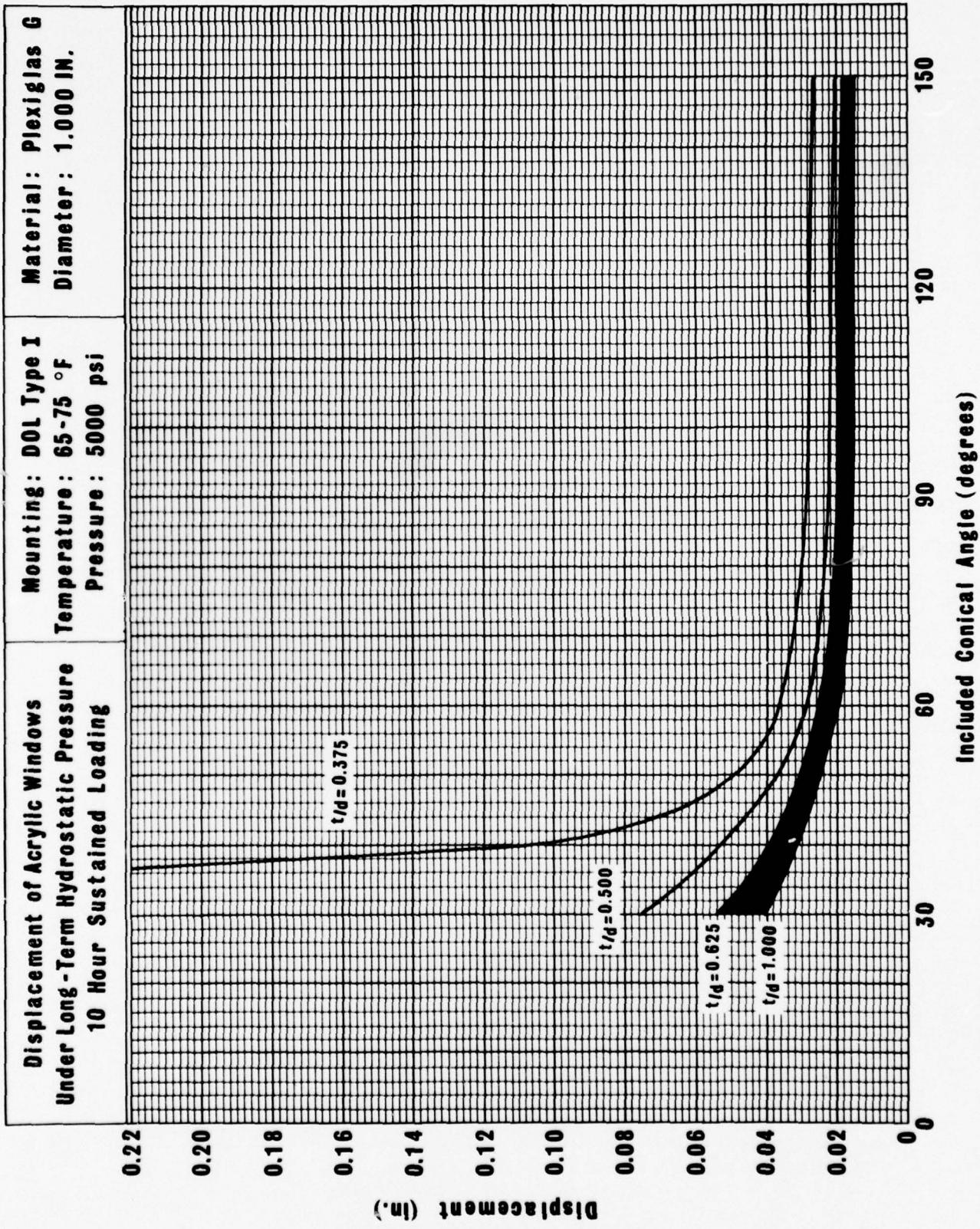
END  
DATE  
FILED  
8-79  
DOC

### B.2.1 Axial Displacements (5000 Pounds Per Square Inch)

The data in this section are concerned with the axial displacements of conical frustums with included angles of 30, 60, 90, 120, and 150 degrees (0.5, 1.04, 1.57, 2.09, and 2.6 radians) under long-term pressure loading at 5000 pounds per square inch (34.4 megapascals) at ambient room temperature in mountings with  $D_i/D_f = 1.0$ .\*

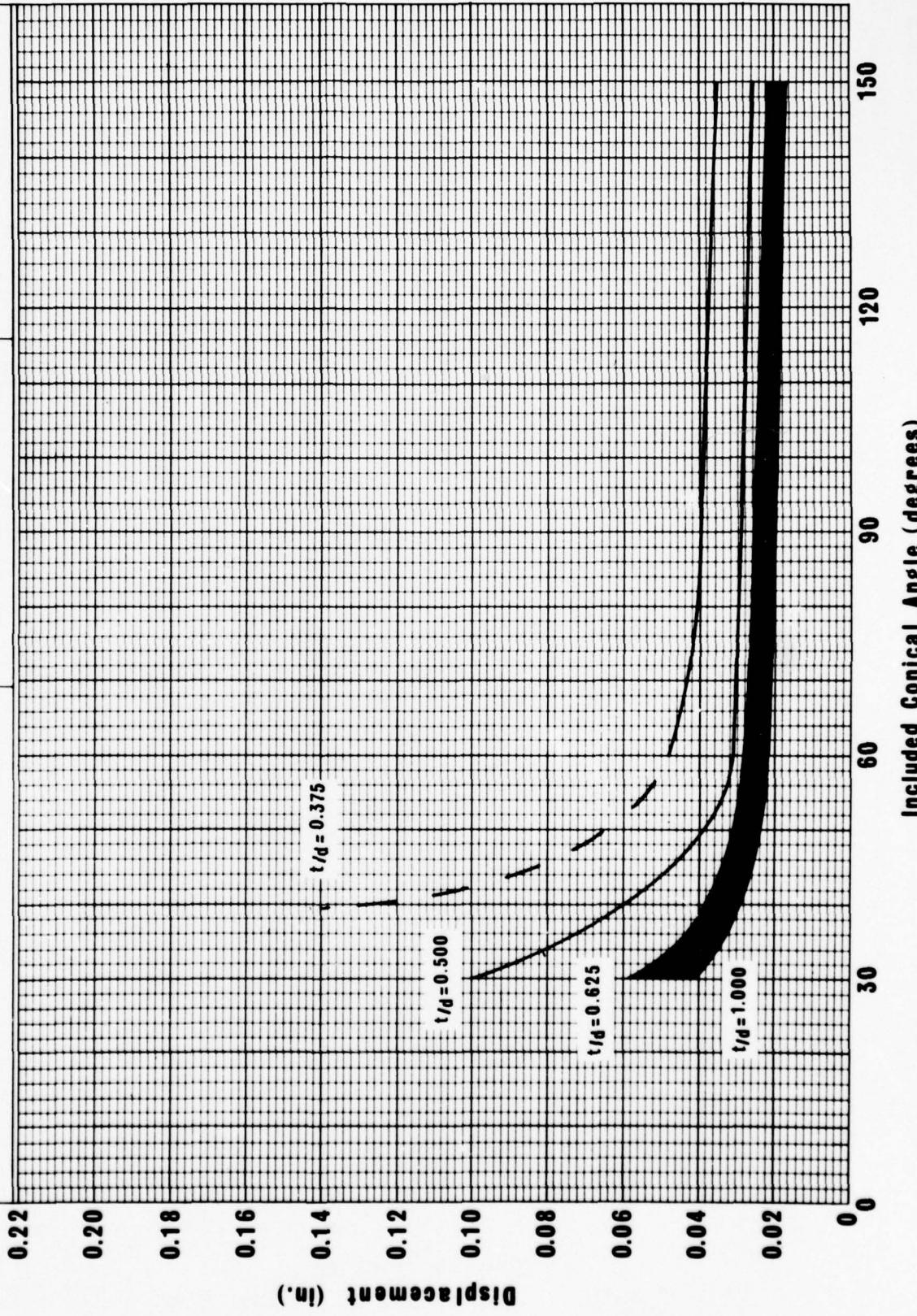
---

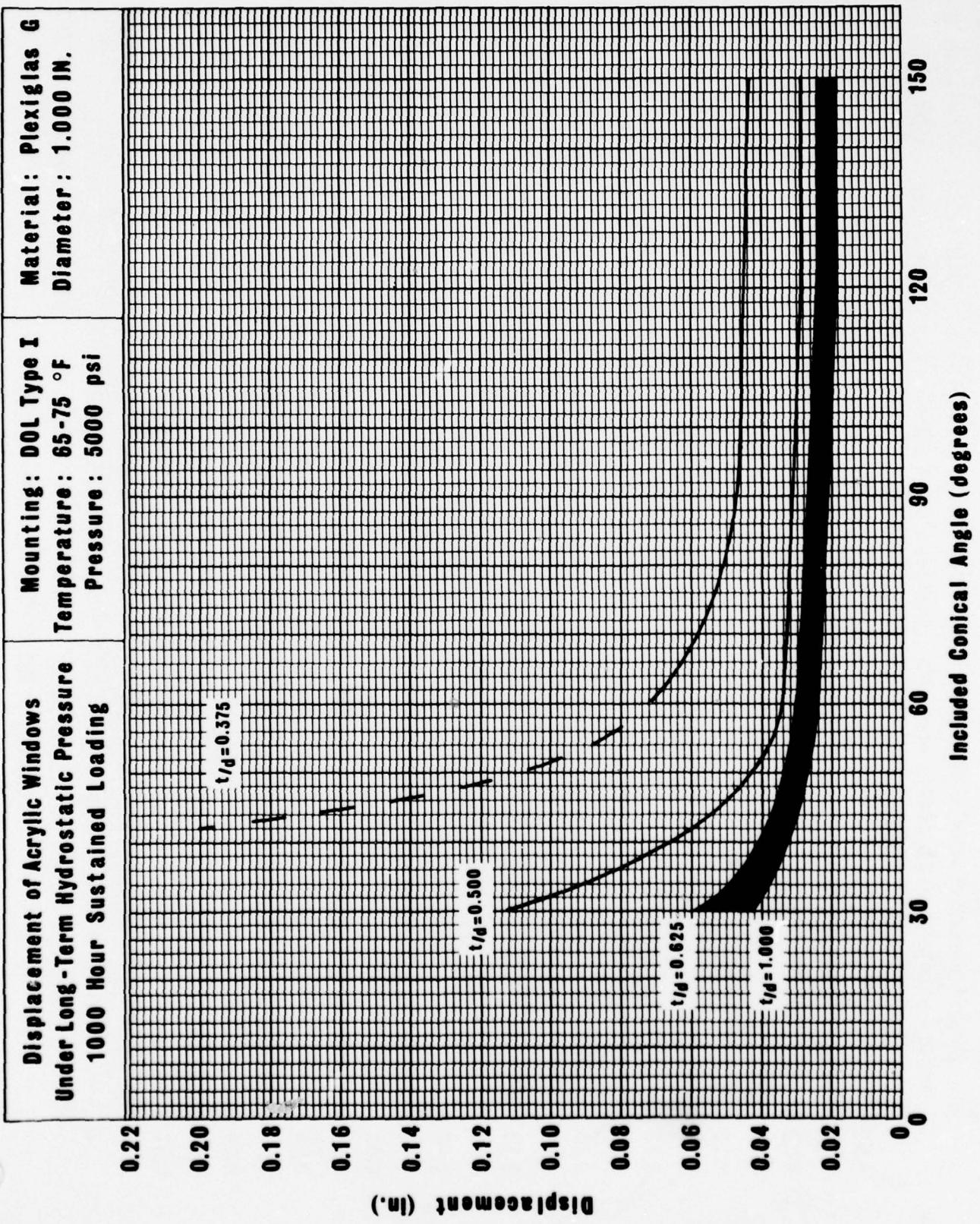
\*On many figures in this appendix  $D_i$  is noted as D or d, thus  $t/D_i = t/D = t/d$ .



**Displacement of Acrylic Windows  
Under Long - Term Hydrostatic Pressure  
100 Hour Sustained Loading**

**Mounting: DOL Type I      Material: Plexiglas G  
Temperature: 65-75 °F      Diameter: 1.000 IN.  
Pressure: 5000 psi**

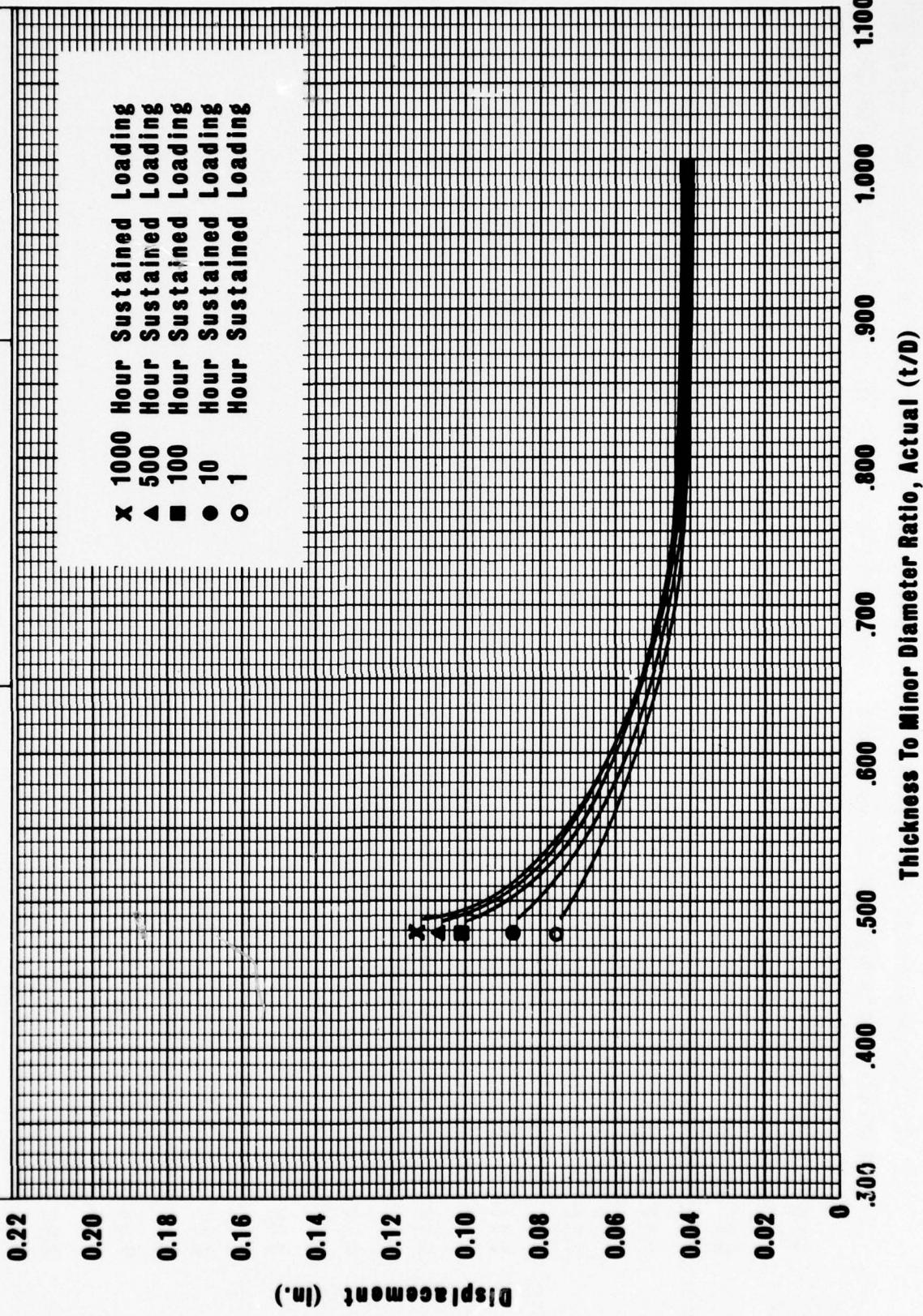




**Displacement of Acrylic Windows  
Under Long - Term Hydrostatic Pressure**  
**30° Cones**

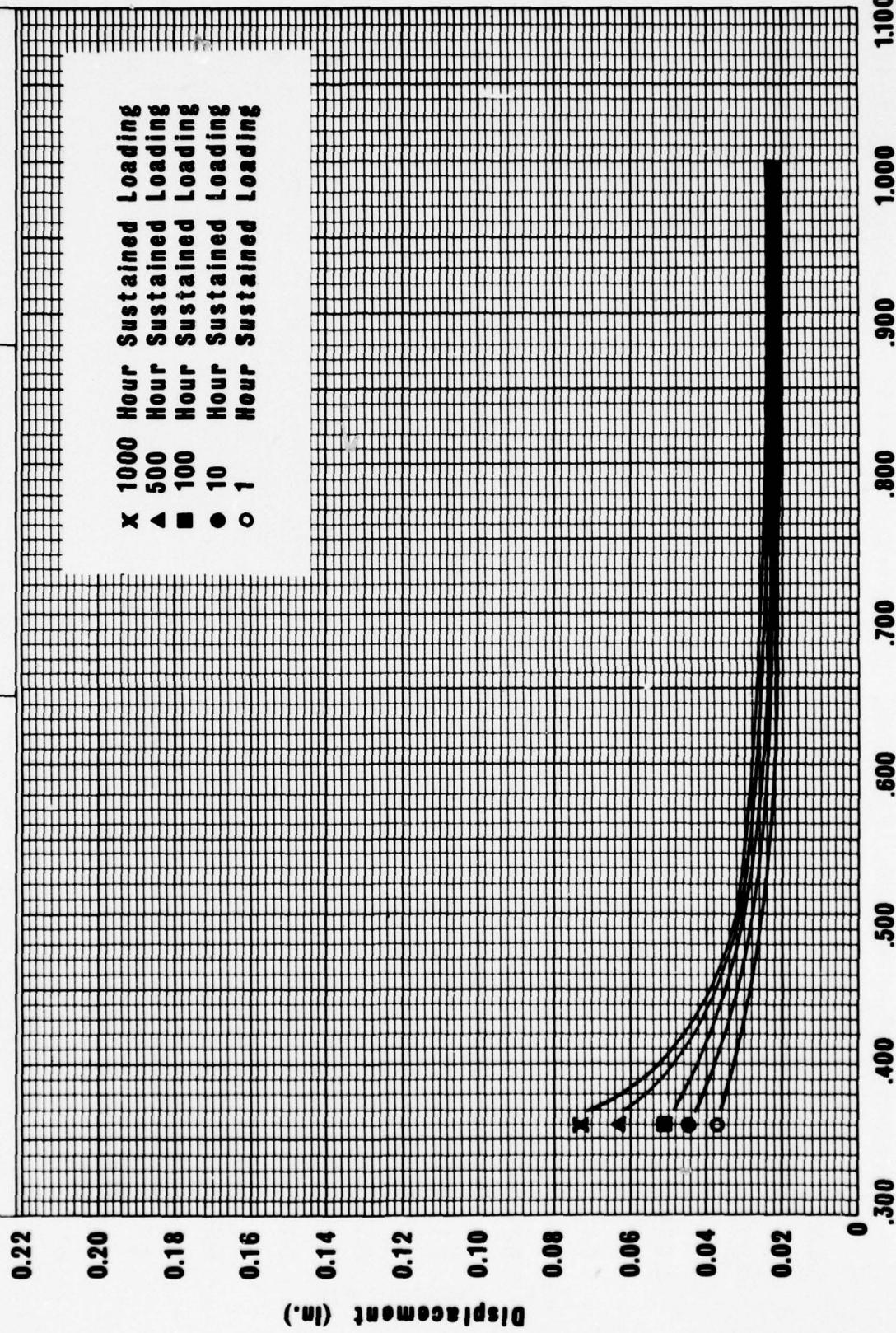
Mounting: DOL Type I  
Temperature: 65-75 °F  
Pressure: 5,000 psi  
Material: Plexiglas G  
Diameter: 1.000 IN.

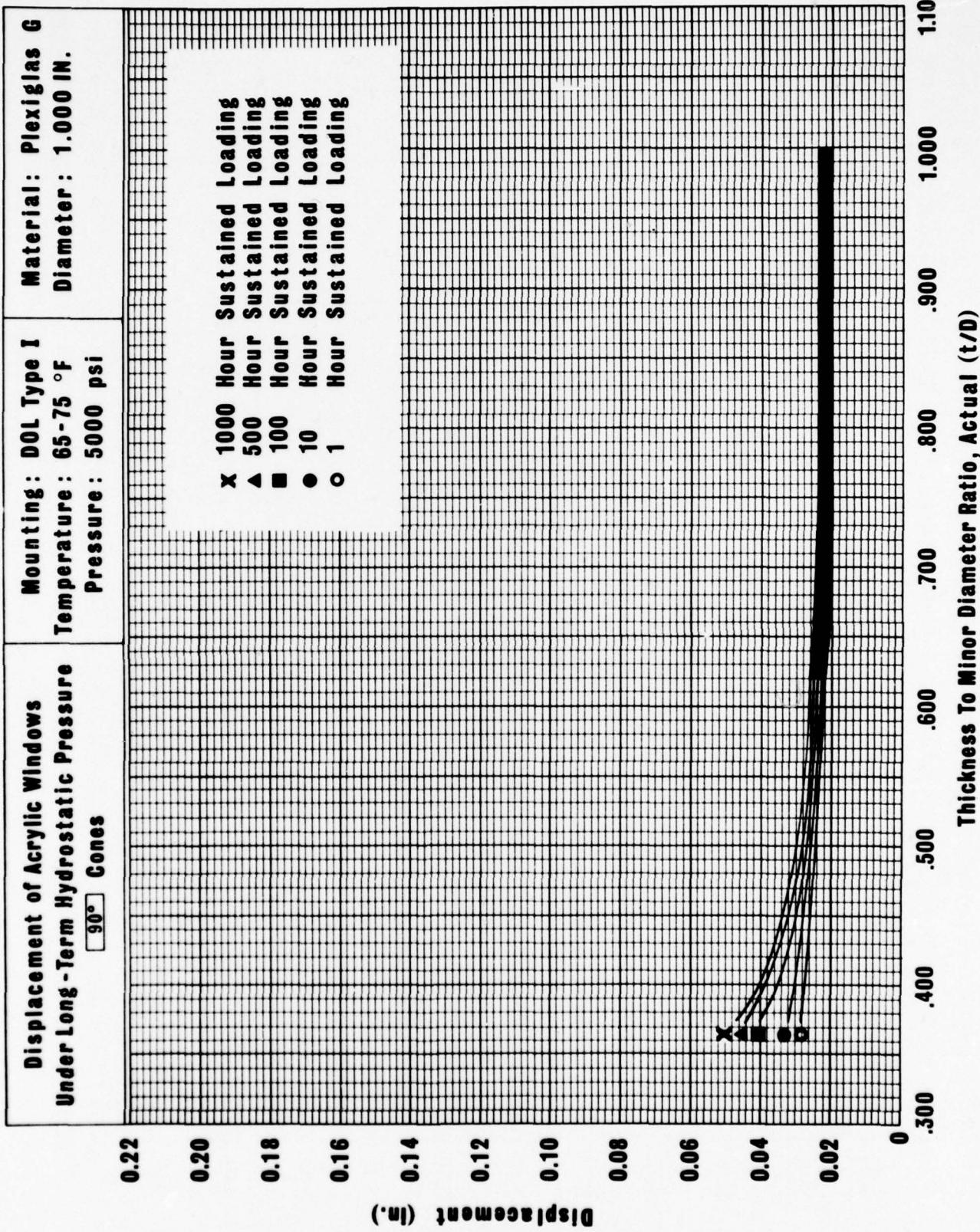
x 1000 Hour Sustained Loading  
▲ 500 Hour Sustained Loading  
■ 100 Hour Sustained Loading  
● 10 Hour Sustained Loading  
○ 1 Hour Sustained Loading

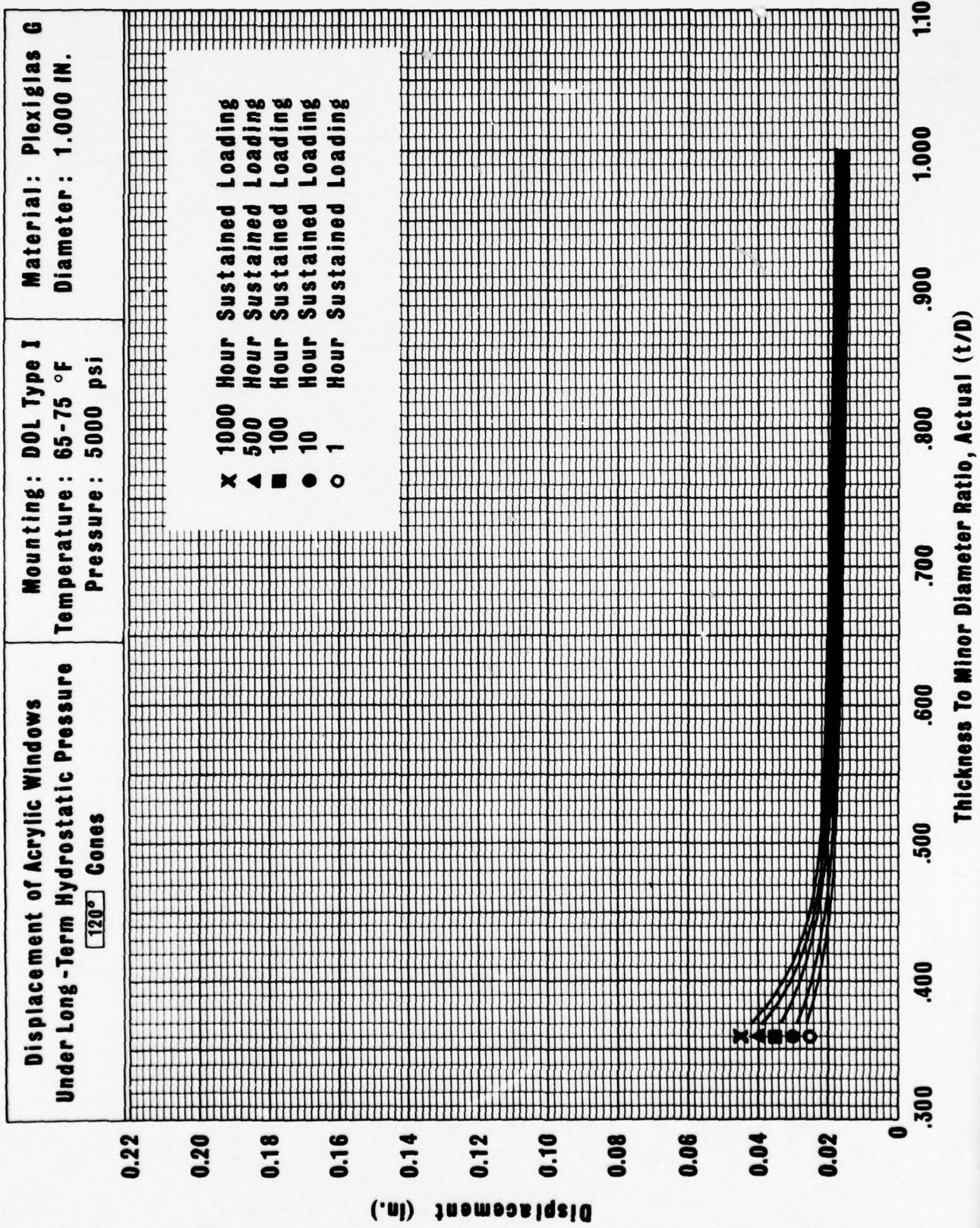


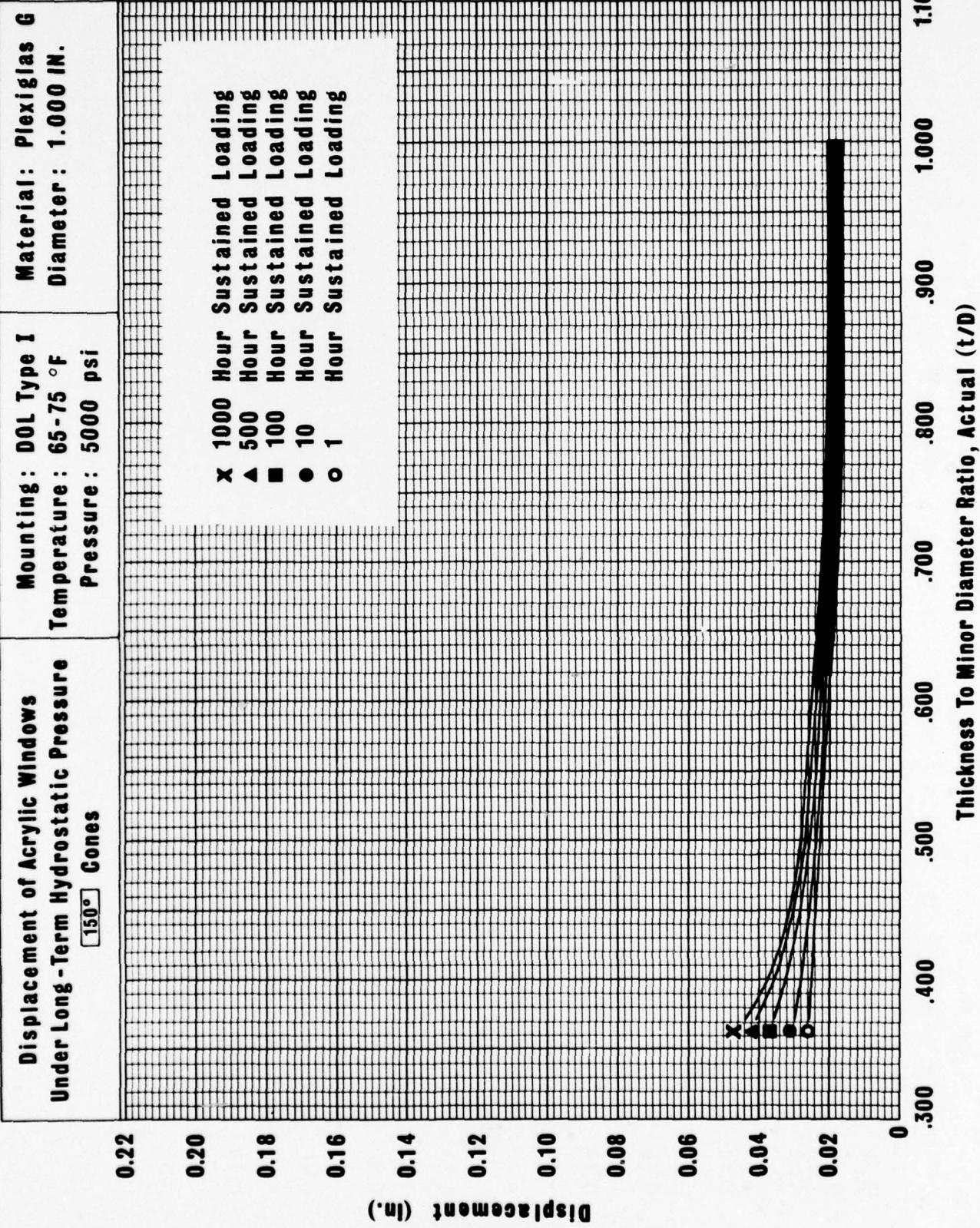
**Displacement of Acrylic Windows  
Under Long-Term Hydrostatic Pressure**  
 **Cones**  
 **60° Cones**

**Mounting:** DOL Type I    **Material:** Plexiglas G  
**Temperature:** 65-75 °F    **Diameter:** 1.000 IN.









### B.2.2 Axial Displacements (10,000 Pounds Per Square Inch)

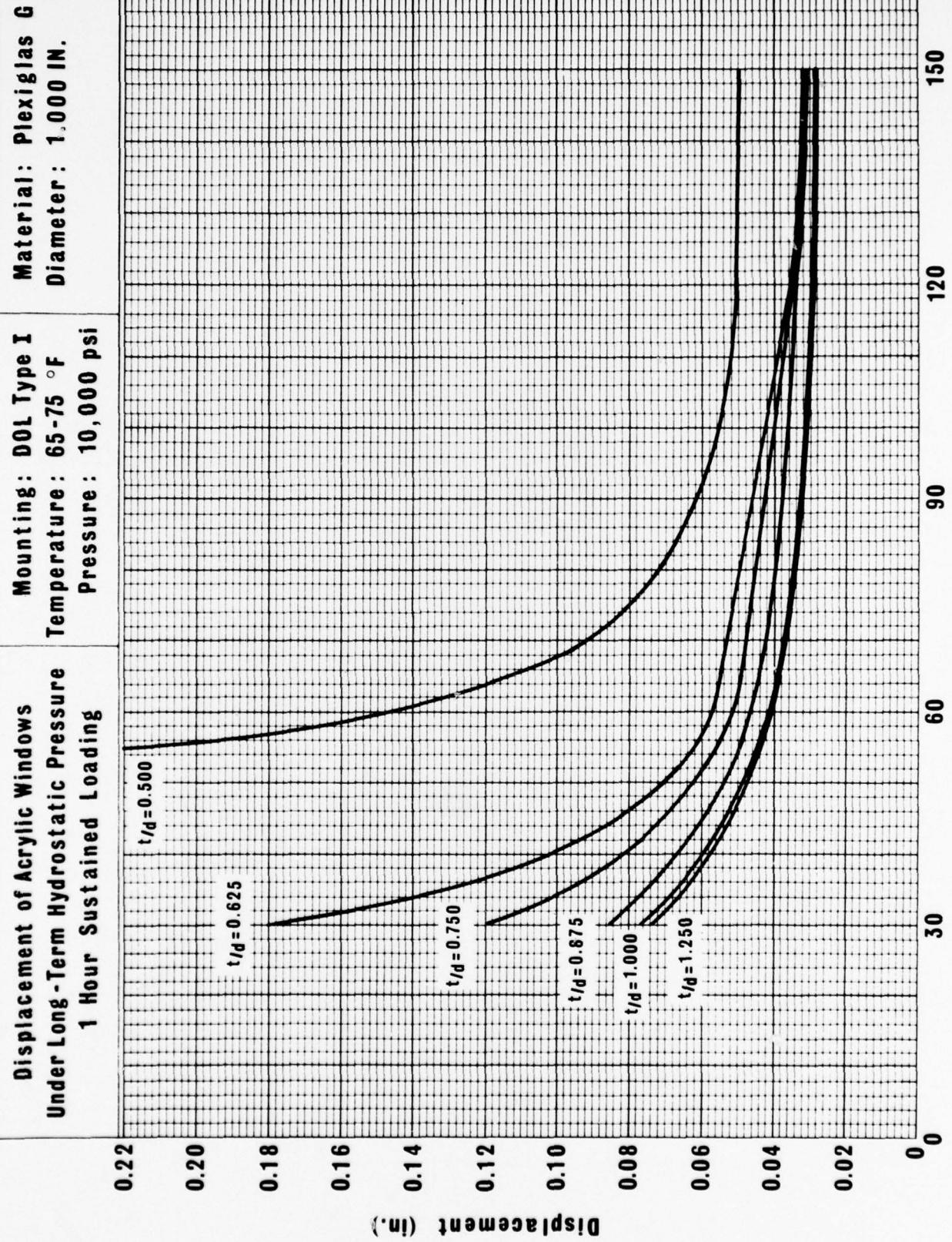
The data in this section are concerned with the axial displacements of conical frustums with included angles of 30, 60, 90, 120, and 150 degrees (0.5, 1.04, 1.57, 2.09, and 2.6 radians) under long-term pressure loading at 10,000 pounds per square inch (68.9 megapascals) at ambient room temperature in mountings with  $D_i/D_f = 1.0$ .\*

---

\*On many figures in this appendix  $D_i$  is noted as D or d, thus  $t/D_i = t/D = t/d$ .

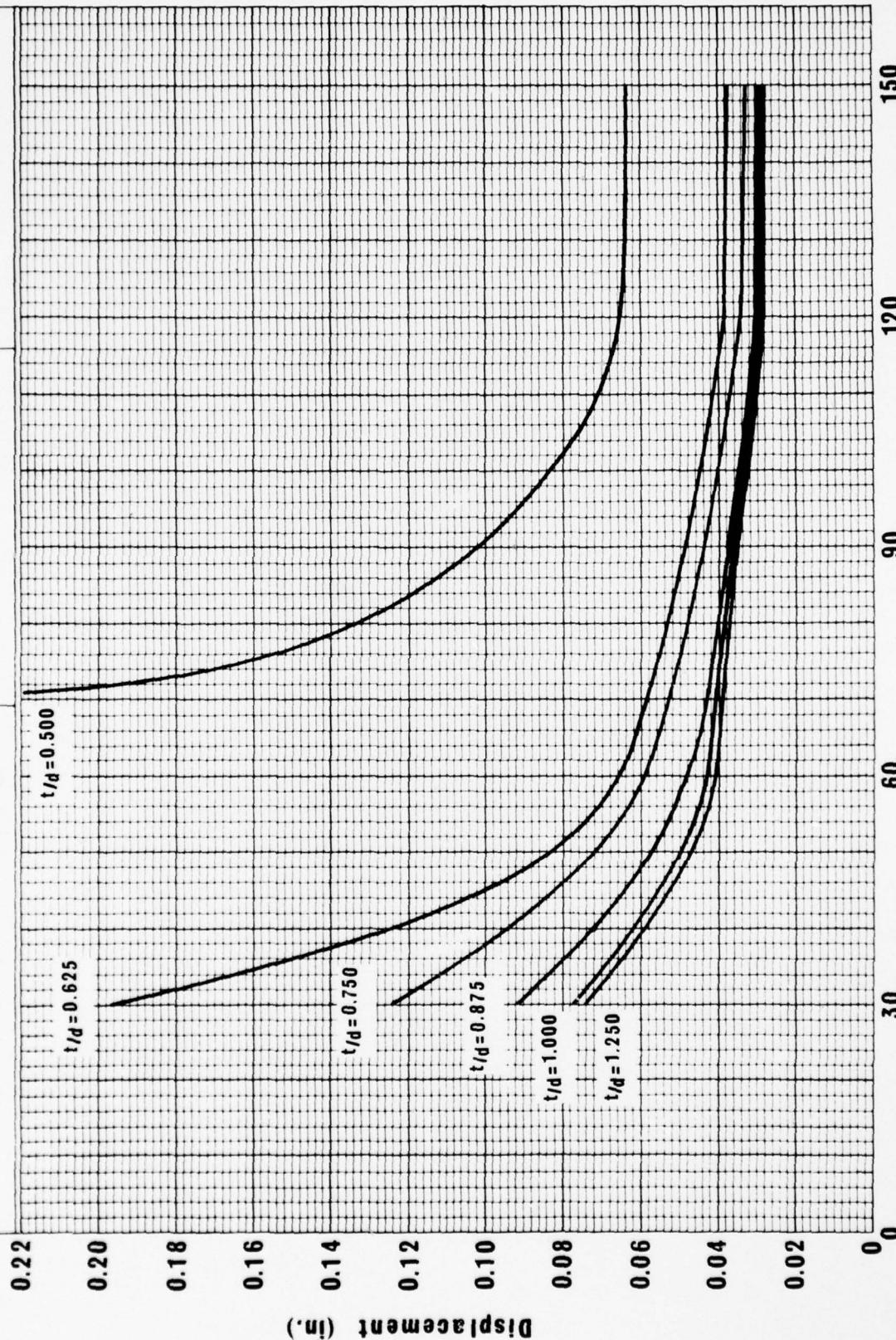
**Displacement of Acrylic Windows  
Under Long-Term Hydrostatic Pressure  
1 Hour Sustained Loading**

**Mounting: DOL Type I  
Temperature: 65-75 °F  
Pressure: 10,000 psi**



**Displacement of Acrylic Windows  
Under Long - Term Hydrostatic Pressure  
10 Hour Sustained Loading**

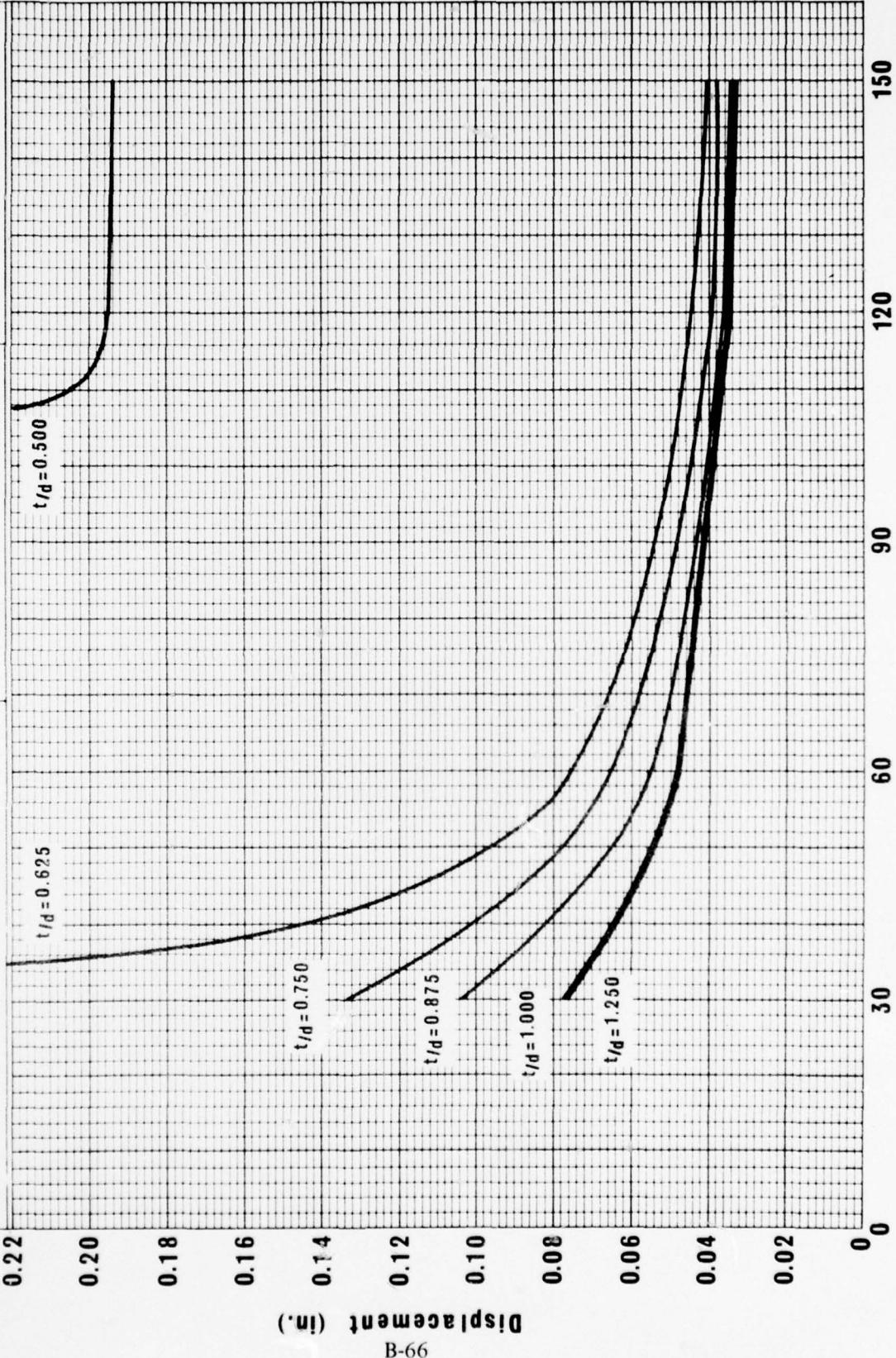
**Mounting:** DOL Type I      **Material:** Plexiglas G  
**Temperature:** 65-75 °F      **Diameter:** 1.000 IN.  
**Pressure:** 10,000 psi



**Displacement of Acrylic Windows  
Under Long - Term Hydrostatic Pressure  
100 Hour Sustained Loading**

**Mounting : DOL Type I  
Temperature : 65-75 °F  
Pressure : 10,000 psi**

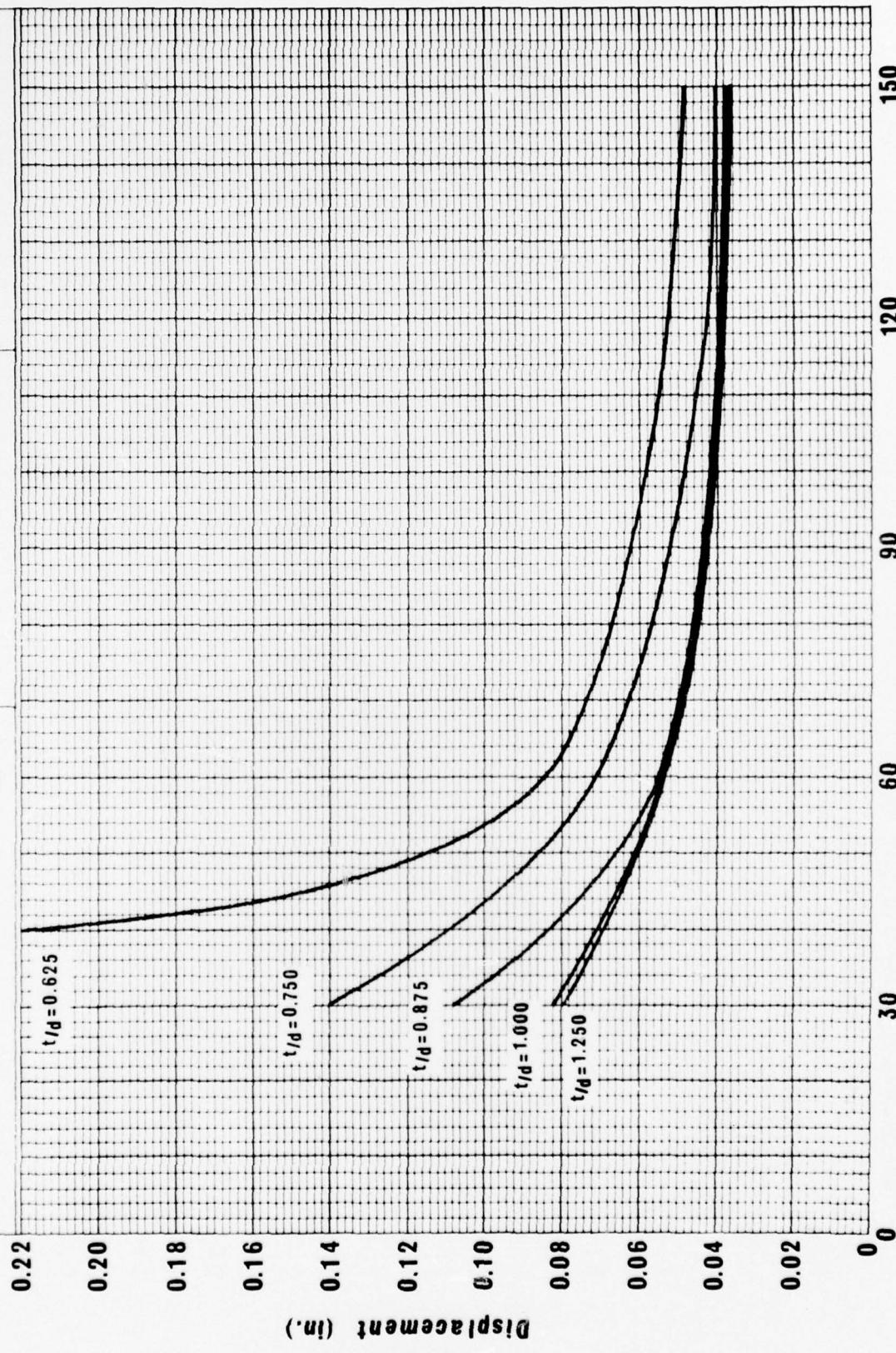
**Material: Plexiglas G  
Diameter: 1.000 IN.**

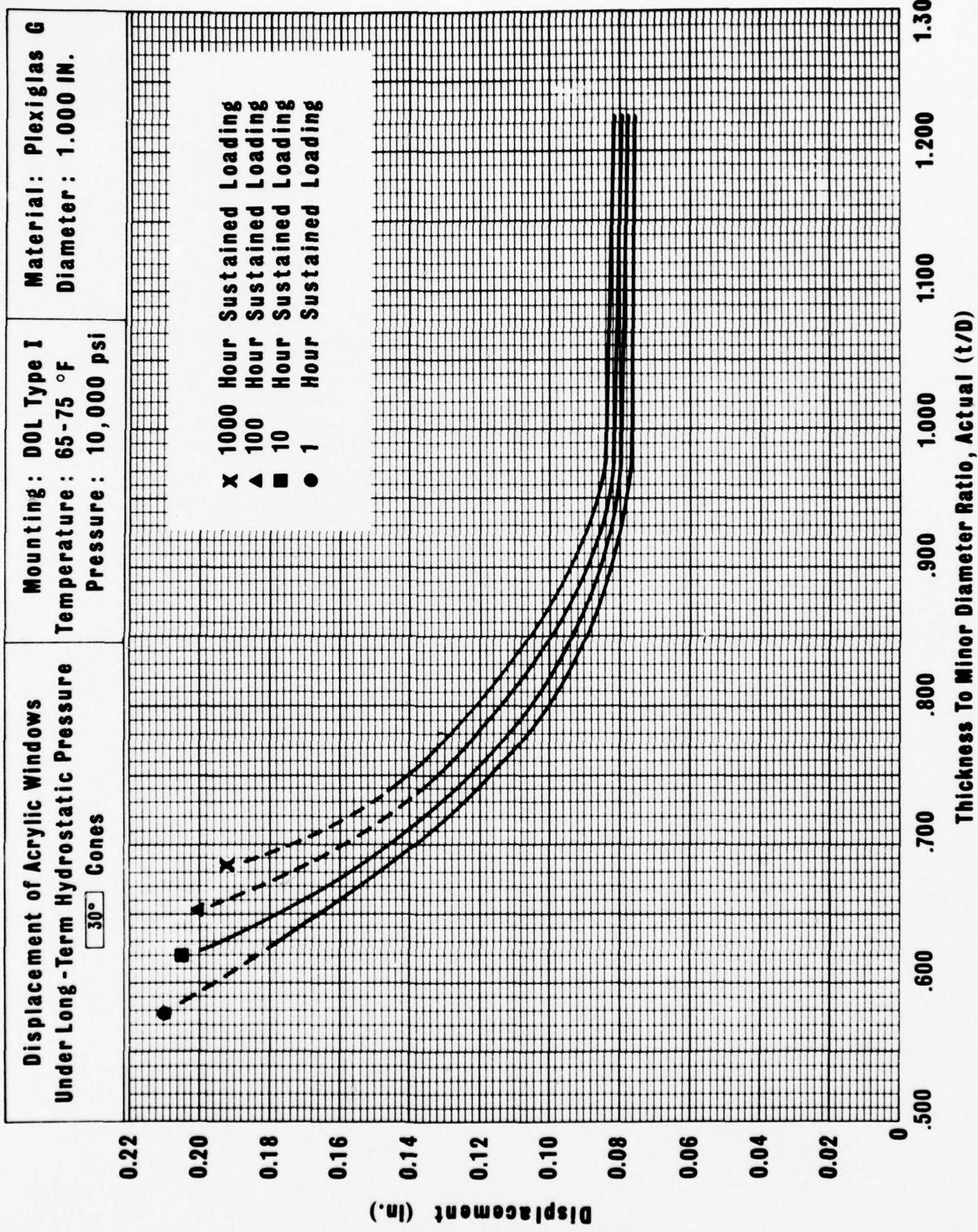


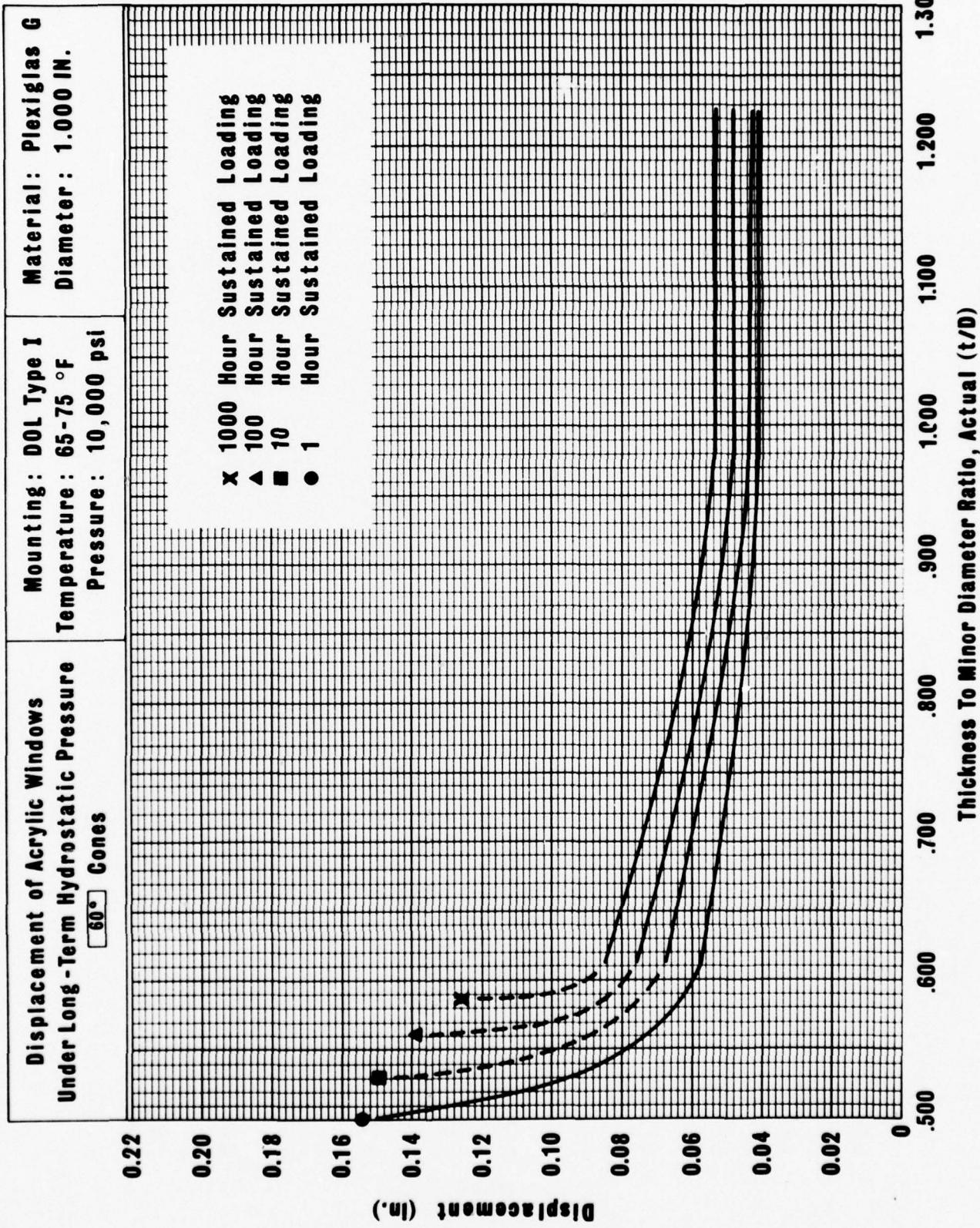
B-66

Displacement of Acrylic Windows  
Under Long-Term Hydrostatic Pressure  
1000 Hour Sustained Loading

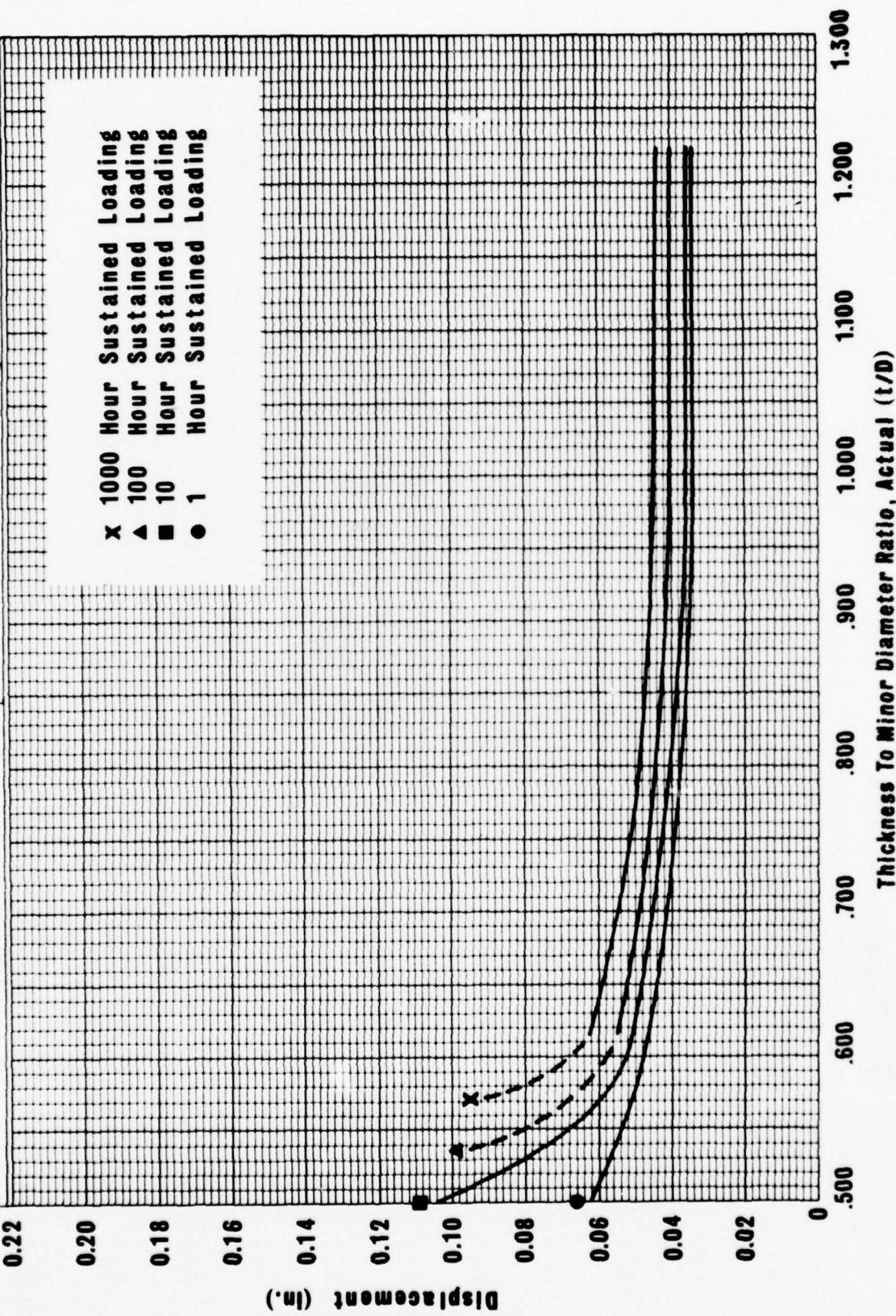
Mounting: DOL Type I  
Temperature: 65-75 °F  
Pressure: 10,000 psi  
Material: Plexiglas G  
Diameter: 1.000 in.

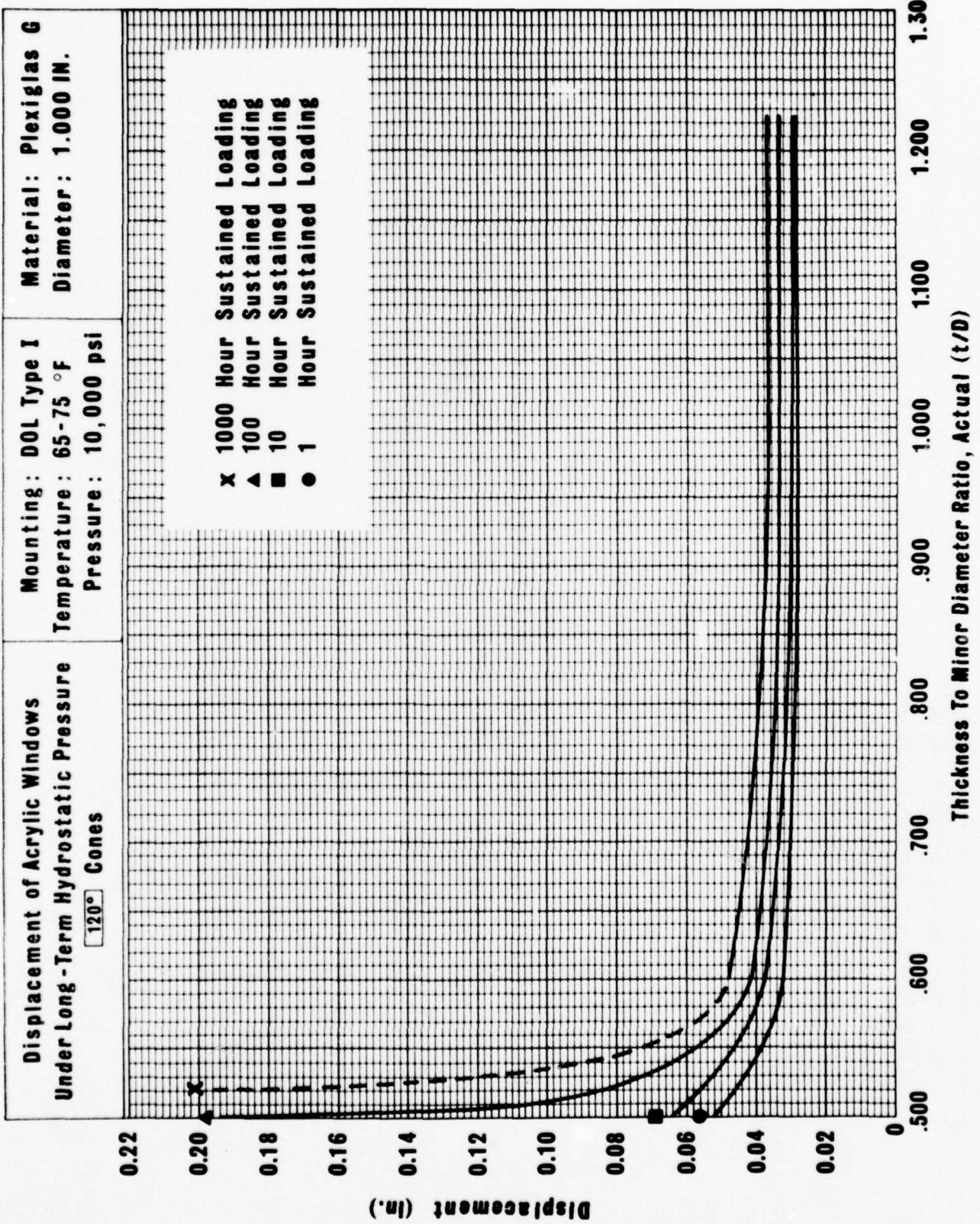


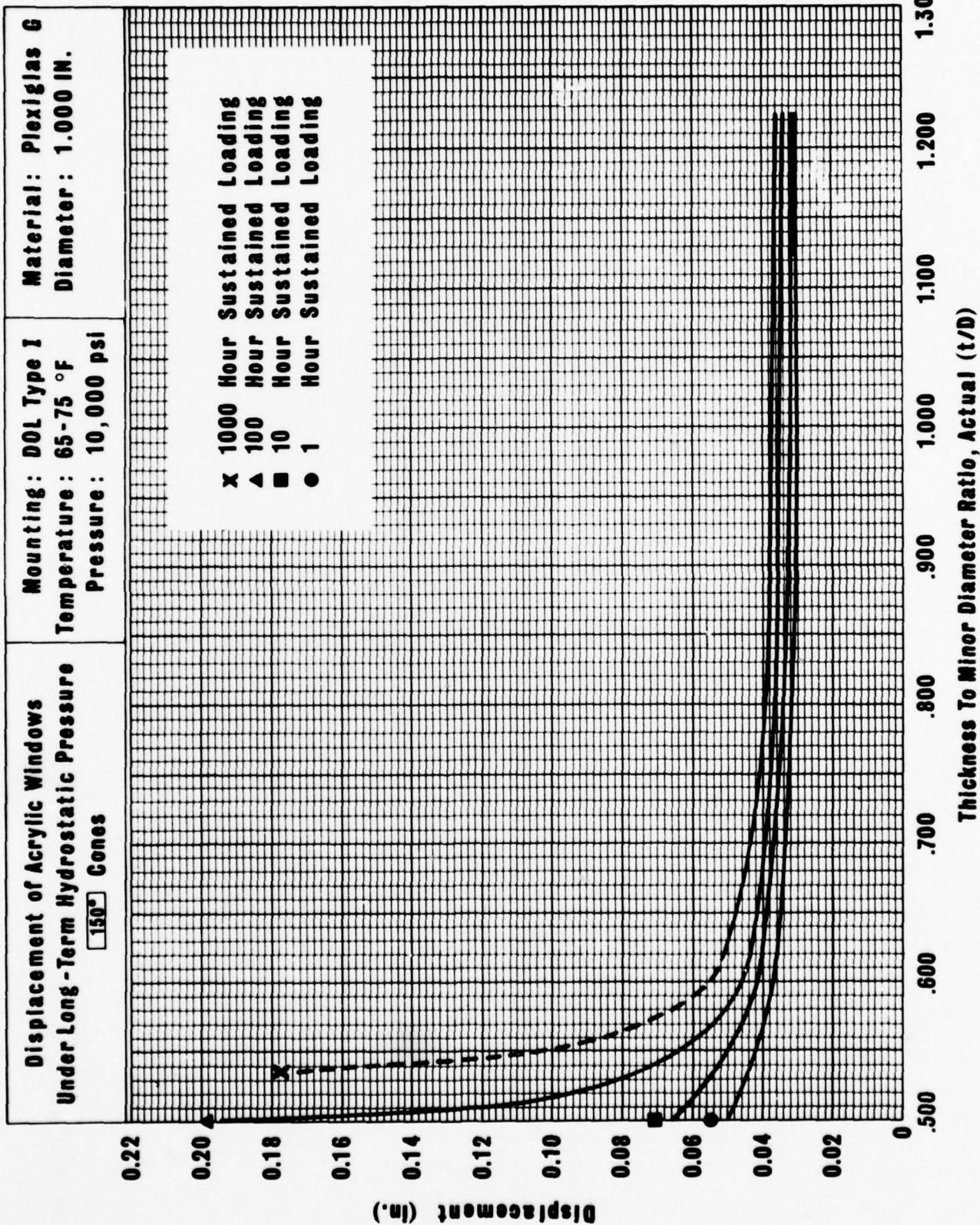




Displacement of Acrylic Windows Under Long-Term Hydrostatic Pressure	Mounting: DOL Type I	Material: Plexiglas G
90° Cones	Temperature: 65-75 °F	Diameter: 1.000 IN.
	Pressure: 10,000 psi	





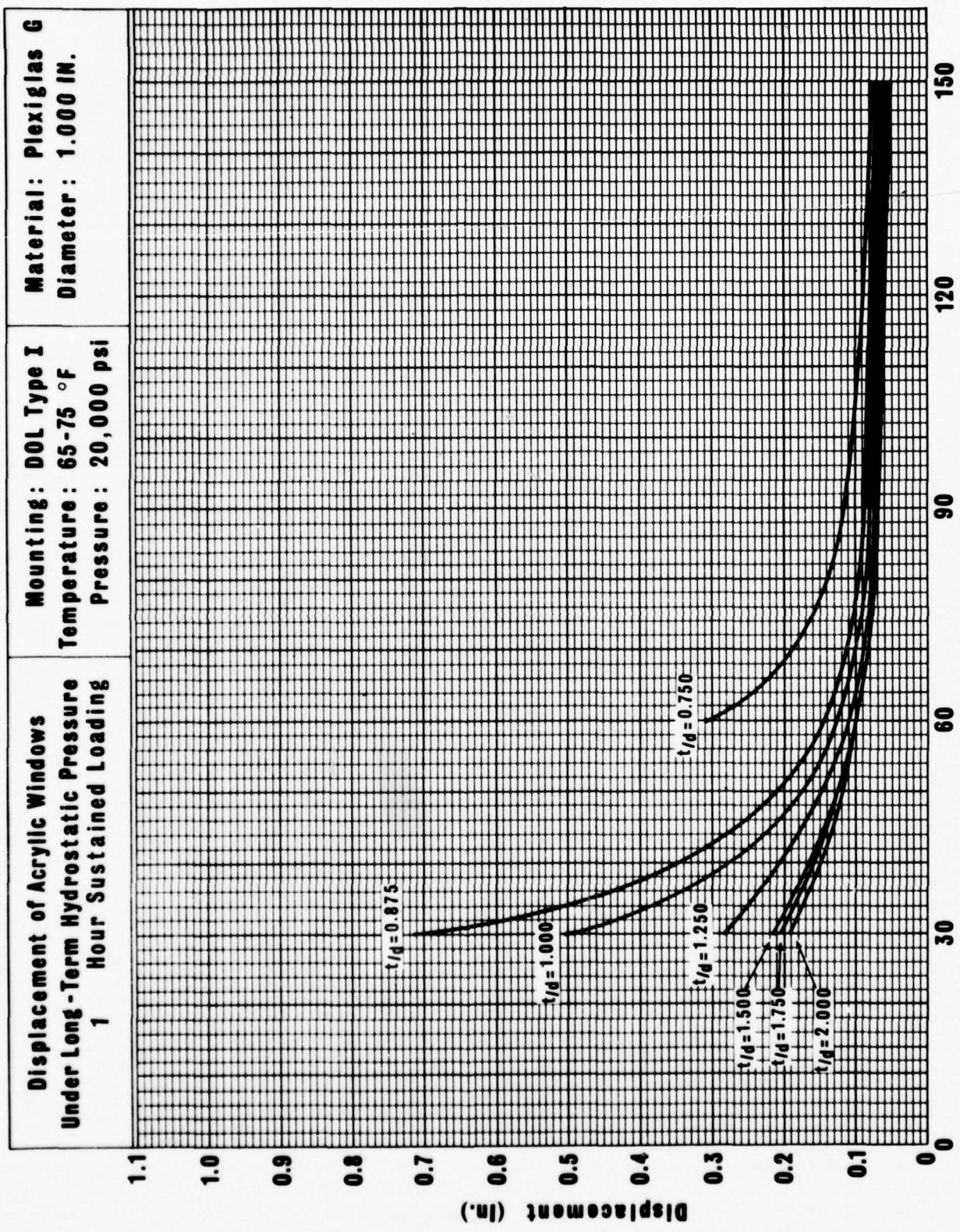


### B.2.3 Axial Displacements (20,000 Pounds Per Square Inch)

The data in this section are concerned with the axial displacements of conical frustums with included angles of 30, 60, 90, 120, and 150 degrees (0.5, 1.04, 1.57, 2.09, and 2.6 radians) under long-term pressure loading at 20,000 pounds per square inch (137.9 megapascals) at ambient room temperature in mountings with  $D_i/D_f = 1.0$ .\*

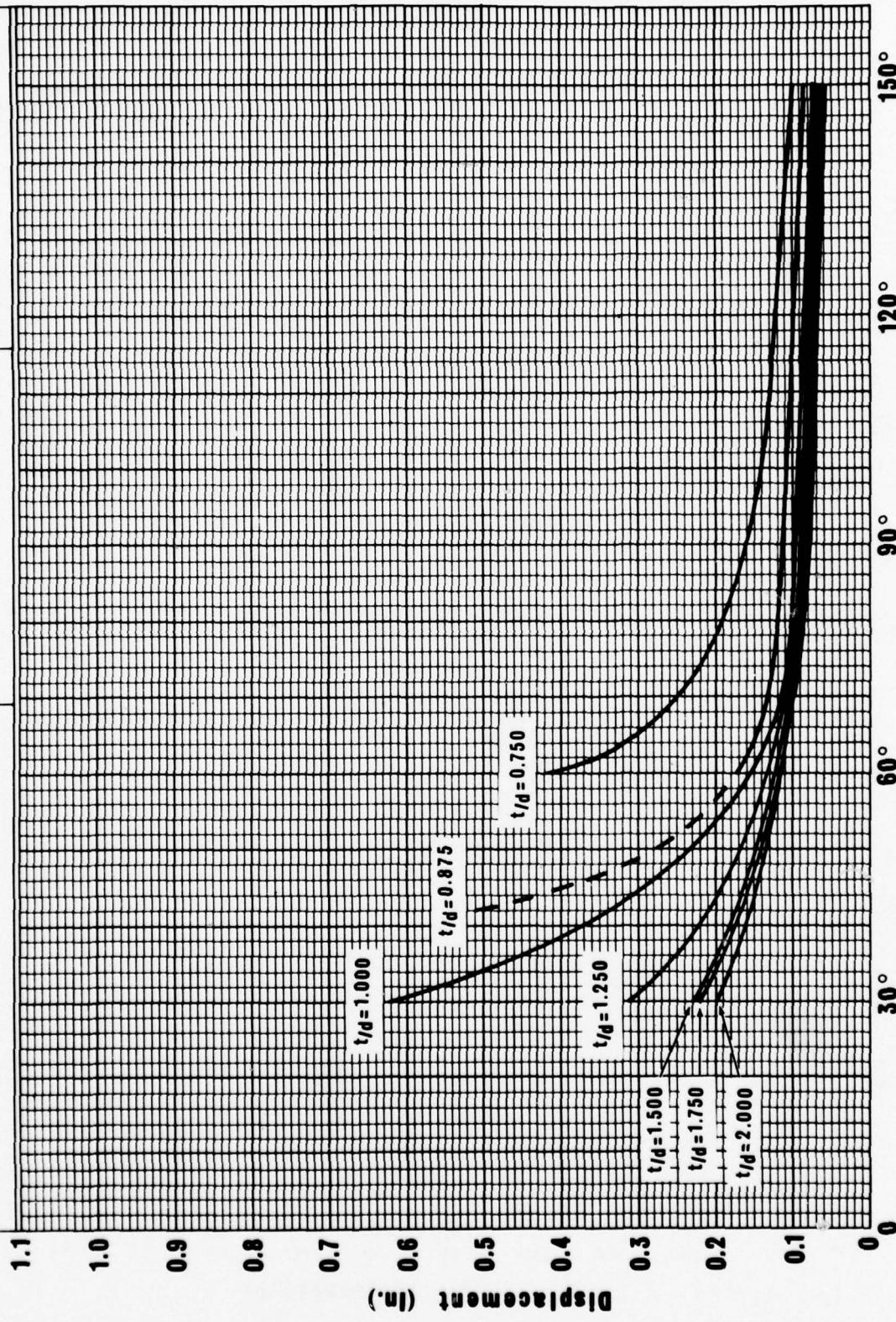
---

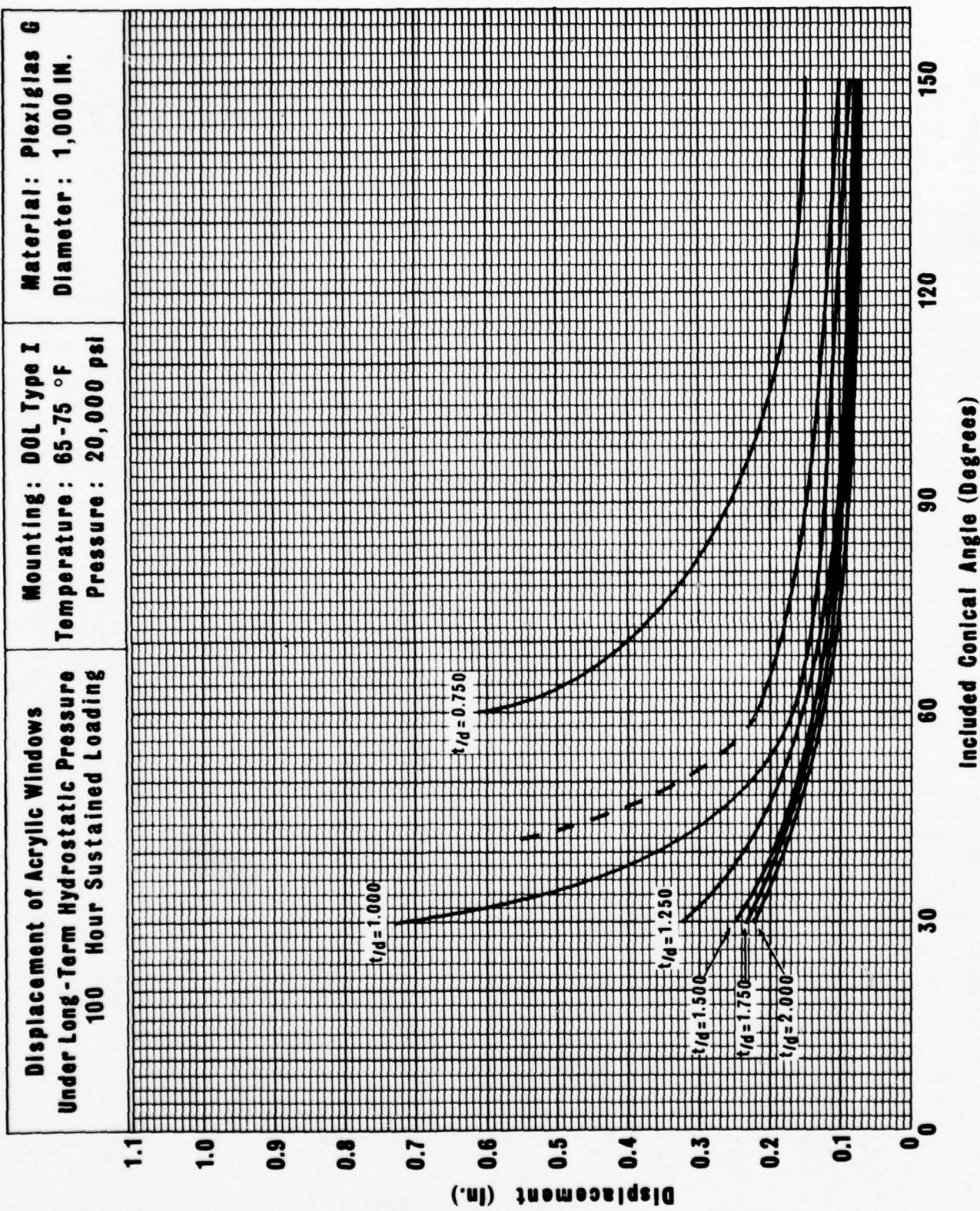
\*On many figures in this appendix  $D_i$  is noted as D or d, thus  $t/D_i = t/D = t/d$ .



**Displacement of Acrylic Windows  
Under Long-Term Hydrostatic Pressure  
10 Hour Sustained Loading**

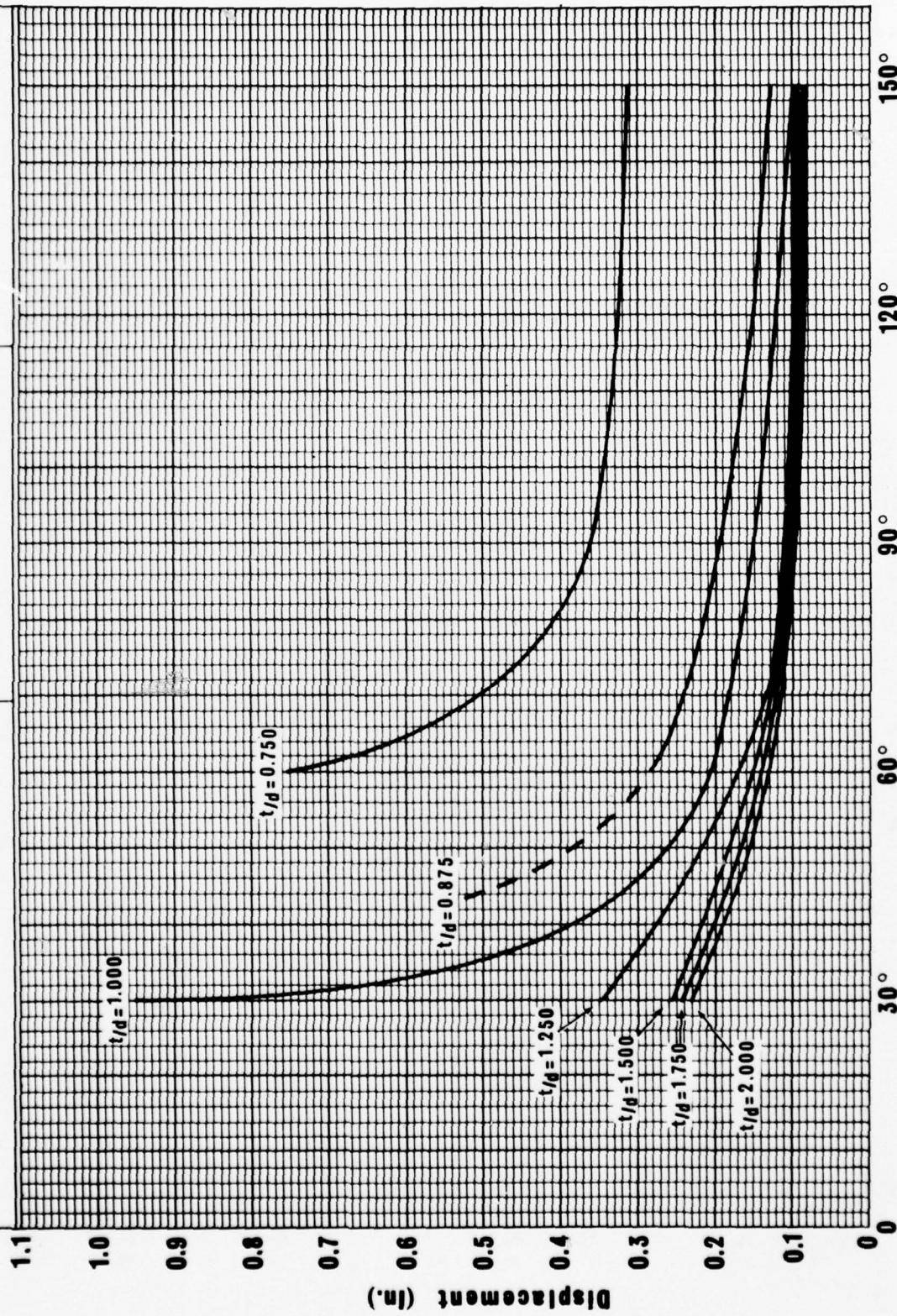
Mounting: DOL Type I  
Temperature: 65-75 °F  
Diameter: 1,000 IN.  
Pressure: 20,000 psi

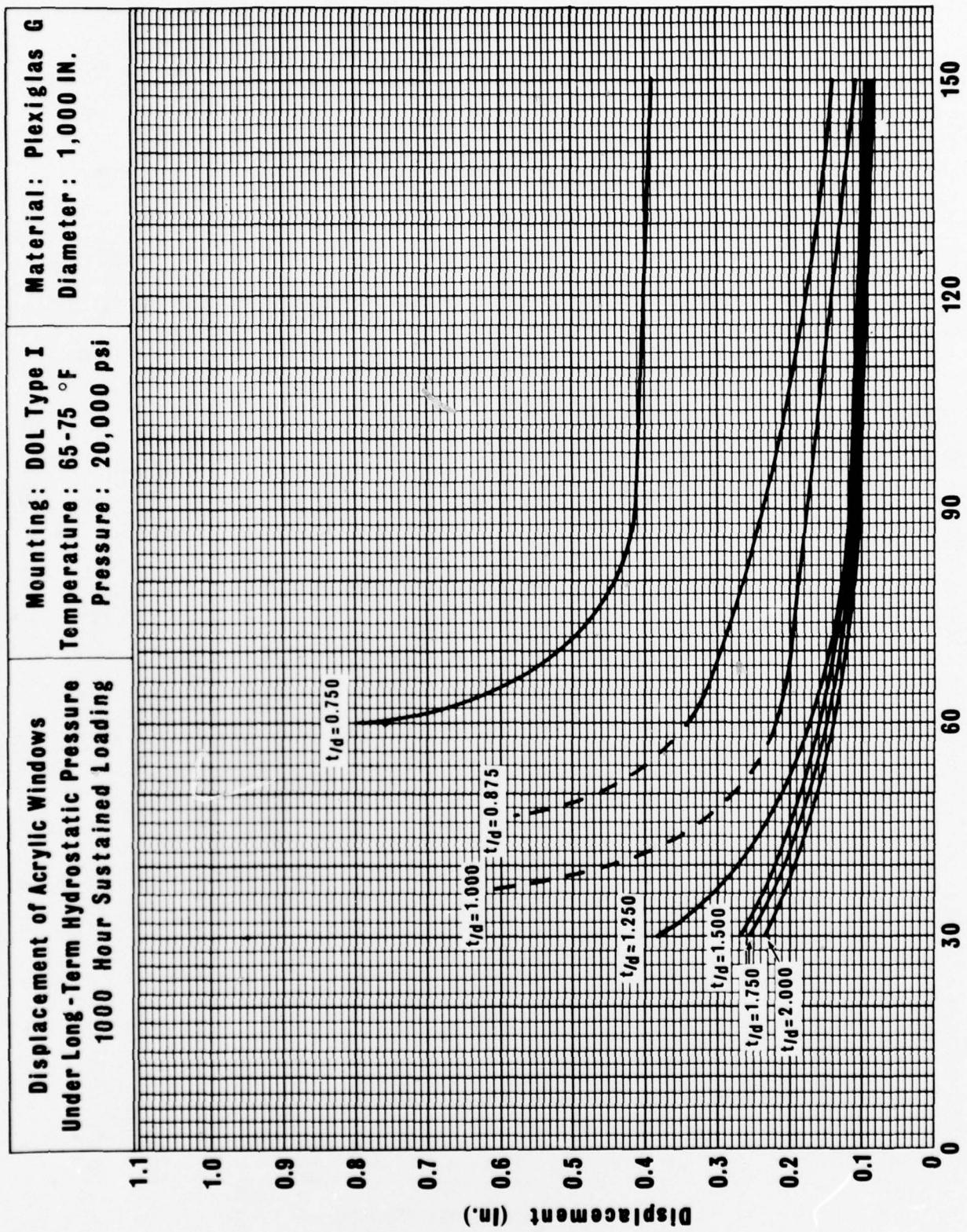




**Displacement of Acrylic Windows  
Under Long-Term Hydrostatic Pressure  
500 Hour Sustained Loading**

**Mounting:** DOT Type I    **Material:** Plexiglas G  
**Temperature:** 65-75 °F    **Diameter:** 1,000 IN.  
**Pressure:** 20,000 psi

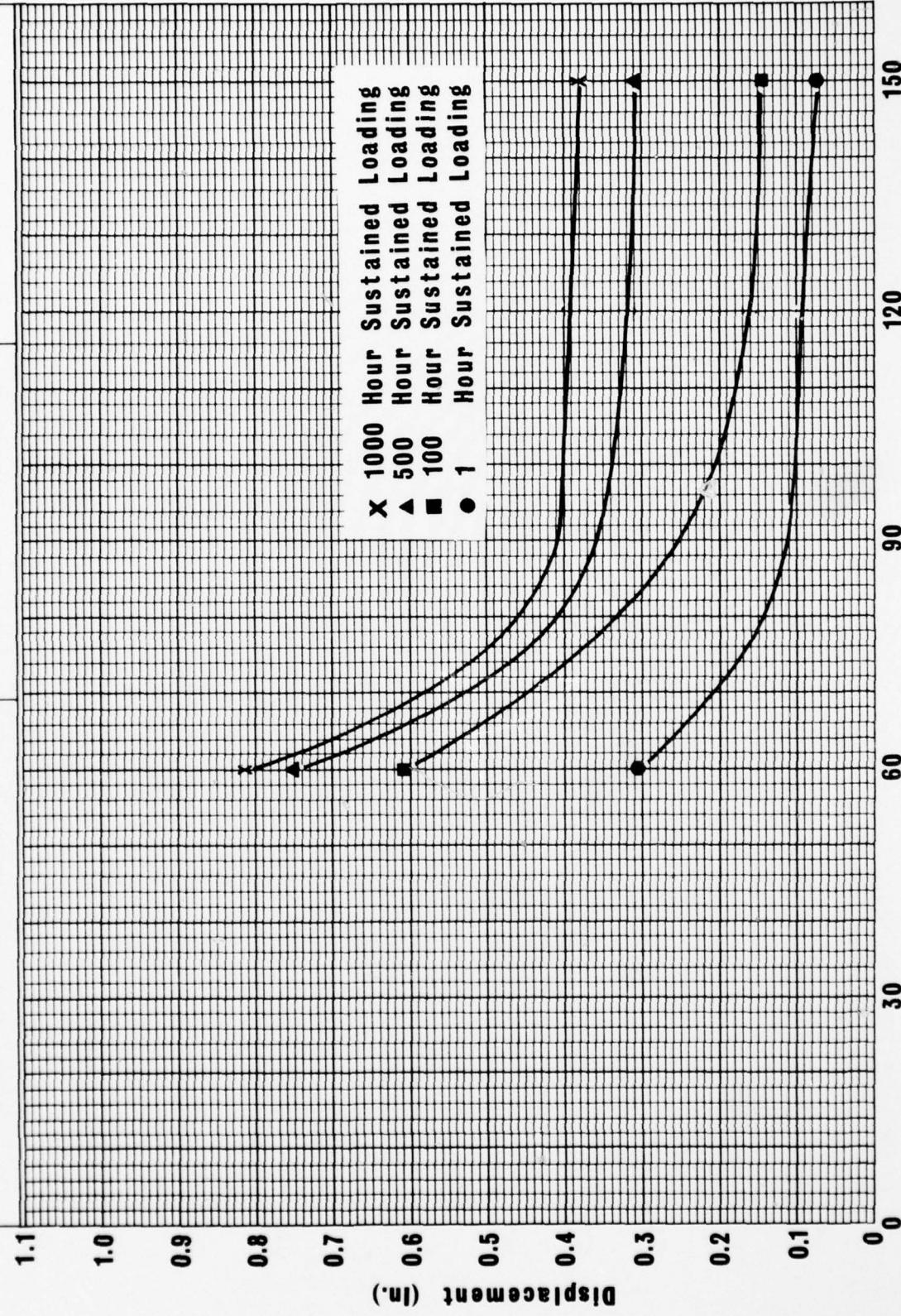




**Displacement of Acrylic Windows  
Under Long-Term Hydrostatic Pressure  
0.750 Nominal t/D Ratio**

Mounting: DOL Type I  
Temperature: 65-75 °F  
Pressure: 20,000 psi

Material: Plexiglas G  
Diameter: 1.000 IN.



**Displacement of Acrylic Windows  
Under Long - Term Hydrostatic Pressure**

**0.875 Nominal t/D Ratio**

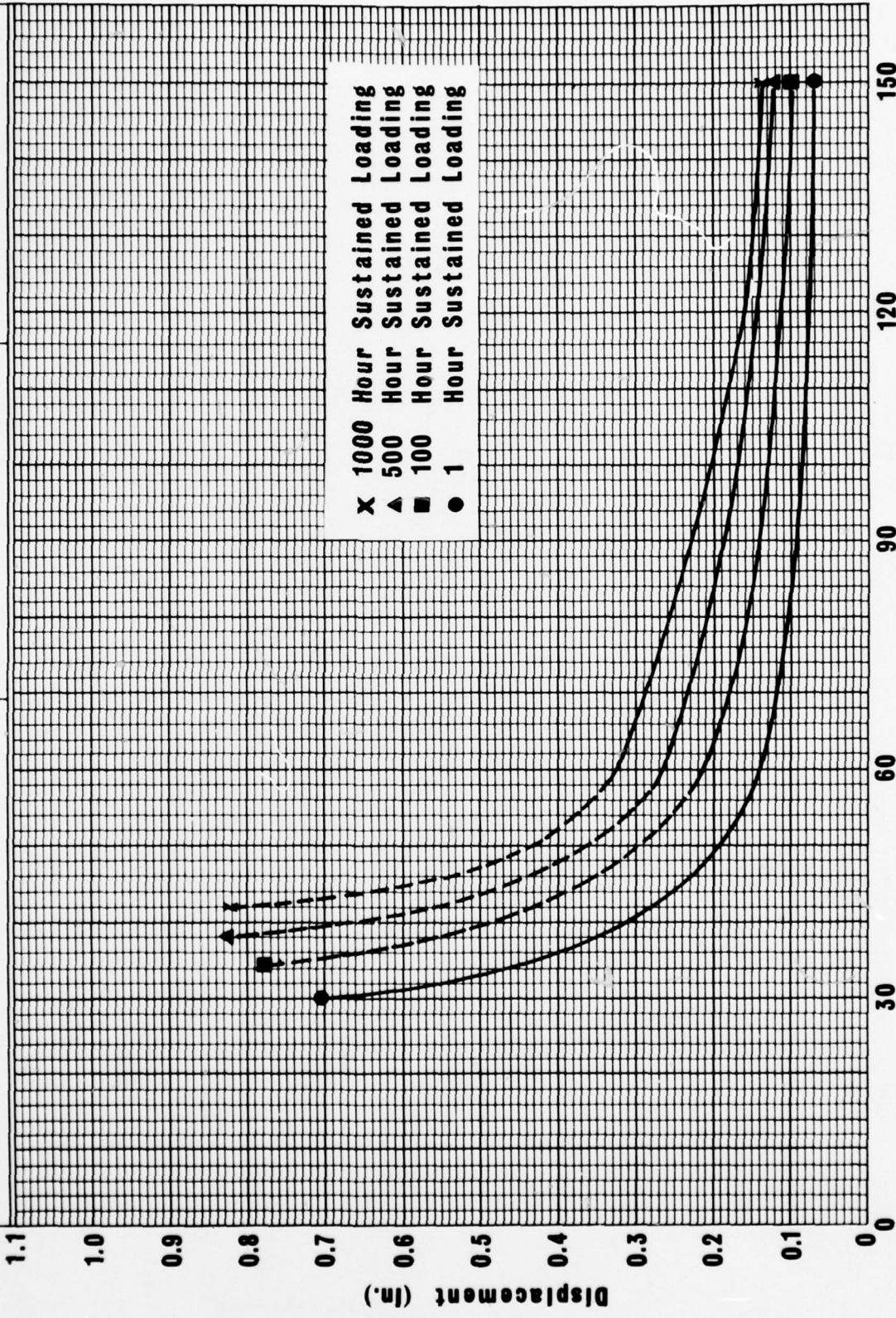
**Mounting: DOL Type I**

**Material: Plexiglas G**

**Diameter: 1.000 IN.**

**Temperature: 65-75 °F**

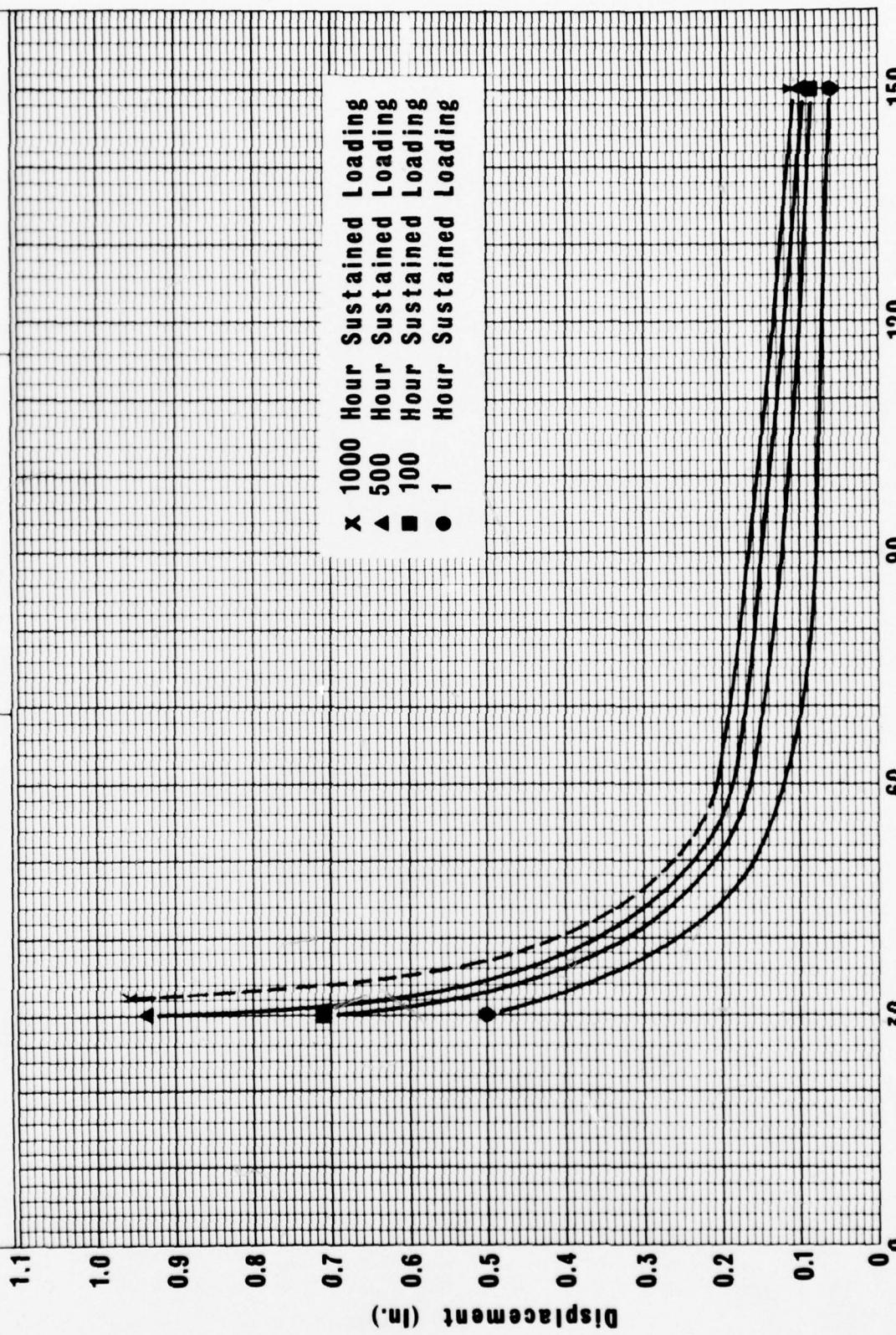
**Pressure : 20,000 psi**



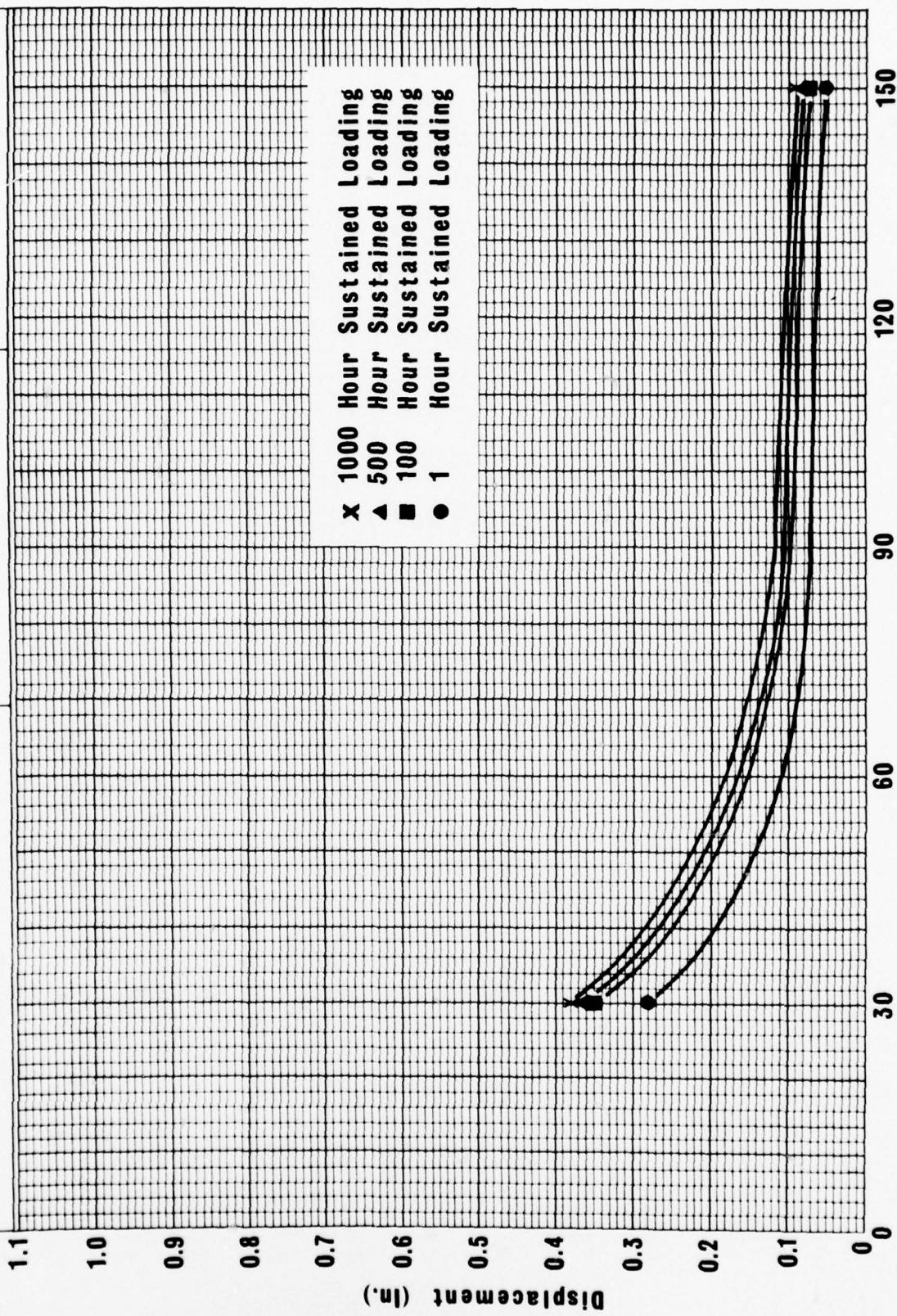
**Displacement of Acrylic Windows  
Under Long-Term Hydrostatic Pressure**

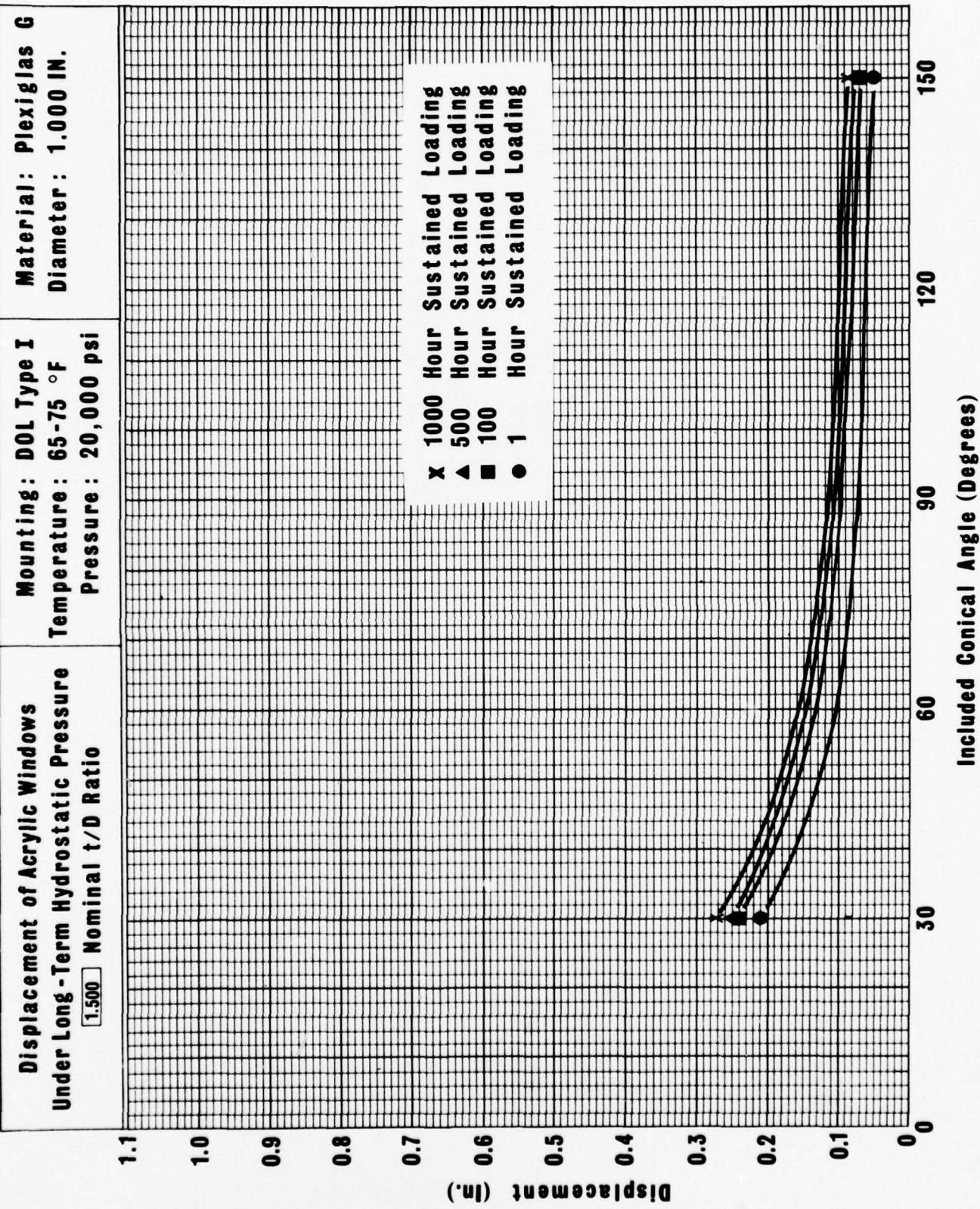
1.000	Nominal t/D Ratio
-------	-------------------

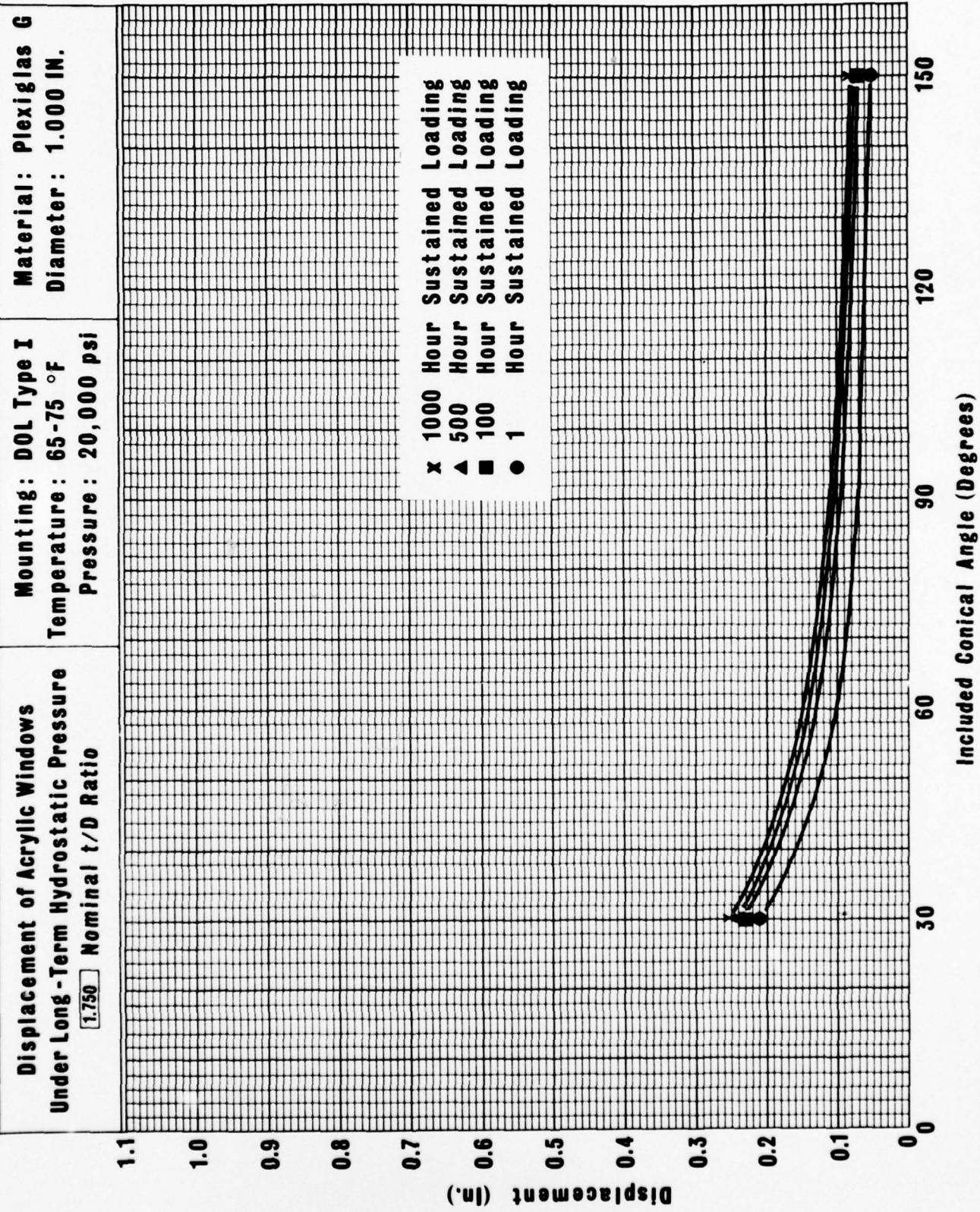
Mounting: DOL Type I      Material: Plexiglas G  
Temperature: 65-75 °F      Diameter: 1.000 IN.  
Pressure: 20,000 psi

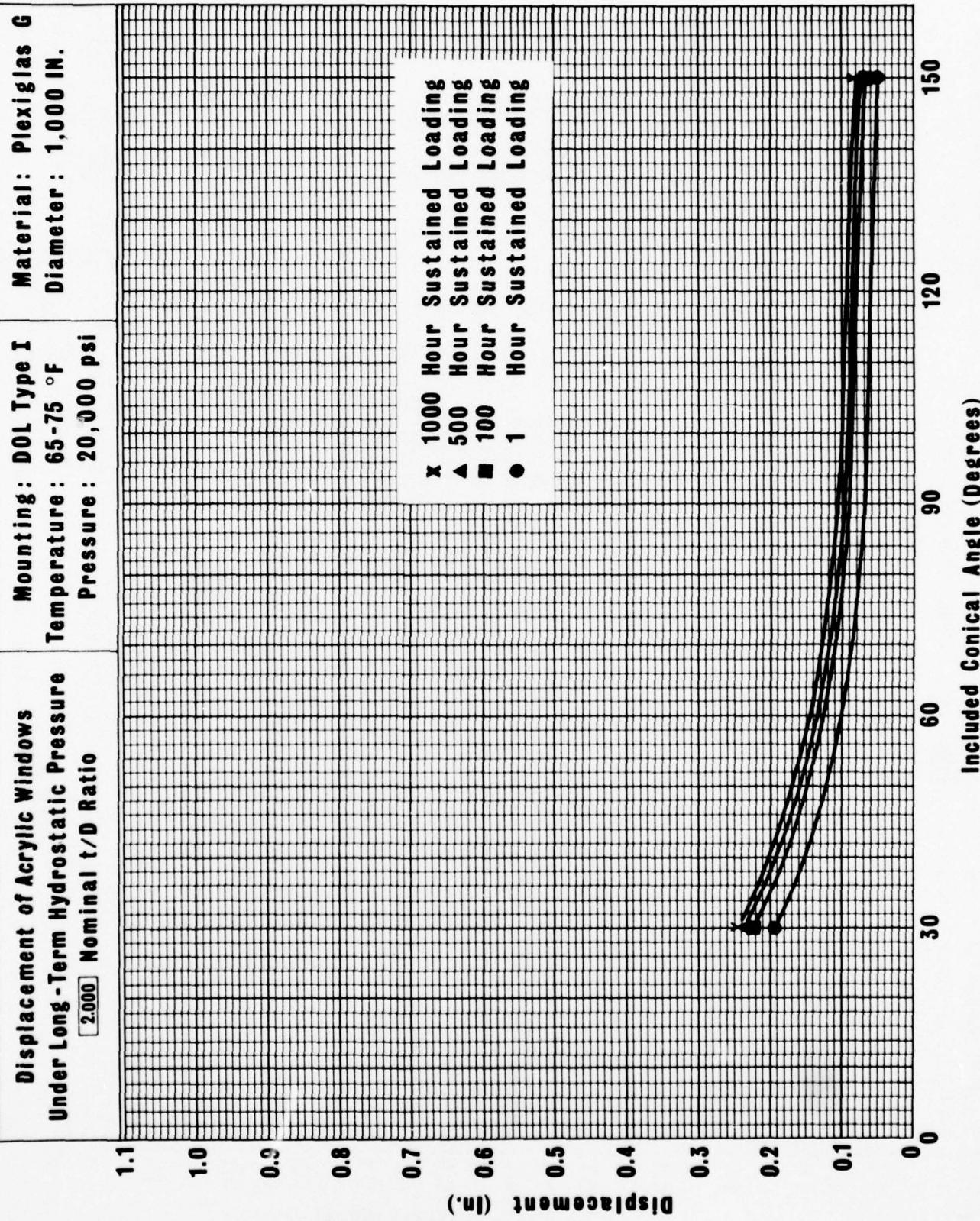


<b>Displacement of Acrylic Windows Under Long - Term Hydrostatic Pressure</b>	<b>Mounting:</b> DOL Type I	<b>Material:</b> Plexiglas G
<input checked="" type="checkbox"/> 1.250 Nominal t/D Ratio	Temperature: 65-75 °F	Diameter: 1.000 IN.
	Pressure: 20,000 psi	







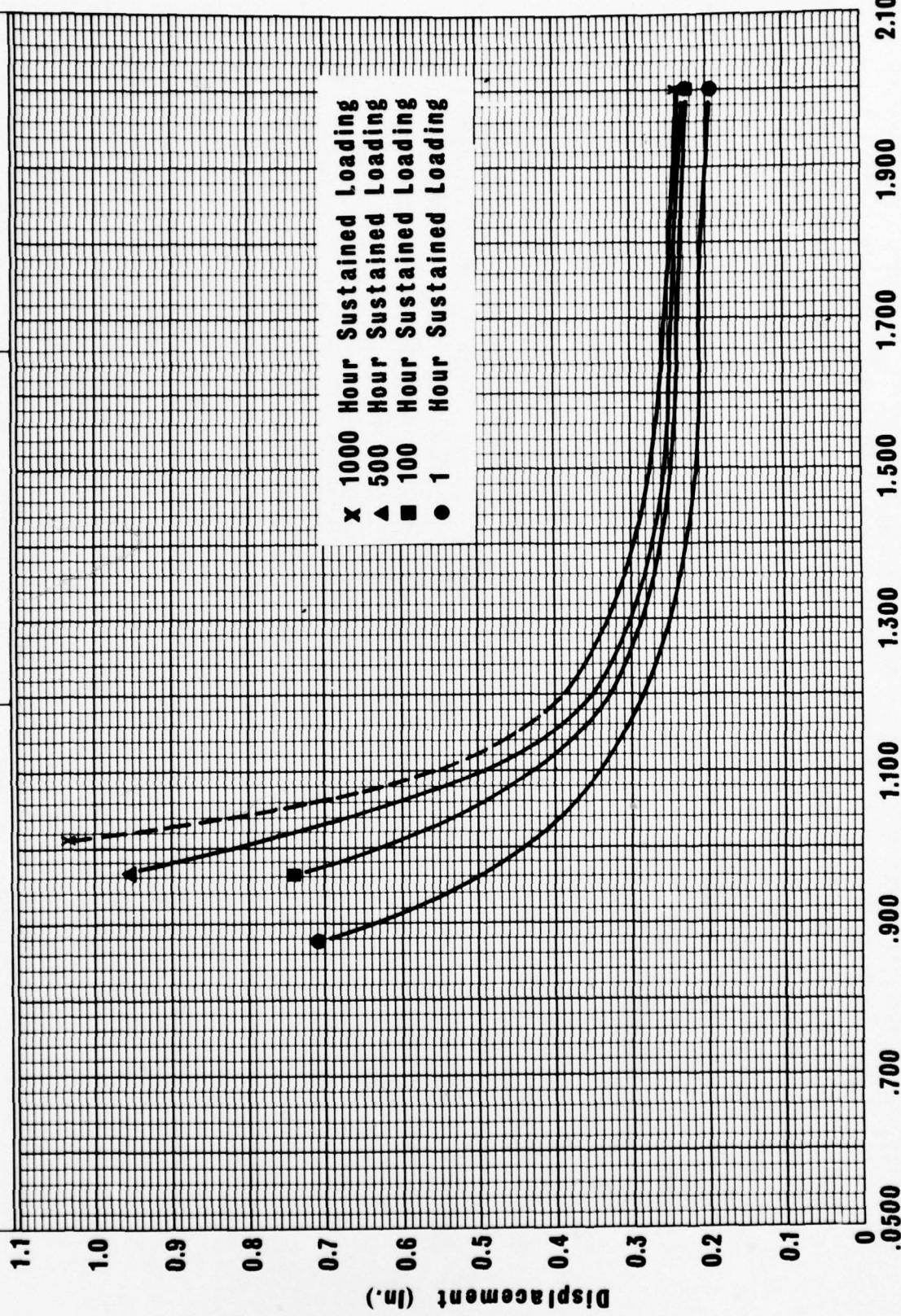


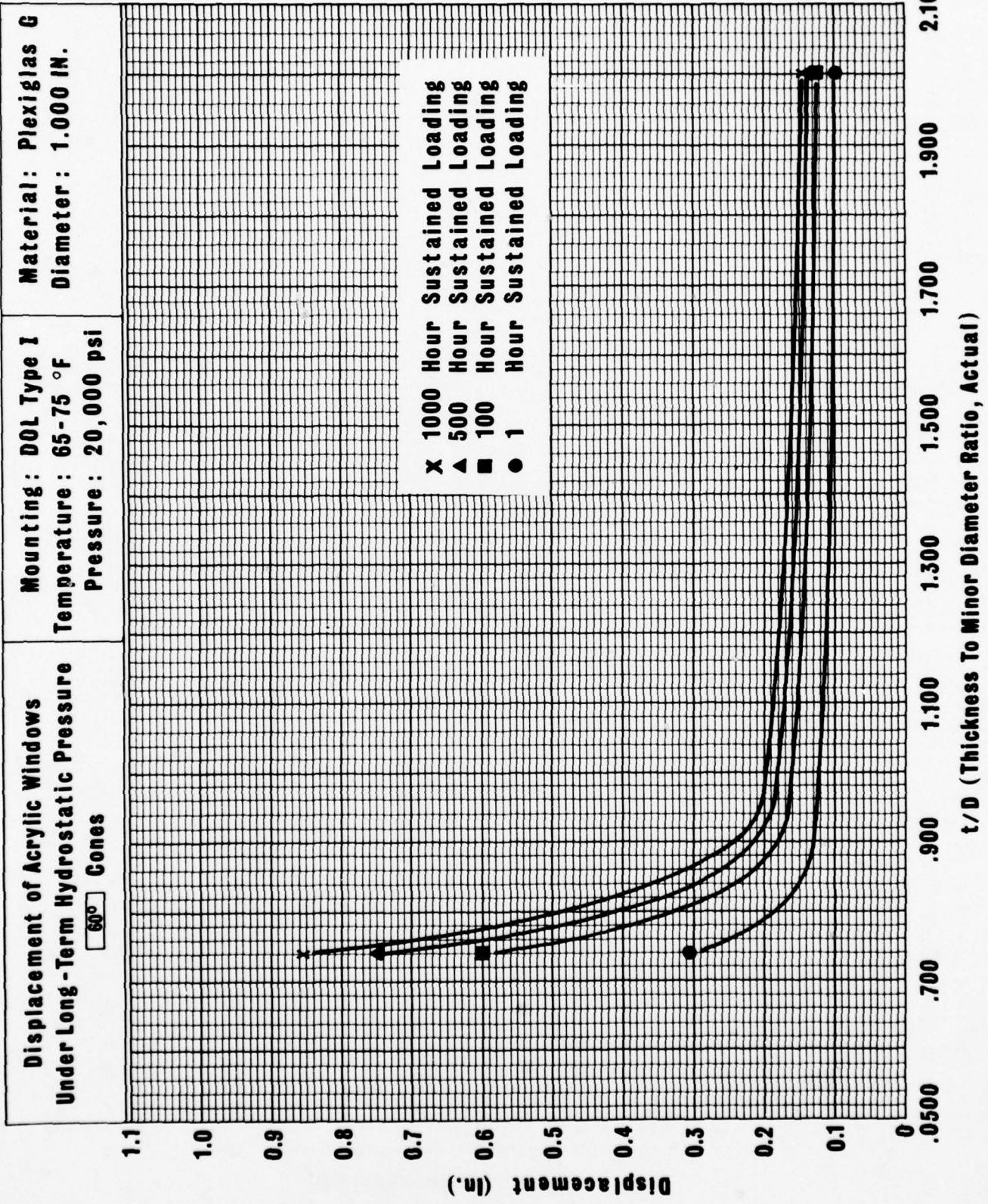
**Displacement of Acrylic Windows  
Under Long - Term Hydrostatic Pressure**

**[30°] Cones**

**Mounting: DOL Type I      Temperature: 65 - 75 °F  
Pressure: 20,000 psi**

**Material: Plexiglas G  
Diameter: 1.000 IN.**



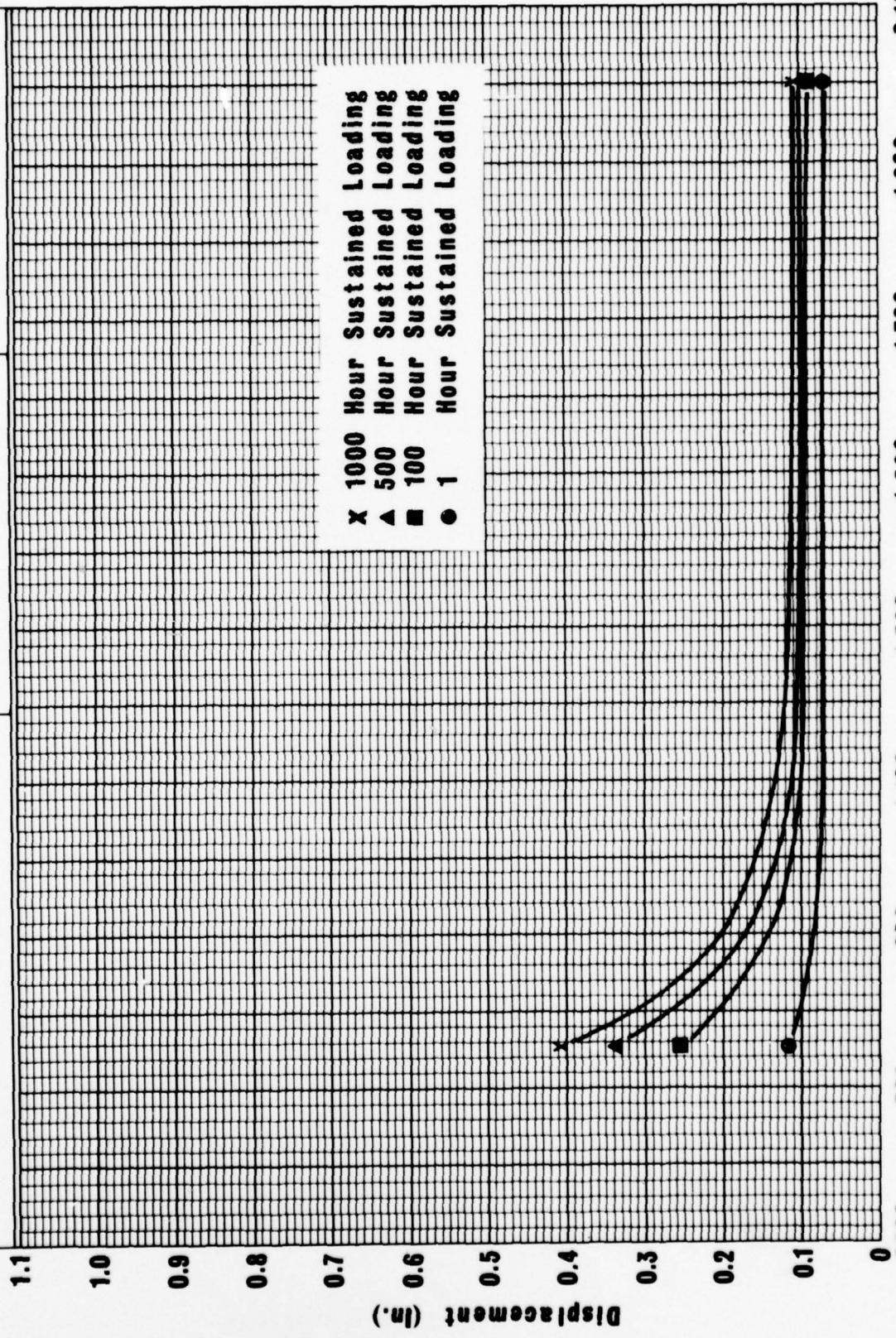


**Displacement of Acrylic Windows  
Under Long-Term Hydrostatic Pressure**

**90° Cones**

Mounting: DOL Type I  
Temperature: 65-75 °F  
Pressure: 20,000 psi

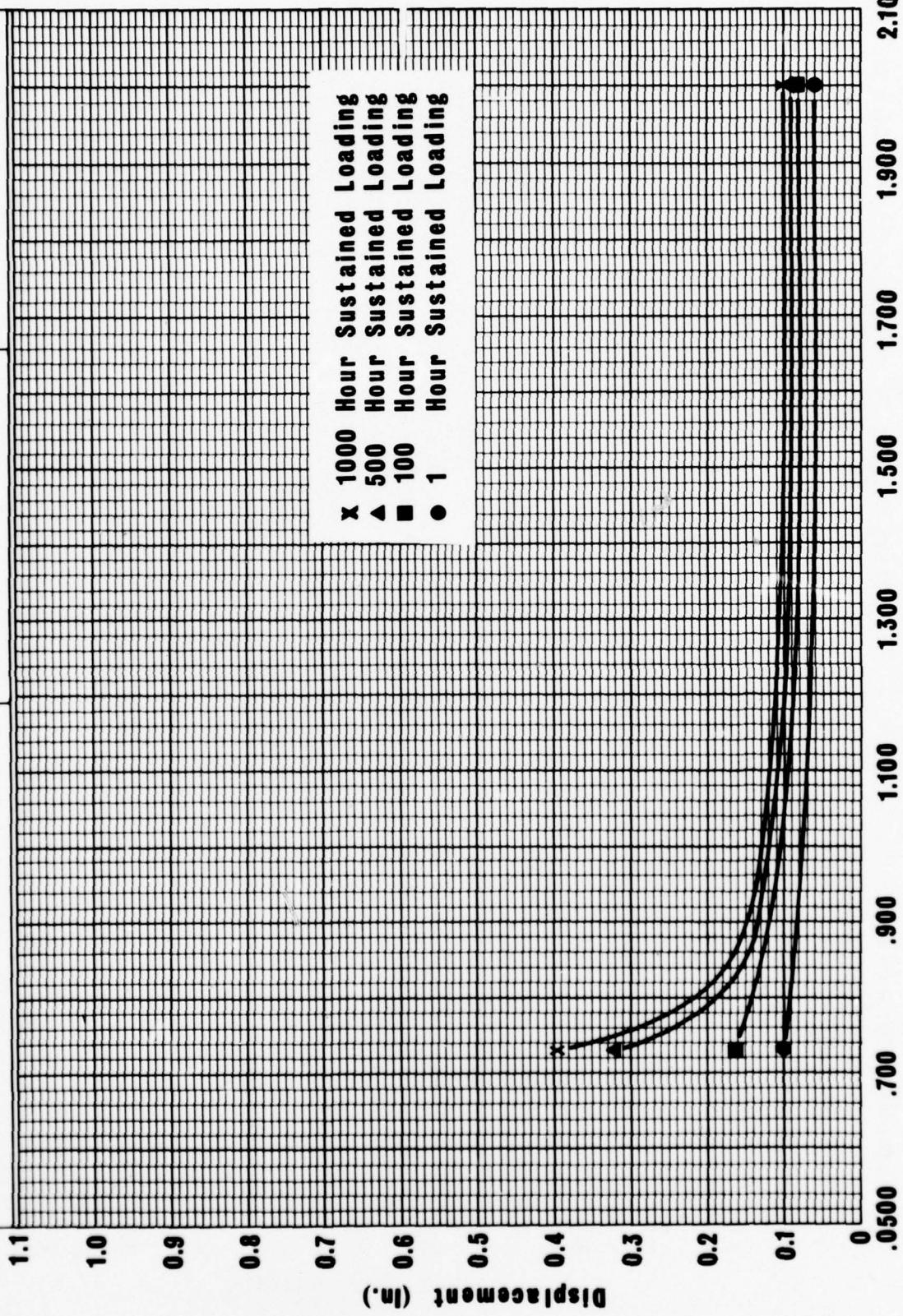
Material: Plexiglas G  
Diameter: 1.000 in.



**Displacement of Acrylic Windows  
Under Long - Term Hydrostatic Pressure**

**120° Cones**

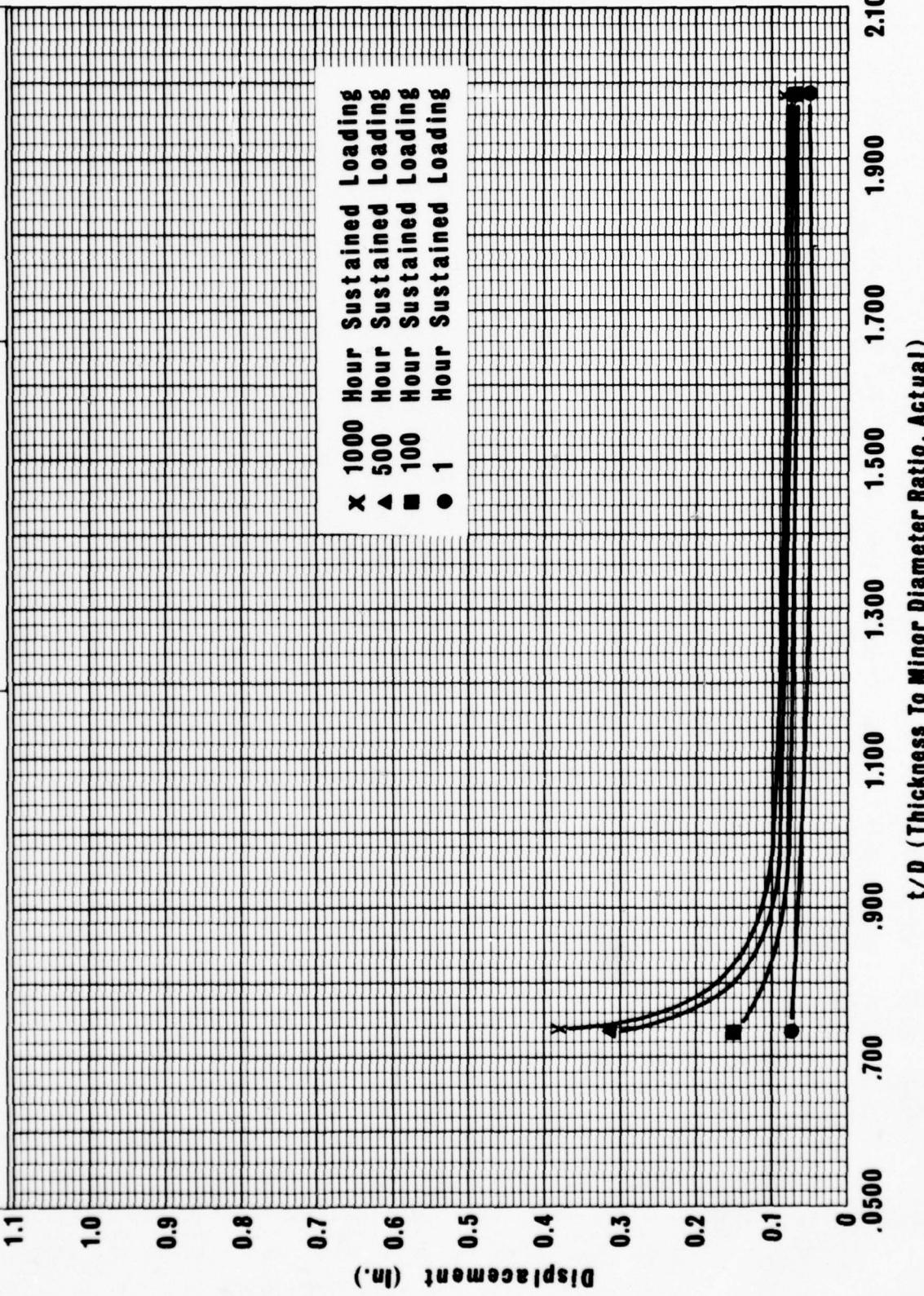
Mounting: DOL Type I      Material: Plexiglas G  
Temperature: 65-75 °F      Diameter: 1.000 IN.  
Pressure: 20,000 psi



**Displacement of Acrylic Windows  
Under Long-Term Hydrostatic Pressure**

$150^\circ$  Cones

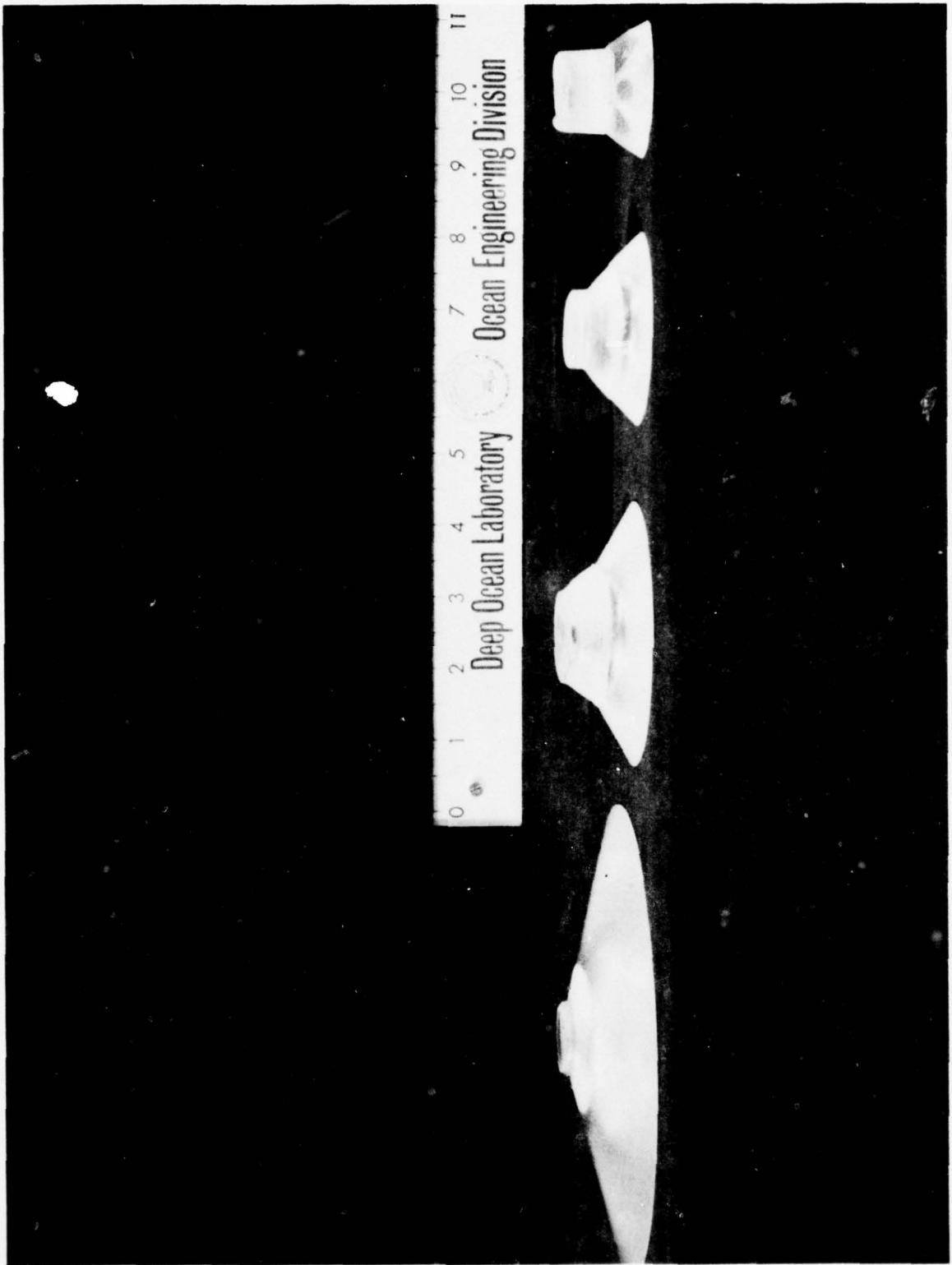
Mounting: DOL Type I      Material: Plexiglas G  
Temperature: 65-75 °F      Diameter: 1.000 IN.  
Pressure: 20,000 psi



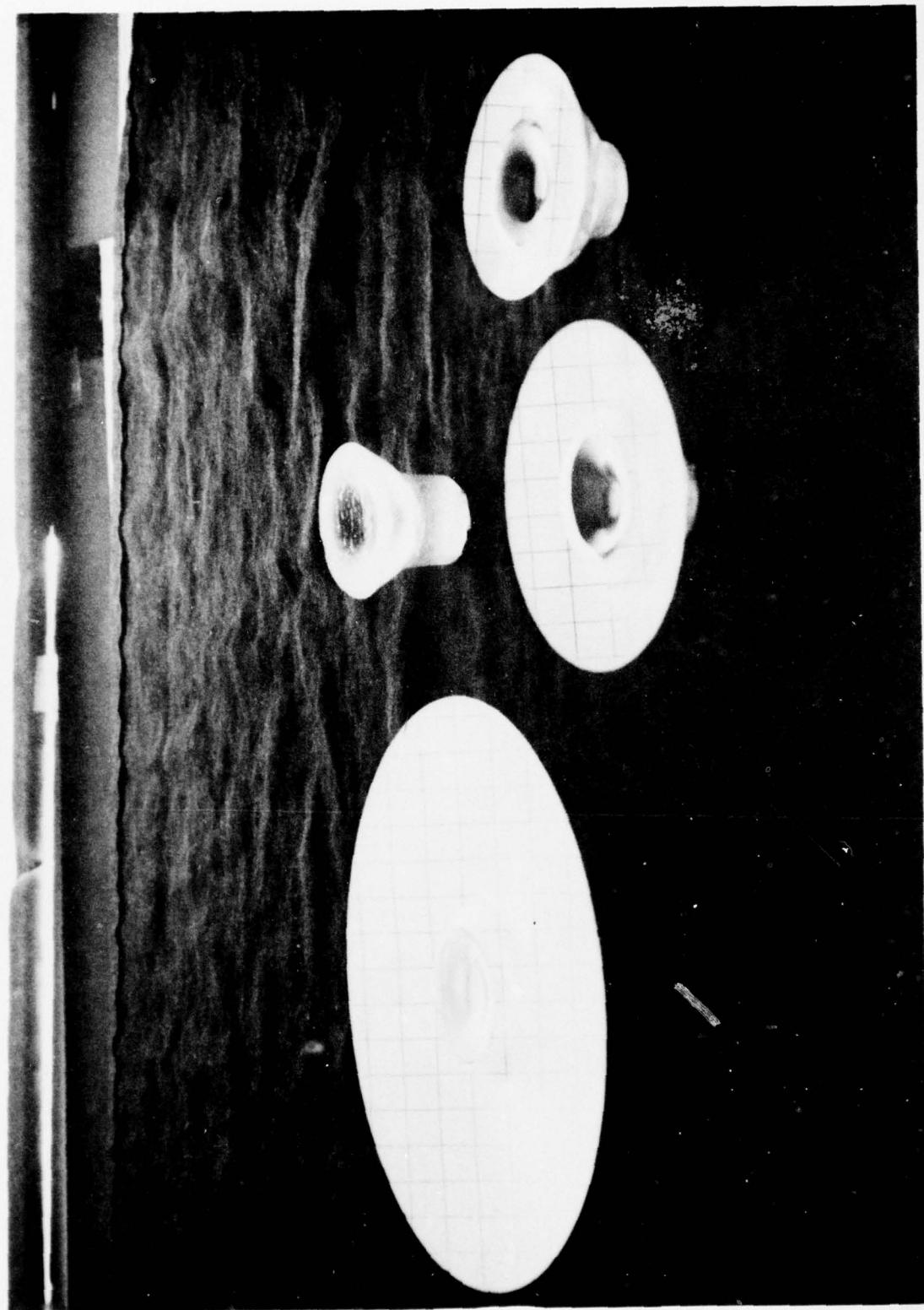
#### **B.2.4 Permanent Deformations**

The data in this section are concerned with the permanent deformations of conical frustums with included angles of 30, 60, 90, 120, and 150 degrees (0.5, 1.04, 1.57, 2.09, and 2.6 radians) after 1000 hours of long-term pressure loading at 20,000 pounds per square inch (137.9 megapascals) at ambient room temperature in mountings with  $D_i/D_f = 1.0$ .

Conical frustums with  $t/D_i = 0.75$ ; elevation.



Conical frustums with  $t/D_1 = 0.75$ , high-pressure face.

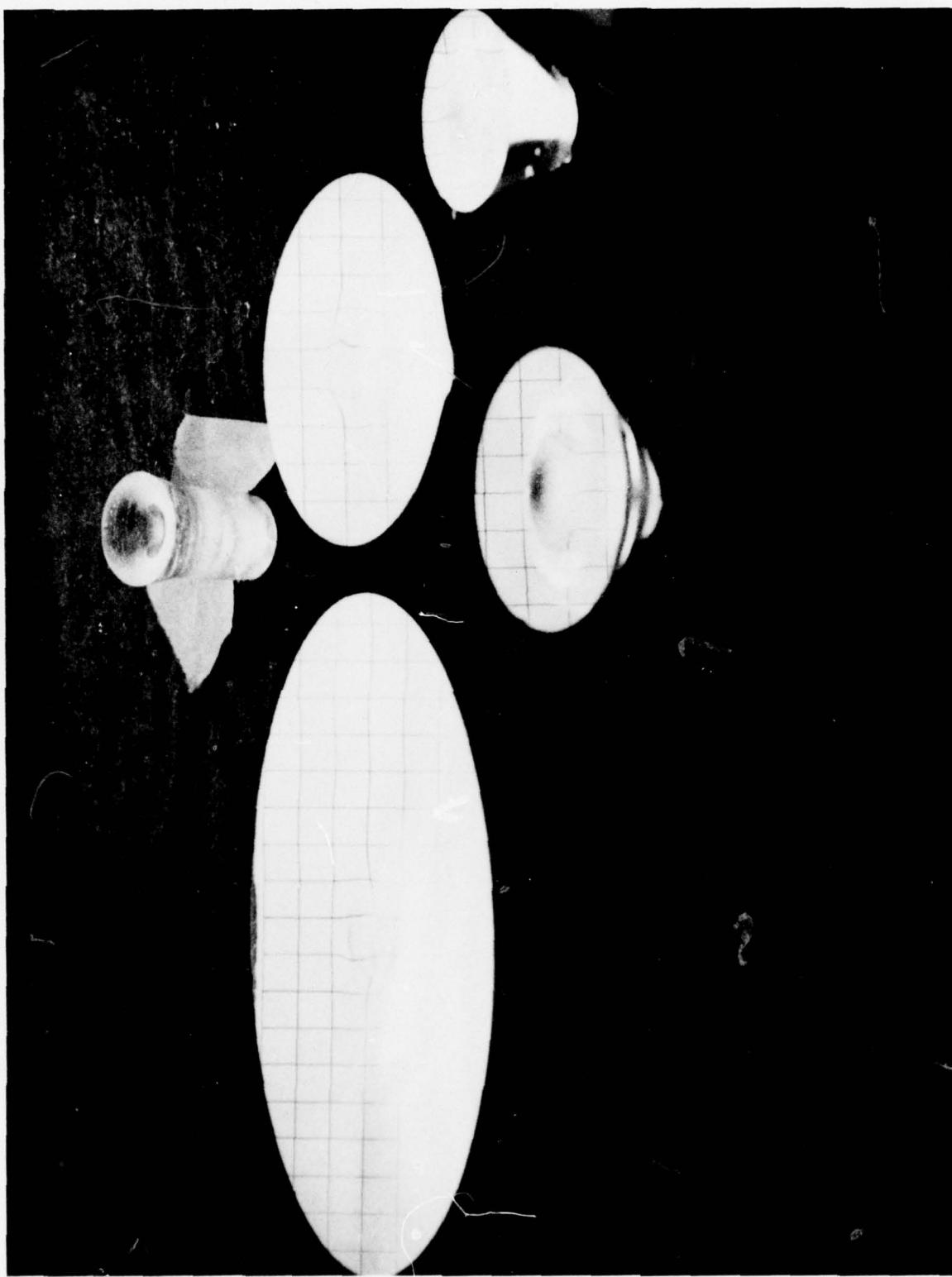


B-93

Conical frustums with  $t/D_1 = 0.875$ , elevation.

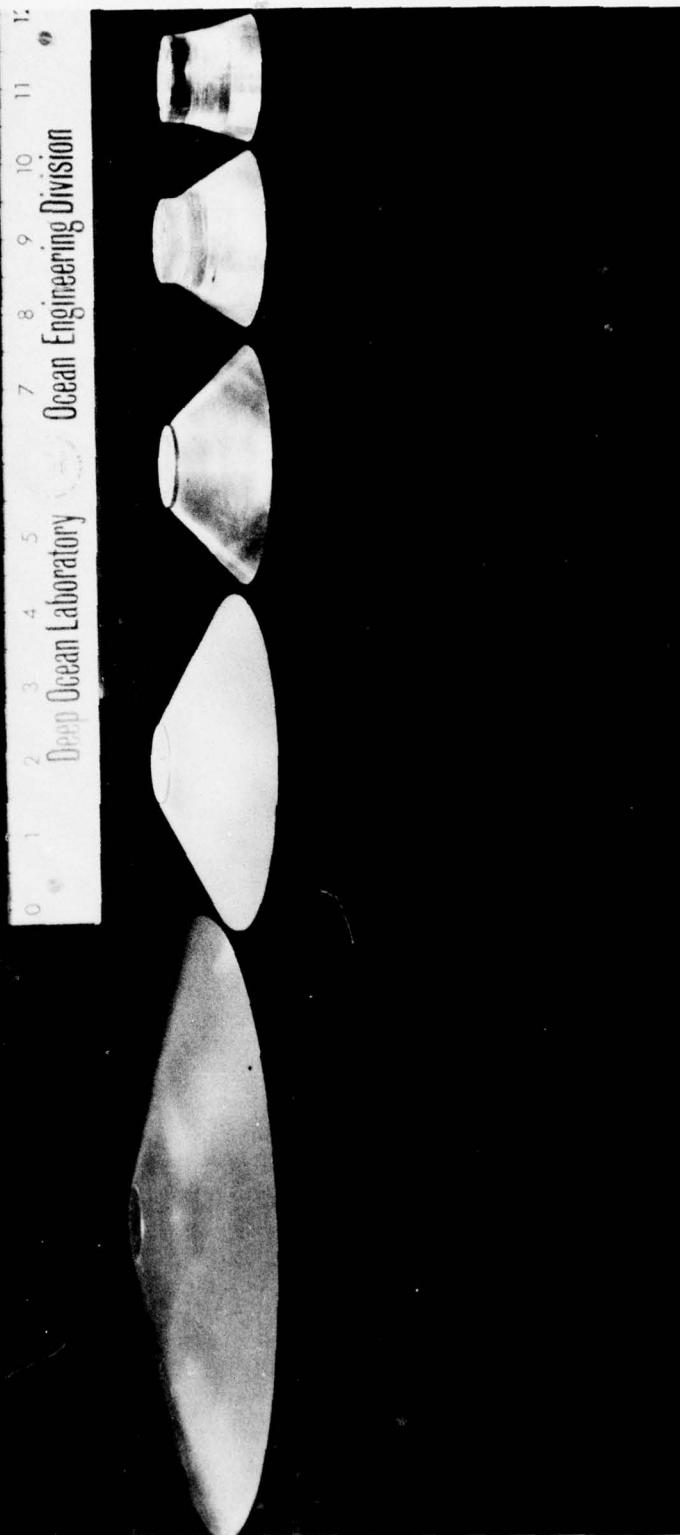


Conical frustums with  $t/D_l = 0.875$ ; high-pressure face.



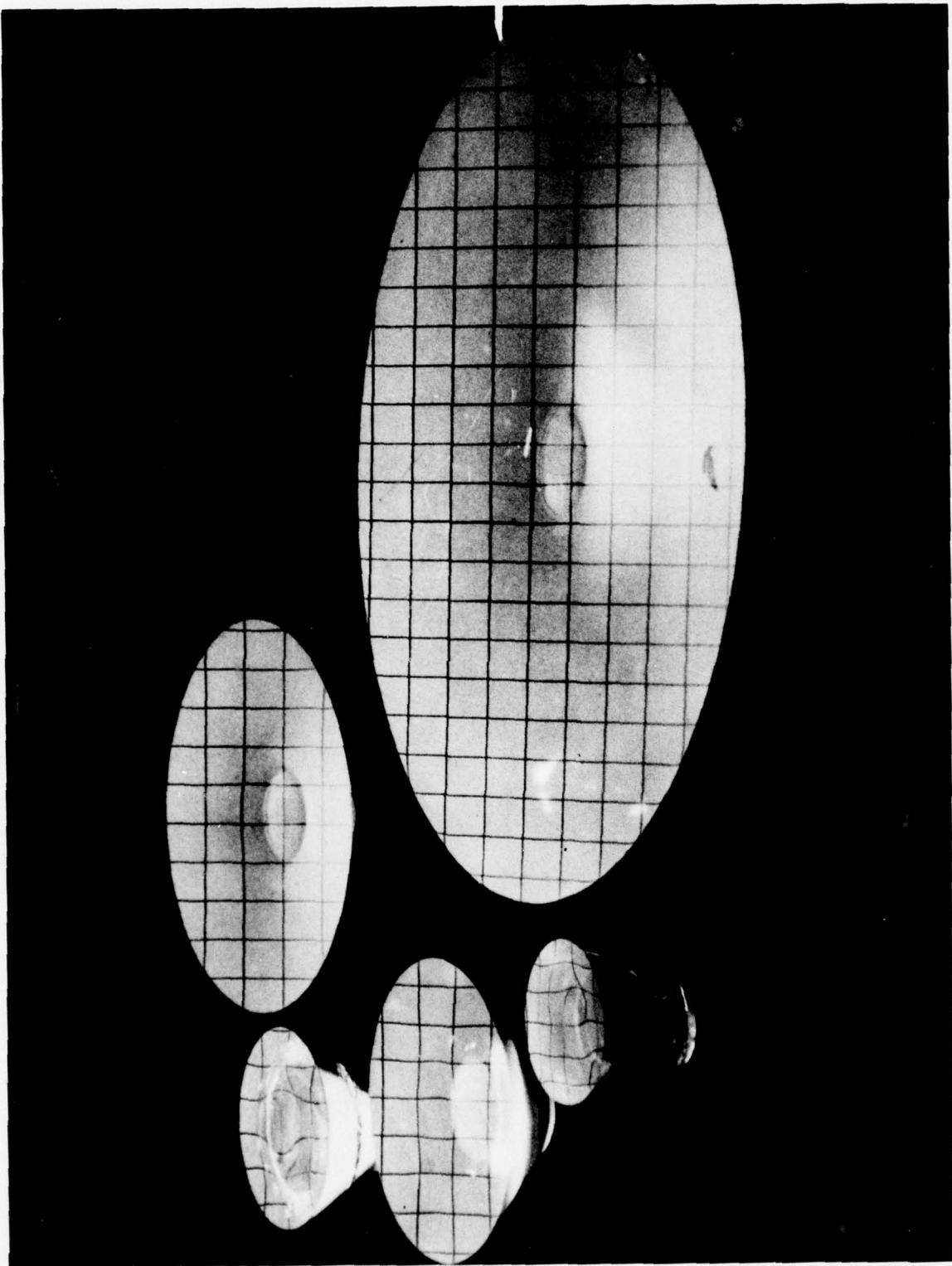
B-95

Conical frustums with  $t/D_1 = 1.0$ ; elevation.



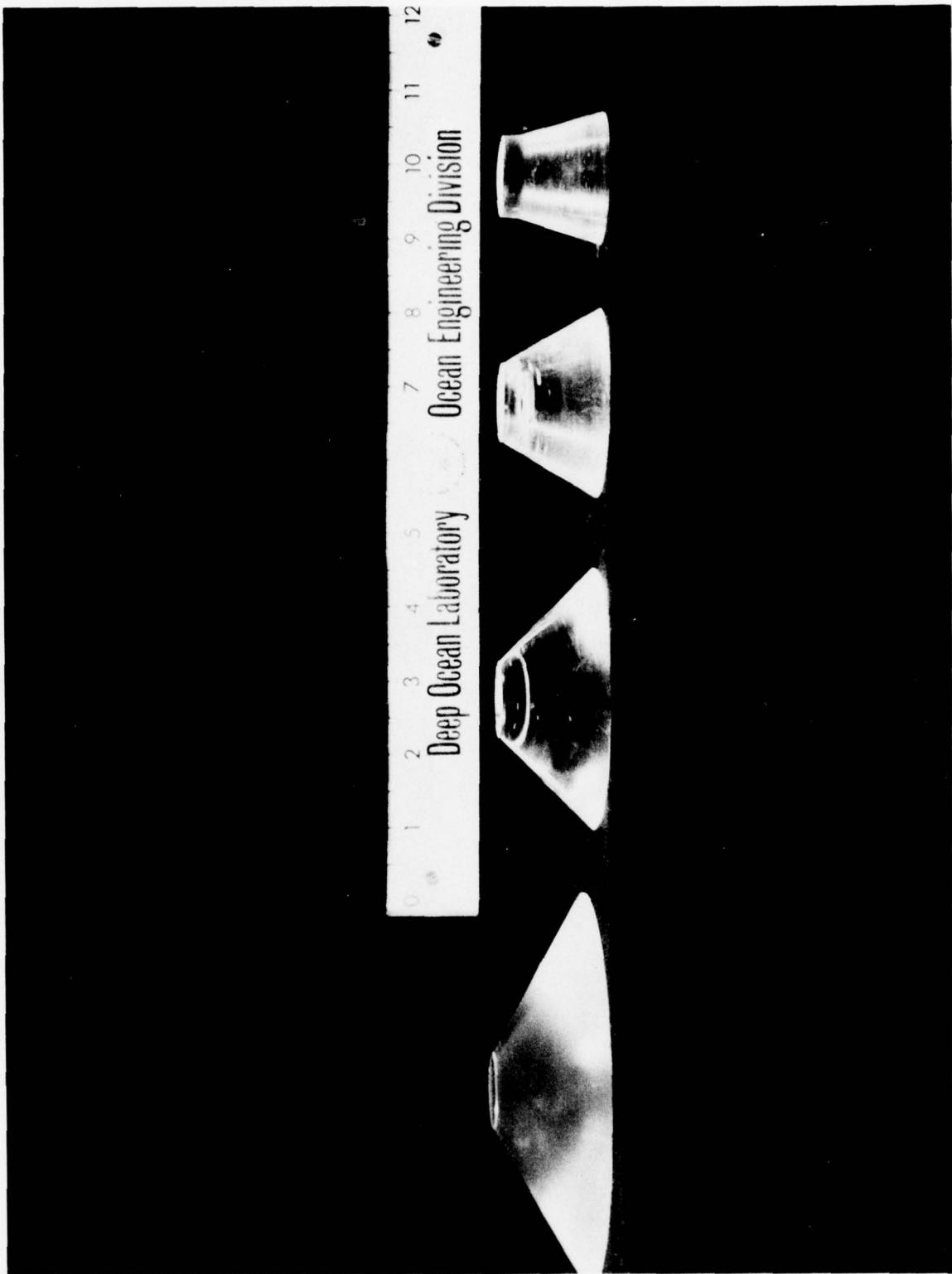
B-96

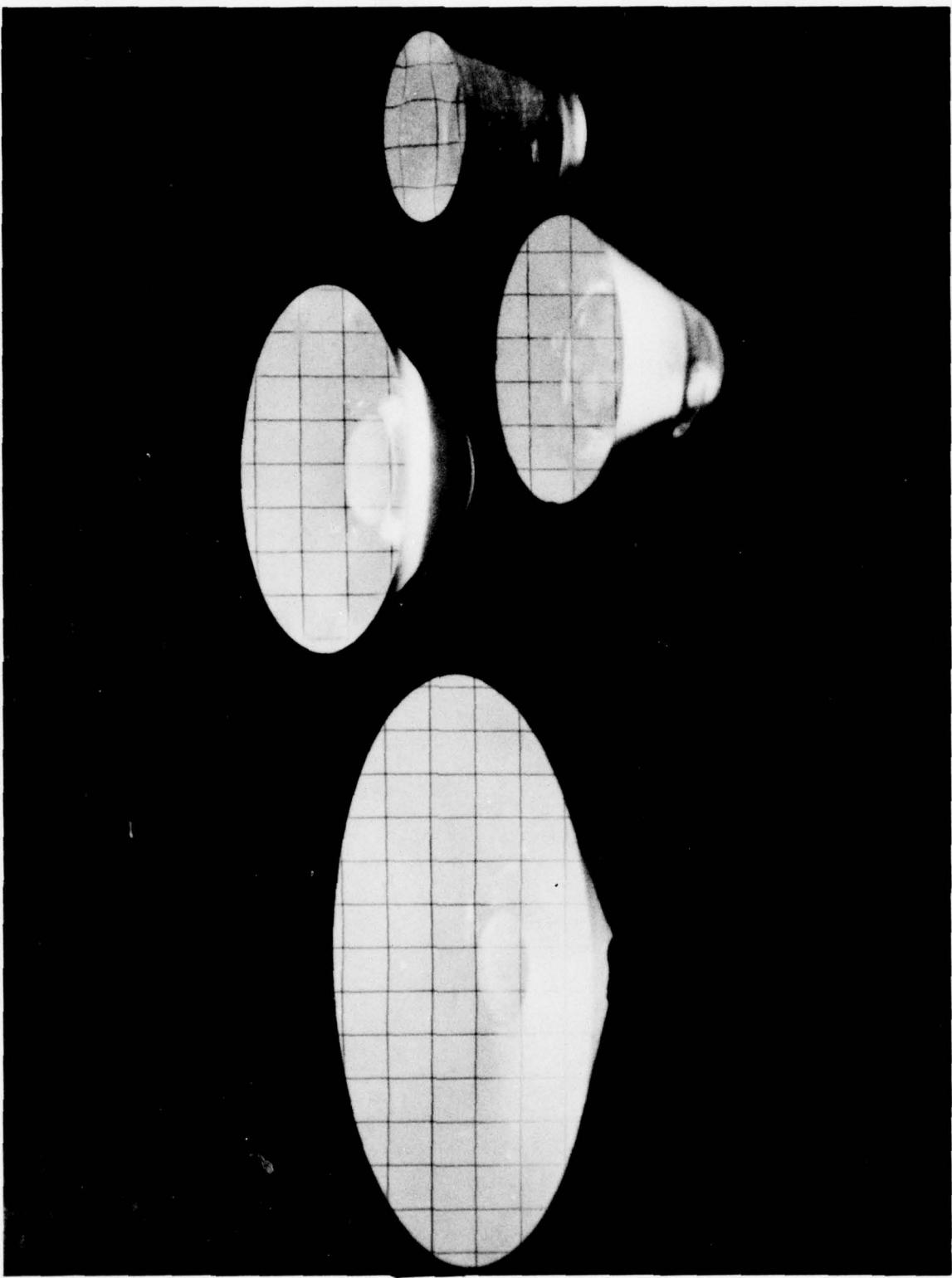
Conical frustums with  $t/D_i = 1.0$ ; high-pressure face.



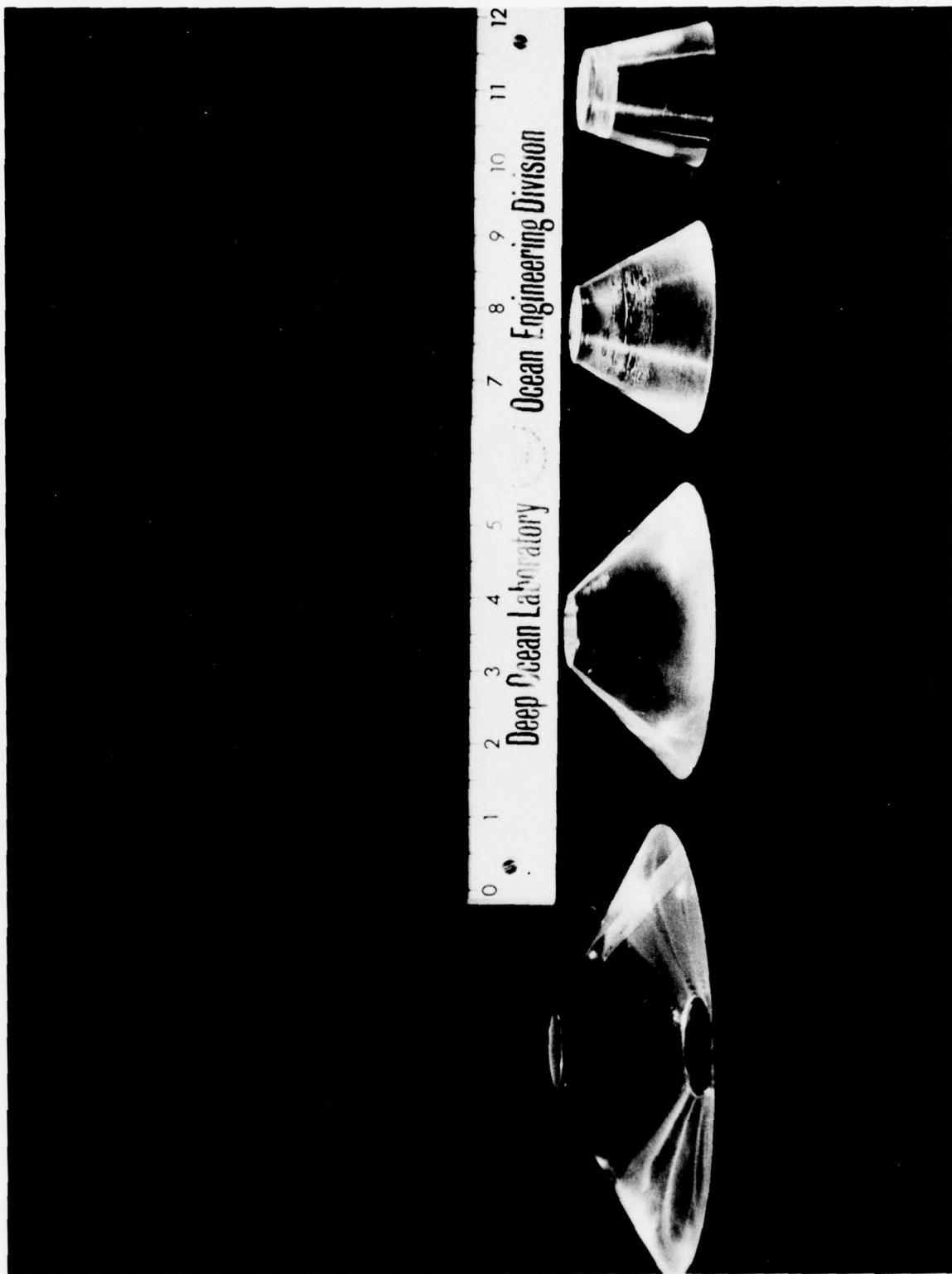
B-97

Conical frustums with  $t/D_1 = 1.25$ ; elevation.





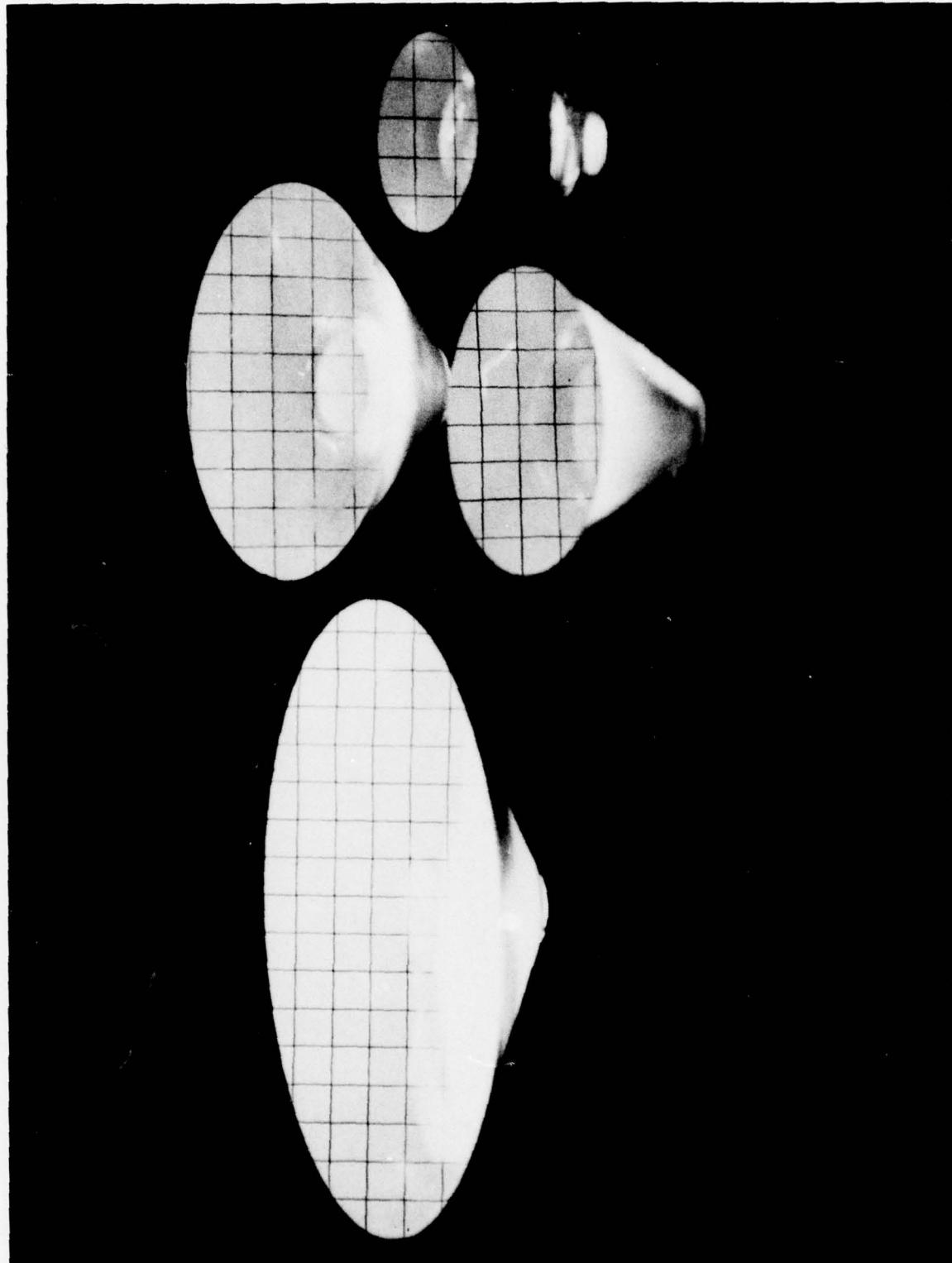
Conical frustums with  $t/D_i = 1.25$ ; high-pressure face.



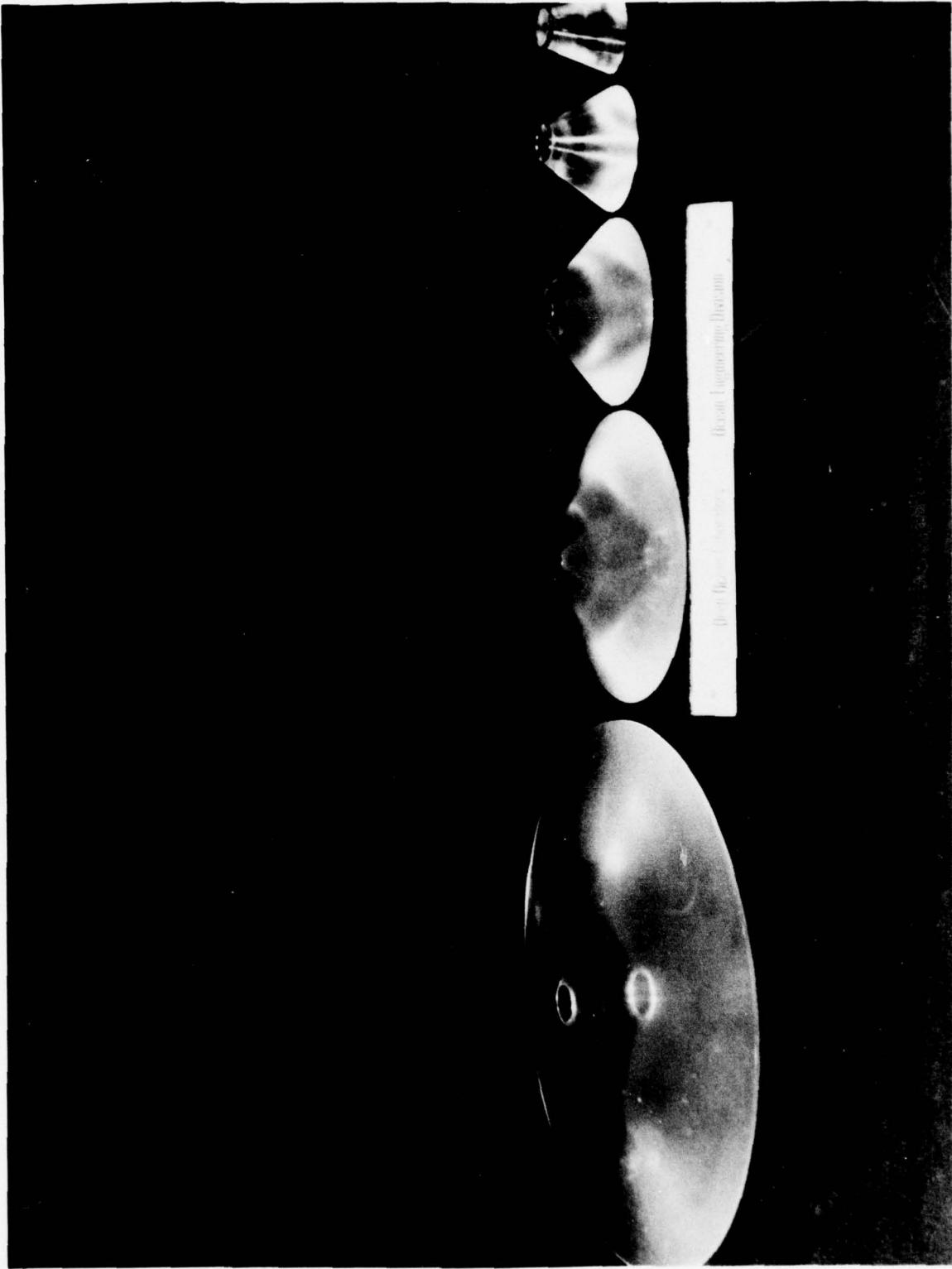
B-100

Conical trustums with  $t/D_1 = 1.5$ ; elevation.

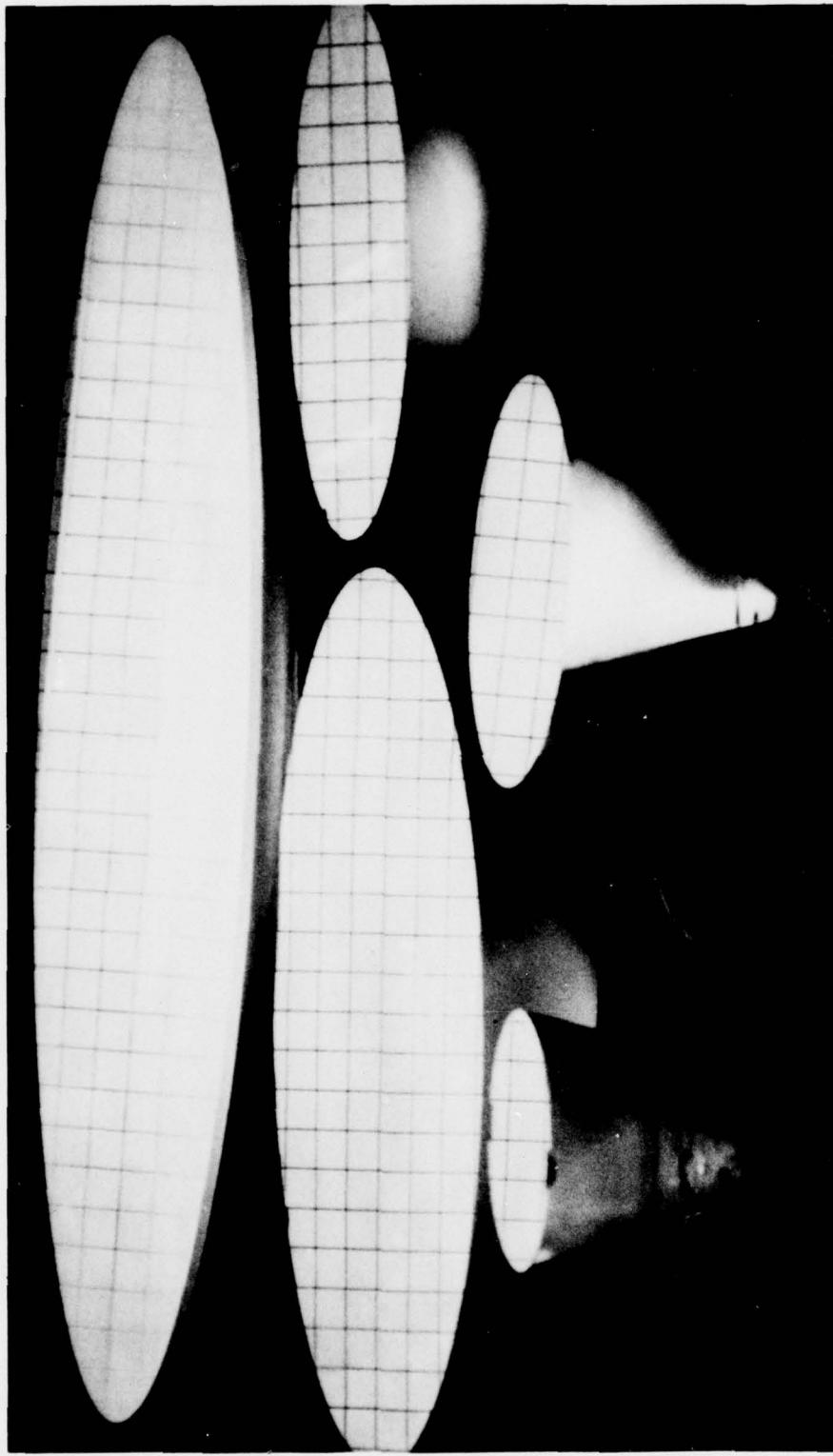
Conical frustums with  $t/D_1 = 1.5$ ; high-pressure face.



B-101

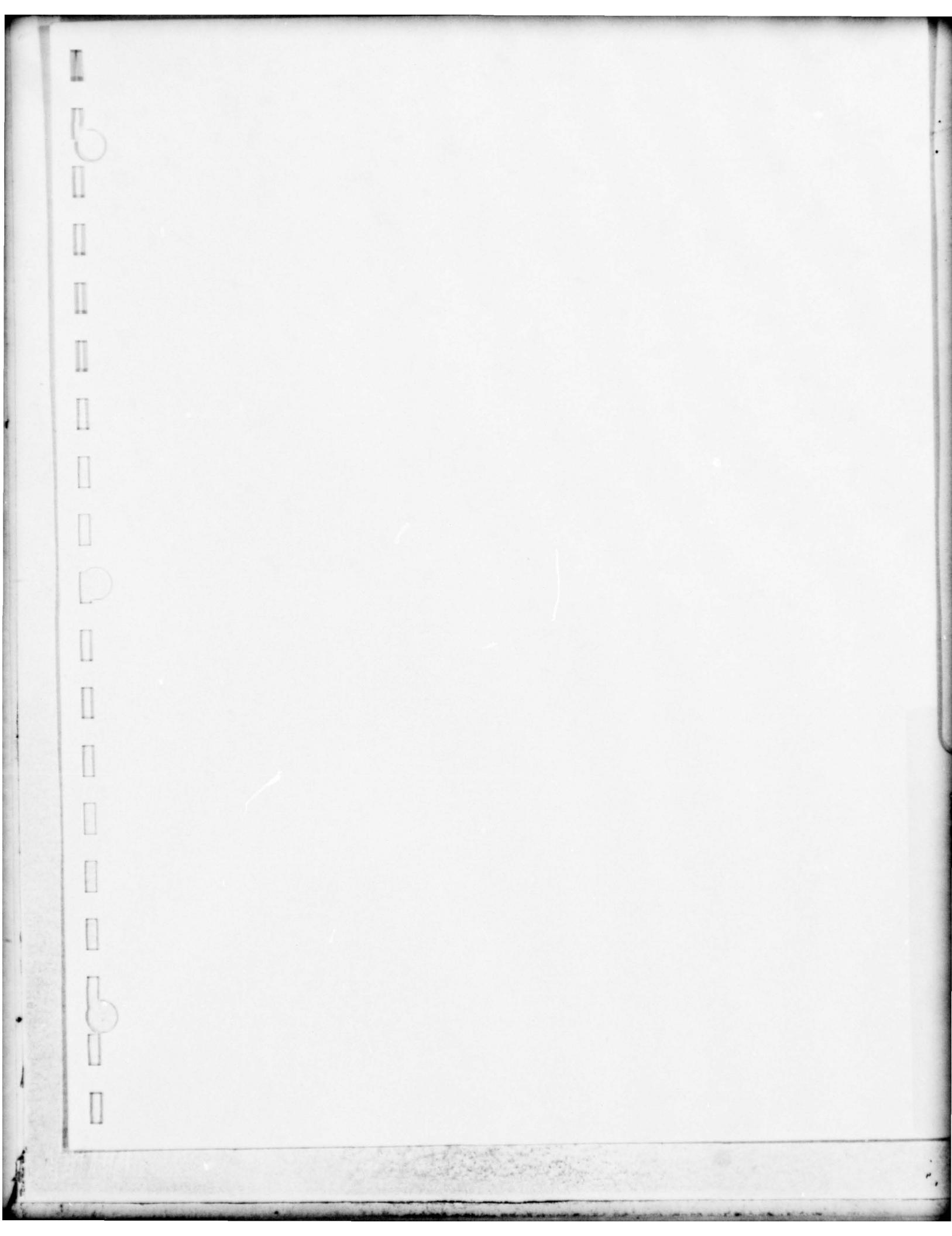


Conical frustums with  $t/D_1 = 2.0$ ; elevation.



Conical frustums with  $t/D_i = 2.0$ ; high-pressure face.

B-103



APPENDIX C. CRITICAL PRESSURES AND DISPLACEMENTS OF  
SPHERICAL SECTORS . . . C-1

C.1 SHORT-TERM PRESSURE LOADING . . . C-1

- C.1.1 Critical Pressures . . . C-2
- C.1.2 Sliding Displacement . . . C-15
- C.1.3 Axial Displacement . . . C-22

C.2 LONG-TERM PRESSURE LOADING . . . C-29

- C.2.1 Time-Dependent Sliding Displacement . . . C-30
- C.2.2 Time-Dependent Axial Displacement . . . C-37

## APPENDIX C. CRITICAL PRESSURES AND DISPLACEMENTS OF SPHERICAL SECTORS

### C.1 SHORT-TERM PRESSURE LOADING

Short-term pressure loading consisted of pressurizing the viewport assembly at a rate of 650 pounds per square inch (4.48 megapascals) per minute until catastrophic failure of the window took place. During the pressurization, axial displacement was measured at the center of the window's low-pressure face. This axial displacement represents the sum of window deflection and sliding inside the conical mounting.

Data generated by windows under short-term loading operationally represent the behavior of windows during a dive by a submersible or during the pressurization process of a hyperbaric chamber. As soon as the submersible ceases to sink or the hyperbaric chamber ceases to be pressurized by its operator, the behavior of the windows starts to deviate from short-term data. Its axial displacement increases even though the pressure loading remains constant and the potential critical pressure value decreases, both as functions of time under a given sustained pressure loading.

As a result of their operational limitations, short-term data should be used only with a complete understanding of their limitations. For this reason, short-term data are generally used only for four purposes:

- a. Evaluation of new window materials, mounting designs, mounting seat finishes, and other design and material variables.
- b. Evaluation of damage to a window in the form of crazing, scratches, cracks, weathering, nuclear radiation, etc.
- c. Determination of the displacements of windows during temporary overpressurization.
- d. Determination of the critical pressures of windows under temporary overpressurization.

The data generated by windows tested in mountings with  $D_i/D_f = D_i/(D_i - 0.2 R_i)^*$  are from the operational standpoint directly applicable, since usually in operational viewports in pressure vessels  $D_i/D_f$  is greater than 1.0.

Data generated by windows at ambient room temperature are directly applicable only to operational conditions at room temperatures (65 to 75°F) (18 to 24°C). For operational temperatures below room temperature, the room-temperature data become conservative, while for temperatures above room temperature they are unacceptable unless properly discounted.

Most data were generated with model-scale windows for reasons of economy. Since it has been proven, however, that there is no size effect for acrylic plastic (while it is known

---

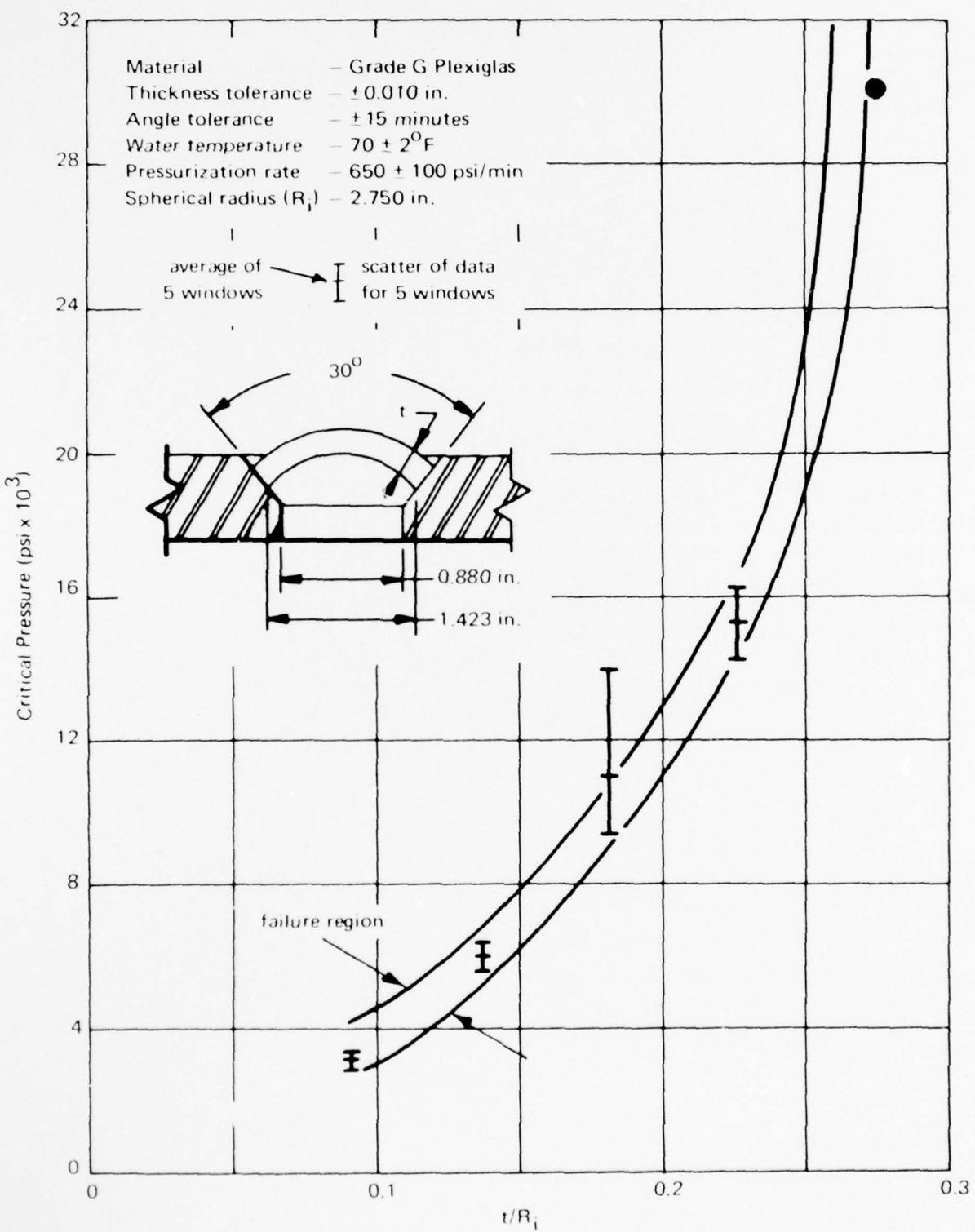
\* $R_i$  refers in this appendix to the internal curvature of the window's surface;  $D_i$  denotes the minor diameter of the window; and  $D_f$  describes the minor diameter of the conical seat in the mounting.

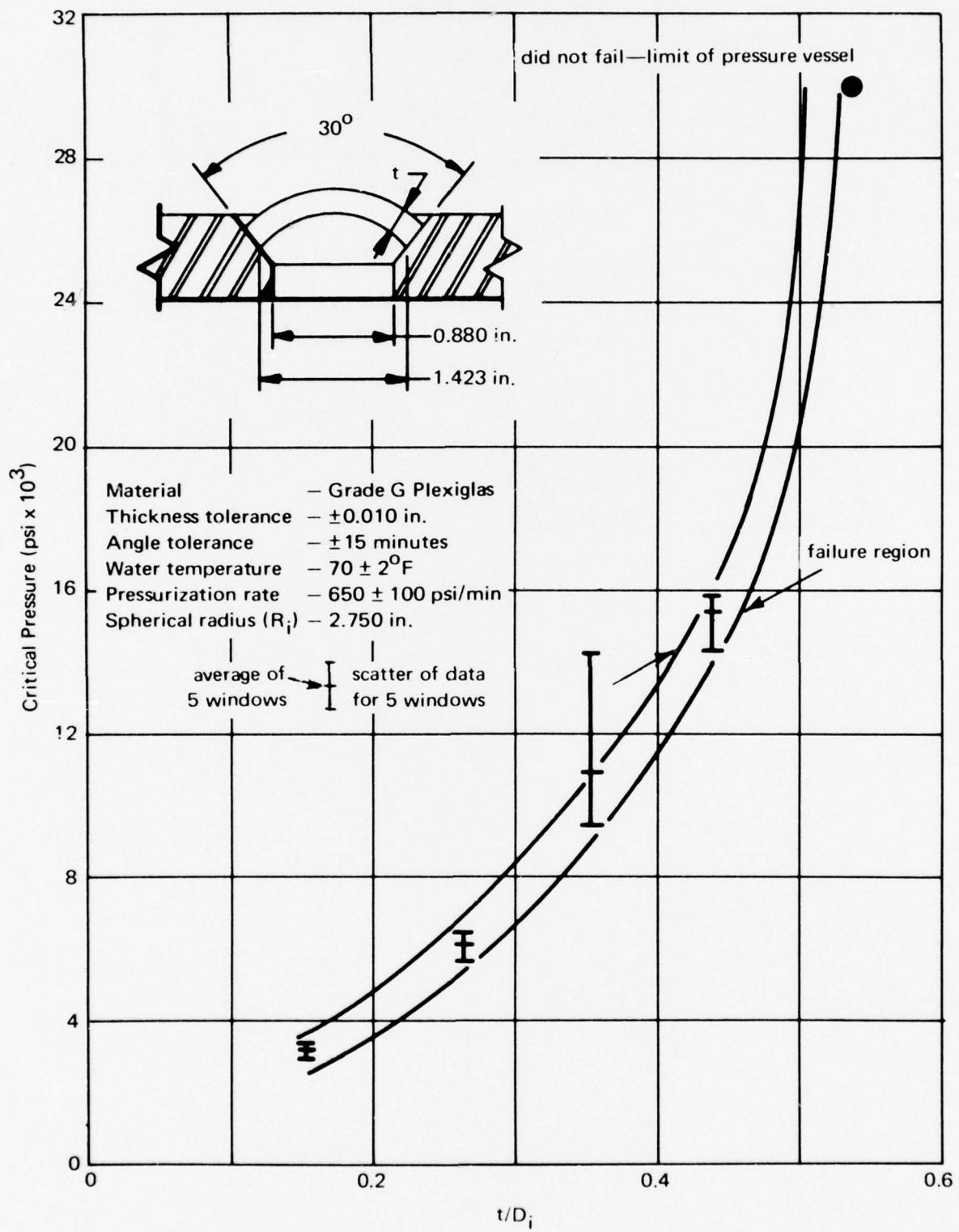
to exist for concrete, glass, and other brittle materials), data from model-scale windows can be used with confidence for predicting the performance of full-scale, acrylic plastic, conical frustums. The critical pressures can be directly used, as the critical pressure for model- and full-scale windows is the same, if both have the same included angle and  $t/D_i$  ratio and are tested in mountings with the same  $D_f/D_i$  ratio. Sliding and axial displacements of full-scale windows can be extrapolated from the displacements of model-scale windows, if the displacements of model-scale windows are multiplied by the ratio of full-scale to model-scale window diameters.

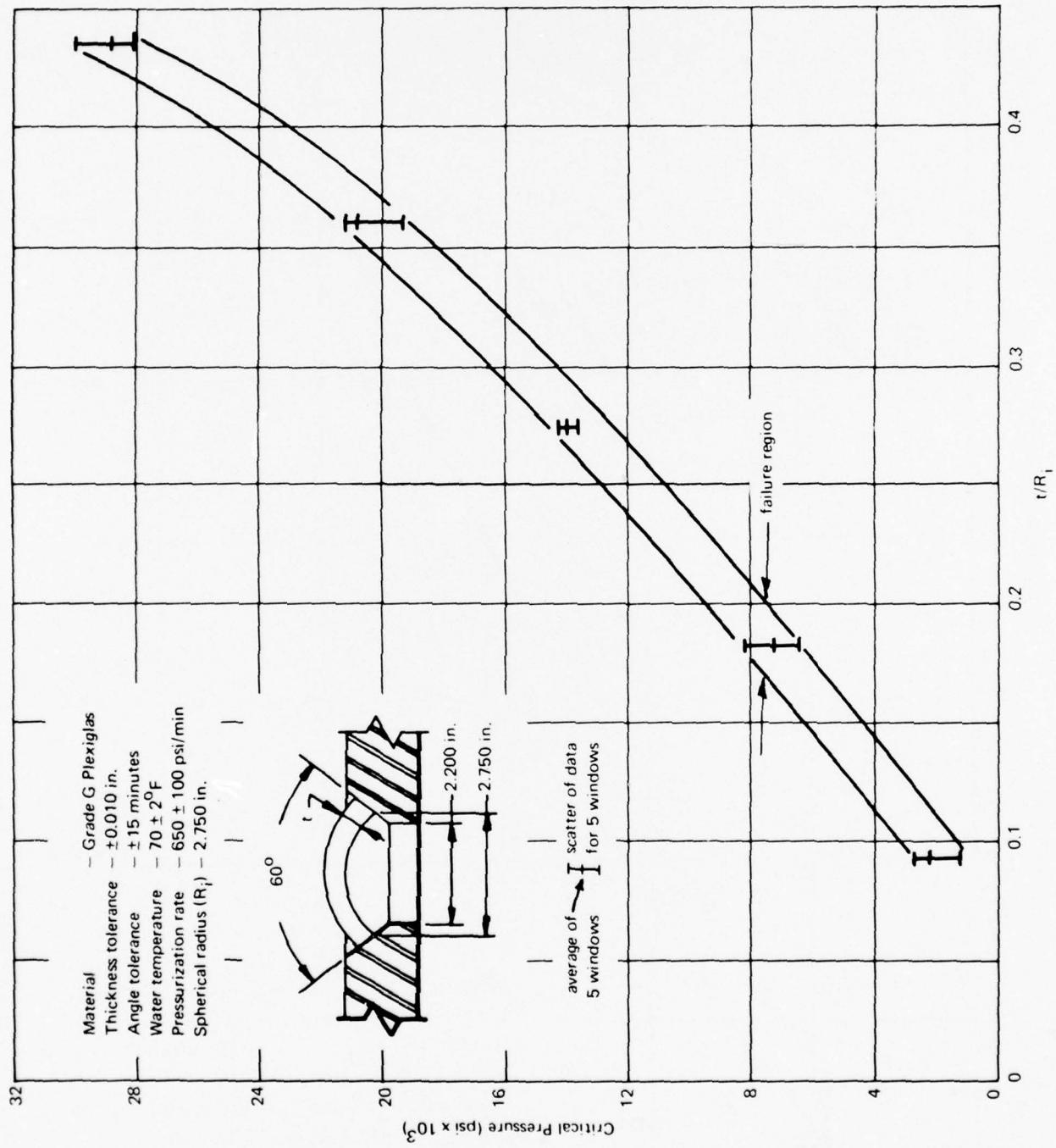
The sliding displacement was measured along the surface of the seat in the steel mounting. To obtain the axial component of sliding in the mounting seat, the recorded sliding values must be multiplied by  $\cos \alpha/2$ , where  $\alpha$  represents the total included angle of the spherical sector.

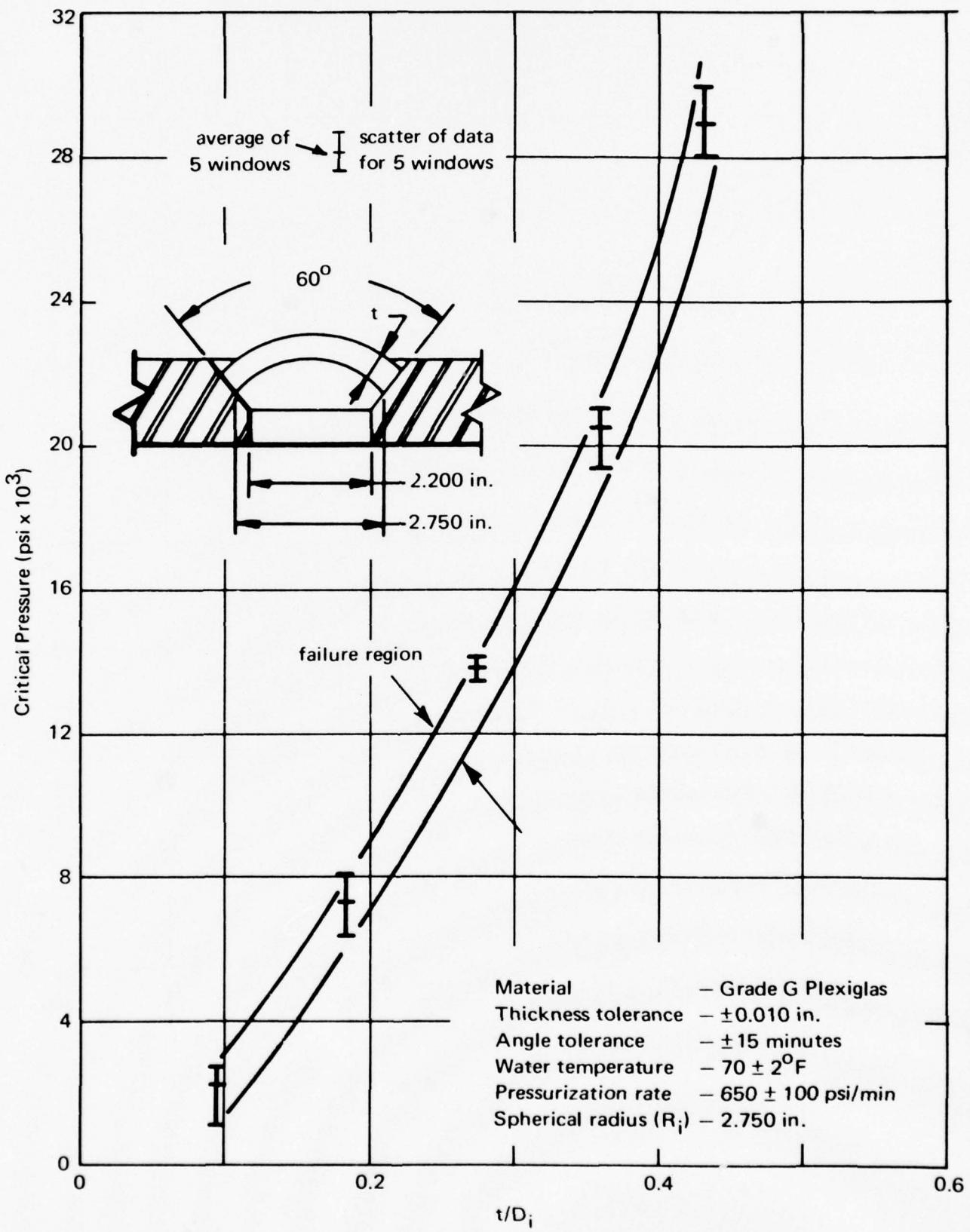
### C.1.1 Critical Pressures

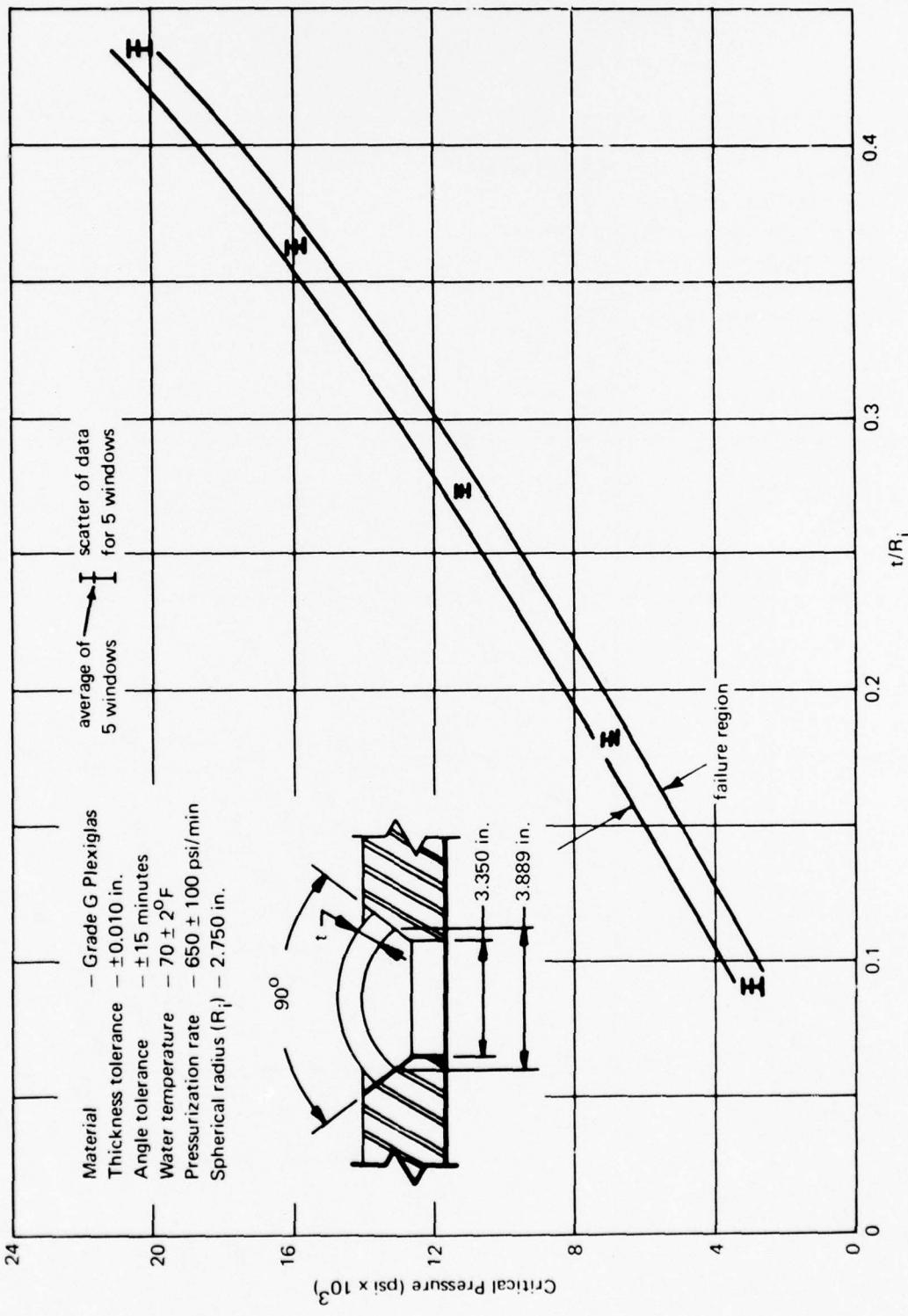
Data in this section are concerned with the critical pressures of spherical sectors with 30-, 60-, 90-, 120-, 150-, and 180-degree (0.5, 1.04, 1.57, 2.09, and 3.14 radians) included angles under short-term pressure loading at ambient room temperature in the mounting with  $D_f = (D_i - 0.2 R_j)$ .

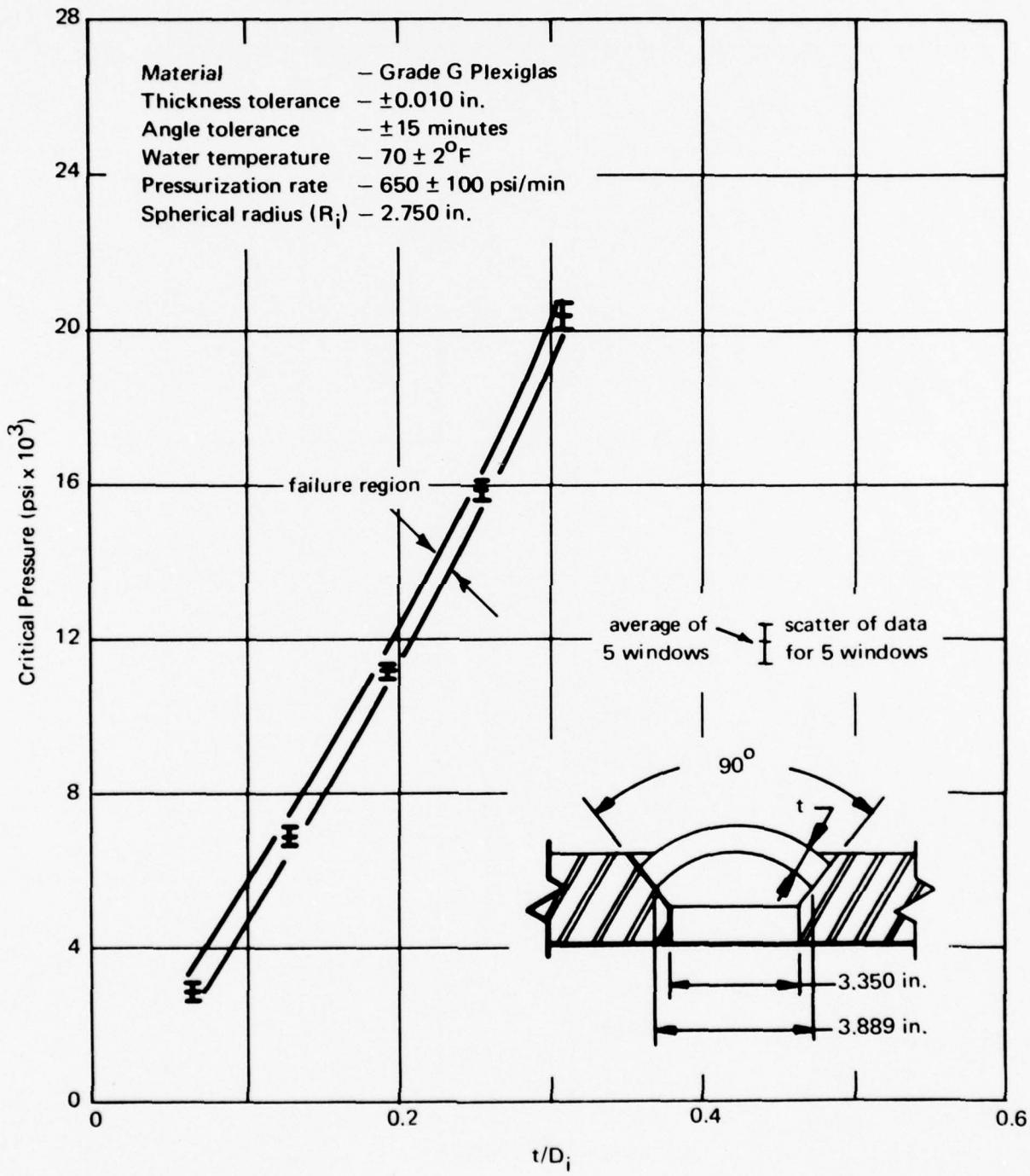


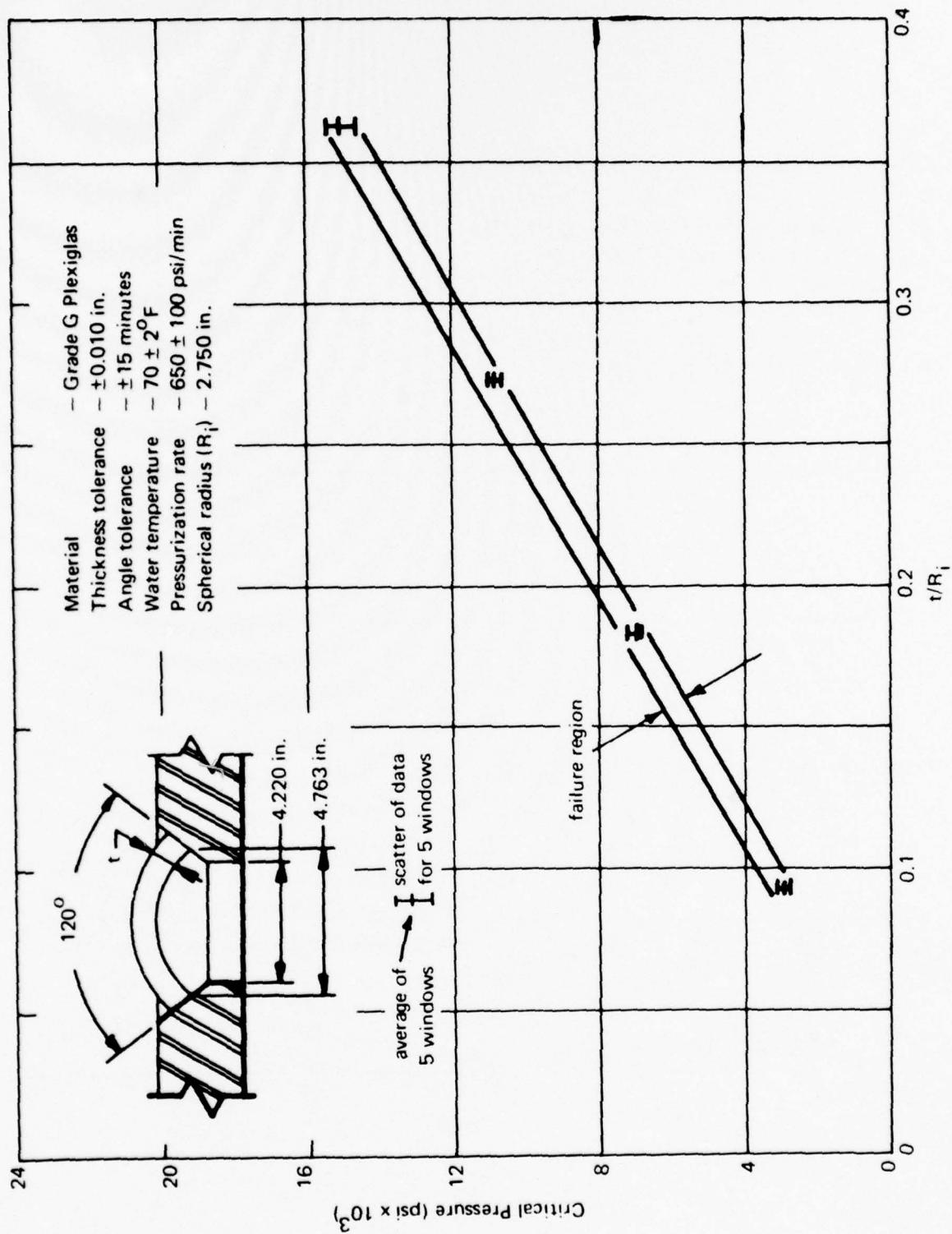


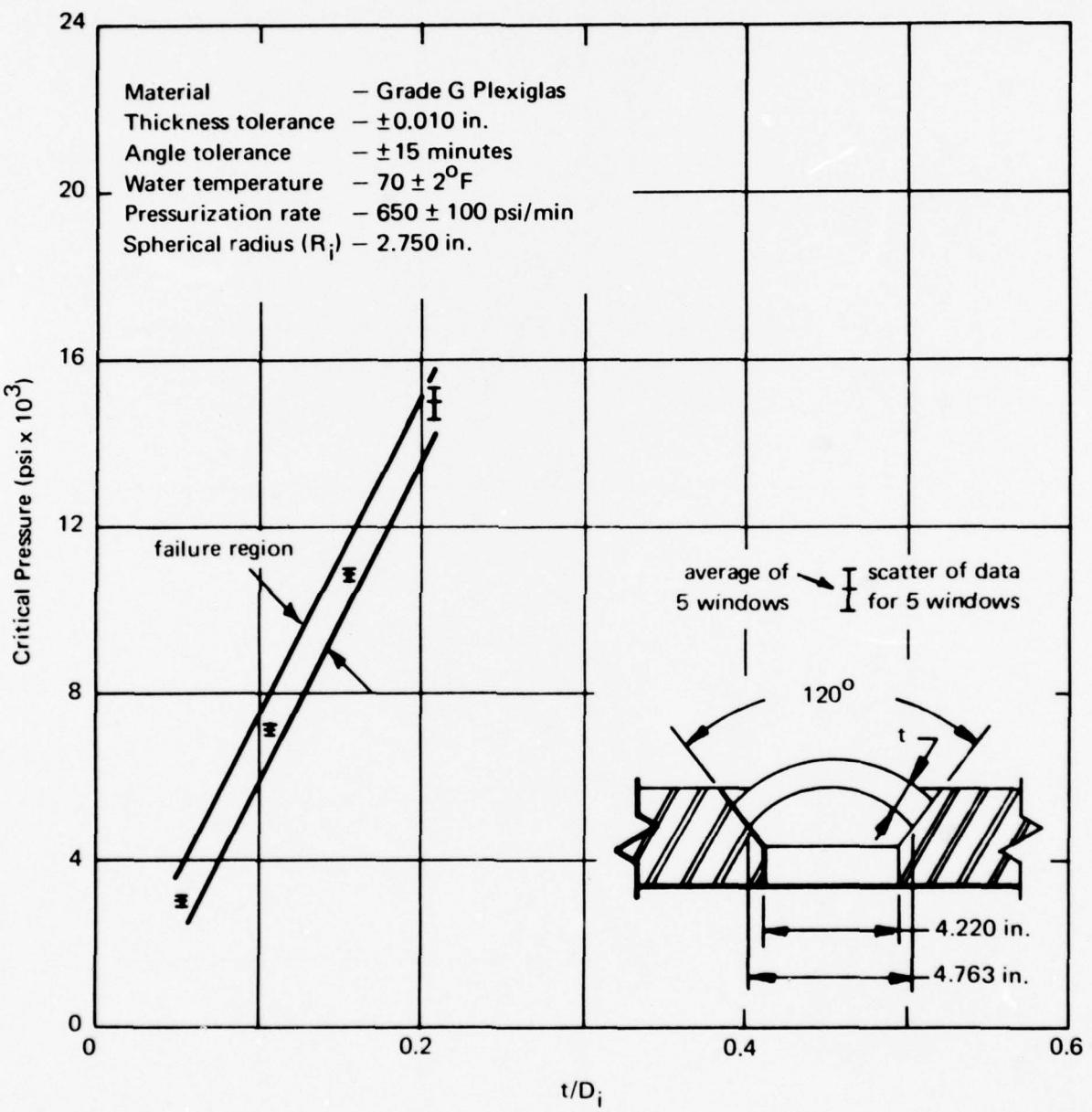




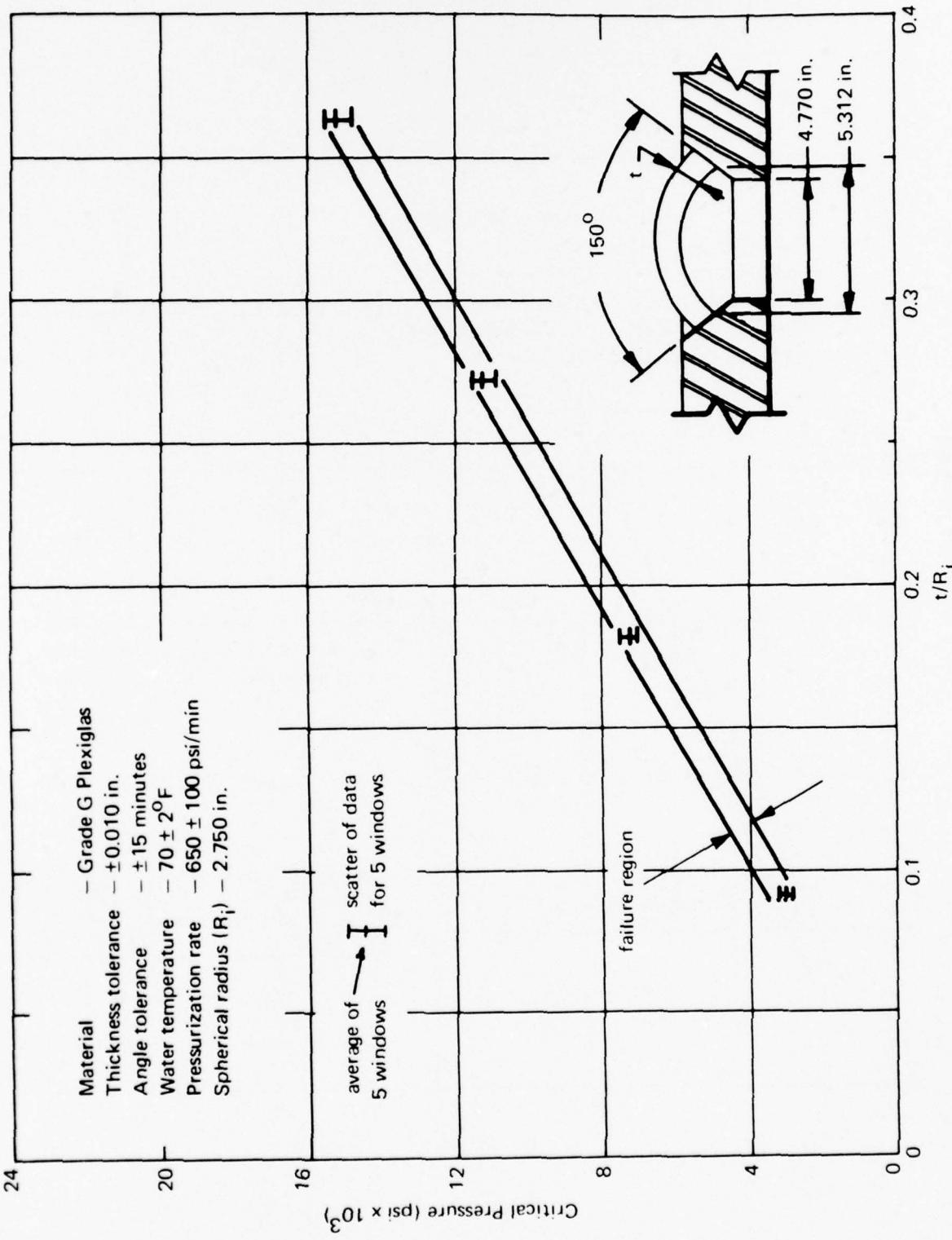


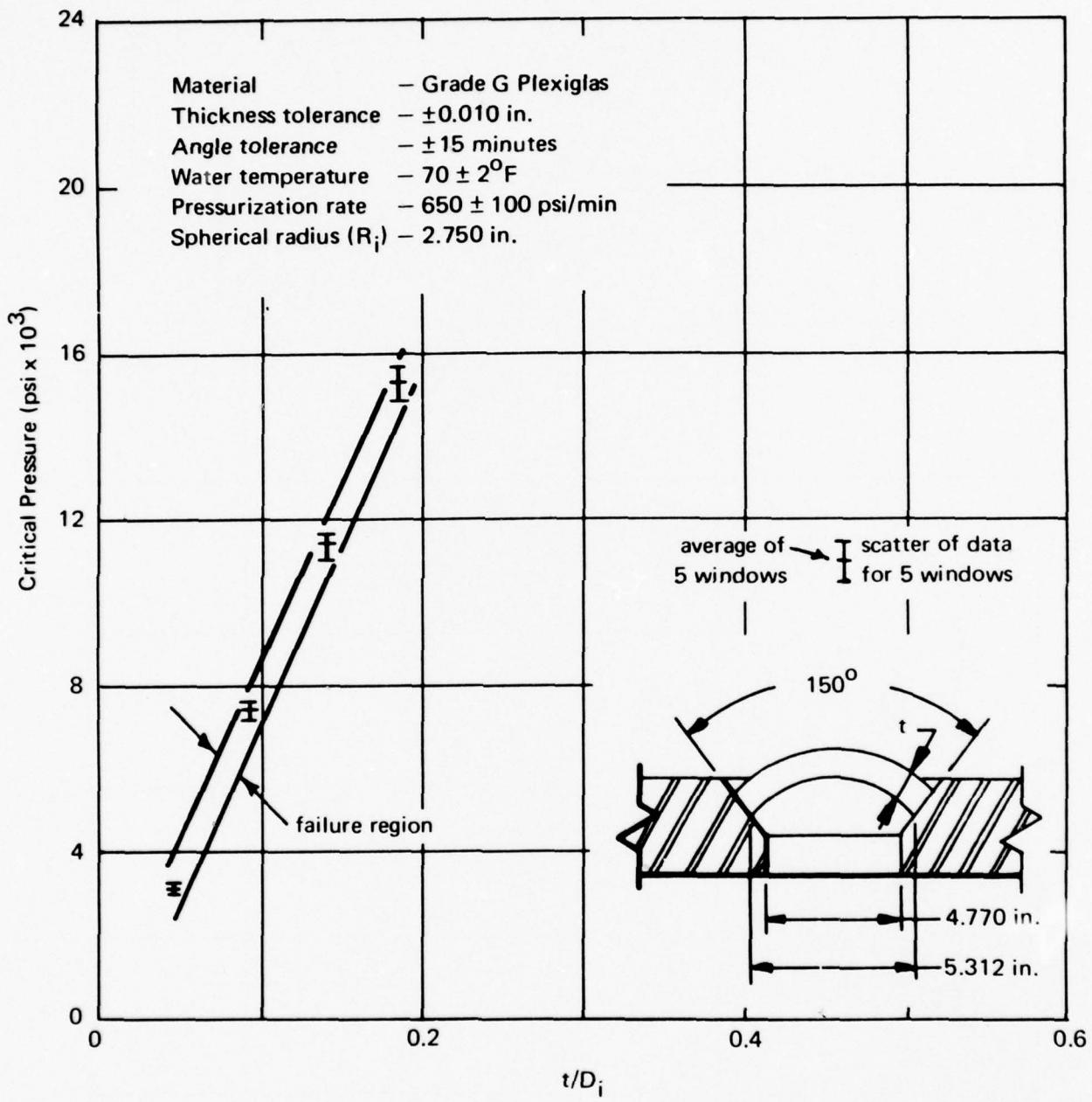


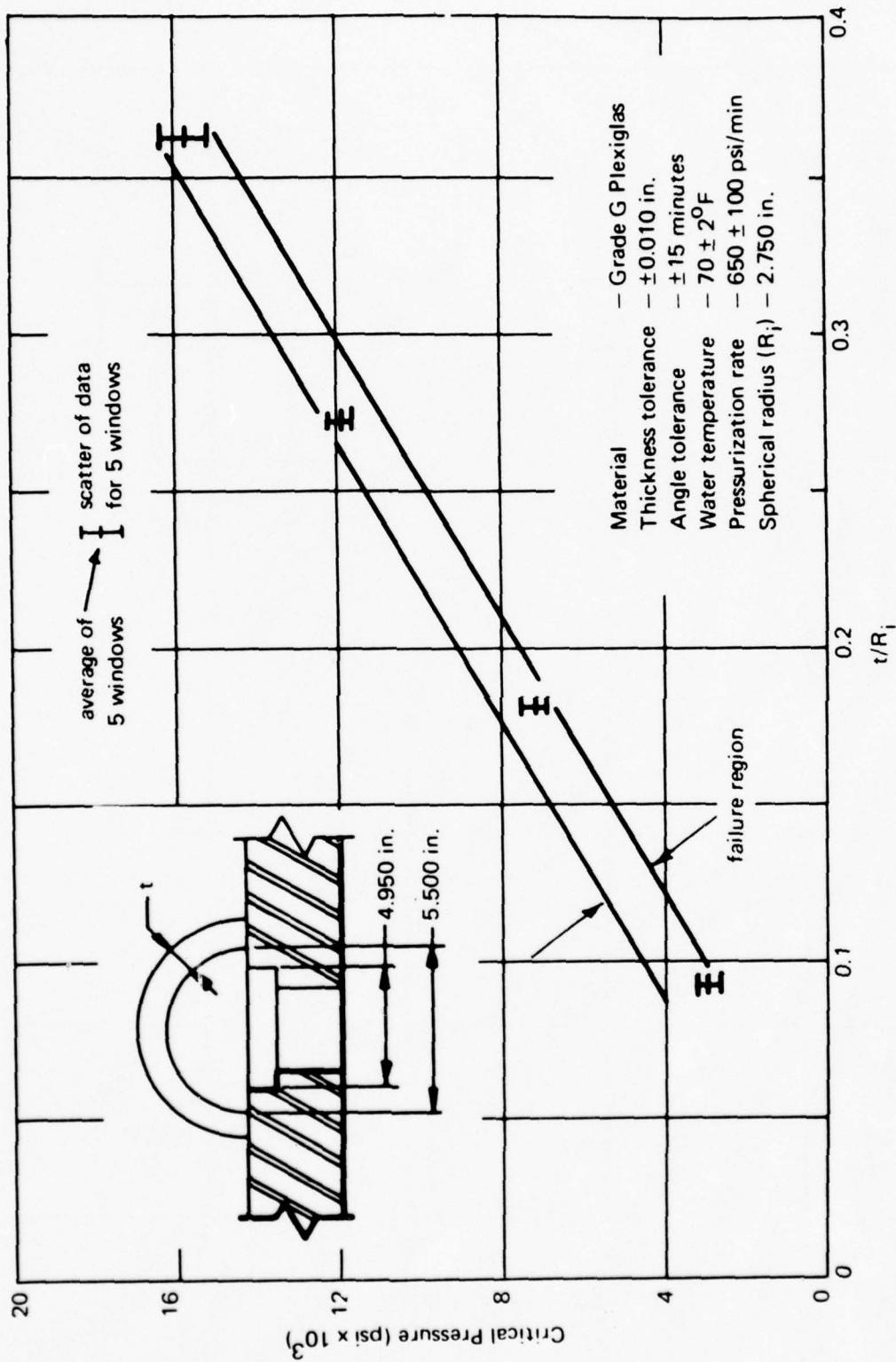


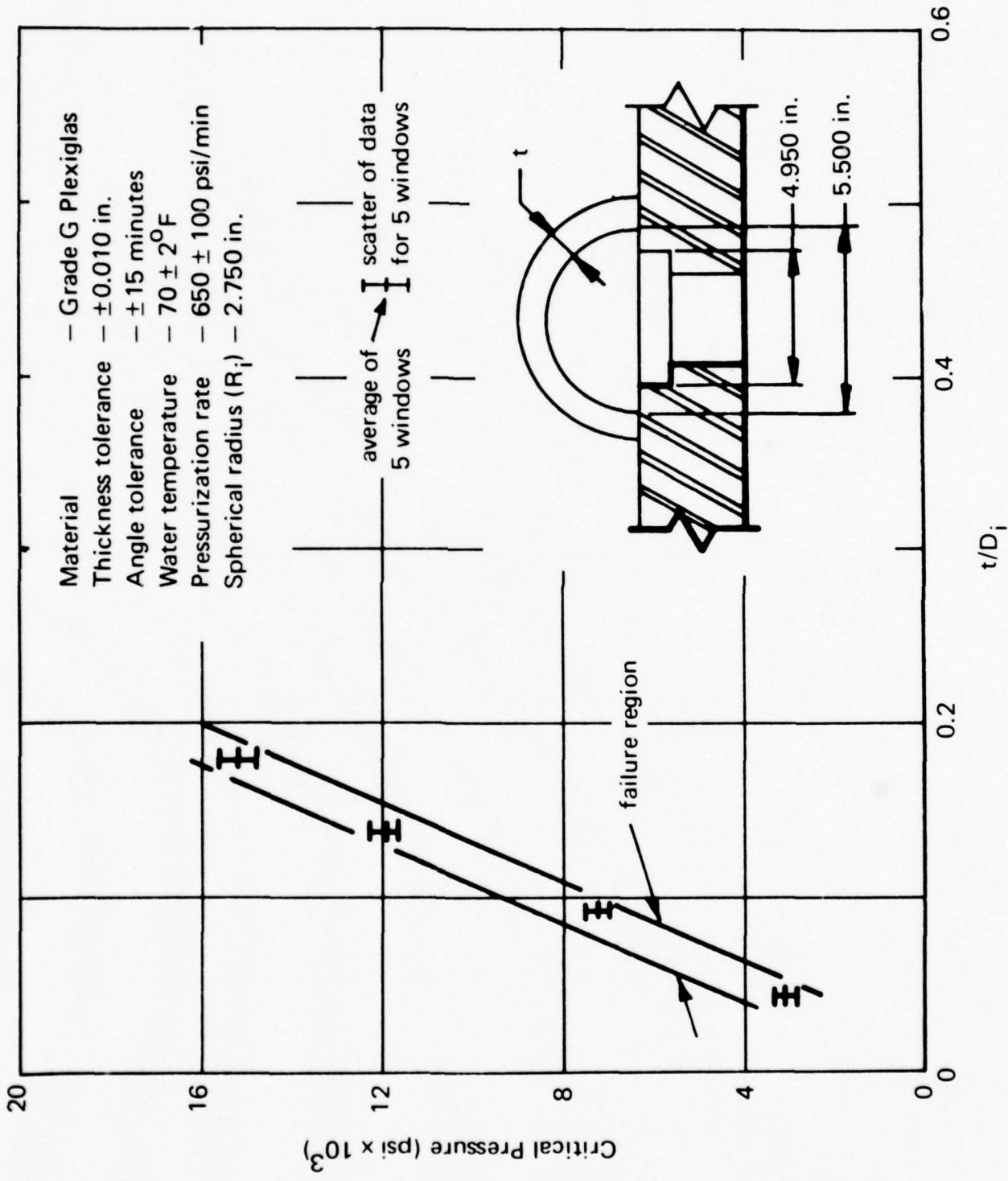


Material - Grade G Plexiglas  
 Thickness tolerance -  $\pm 0.010$  in.  
 Angle tolerance -  $\pm 15$  minutes  
 Water temperature -  $70 \pm 2^{\circ}\text{F}$   
 Pressurization rate -  $650 \pm 100$  psi/min  
 Spherical radius ( $R_i$ ) - 2.750 in.



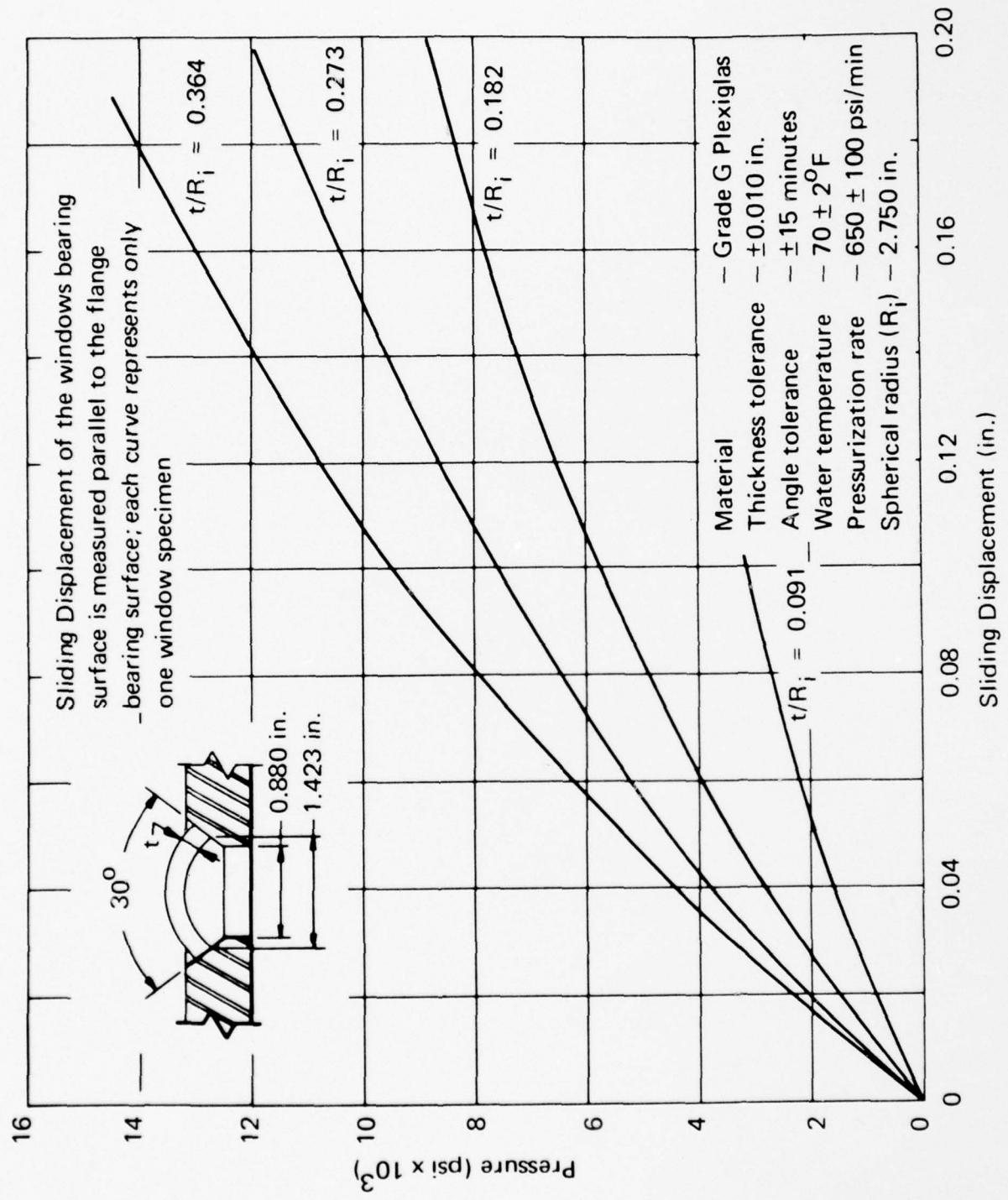


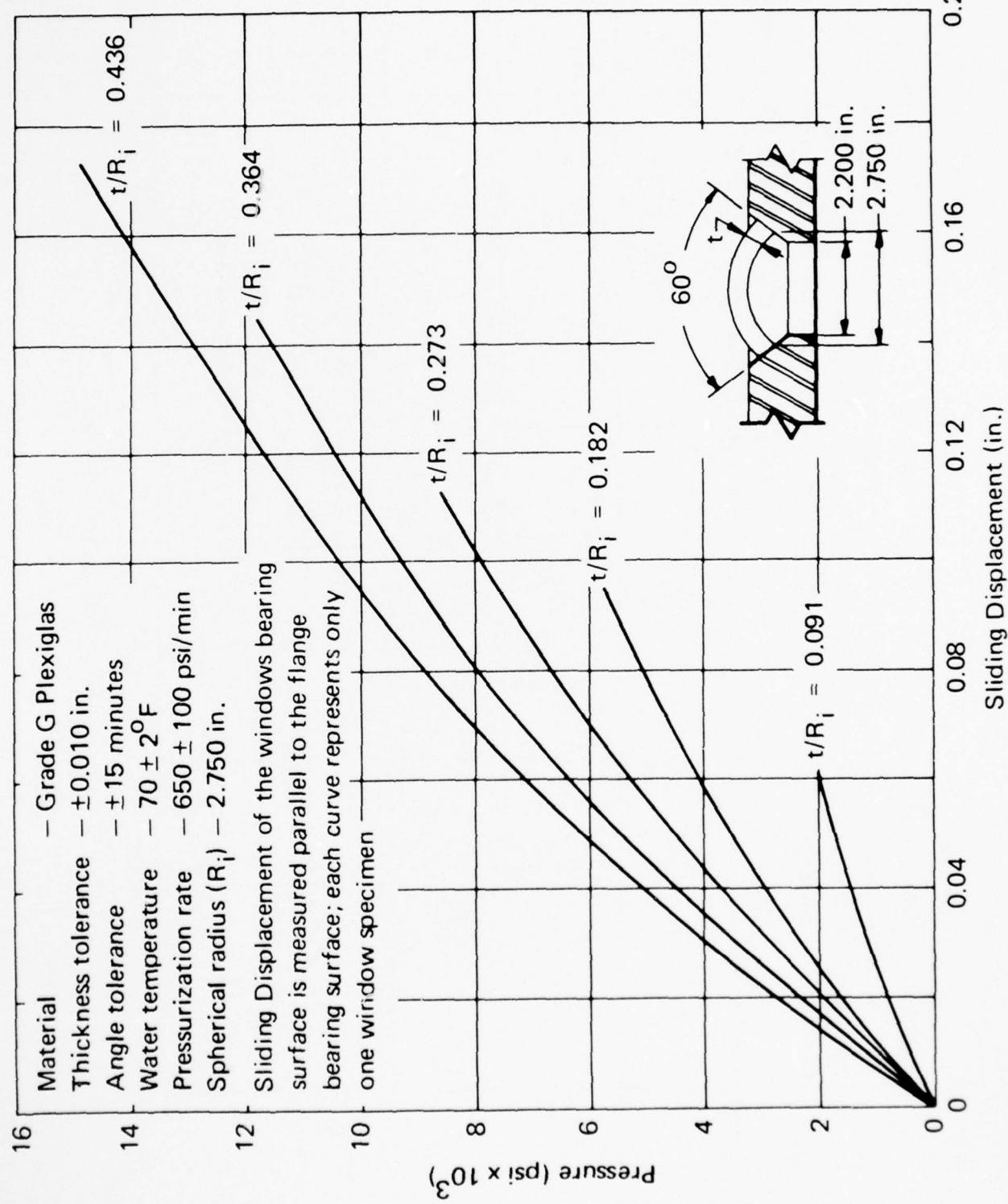


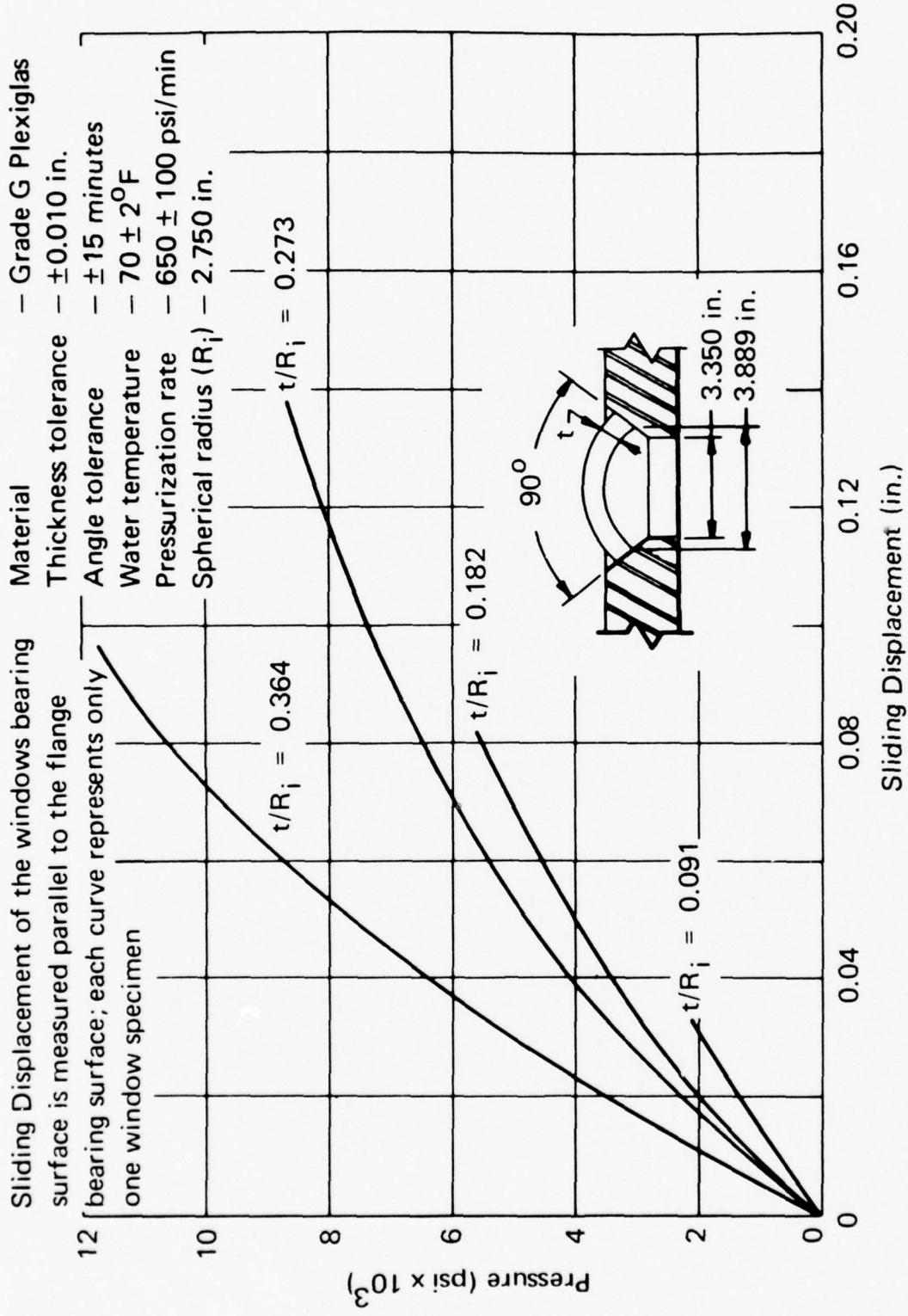


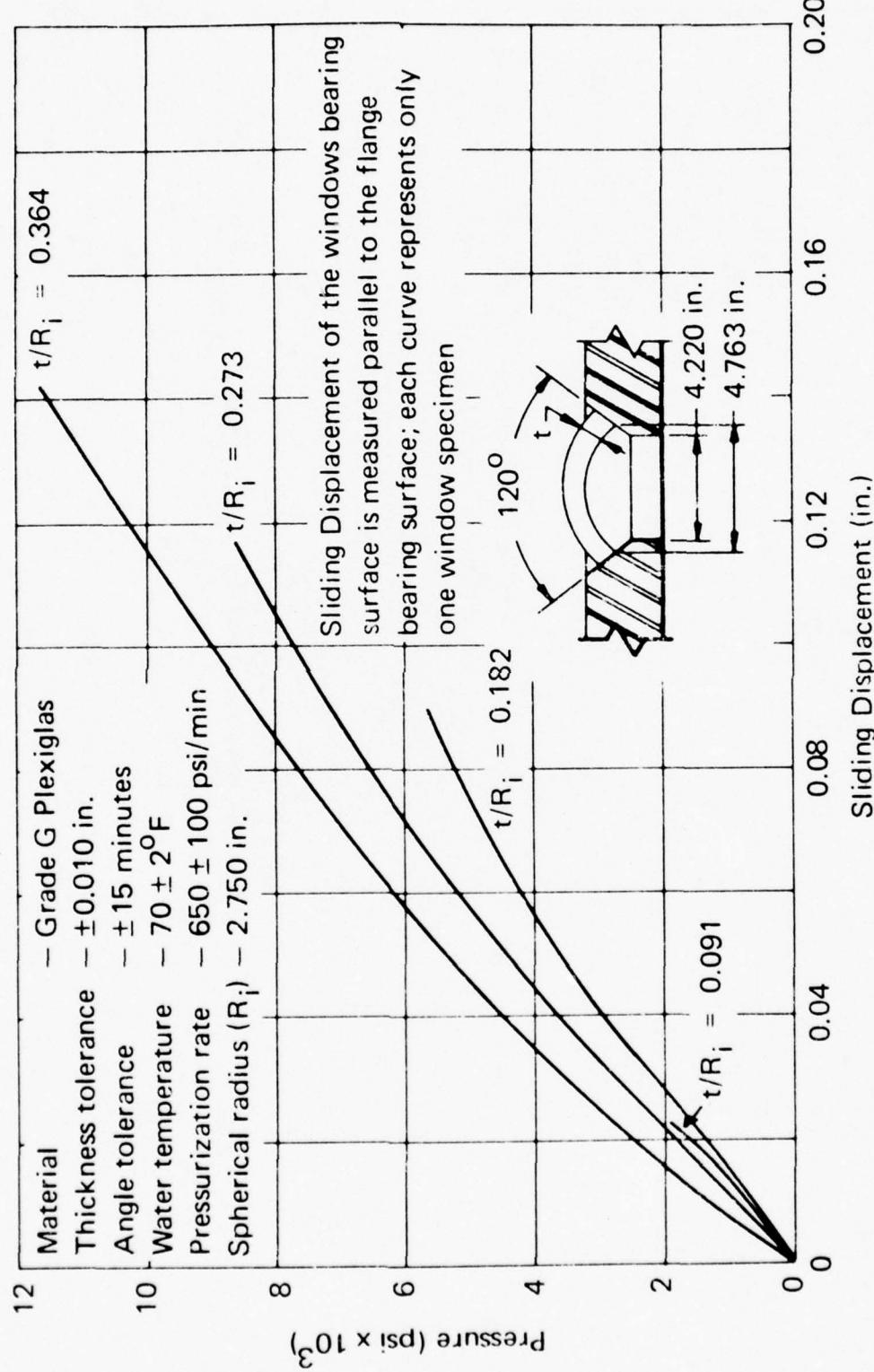
### C.1.2 Sliding Displacement

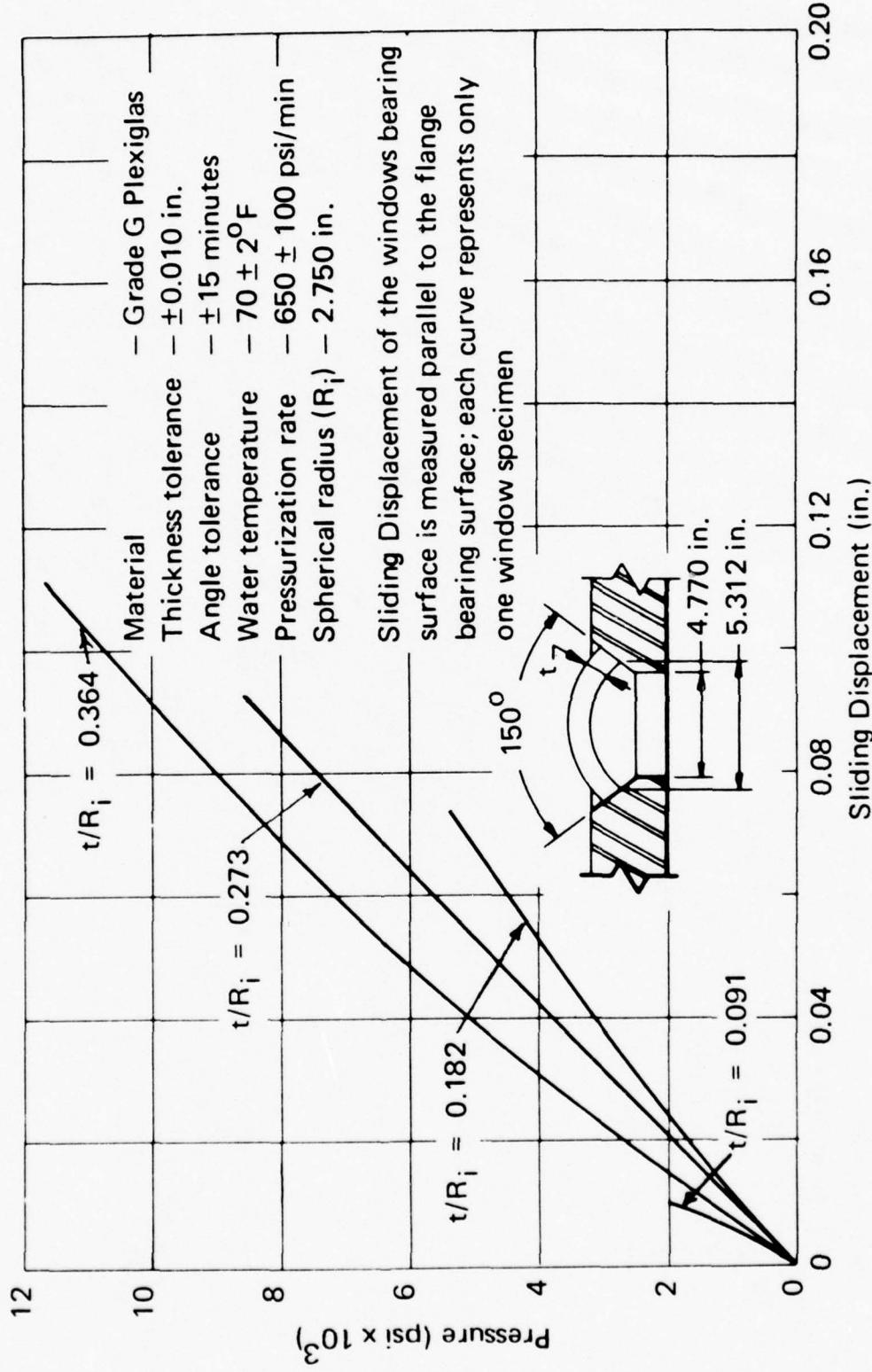
The data in this section are concerned with the sliding displacements of spherical sectors with 30-, 60-, 90-, 120-, 150-, and 180-degree (0.5, 1.04, 1.57, 2.09, 2.6, and 3.14 radians) included angles under short-term pressure loading at ambient room temperatures in the mounting with  $D_f = (D_i - 0.2 R_i)$ .

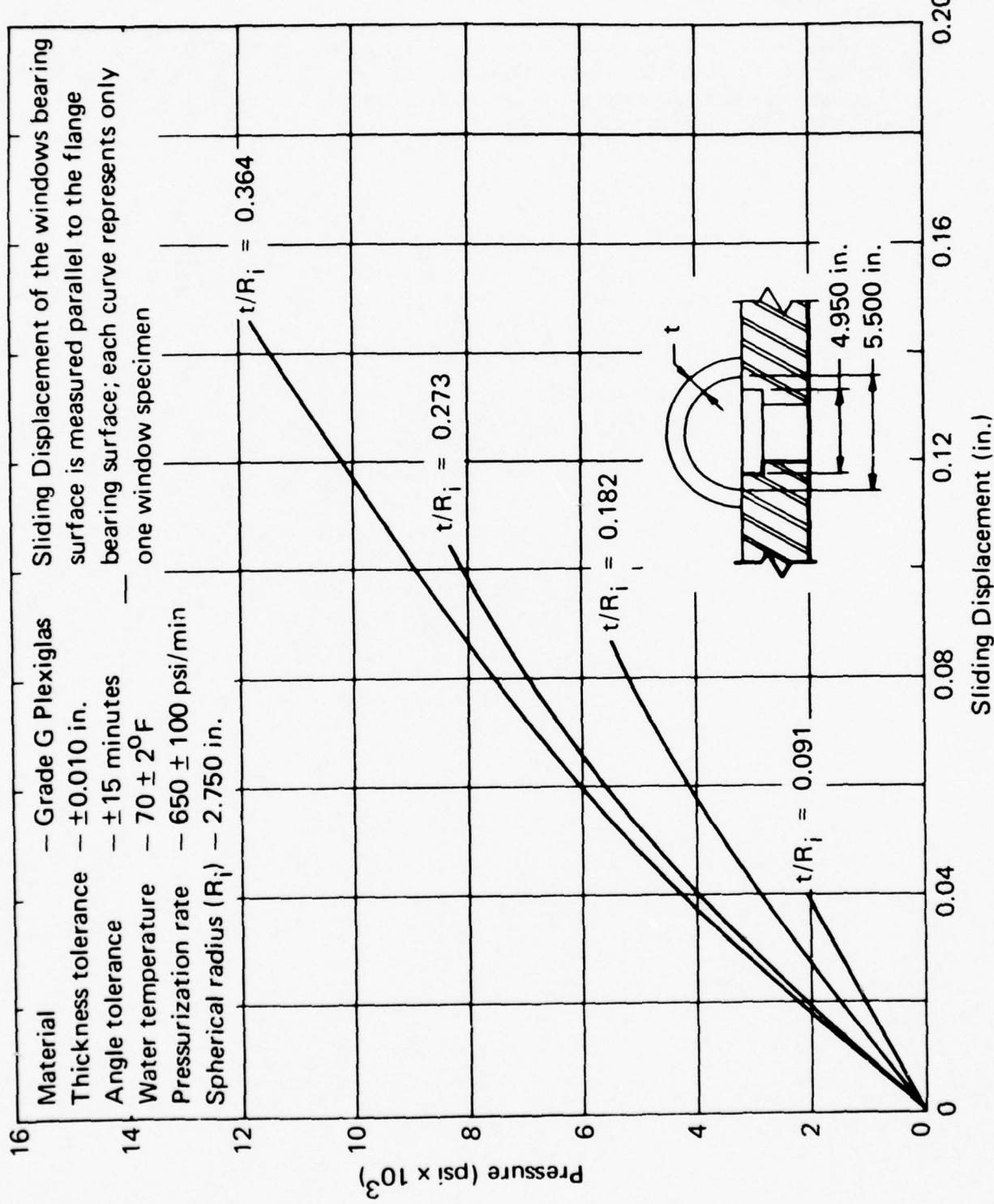








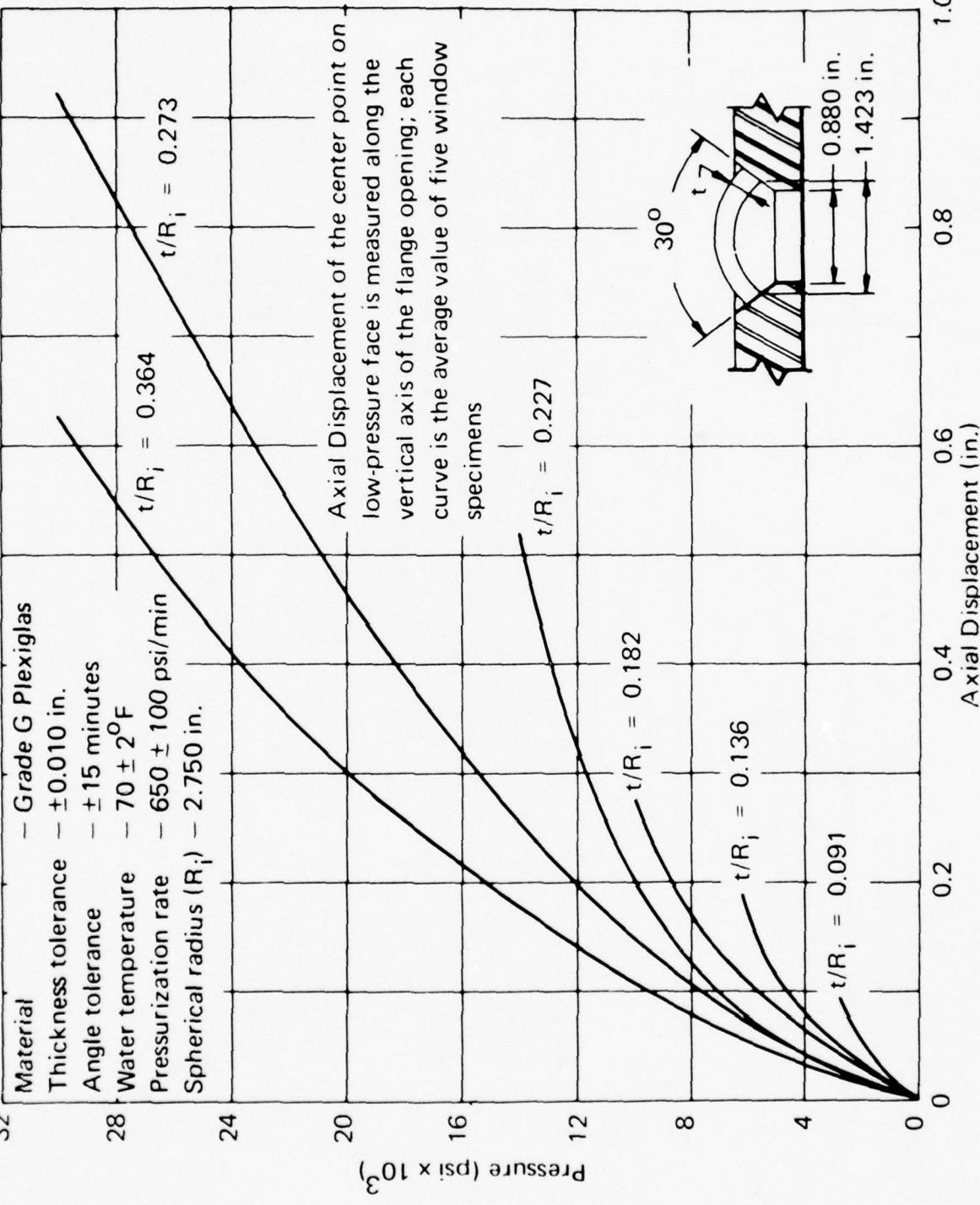




### C.1.3 Axial Displacement

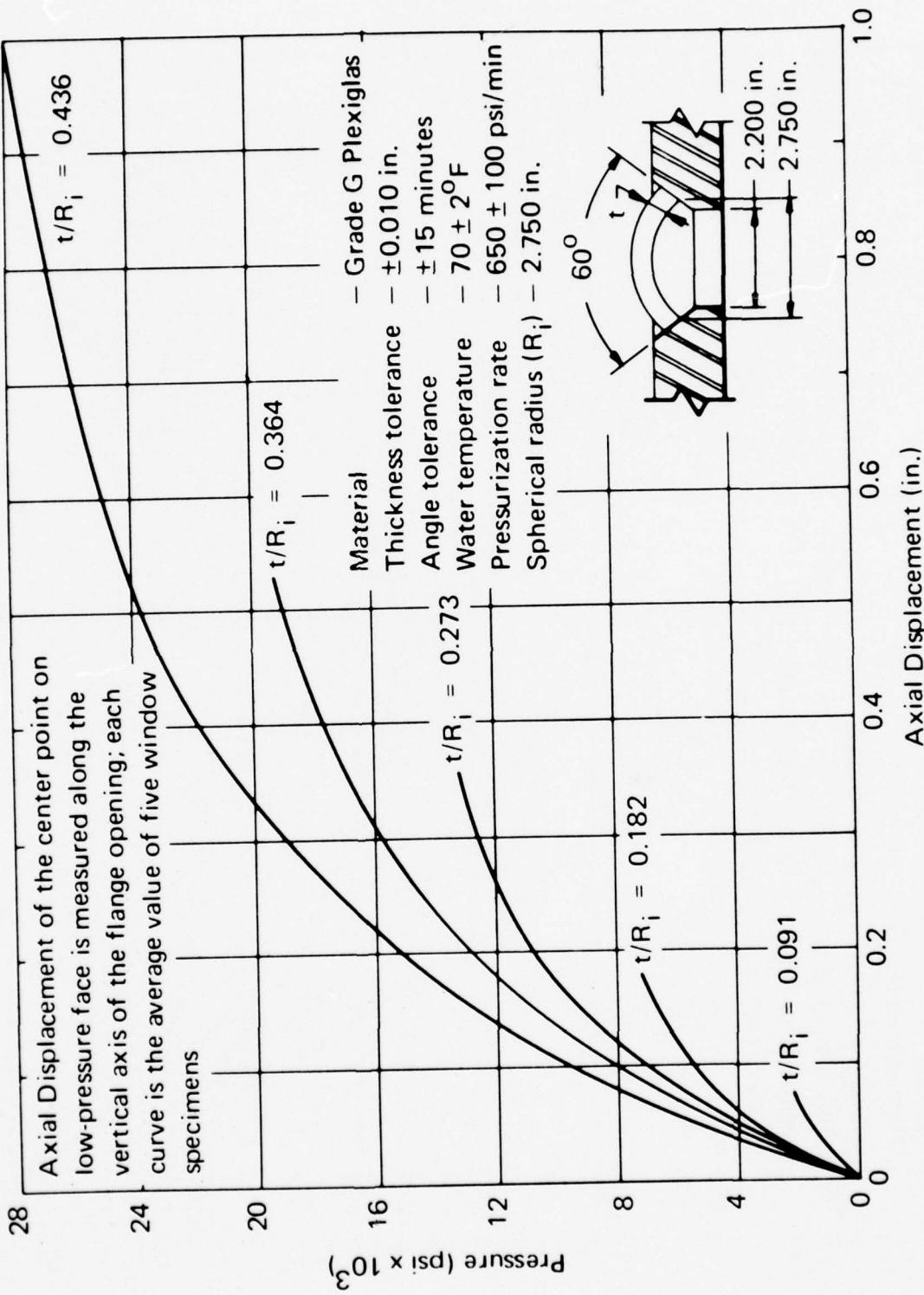
The data in this section are concerned with the axial displacements of spherical sectors with 30-, 60-, 90-, 120-, 150-, and 180-degree ( $0.5, 1.04, 1.57, 2.09, 2.57$ , and  $3.14$  radians) included angles under short-term pressure loading at ambient room temperatures in the mounting with  $D_f = (D_i - 0.2 R_j)$ .

32

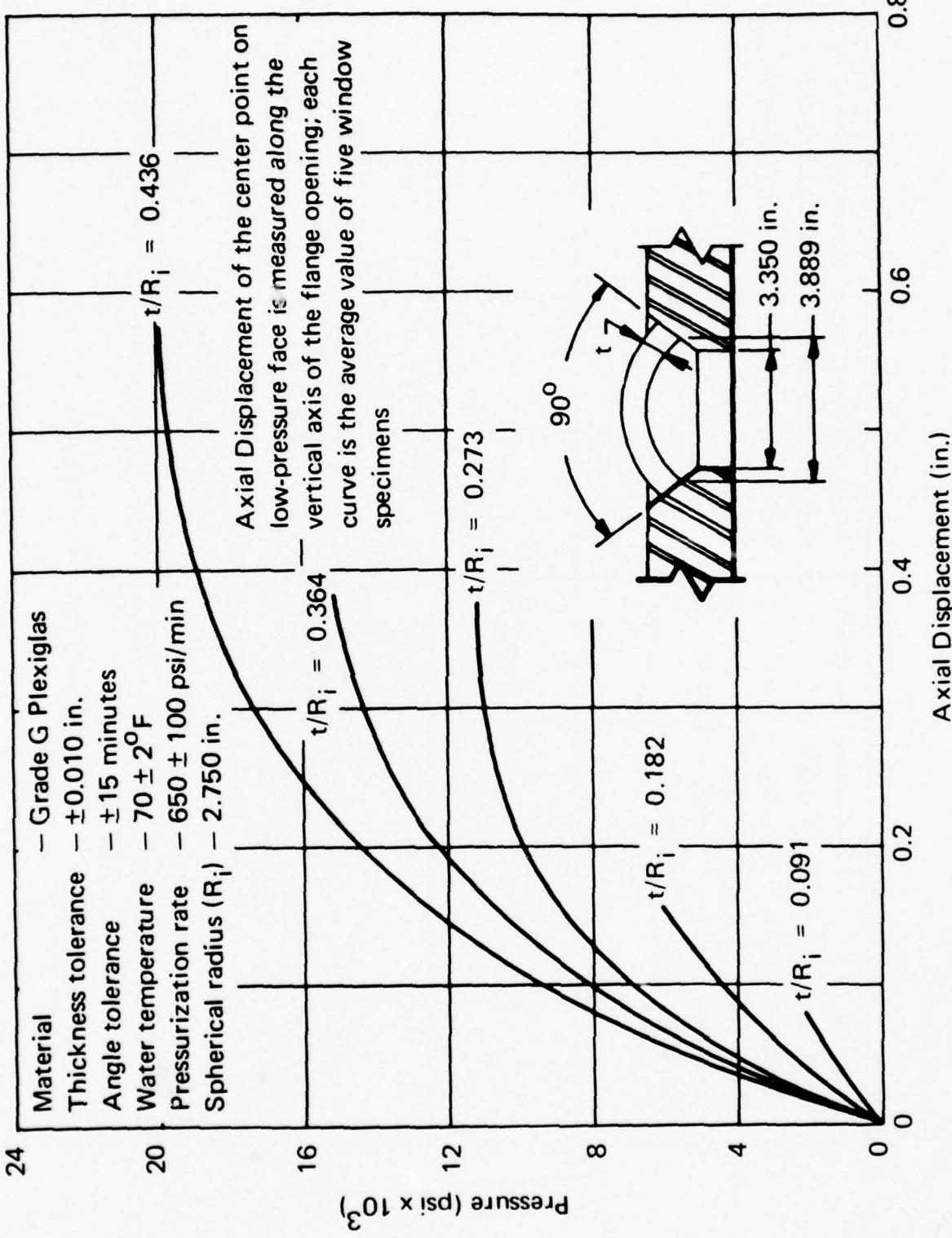


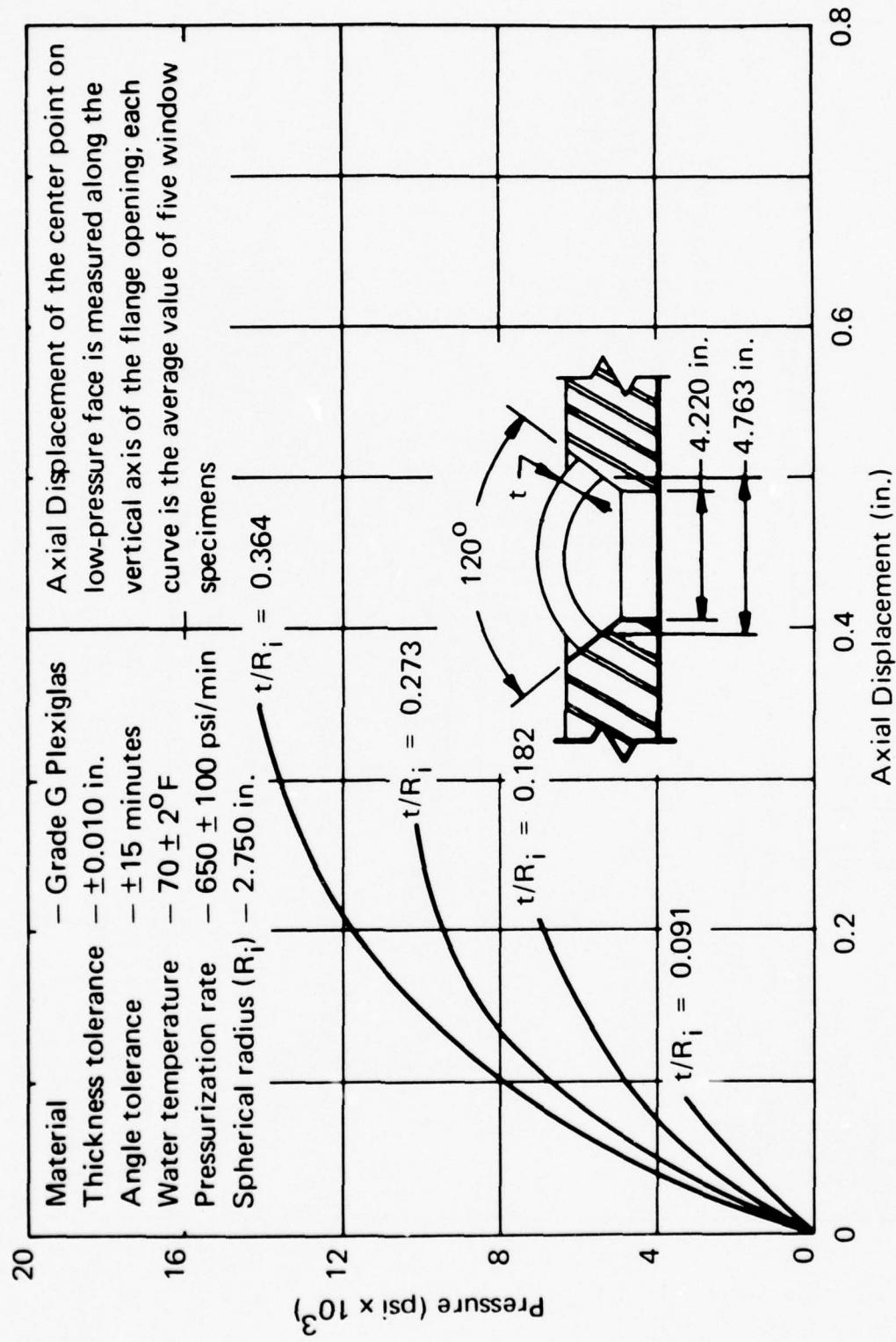
28

Axial Displacement of the center point on low-pressure face is measured along the vertical axis of the flange opening; each curve is the average value of five window specimens

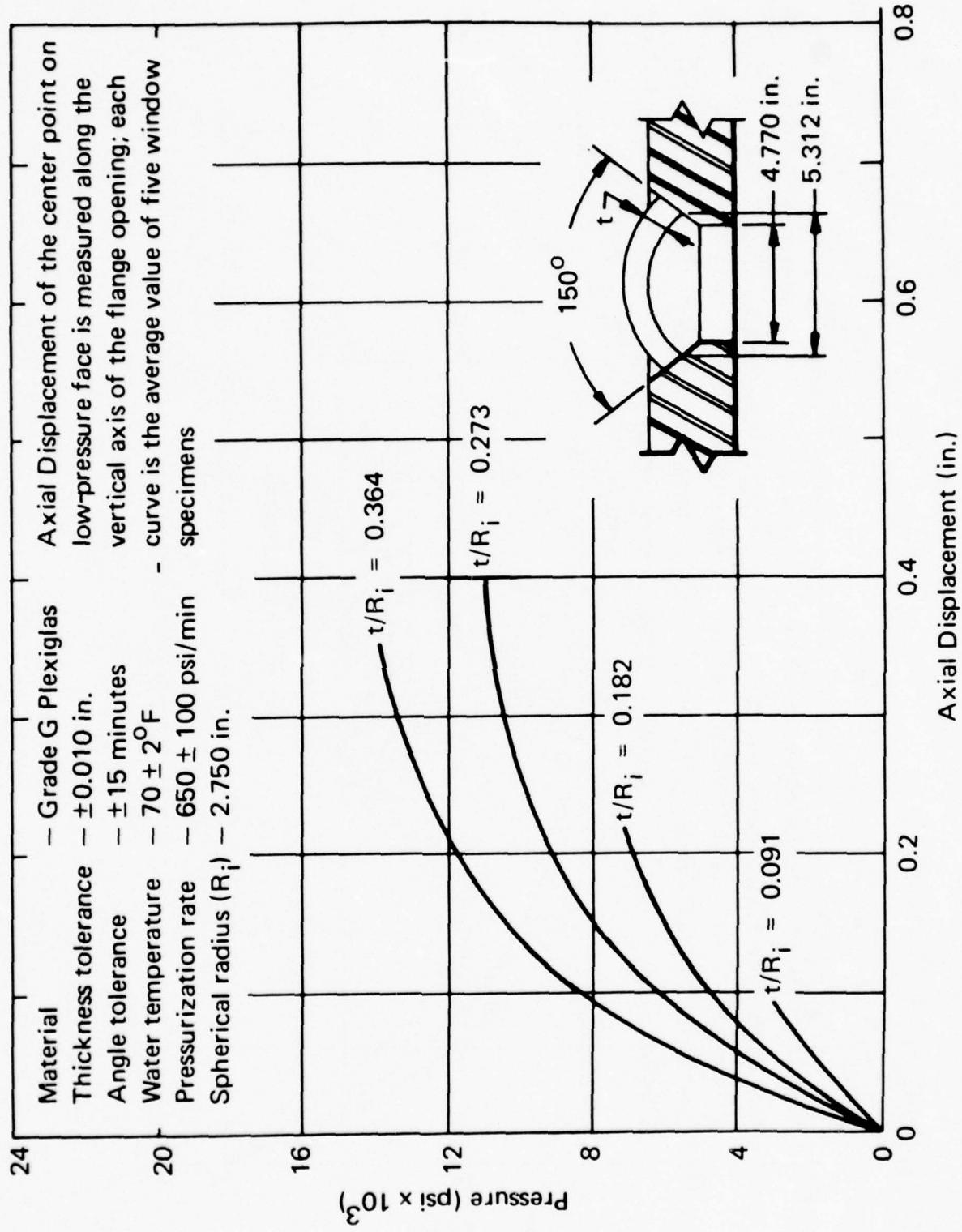


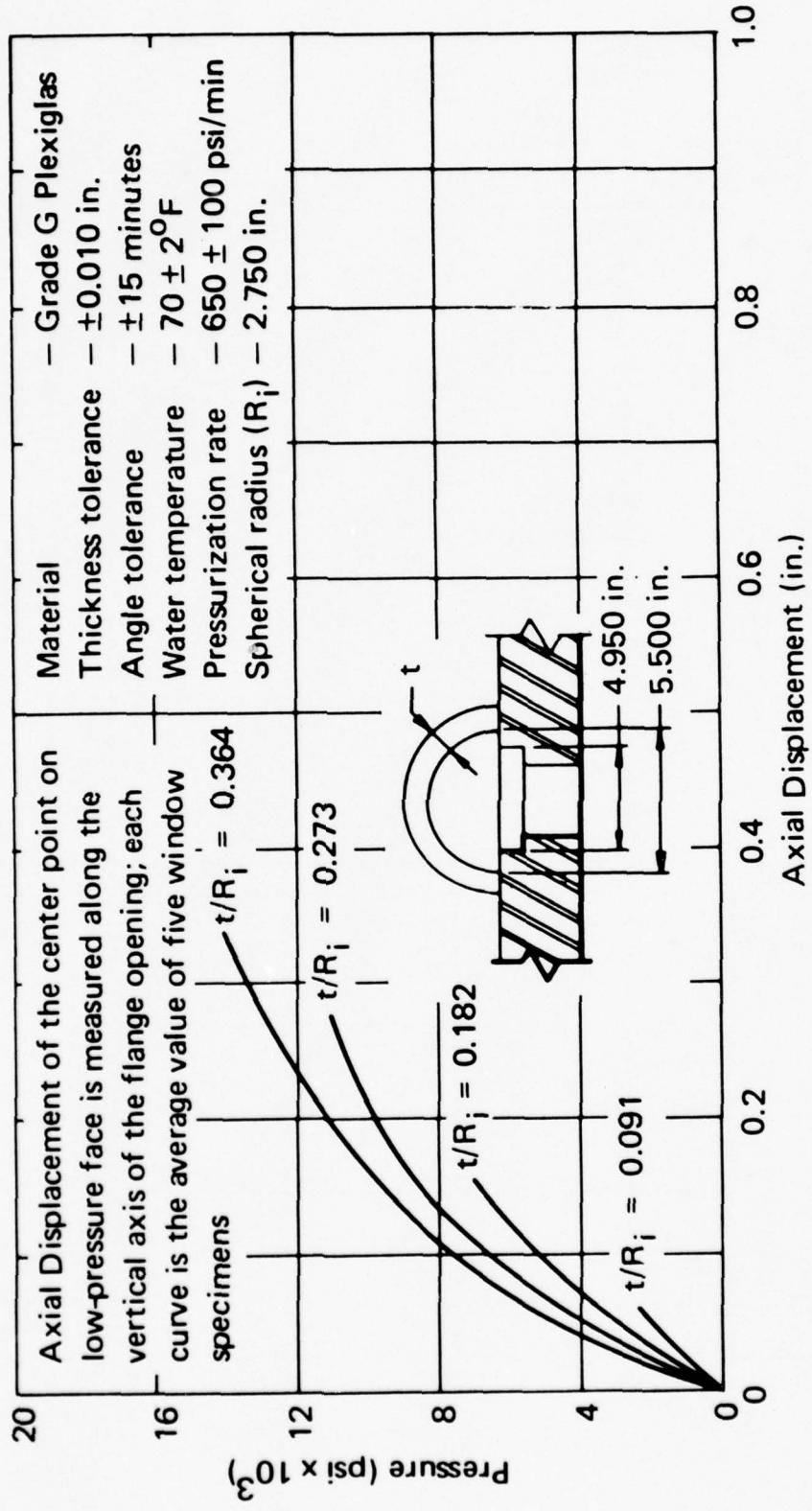
24





24





## C.2 LONG-TERM PRESSURE LOADING

Long-term pressure loading consisted of pressurizing the viewport assembly at a rate of 650 pounds per square inch (4.48 megapascals) per minute to the desired pressure, holding it for several minutes, and then depressurizing to 0 pound per square inch (0 megapascal). The windows were subsequently inspected for cracks, measured for permanent deformation, and photographed. The tests were performed with model-scale windows at room temperature in mountings with  $D_f = (D_i - 0.2 R_i)$ .

The axial and sliding displacements of model-scale windows can be used to predict the axial and sliding displacements of full-scale windows, if the displacements of the model-scale windows are multiplied by the ratio of full-scale to model-scale window diameters. Because the test data were generated at room temperature, they are directly applicable only to operational conditions at room temperature. For operational temperatures below room temperature, the displacement data becomes very conservative as there is a significant decrease in displacement and permanent deformation at lower temperatures. For temperatures above room temperature, the displacement data, as shown, cannot be safely applied.

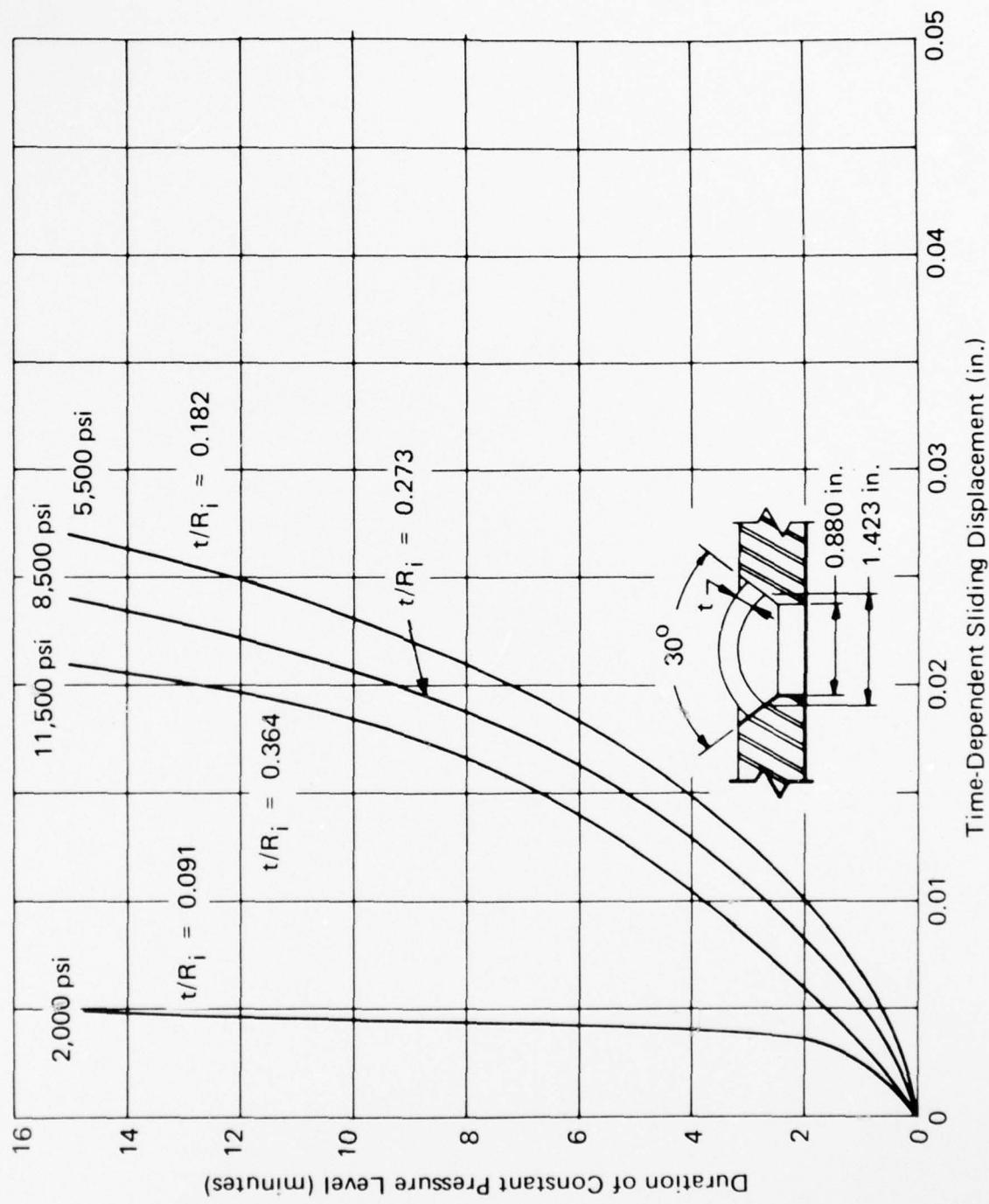
Since all long-term sliding and axial displacement data have been generated in mountings with  $D_i/D_f = D_i/(D_i - 0.2 R_i)$ , they are directly applicable to all operational viewport designs with  $D_i/D_f > 1.0$ . However, to determine the actual value the window's sliding or axial displacement, the time-dependent sliding or axial displacement must be added to the value for the short-term sliding or axial displacement for the given pressure used in the long-term tests.

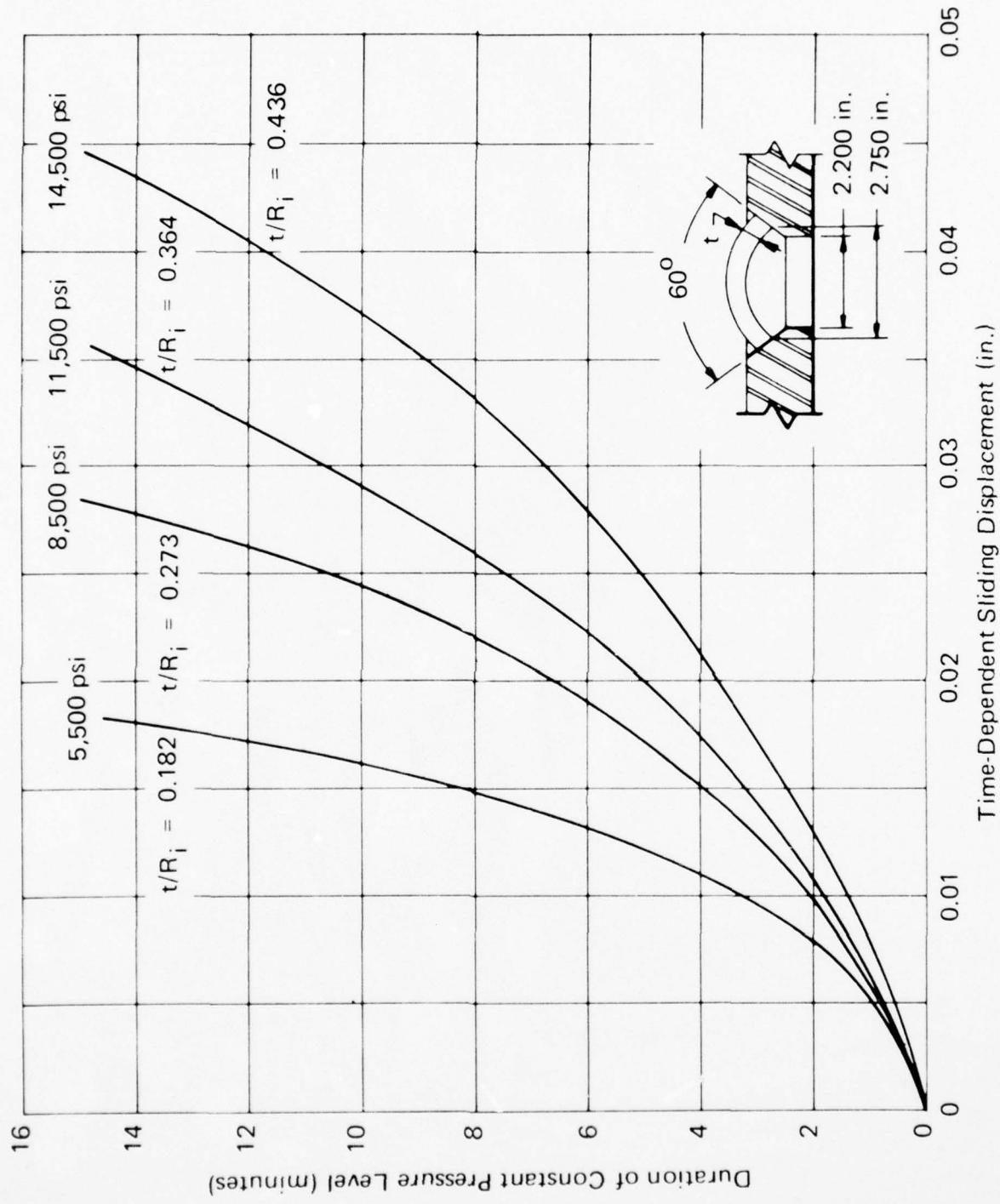
The values of long-term pressure loading were chosen to be less than those for short-term critical pressures, but greater than one-half of critical pressure under short-term loading. Thus, the pressure values for long-term loadings are 2 to 8 times higher than are the typical operational pressures for spherical sectors. Therefore, the displacement data in this section cannot be used for predicting displacements of spherical sectors under typical operational pressures. They are very useful, however, for predicting displacements during accidental overpressurization lasting only a few minutes.

### C.2.1 Time-Dependent Sliding Displacement

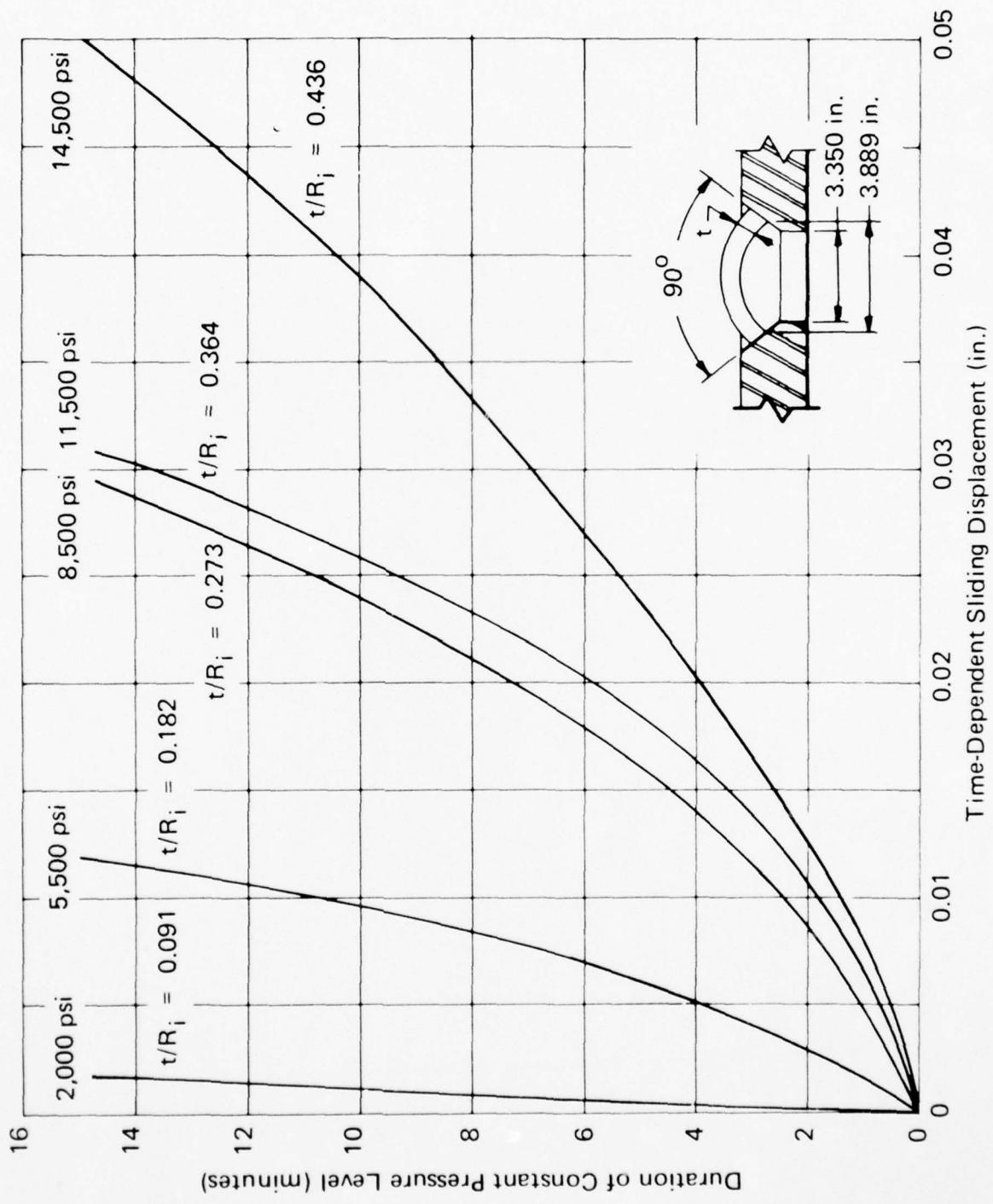
The data in this section are concerned with the time-dependent sliding displacements of spherical sectors with 30-, 60-, 90-, 120-, 150-, and 180-degree ( $0.5, 1.04, 1.57, 2.09, 2.6,$  and  $3.14$  radians) included angles under long-term pressure loading at ambient room temperature in the mounting with  $D_f = (D_i - 0.2 R_i)$ .

Each curve represents only one window specimen

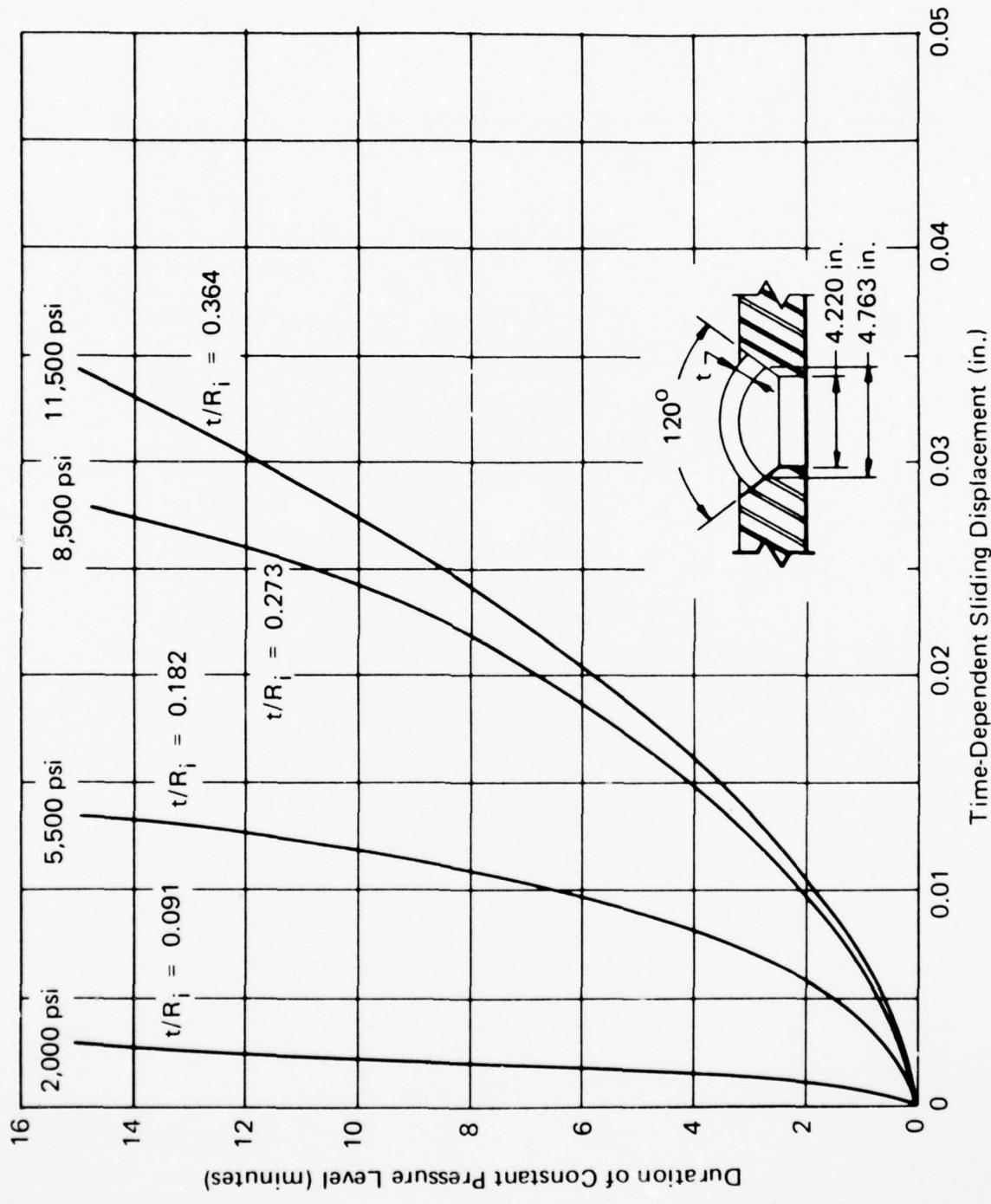


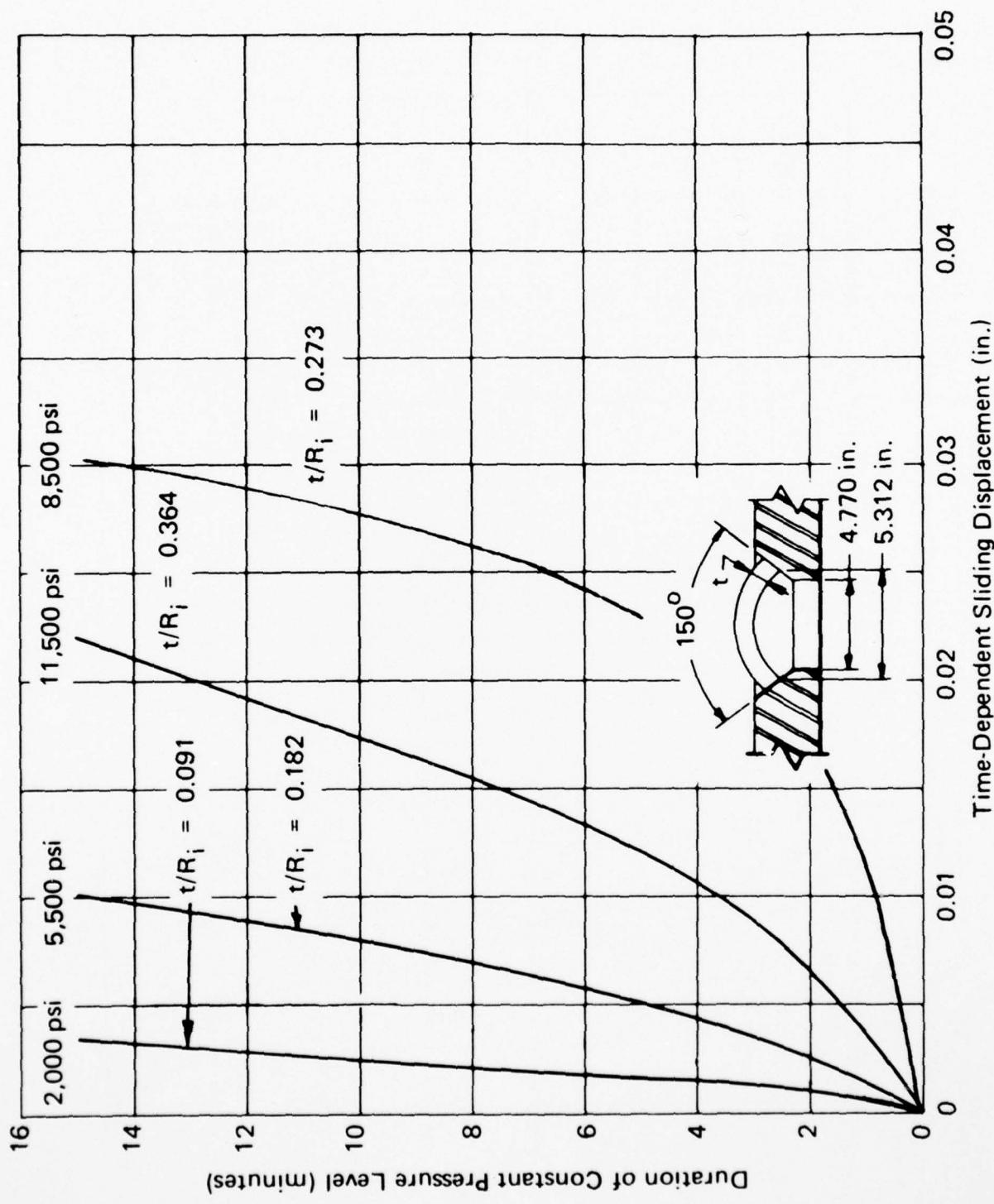


Each curve represents only one window specimen

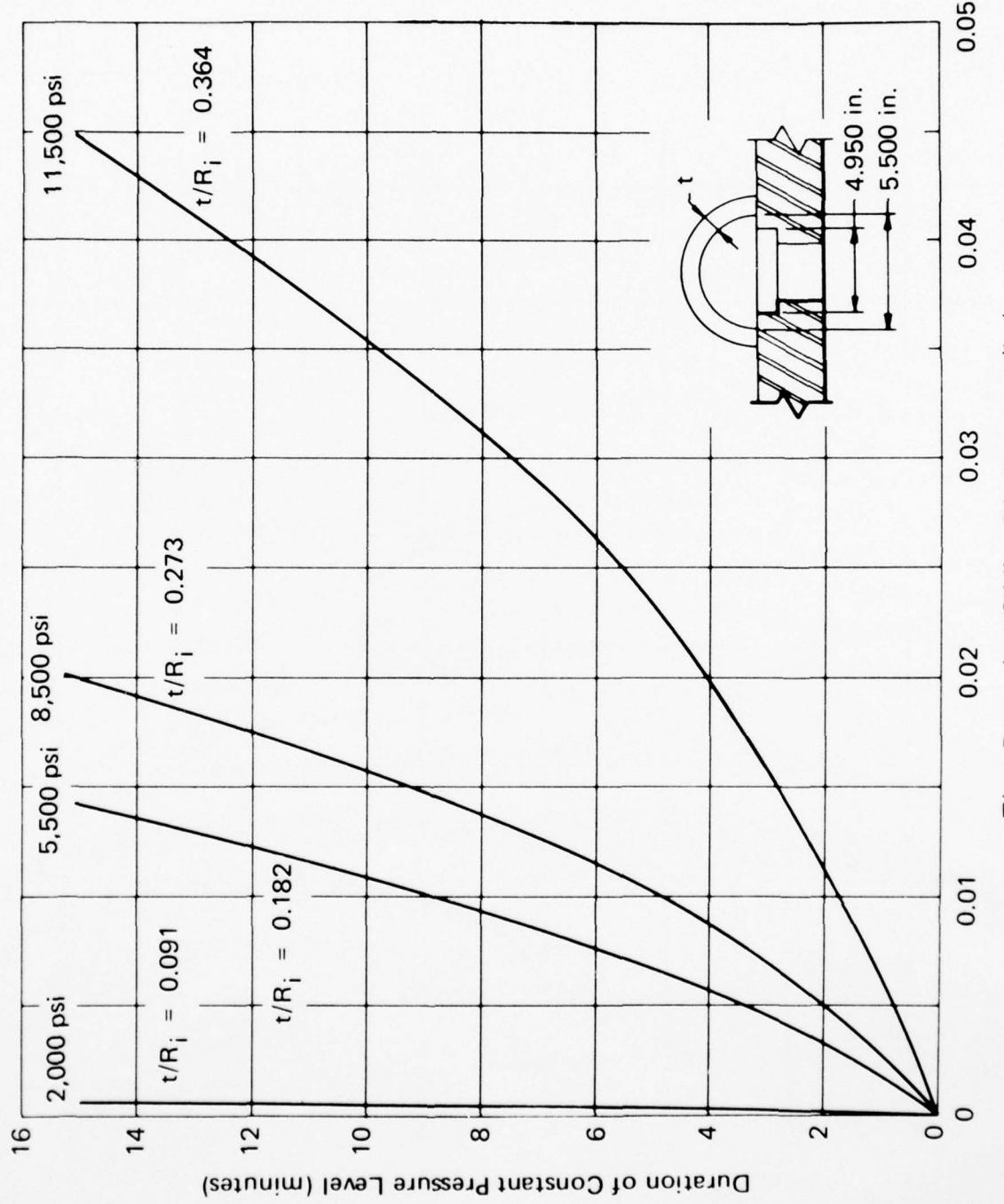


Each curve represents only one window specimen



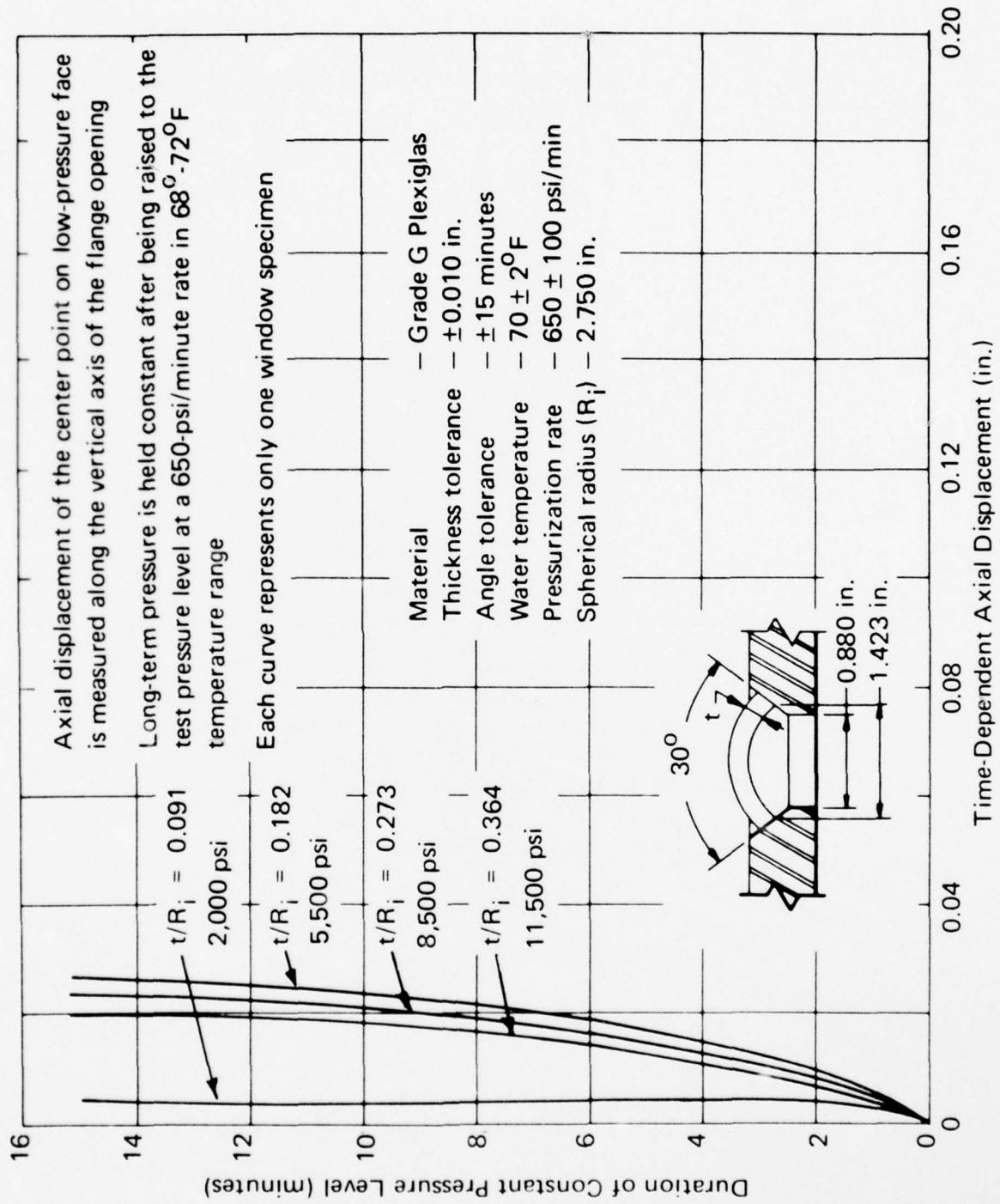


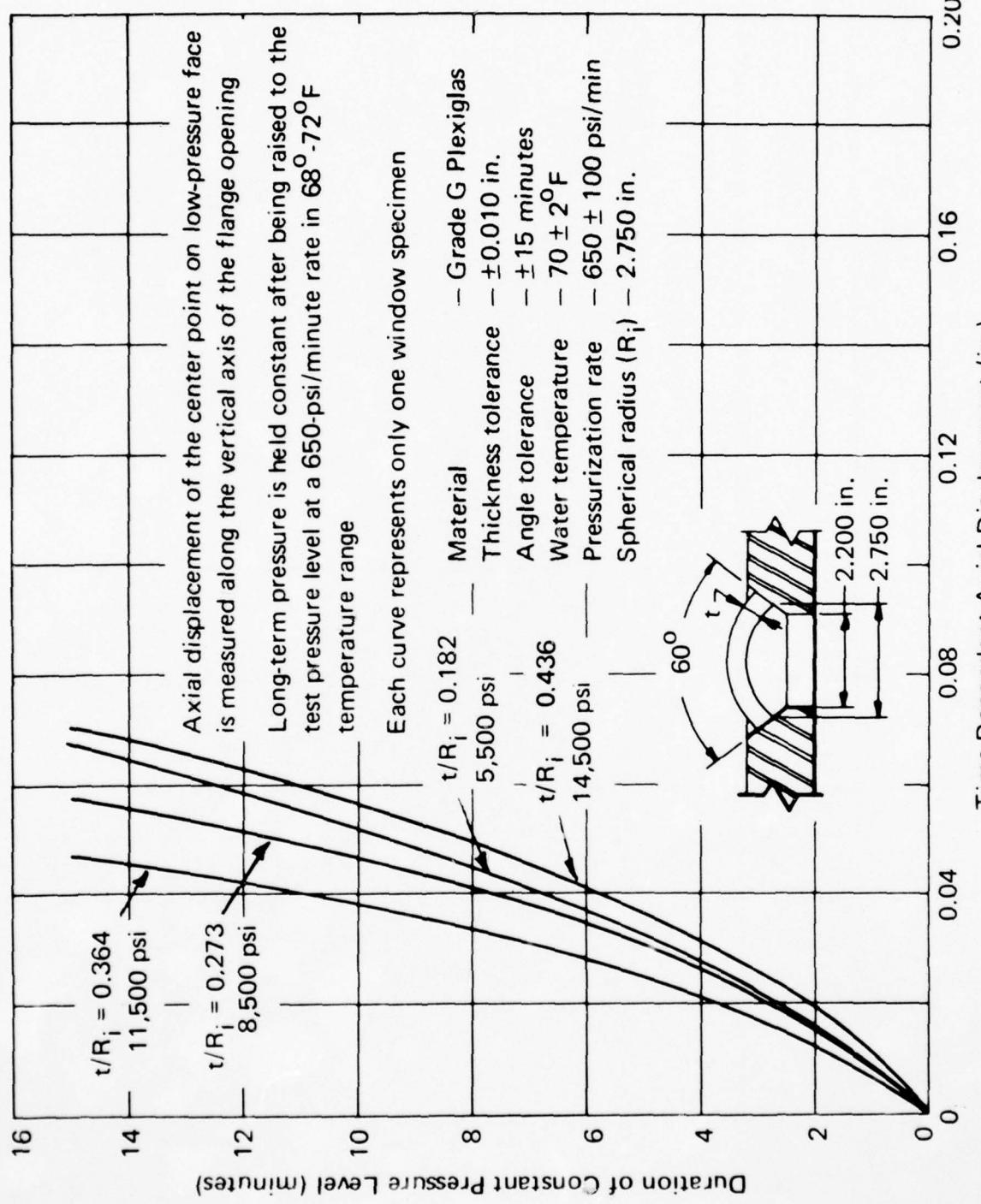
Each curve represents only one window specimen

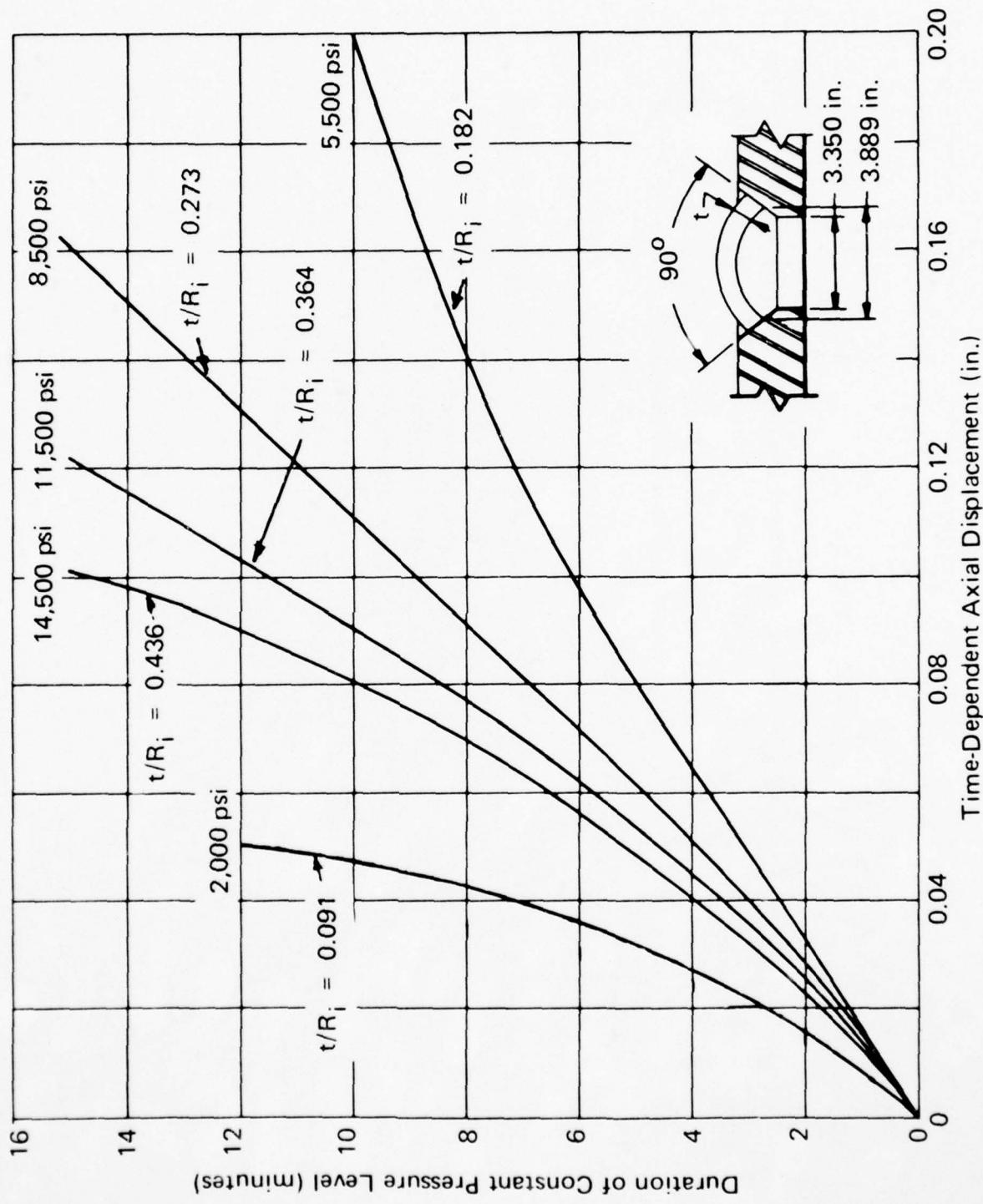


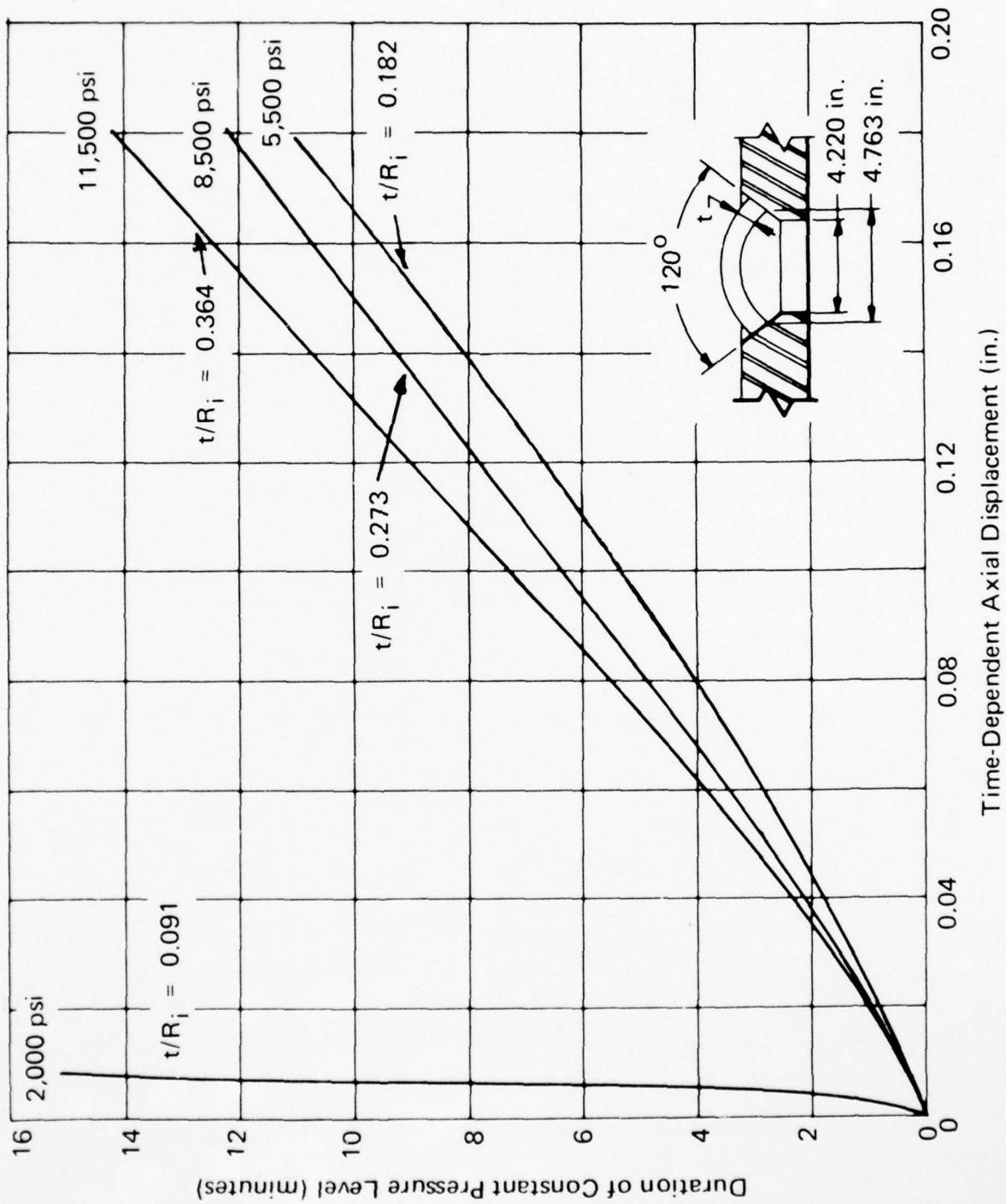
### C.2.2 Time-Dependent Axial Displacement

The data in this section are concerned with the time-dependent axial displacement of spherical sectors with 30-, 60-, 90-, 120-, 150-, and 180-degree (0.5, 1.04, 1.57, 2.09, 2.6, and 3.14 radians) included angles under long-term pressure loading at ambient room temperature in the mounting with  $D_f = (D_i - 0.2 R_i)$ .









Each curve represents only one window specimen

